中国科学院大学
University of Chinese Academy of Sciences

中国科学院高能物理研究所
Institute of High Energy Physics Chinese Academy of Sciences

Search for Higgs Boson Decays to Four τ-leptons with the ATLAS Detector and Developments of Silicon Detector

PhD Thesis Defense

by **Hao Zeng**

Supervisor: Professor João Pedro Barreiro Guimarães da Costa

Institute of High Energy Physics, Chinese Academy of Sciences

May, 16th, 2025

The Standard Model of Particle Physics

- The Standard Model is the theory that explains the fundamental particles and their interparticle forces
- The particles in the SM includes:
  - Fermions: building blocks of matter, leptons and quarks, three generations
  - Bosons: force carriers
- The forces in the SM:
  - Electromagnetic (γ)
  - Strong (g)
  - Weak ($W^{\pm}, Z^{0}$)
  - Gravity is unexplained in the current SM

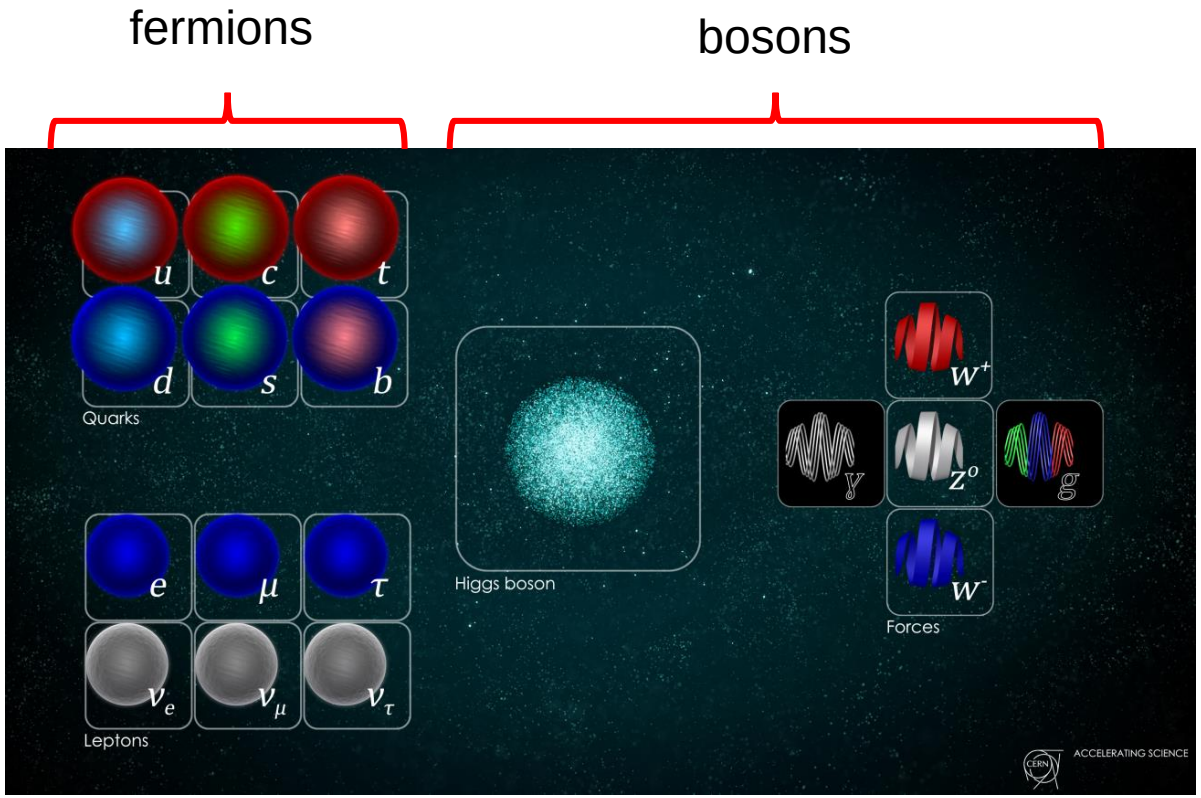

The SM Higgs Boson

- The only particle in SM with zero spin
- Discovered in 2012 by both ATLAS and CMS experiments
- Latest measured mass: 125.20 ± 0.11 GeV
- Responsible for providing mass to all fundamental particles, only couples to particles with mass:

$$\mathcal{L} = -g_{Hf\bar{f}}\bar{f}fH + \frac{g_{HHH}}{6}H^3 + \frac{g_{HHHH}}{24}H^4 + \delta_V V_\mu V^\mu \left(g_{HVV}H + \frac{g_{HHVV}}{2}H^2\right)$$

$$g_{Hf\bar{f}} = \frac{m_f}{v}, \qquad g_{HVV} = \frac{2m_V^2}{v}, \quad g_{HHVV} = \frac{2m_V^2}{v^2}$$

$$g_{HHH} = \frac{3m_H^2}{v}, \quad g_{HHHH} = \frac{3m_H^2}{v^2},$$

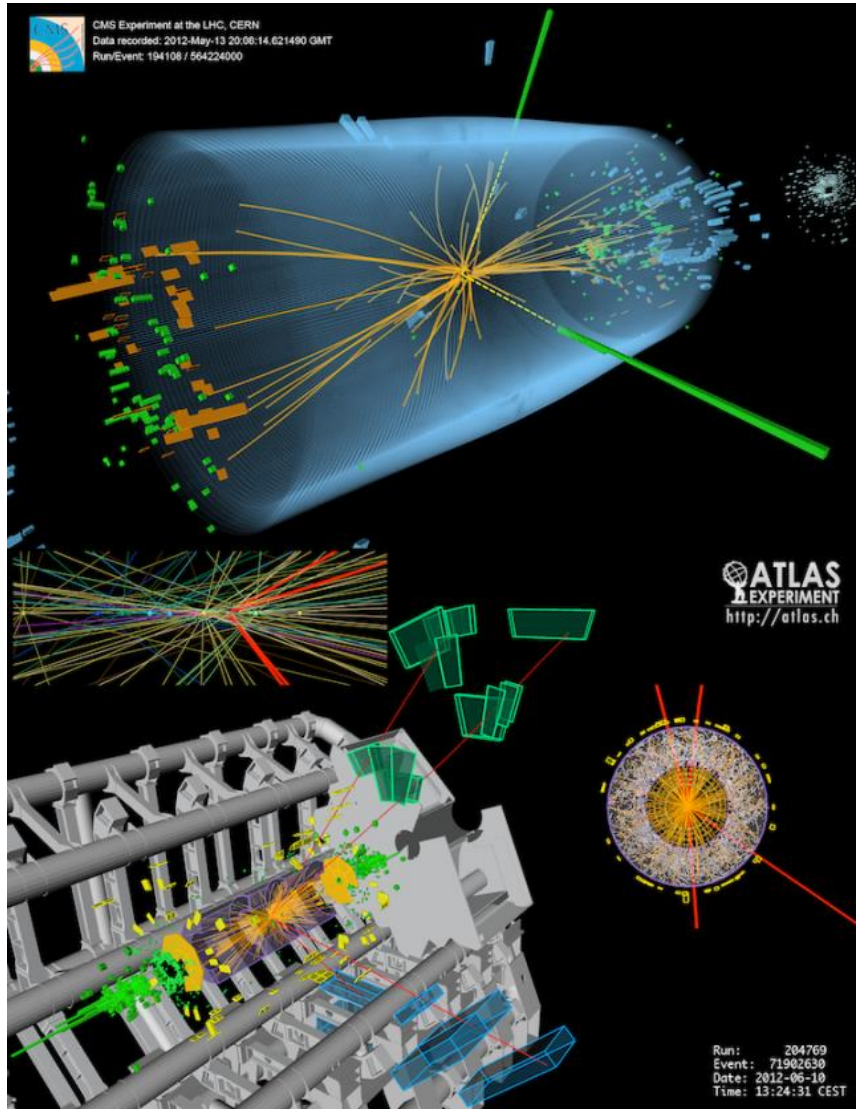

The SM Higgs Boson

- The only particle in SM with zero spin
- Discovered in 2012 by both ATLAS and CMS experiments
- Latest measured mass: 125.20 ± 0.11 GeV
- Responsible for providing mass to all fundamental particles, only couples to particles with mass:

$$\mathcal{L} = -g_{Hf\bar{f}}\bar{f}fH + \frac{g_{HHH}}{6}H^3 + \frac{g_{HHHH}}{24}H^4 + \delta_V V_\mu V^\mu \left(g_{HVV}H + \frac{g_{HHVV}}{2}H^2\right)$$

$$g_{Hf\bar{f}} = \frac{m_f}{v}, \qquad g_{HVV} = \frac{2m_V^2}{v}, \quad g_{HHVV} = \frac{2m_V^2}{v^2}$$

$$g_{HHH} = \frac{3m_H^2}{v}, \quad g_{HHHH} = \frac{3m_H^2}{v^2},$$

Higgs decay modes

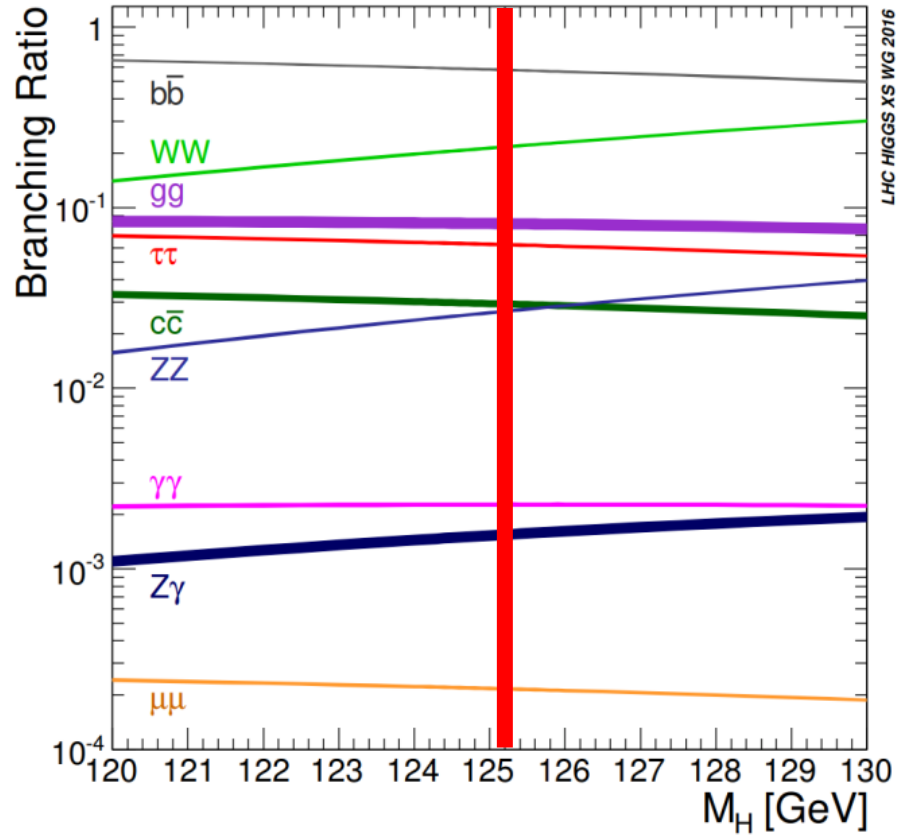

The Standard Model is incomplete

- Even though the Standard Model has been tested through numerous experiments and has demonstrated its robustness, there are still many questions that it can not answer
  - The nature of dark matter
  - The origin of neutrino mass
  - The matter-antimatter asymmetry problem
  - The question of naturalness
  - …

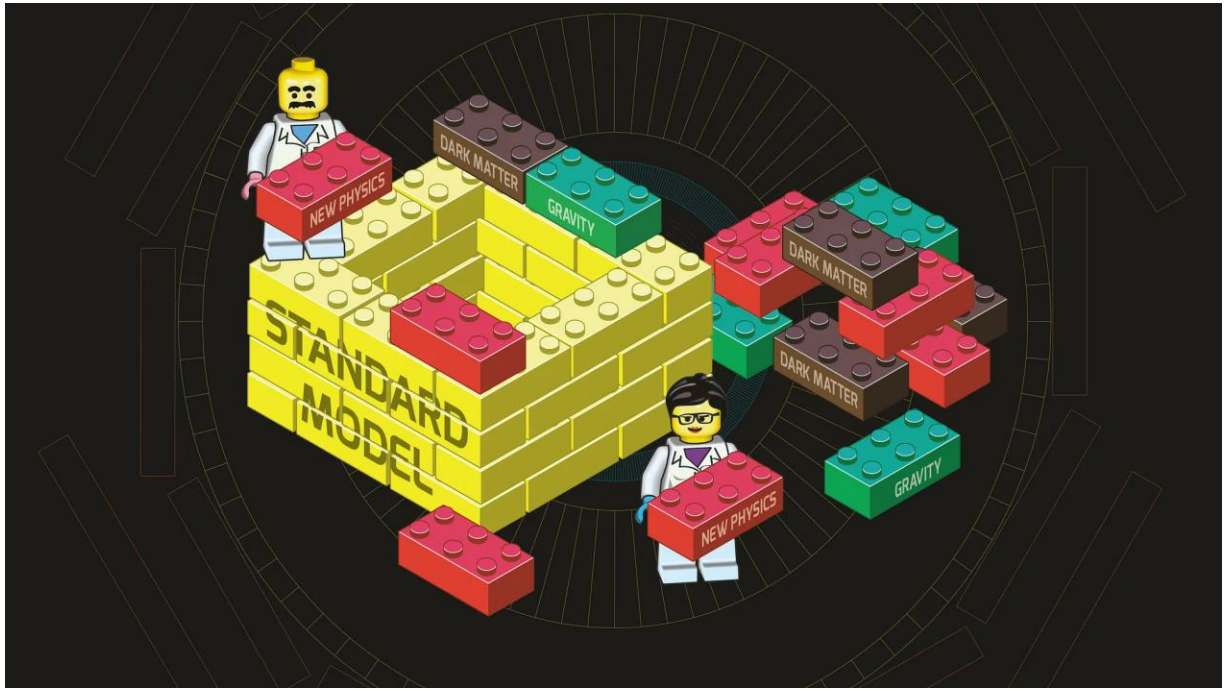

Motivation for Exotic Higgs Decays Search

- Exotic Higgs decays to BSM particles offer a way for probing new physics.
  - Higgs can act as a "portal" for hidden-sector particles interacting with SM
  - Predicted in models of dark matter, electroweak baryogenesis, and neutral naturalness
- 2HDM+s Model:
  - The SM is augmented by a light scalar or pseudoscalar particle $\boldsymbol{a}$
    - $H \to aa$
  - The light particle can inherit the Yukawa coupling pattern of Higgs
    - The couplings between a and SM particles are depending on the $\boldsymbol{m_a}$ and the rotation angle between the doublet Higgs bosons $\boldsymbol{\tan\beta}$
    - $H \to aa \to 4\tau$

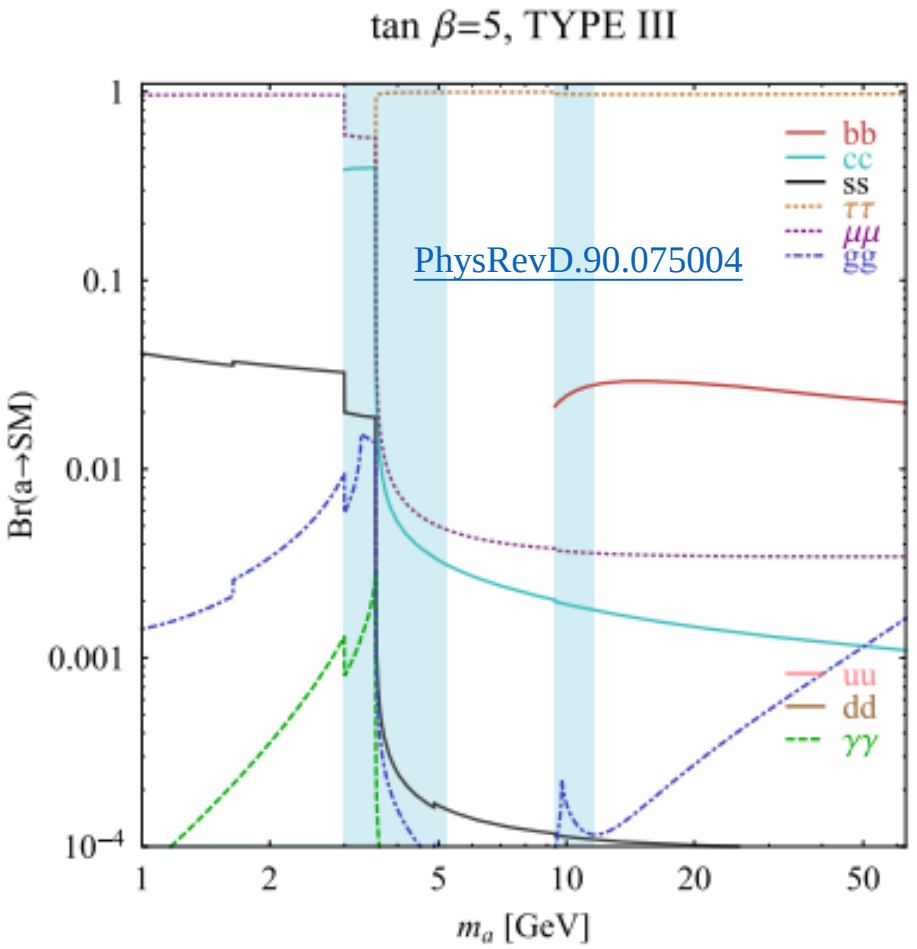

How to Produce Higgs

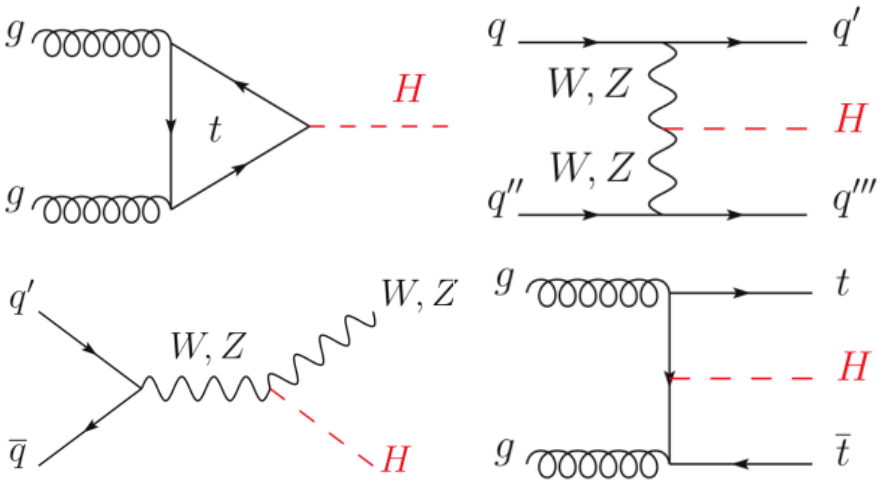

Proton-proton collider
LHC

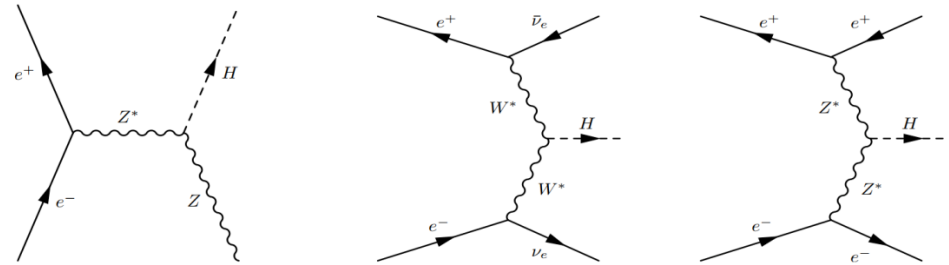

e^-e^+ collider
CEPC

The Large Hadron Collider

- The Large Hadron Collider (LHC) is the world's largest and most powerful particle accelerator
  - Proton-proton collider machine
  - Two-ring superconducting hadron accelerator and collider installed within a **27** km long tunnel
  - Located at the border of France and Switzerland
  - Four main experiments: ATLAS, CMS, ALICE and LHCb.

Circular Electron Positron Collider (CEPC)

- The CEPC was proposed by the Chinese HEP community in late 2012 after the Higgs discovery.
- It aims to start operation in 2030s, as a Higgs / Z / W factory.
- Huge amount of physics can be studied in CEPC:
  - High precision Higgs and EW measurements, studies of flavor physics & QCD, and probes of new physics beyond the SM (exotic Higgs decays).
- The CEPC reference detector TDR is planned to release in the next couple months.

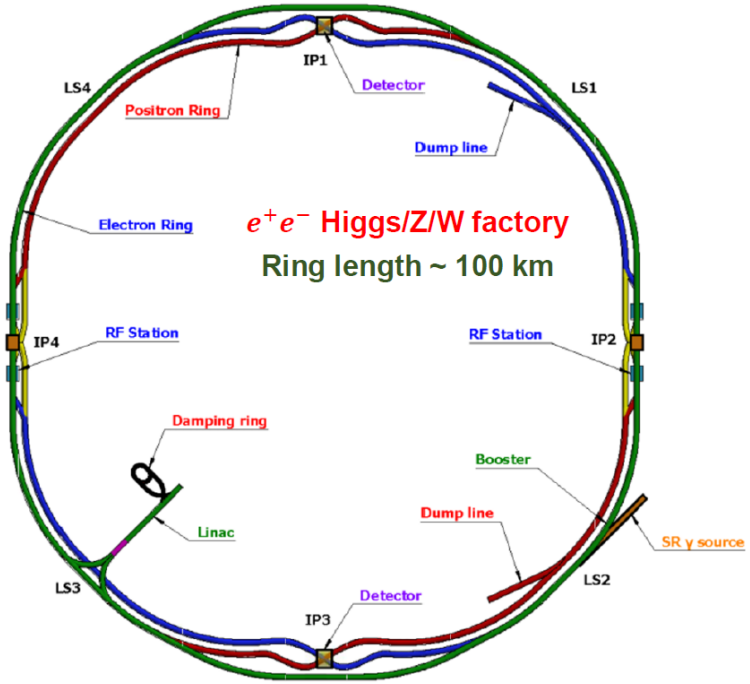

Limits for Exotic Higgs Decays at LHC

- Many searches for exotic Higgs boson decays $H \to aa$ have been conducted by the ATLAS and CMS Collaborations
  - The plot summarizes the limits up to 2022

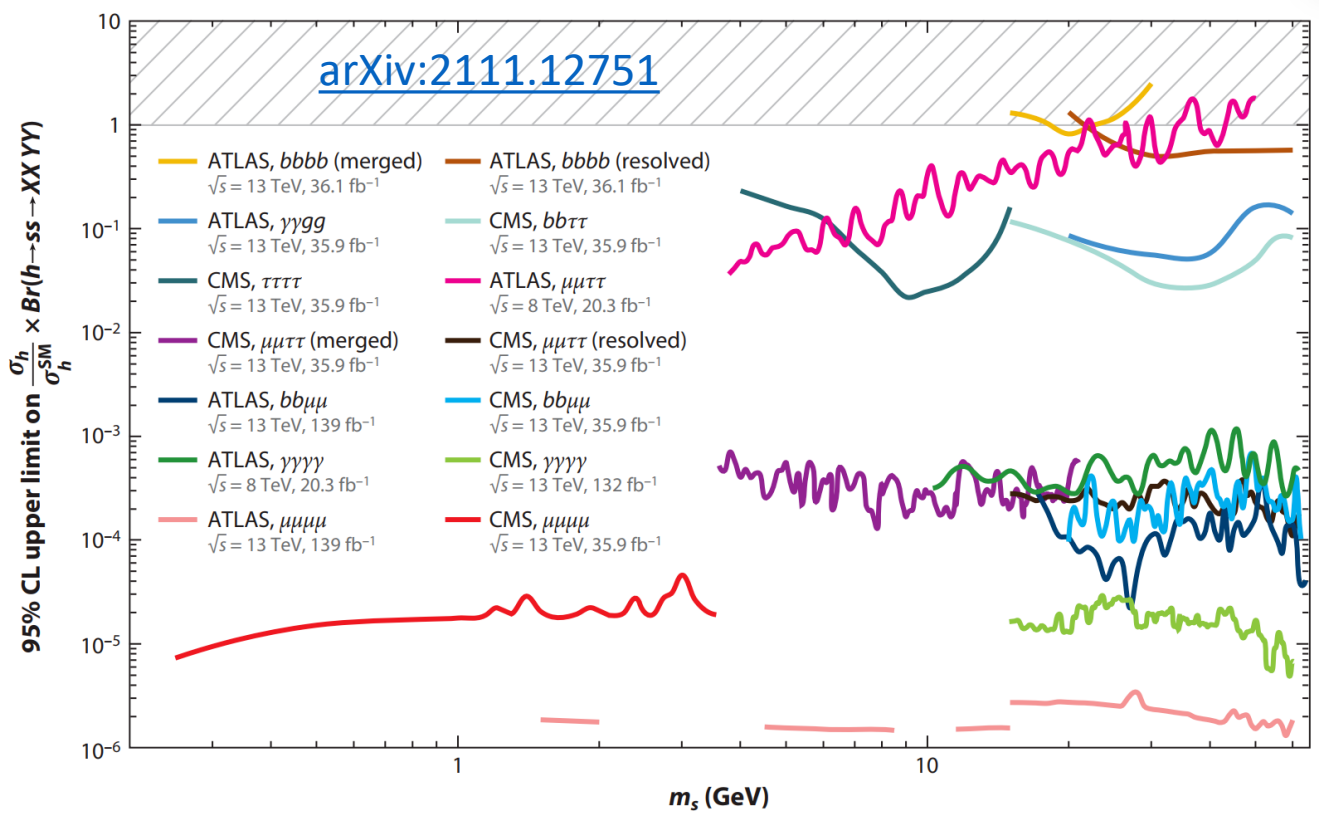

Recent results

ATLAS

$bb\tau\tau$: PRD 110 (2024) 052013

$\gamma\gamma\gamma\gamma$: EPJC 84 (2024) 742

$\gamma\gamma\tau\tau$: JHEP 03 (2025) 190

CMS

$\mu\mu(\tau\tau)bb$: EPJC 84 (2024) 493

$bbbb$: JHEP 06 (2024) 097

$\gamma\gamma\gamma\gamma$: PRL 131 (2023) 101801

$\gamma\gamma\gamma\gamma$: JHEP 07 (2023) 148

Why $H \to aa \to 4\tau$?

- The branching ratio of $a \to \tau^+\tau^-$ are dominant in the 2HDM + S for type-III Yukawa couplings with $\tan\beta > 1$
- 4τ channel has not been covered by ATLAS
  - Especially the boosted 4τ search

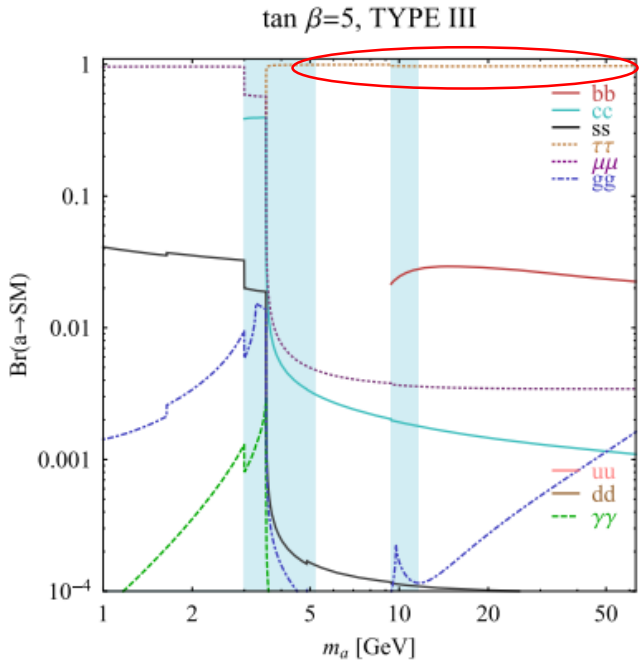

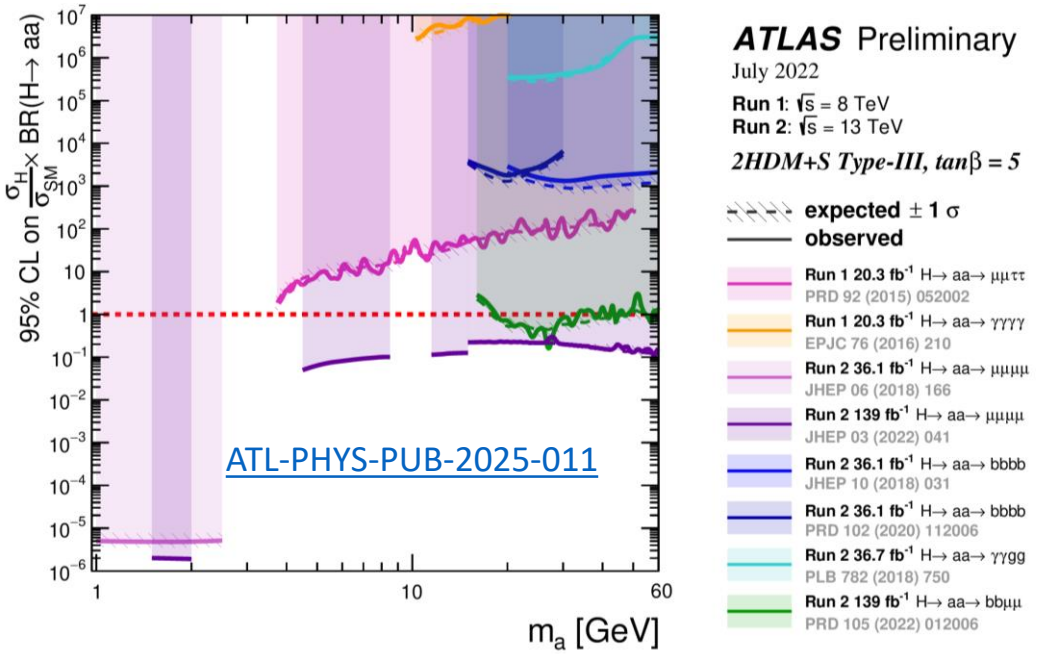

The ATLAS Detector

- Multipurpose particle detector
  - 44 m long, 25 m in diameter, 7000 tons
- Forward-backward symmetric cylindrical design covering almost 4π solid angle
- Various sub-detector system to reconstruct different type of particles
  - Inner detector
  - Calorimeter system
  - Muon spectrometer
- Using the ATLAS 2015-2018 data (140 fb^{-1})

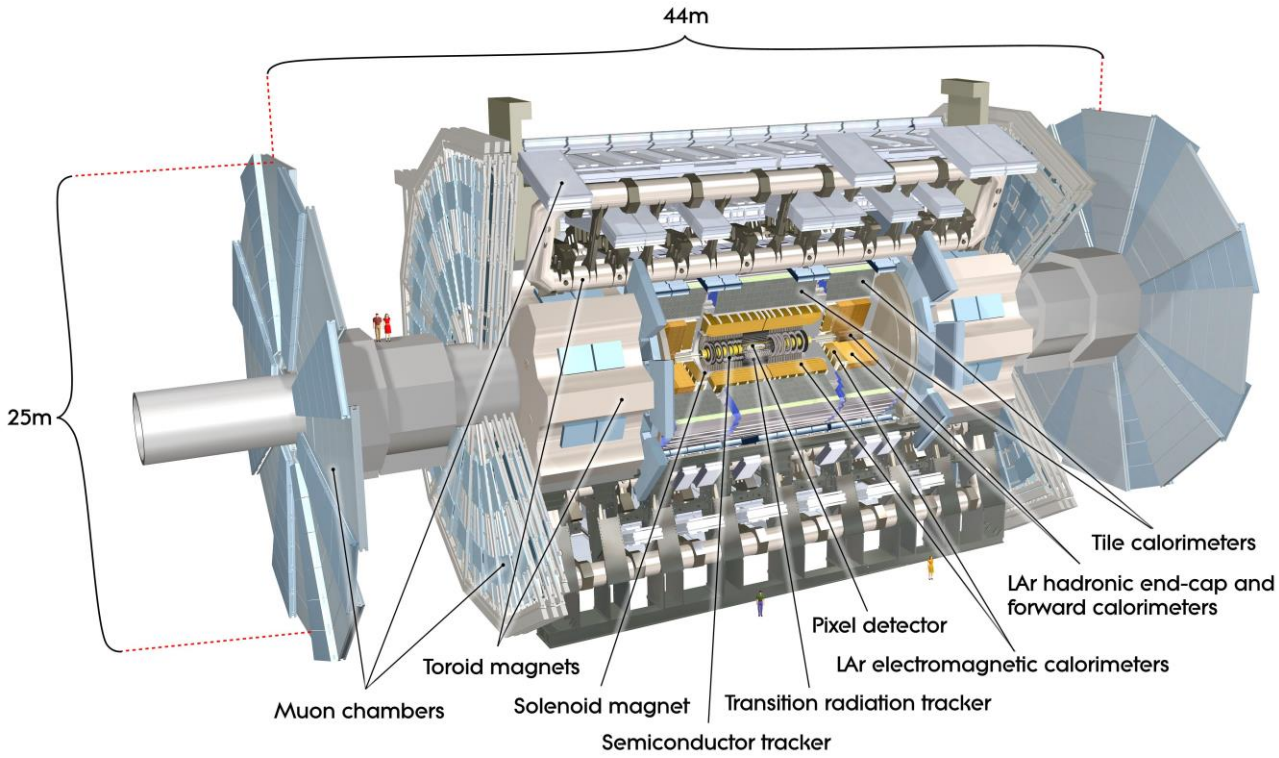

Object Reconstruction in ATLAS Detector

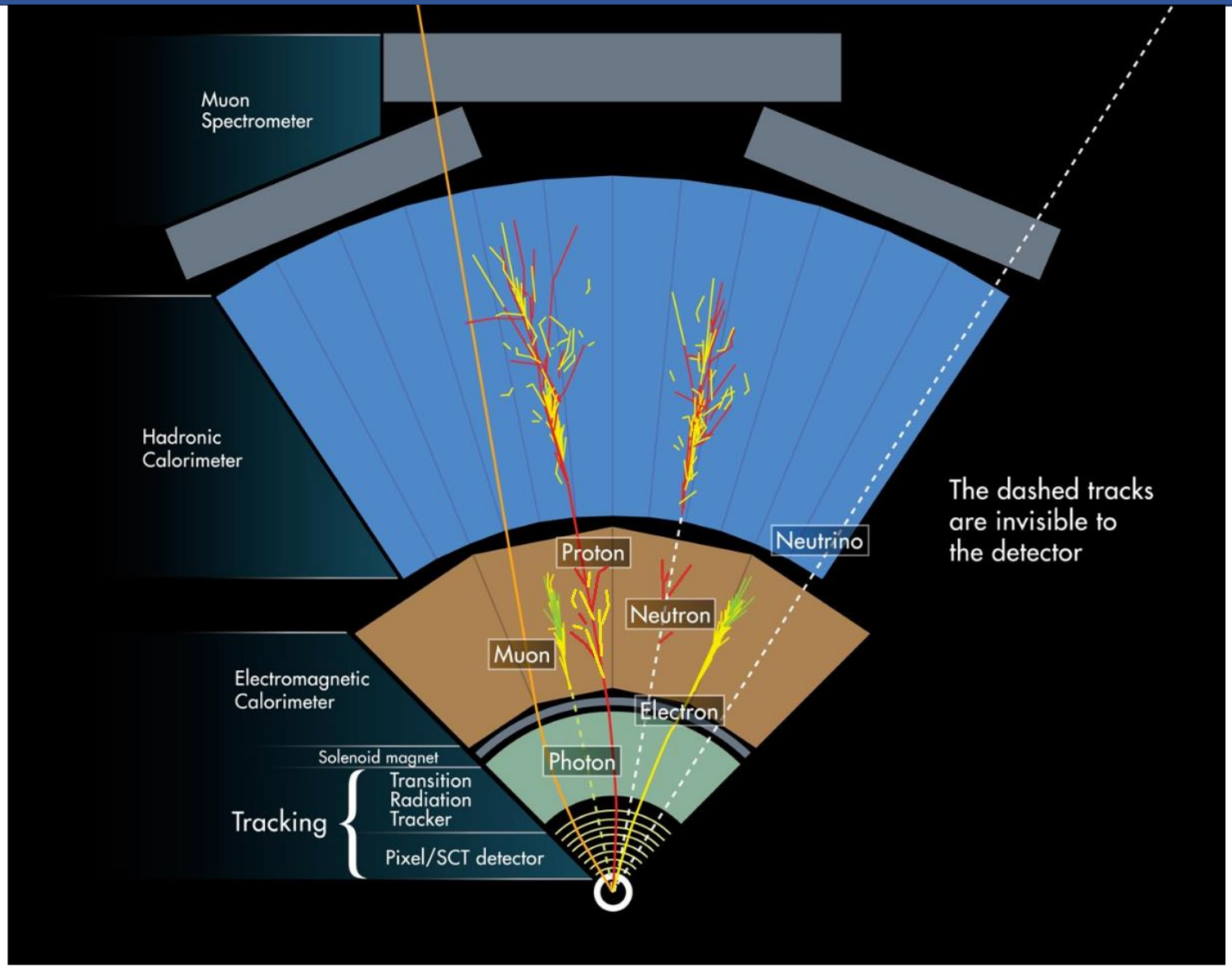

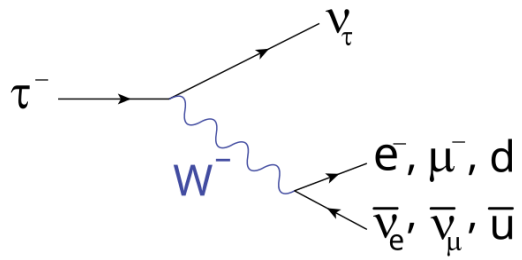

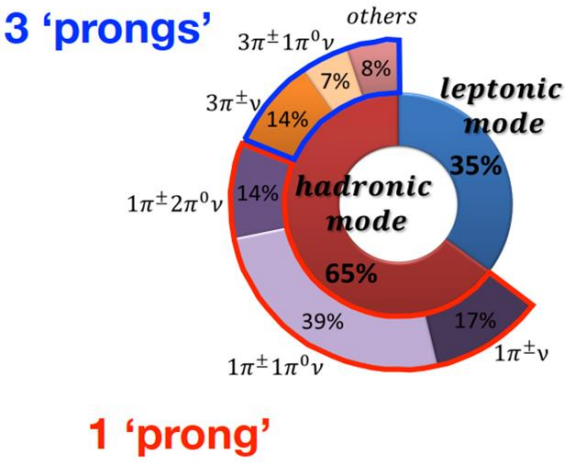

The Upgrade of LHC

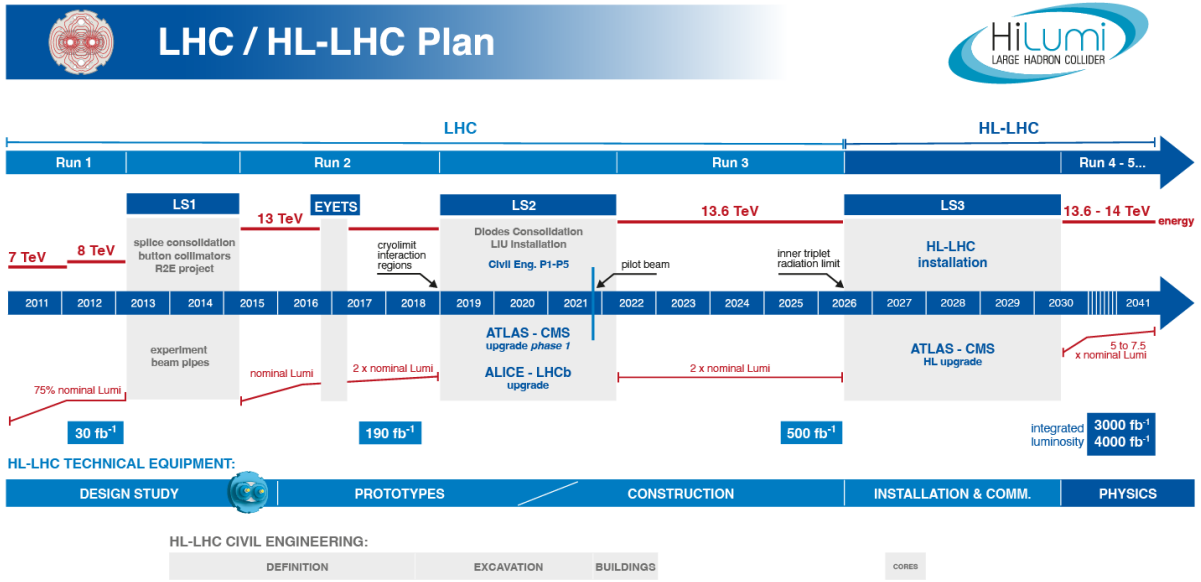

- Instantaneous luminosity to increase from 2.0 to 7.5 × $10^{34} s^{-1} cm^{-2}$
- Pile-up to increase from currently 55 to 200

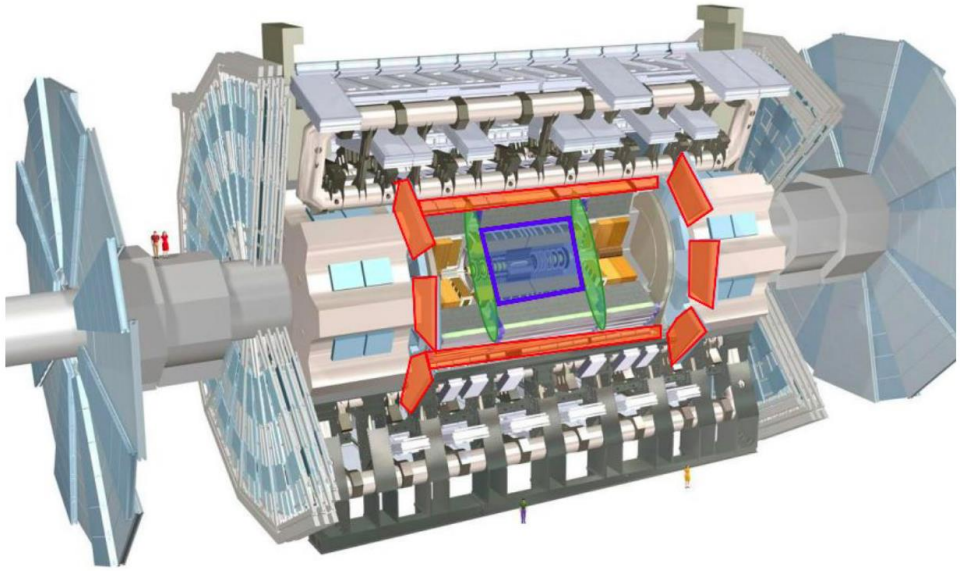

- **New tracker (ITk)**
  - Less material & finer segmentation
- **High Granularity Timing Detector (HGTD)**
  - Providing 30 – 50 ps time resolution per track
  - Improved pile-up separation
- **New muon chambers**
  - Improved trigger efficiency/momentum resolution, reduced fake rate

$H \rightarrow 2a \rightarrow 4\tau$ Analysis

Overview of 4τ Analysis

- Mass range of $4 < m_a < 15$ GeV
  - The most challenge mass range of 4τ search
- $a \to \tau_\mu \tau_h$ decay mode (23% branching ratio of di-τ decay)
  - Using di-muon trigger to go lower muon p_T threshold
- Boosted di-τ due to low mass of a
- Merged di-τ identification (ID)→ resolved with the muon removal technique
- Dominant background is the fake $\mu\tau_{had}$ from QCD → estimated using data-driven method

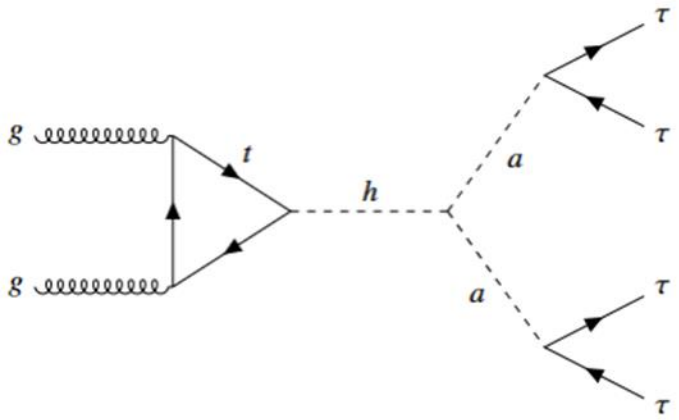

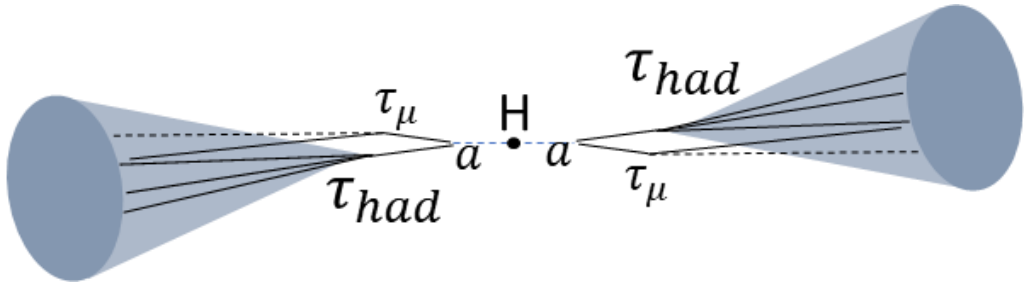

Challenge: Boosted Low-p_T di-τ Identification

- Because of the low mass of a, the distance between τ_l and τ_{had} will be very small even for low p_T
  - $\Delta R(\tau_l, \tau_{had}) \approx 2m_a/p_T^a$
- The decay products of τ_l and τ_{had} are mixed in the detector.
- The standard tau identification does not work

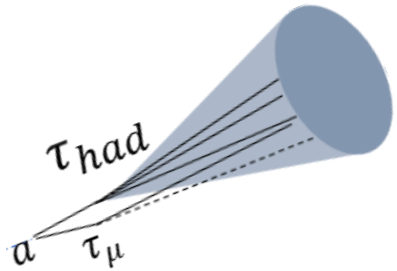

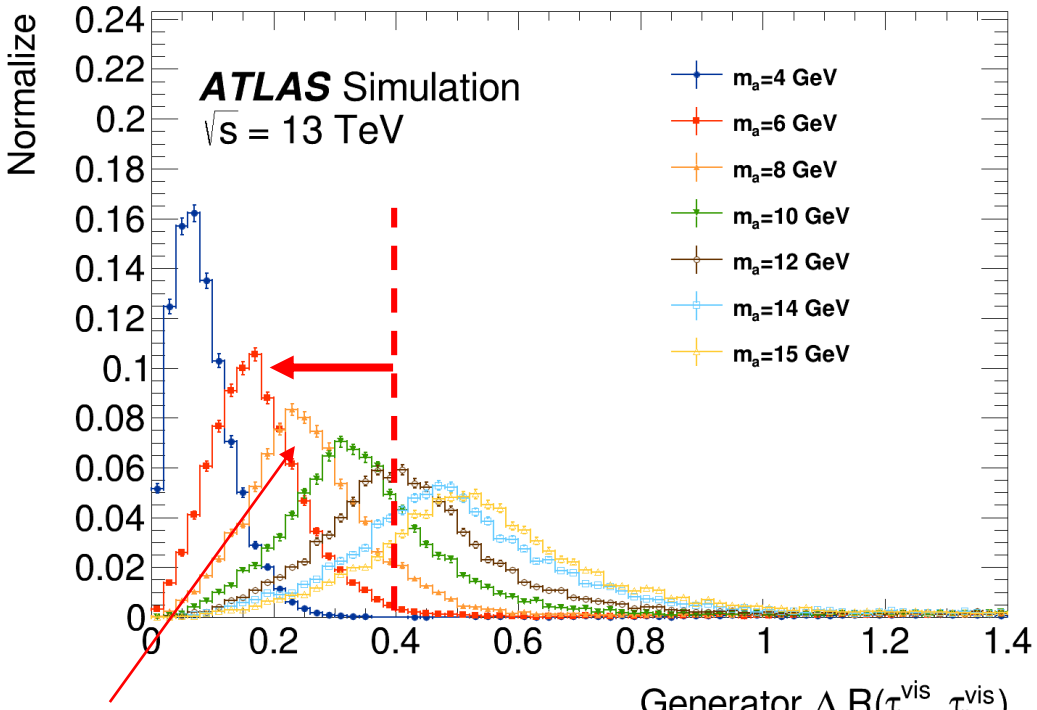

Merged taus

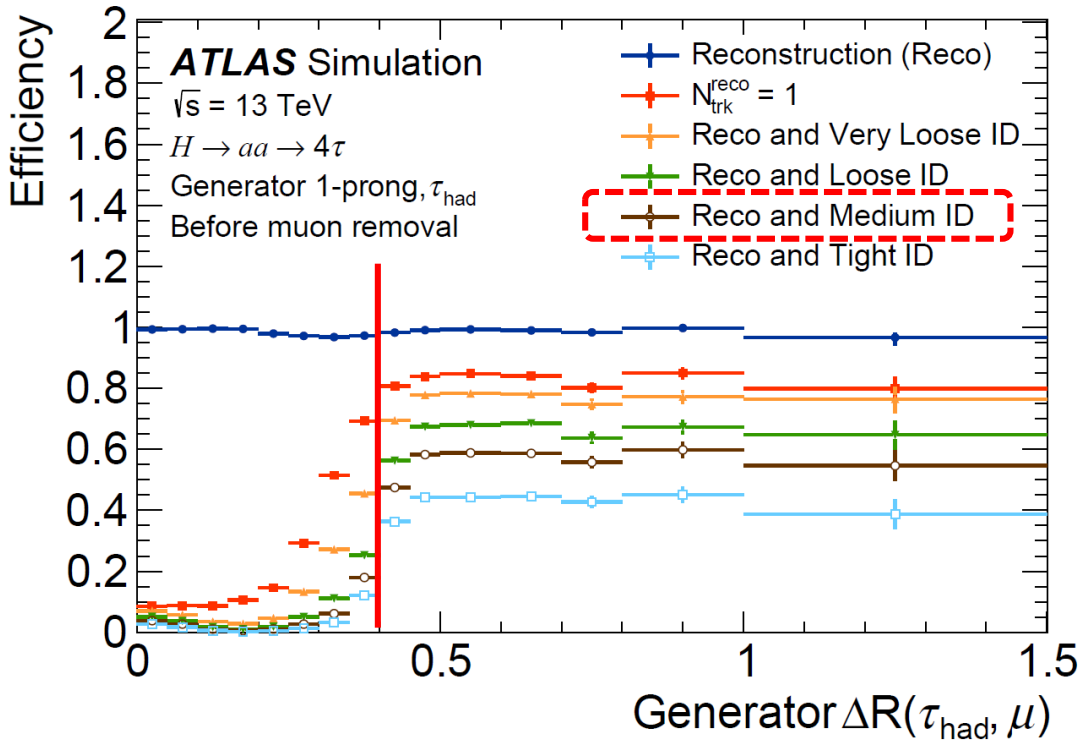

Standard tau identification efficiency

Muon Removal Technique

- Merged $\tau_\mu \tau_{had}$ correction algorithm:
  - Overlapped muons are removed from tau seed jet .
    - Both the **Muon tracks** and **associated energy** are removed
  - Re-calculate the relevant tau identification variables after muon removal.
  - Use the official ATLAS tau performance results for the analysis
  - An extra efficiency uncertainty was extracted for the muon removal method
  - The τ_{had} four-momentum is corrected to the same energy scale as for the isolated τ_{had} using a MC-based correction method.
- Tau id efficiency was recovered after muon removal

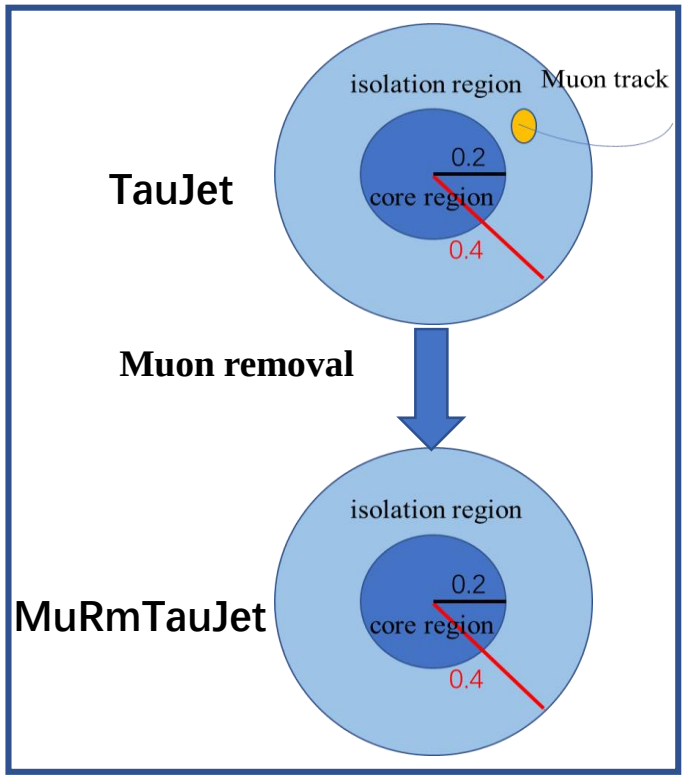

Tau Reco and ID Efficiency after Muon Removal

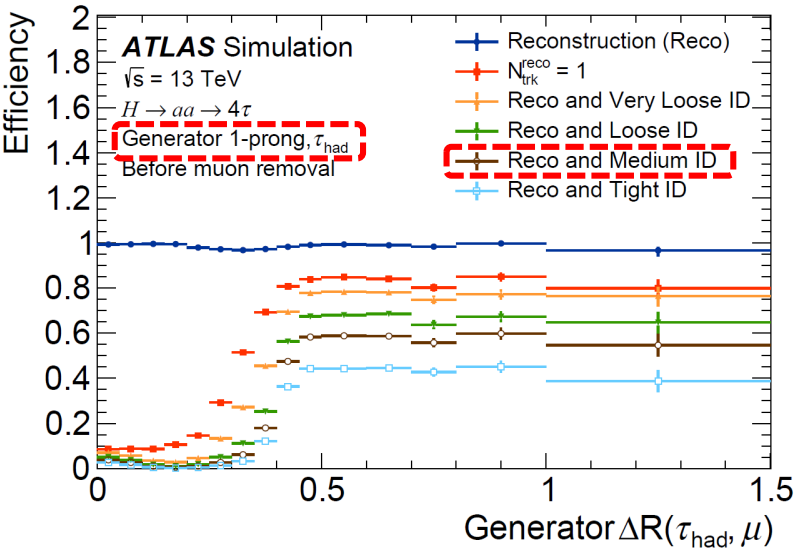

Muon Removal

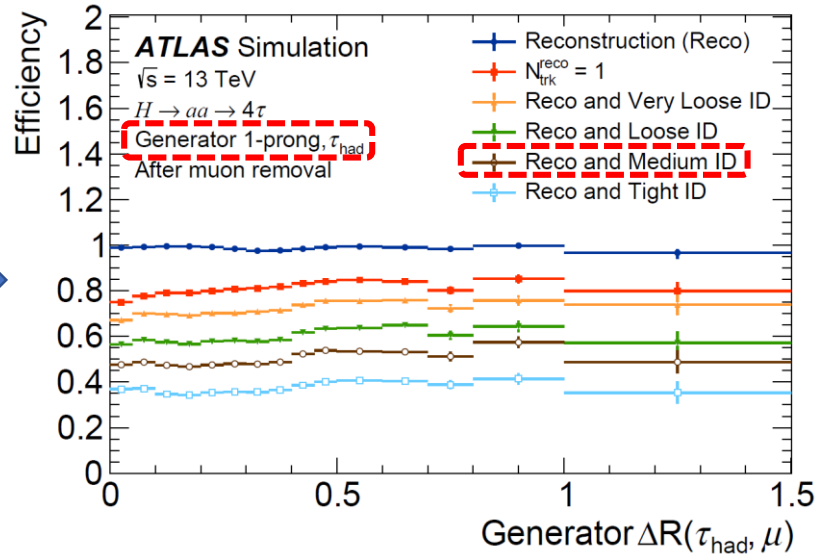

- The efficiencies of merged taus were recovered (improved by an order of 10)
- ΔR has very small effect on the tau efficiencies after the muon removal

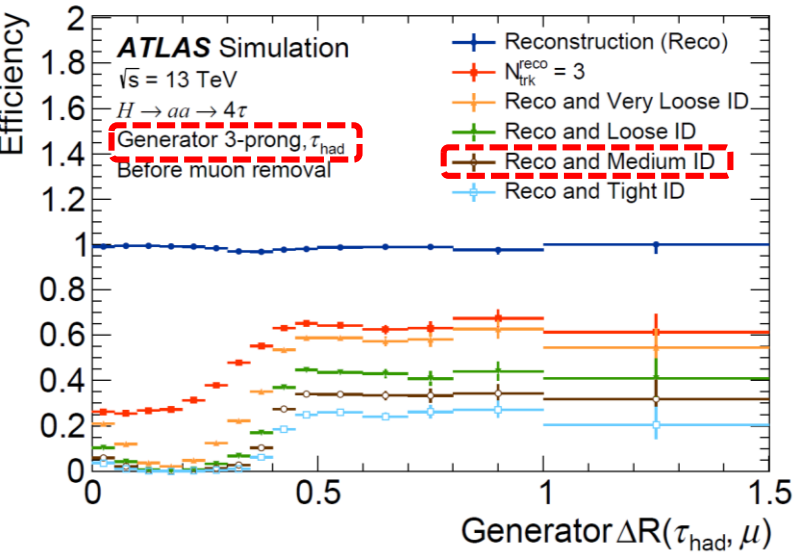

Muon Removal

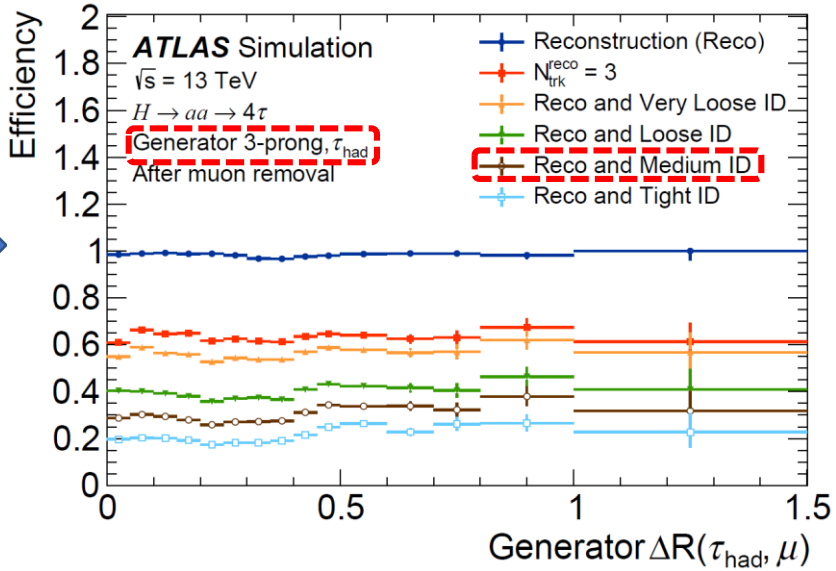

Tau momentum correction

- MC-based correction procedures:
  - Derive the ratio of reco p_T^{OL} to reco p_T^{iso}, $R(p_T^{OL,UnCorr}, n_p, p_T^{\mu})$, in the same truth p_T
  - Correct p_T^{OL} to p_T^{iso} :
    - $p_T^{OL,Corr} = p_T^{OL,UnCorr} / R(p_T^{OL,UnCorr}, n_p, p_T^{\mu})$
  - Correct the η and ϕ based on the momentum conservation
- After the p_T correction, the mean value of p_T^{reco} / p_T^{truth} is moving to 1, which means the average p_T^{reco} is corrected to p_T^{truth}
- The resolution of p_T^{OL} also improves a lot after the correction
- The η and ϕ resolutions are improved very significantly after the correction
- The MC-based correction is applied after all signal selection

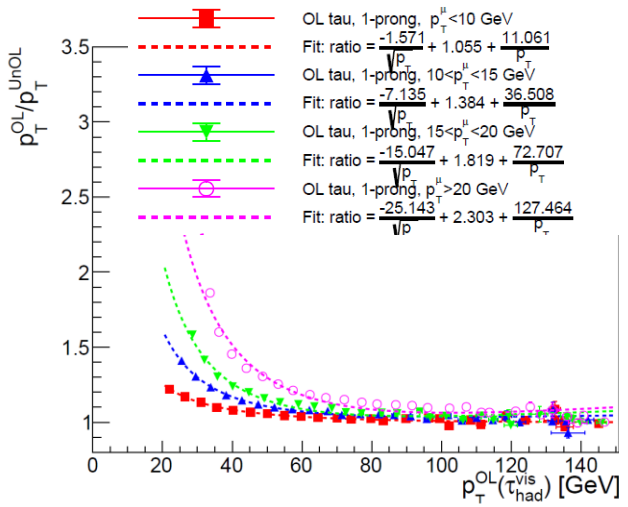

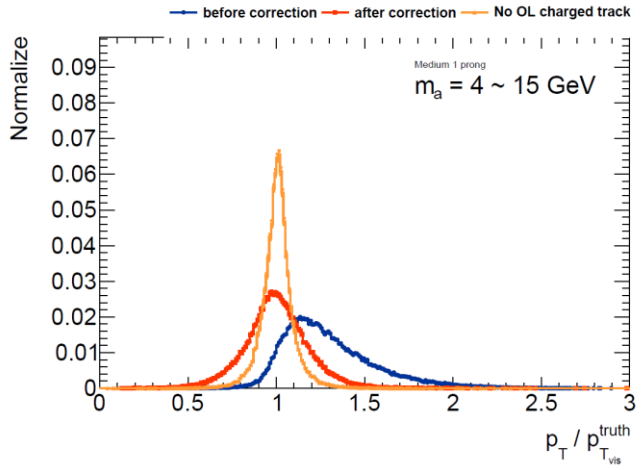

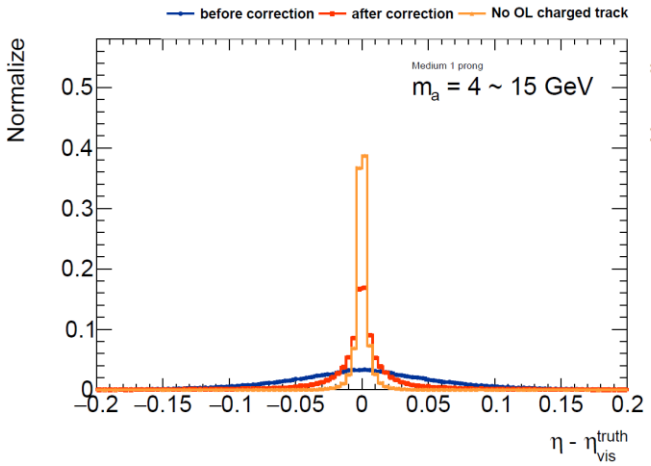

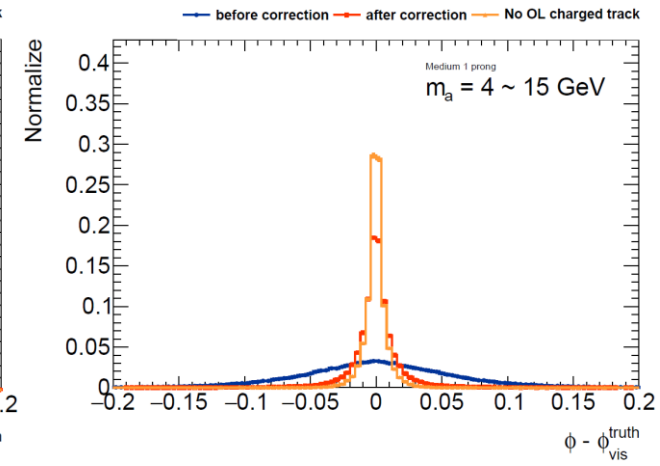

Di-τ tagger method

- The di-τ tagger is an alternative method to resolve the boosted low-p_T di-τ identification:
  - Consider the di-τ pair as one object
  - Use machine learning method to develop the tagger
  - Good discrimination between signal and background

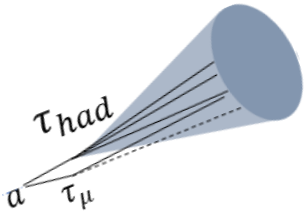

- Challenge is to measure the tagger efficiency in data → measure the scale factors
  - Merged di-τ from Z boson decay requires $p_T^Z \approx 450$ GeV ($\Delta R(\tau,\tau) \approx 2m_Z/p_T^Z$)
  - Merged di-τ from 10 GeV a boson decay only requires $p_T^a \approx 50$ GeV
  - Different kinematics → can not directly apply to low-p_T di-τ case

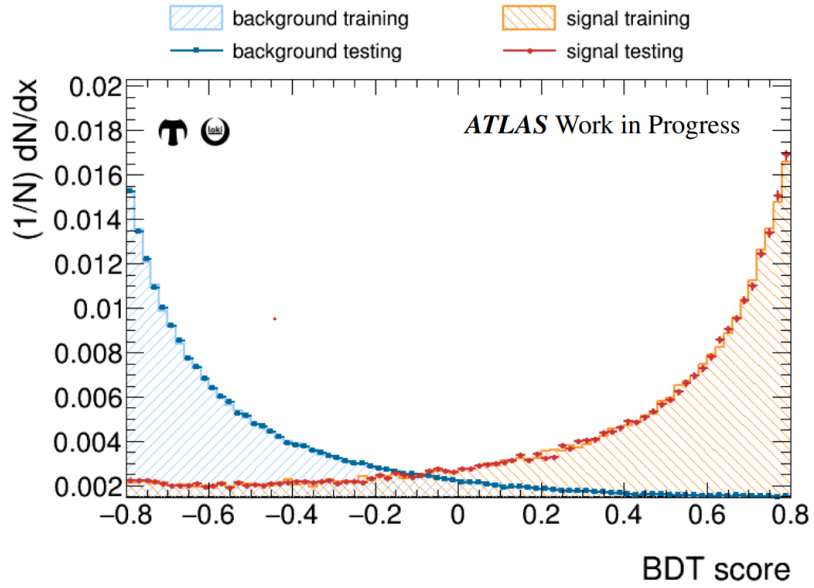

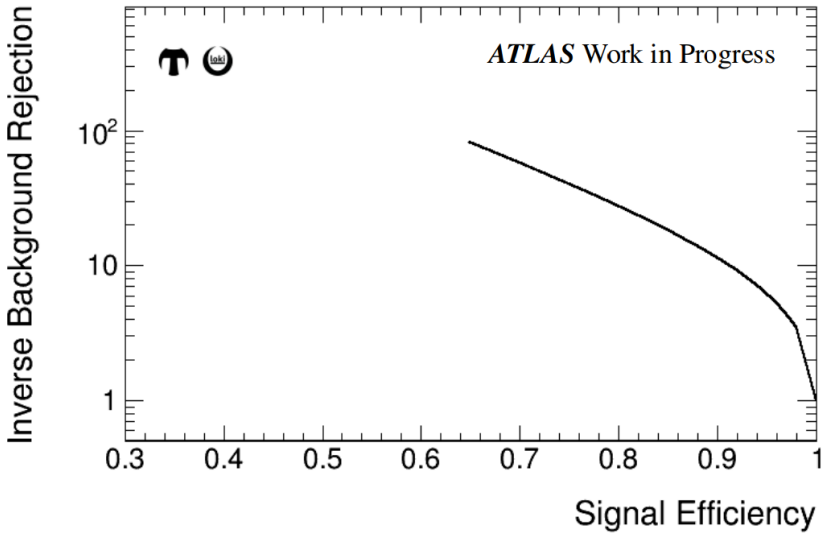

Di-τ tagger efficiency measurement

- Investigating to use $\Upsilon \to \tau_{had}\tau_{\mu}$ process to measure the tagging efficiency in data
  - The mass of Υ (9.46 GeV) is similar to m_a $(4-15$ GeV)
- High-μ data:
  - No high efficiency trigger for $\Upsilon \to \tau_{had}\tau_{\mu}$
- Low-μ data:
  - Check how many Υ in the data via $\Upsilon \to \mu\mu$ process
  - Fitting $\Upsilon \to \mu\mu$ invariant mass in low-mu data → Extract the number of Υ
  - Only 334 Υ →difficult to extract $\Upsilon \to \tau_h\tau_{\mu}$ from background

High-μ

Trigger	Upsilon yields
HLT_mu24	210
HLT_mu50	896
HLT_mu4_j15_gsc35_boffperf_split_dr05_dz02	<10

Low-μ

Center energy	N($\Upsilon \to \mu\mu$)	$Br(\tau\tau \to \mu\tau_{had})$	$N(\Upsilon \to \tau_\mu\tau_{had})$
13TeV	1306	0.23	300
5TeV	147	0.23	34
total $N\left(\begin{matrix}\Upsilon \to \tau_\mu\tau_{had},\\ \Delta R(\mu,\tau) < 0.4\end{matrix}\right)$			334

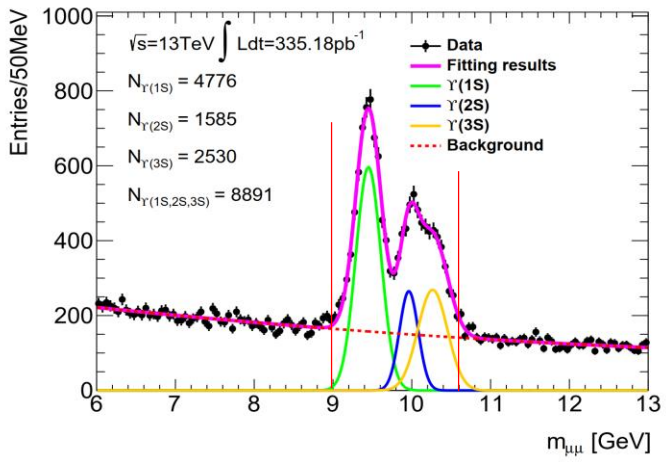

$\Delta R(\mu,\mu) < 0.4$

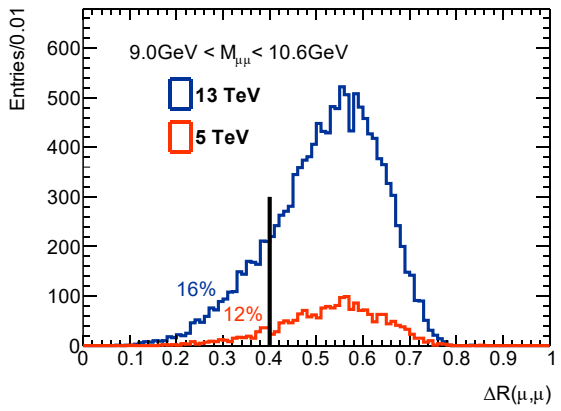

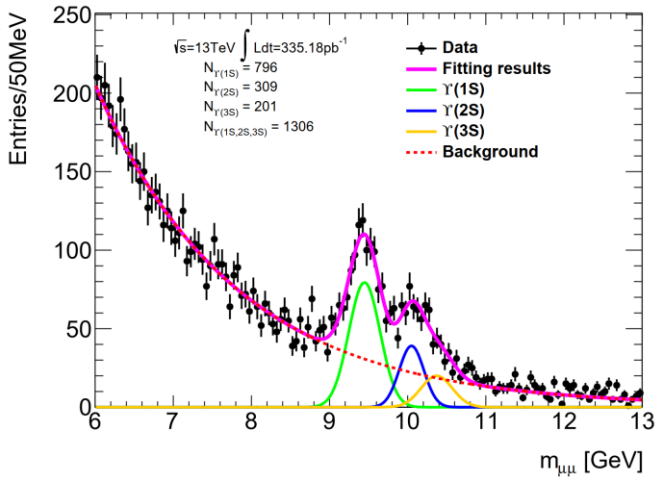

Object Definition

- The requirements of the baseline and signal objects:

	Baseline requirements	Signal requirements
Muons	• $p_T > 5$ GeV, $\|\eta\| < 2.5$ • ATLAS Medium identification (ID) working point (WP) • $z_0 sin\theta < 0.5$ mm • $\frac{d_0}{\sigma_{d_0}} < 7$ • No Isolation requirements	• $p_T > 5$ GeV, $\|\eta\| < 2.5$ • ATLAS Medium ID WP • $z_0 sin\theta < 0.5$ mm • $\frac{d_0}{\sigma_{d_0}} < 4$ • ATLAS PflowLoose Isolation WP
Taus (after muon removal)	• $p_{T,\tau}^{Uncorr} > 20$ GeV • $\|\eta_\tau^{Uncorr}\| < 2.5$, exclude $1.37 < \|\eta_\tau^{Uncorr}\| < 1.52$ • RNNID > 0.01 • 1 or 3 charged tracks	• $p_{T,\tau}^{Uncorr} > 25$ GeV • $\|\eta_\tau^{Uncorr}\| < 2.5$, exclude $1.37 < \|\eta_\tau^{Uncorr}\| < 1.52$ • Medium ID WP • 1 or 3 charged tracks

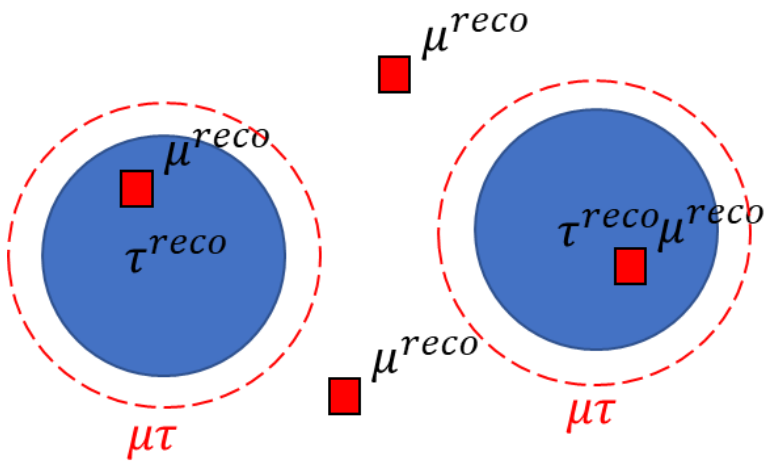

- Looser than usual to increase the muon efficiency from tau decay
- Used to reconstruct the Z in the Z+jets control region
- Uncorrected tau momentum is used in the tau object selection
- Increase the statistics for fake estimation
- Select the closest $\mu\tau_{had}$ pairs with $\Delta R(\mu, \tau) < 0.4$ and $m_{\mu\tau_{had}} < 15$ GeV.

Event selection

- Pre-selection:
  - Good data quality
  - Triggers: di-muon + single muon triggers
  - Has primary vertex
  - At least three leptons
- Event selection in the SRs:
  - Leading $p_T^{\mu} > 14$ GeV
  - Leading $p_{T,\tau}^{Uncorr} > 30$ GeV, sub-leading $p_{T,\tau}^{Uncorr} > 25$ GeV
  - 2 signal $\mu\tau_{had}$ pairs ($\Delta R(\mu, \tau_{had}) < 0.4$, $m_{\mu\tau_{had}} < 15$ GeV and τ_{had} passing Medium RNN ID)
  - $60 < m_{2\mu\tau_{had}}^{Uncorr} < 120$ GeV
  - $SS\mu$ channel: same-sign charge muons
  - $OS\mu$ channel: opposite-sign charge muons and $m_{\mu\mu} < 50$ GeV

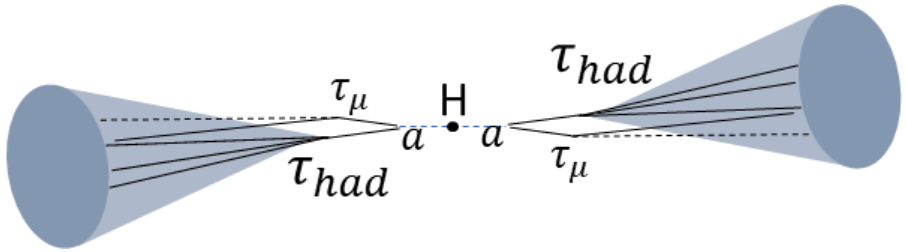

Trigger Type	Year	HLTs
Single Muon	2015-2018	HLT_mu50
Di-muon	2015	HLT_mu18_mu8noL1 HLT_2mu10
	2016-2018	HLT_mu22_mu8noL1 HLT_2mu14

Region definition

$2\mu, 2\ \mu\tau_{\mathrm{had}}$ pairs

Enhance the sensitivity for higher masses ($m_a = [10,15]$ GeV)

More sensitive to lower masses ($m_a = [4,6]$GeV)

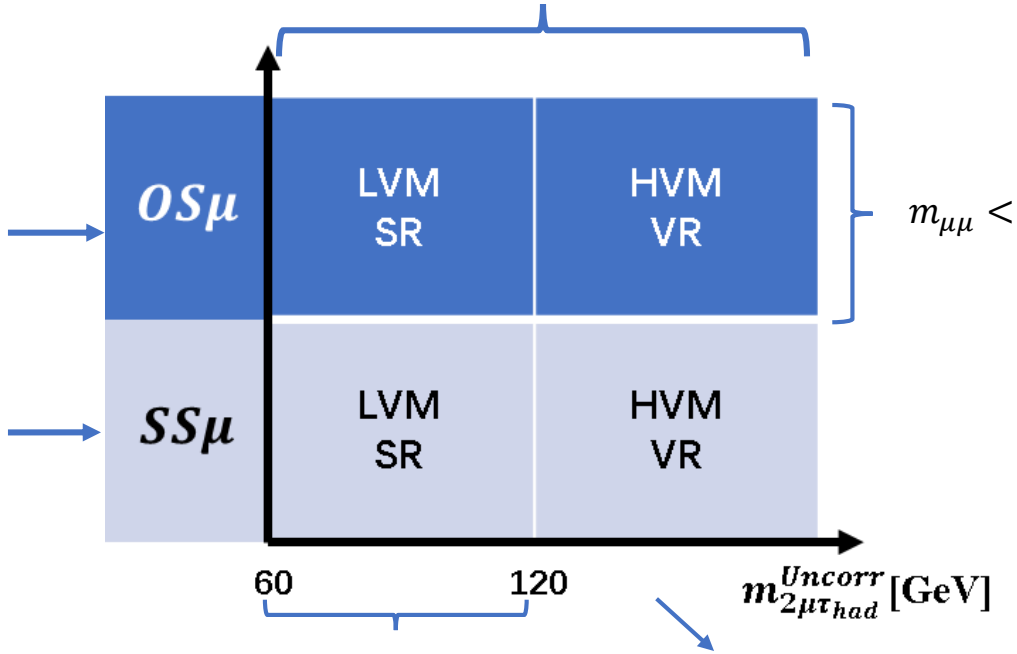

$m_{\mu\mu} < 50$ GeV

Low Visible Mass High Visible Mass

$3\mu, 1\ \mu\tau_{\mathrm{had}}$ pair

Measure the $\mu\tau$ fake factors

$m_{\mu\mu} \in [71,111]$

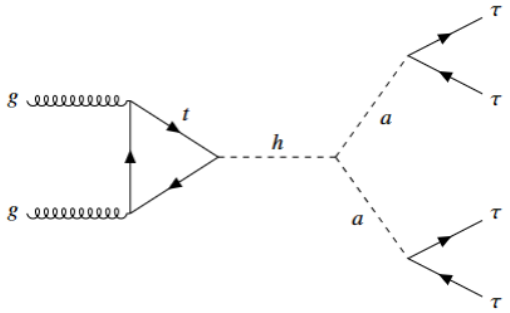

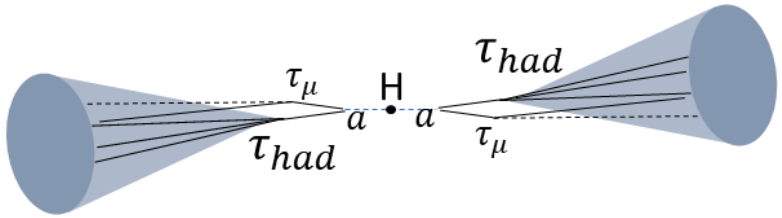

Background Estimation

- Prompt background
  - Estimate using MC: $q\bar{q}/gg \rightarrow ZZ^*, H \rightarrow ZZ^*$ (< 0.1%)
- Non-prompt/fake $\mu\tau_{\mathrm{had}}$ background
  - Data-driven fake factor (FF) method
  - Measure the FF of $\mu\tau_{\mathrm{had}}$ in the $Z(\mu\mu) + \mathrm{jets}(\mu\tau_{\mathrm{had}})$ control region
    - $FF = N^{Z+\mathrm{jets}}_{\text{pass ID}} / N^{Z+\mathrm{jets}}_{\text{fail ID}} = f/(1-f)$
  - FF parameterized as function of $p_{\mathrm{T}}^{\mathrm{Uncorr}}$ and $N_{\mathrm{trk}}^{\mathrm{reco}}$ ($FF(p_{\mathrm{T}}^{\mathrm{Uncorr}}, N_{\mathrm{trk}}^{\mathrm{reco}})$)
  - Apply the FFs to $2\mu\tau_{\mathrm{had}}$ regions by using the events with at least one $\mu\tau_{had}$ candidate failing ID

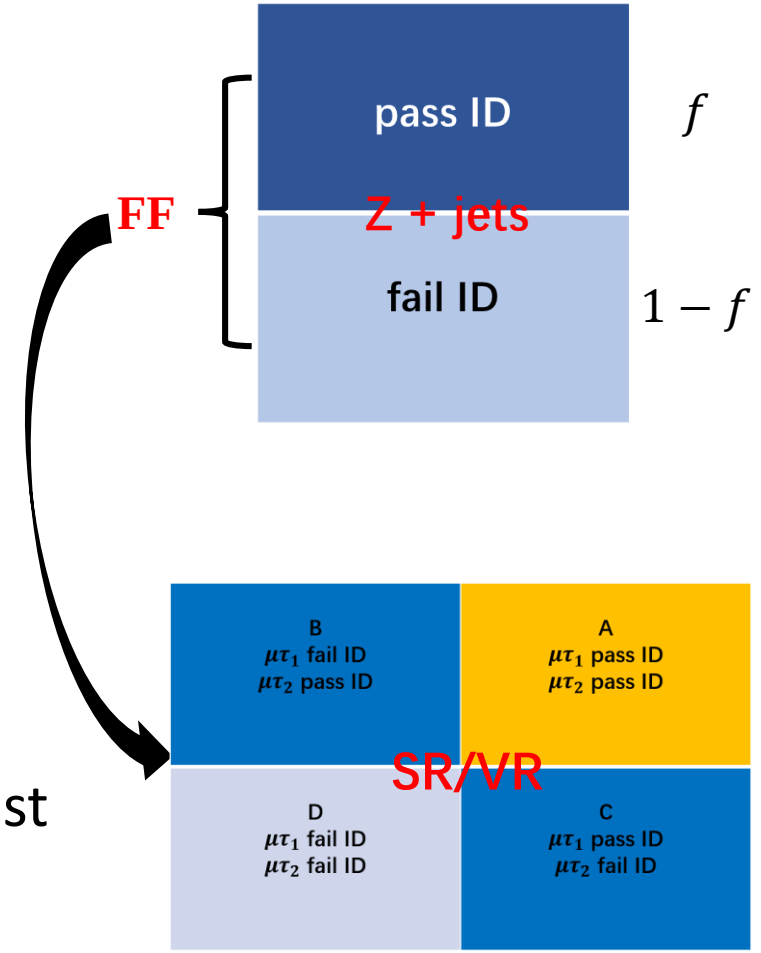

A: $\mu\tau_1$ pass ID, $\mu\tau_2$ pass ID (SR,VR)
B: $\mu\tau_1$ fail ID, $\mu\tau_2$ pass ID
C: $\mu\tau_1$ pass ID, $\mu\tau_2$ fail ID
D: $\mu\tau_1$ fail ID, $\mu\tau_2$ fail ID

Fake factor measurement in Z + jets region

- Fake Factor parameterized as $f(p_T^{Uncorr}, \tau_{prongness})$
- Nominal binning:
  - p_T^{Uncorr}: (20,30), (30,40), (40,500) GeV
  - prongness: 1 prong, 3 prong
- Other parameterization and binning strategies are used to estimate the FF shape uncertainties
  - $|\eta|^{Uncorr}$: barrel (0,1.37), endcap (1.52,2.5)
  - $p_T^{Uncorr}, p_T^{\mu\tau}$

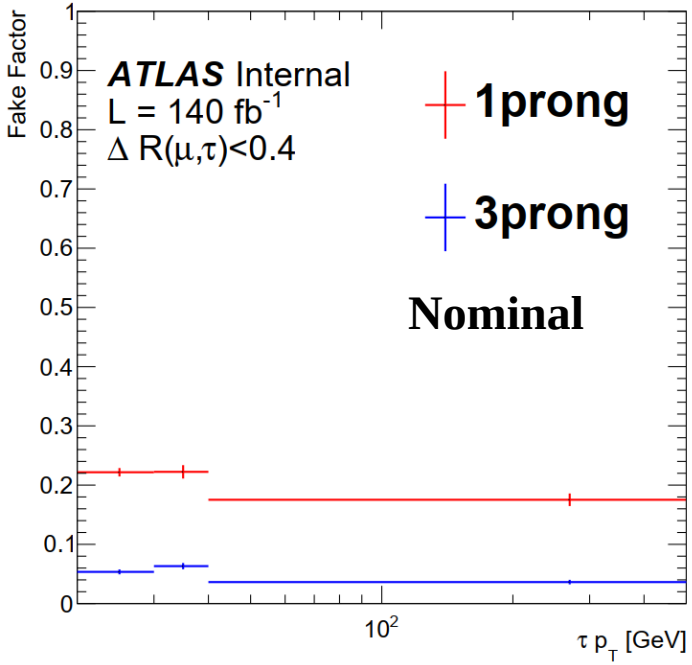

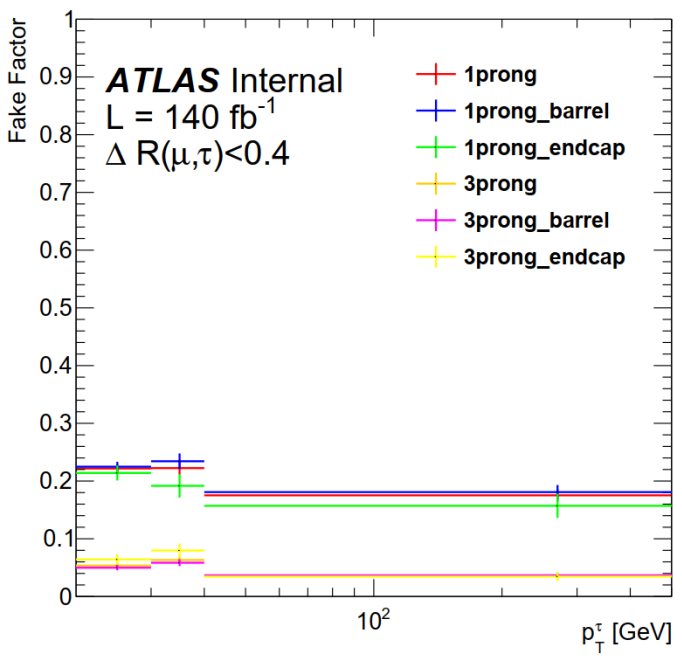

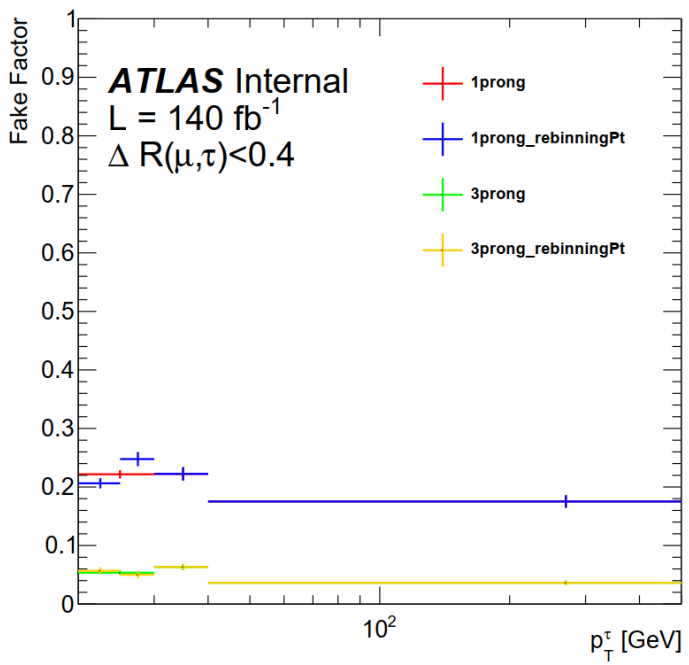

Fake $\mu\tau_{\mathrm{had}}$ background validation

- Apply the fake factor (parametrized as $f(p_{\mathrm{T}}^{\mathrm{Uncorr}}, N_{\mathrm{trk}}^{\mathrm{reco}})$) to the HVM region using the two-object fake estimation equation
- Testing the fake factor method in the HVM validation region
- The fake prediction is agreed with data within the uncertainties
- The relative difference between background prediction and observed data is considered as non-closure uncertainty (8%).

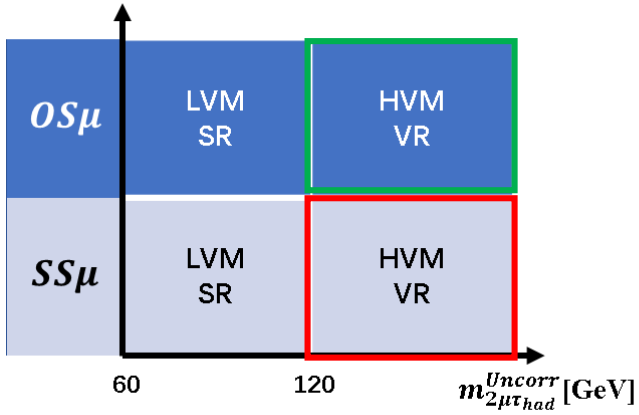

$SS\mu$

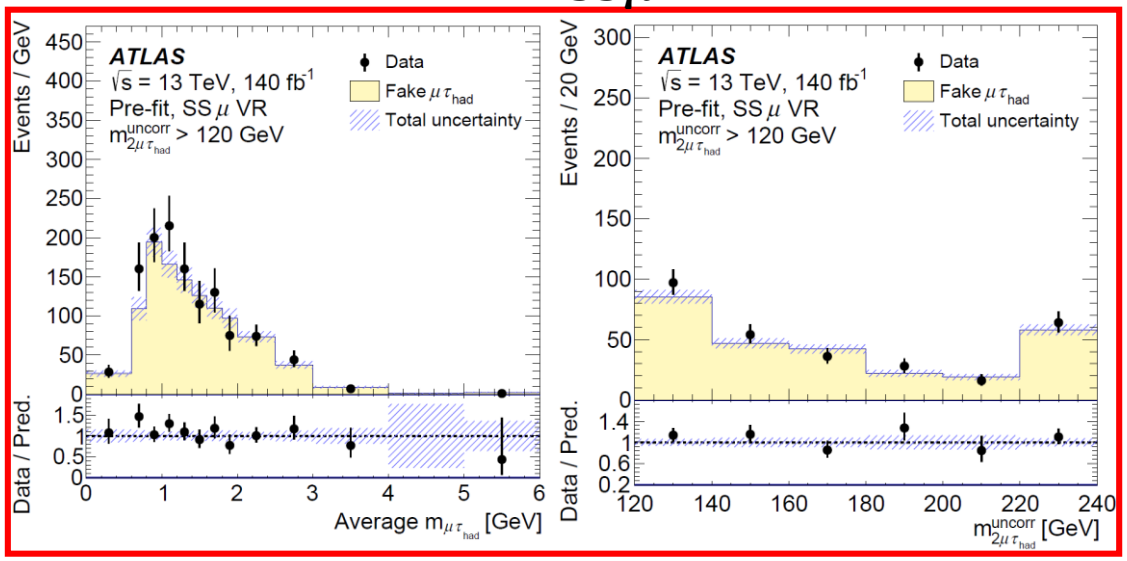

$OS\mu$

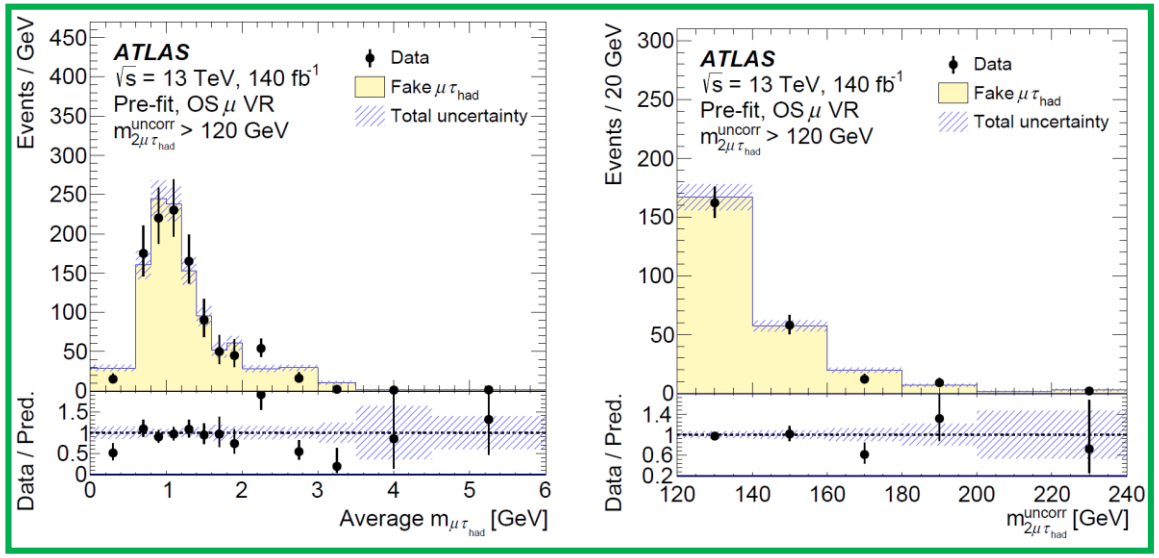

Systematic Uncertainties

Standard systematics

- Experimental uncertainties (from ATLAS performance group)
  - Muon
  - Tau
  - Jet
  - Lumi
  - Pileup
- Theoretical uncertainties
  - QCD (renormalization and factorization) scale uncertainties
    - Cross-section k-factor normalization uncertainty
    - QCD scale shape uncertainty
  - PDF set uncertainties

Custom systematics

- Fake uncertainties
  - Statistic
    - fake_FF_1prong_stat_up
    - fake_FF_1prong_stat_down
    - fake_FF_3prong_stat_up
    - fake_FF_3prong_stat_down

    } Limited number of events in Z+jets CR
  - Parametrization
    - fake_FF_EtaBinning
    - fake_FF_dRBinning
    - fake_FF_MuTauPtBinning
  - Composition
    - fake_FF_Bcomposition
    - fake_FF_2MuTau
    - fake_FF_1jet
    - fake_FF_2jets
    - fake FF dRCut
  - Non-closure
    - fake FF Validation
- Moun Removal Technique Uncertainties
  - Additional Reco+Id efficiency uncertainties

Fake composition uncertainties

- Due to the fake composition difference between Z + jets CR and SR/VR
- Estimated by measuring the FFs in regions with different fake composition
  - With/without Bjets
  - With 1 or 2 jets
  - $2\mu\tau_{had}$ region
  - $\Delta R < 0.4(0.2)$
- Apply the new FFs to SR/VR using the same fake estimation equation

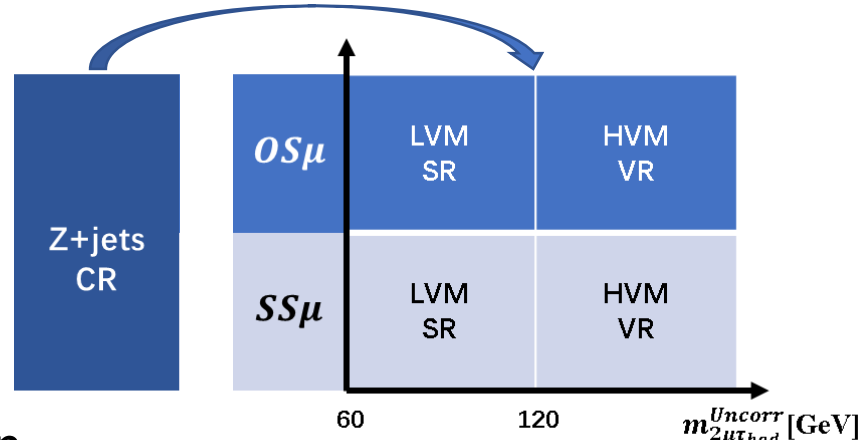

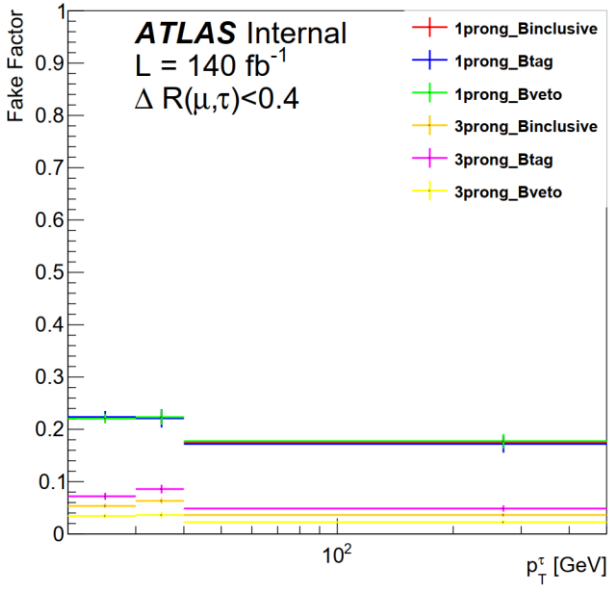

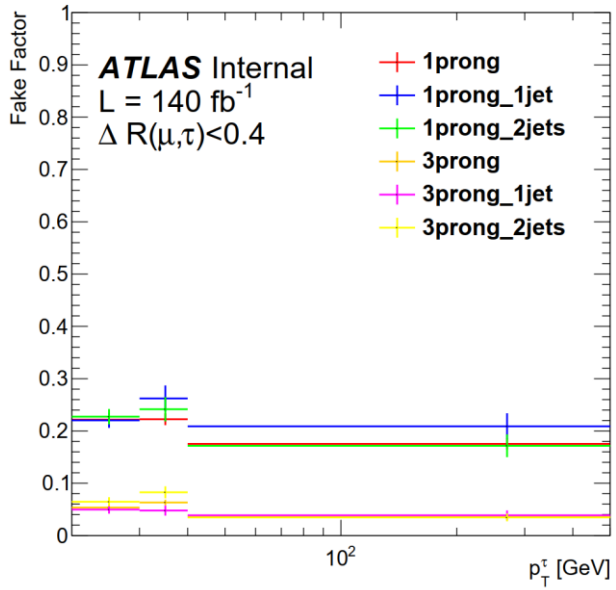

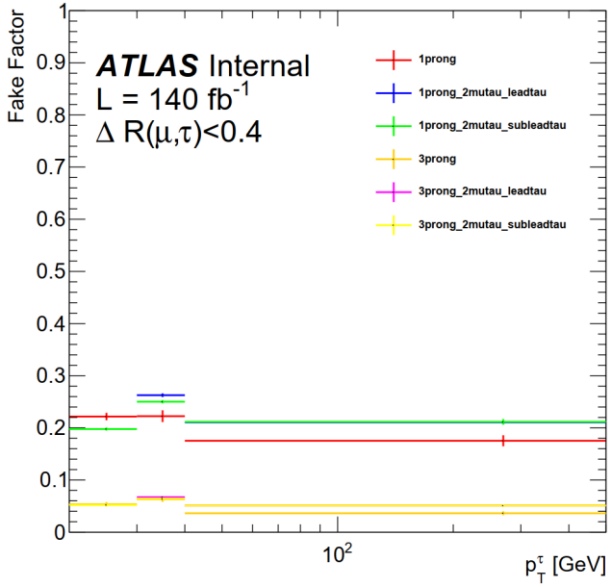

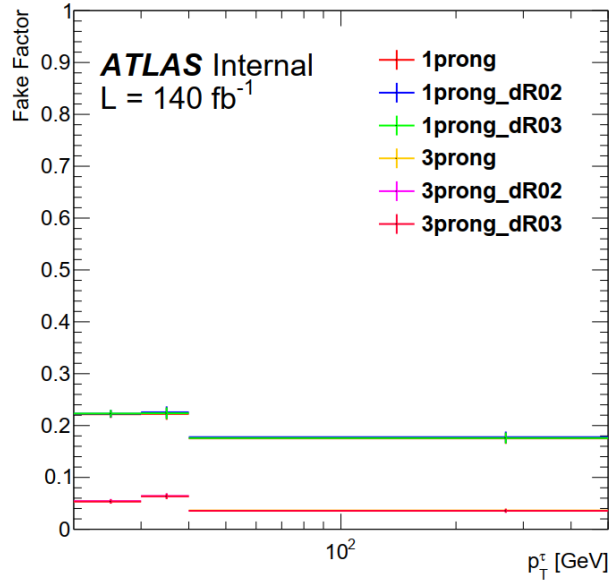

Additional tau efficiency SF uncertainty

- Taking the average difference between merged tau and standard taus
- Medium RNN
  - Object level uncertainty: 1-prong: $\pm 8\%$, 3-prong: $\pm 10\%$
  - Event level uncertainty: take into account two merged taus

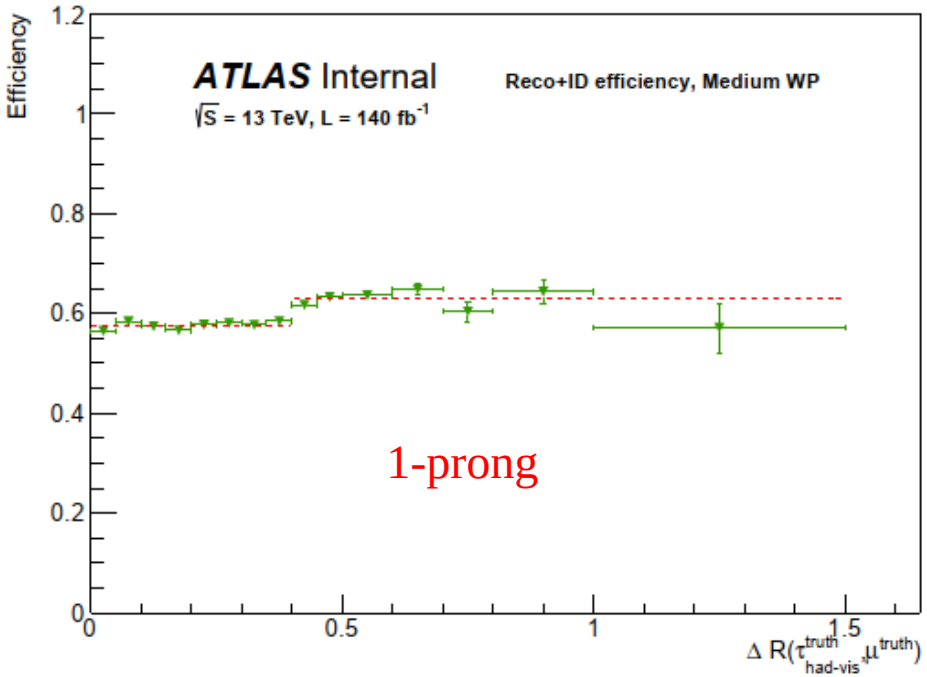

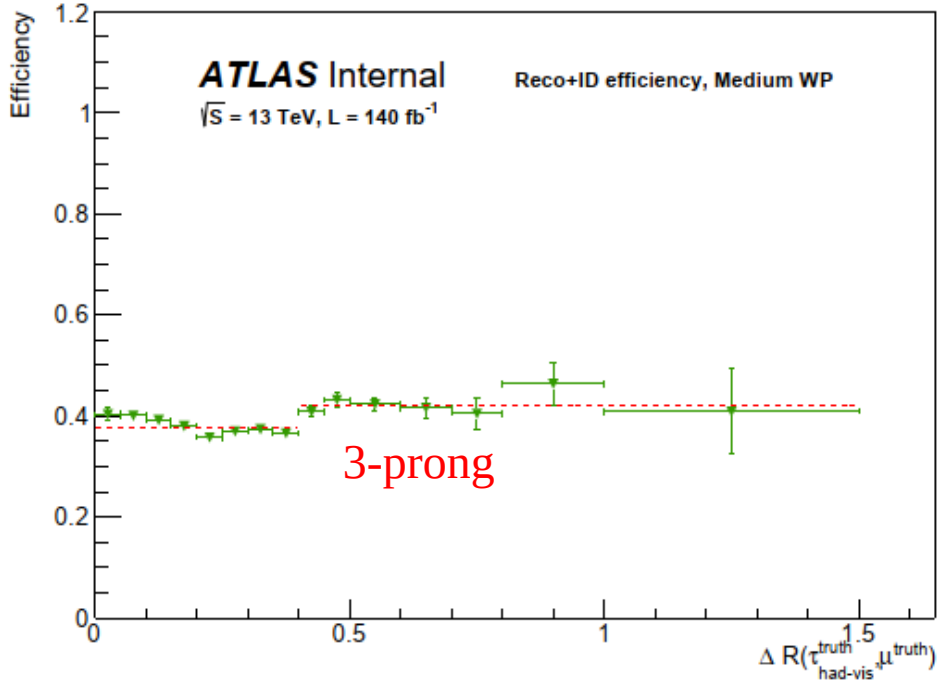

Result

- No significant excess is observed.
  - The background prediction shows very good agreement with the data in both $SS\mu$ and $OS\mu$ channels.

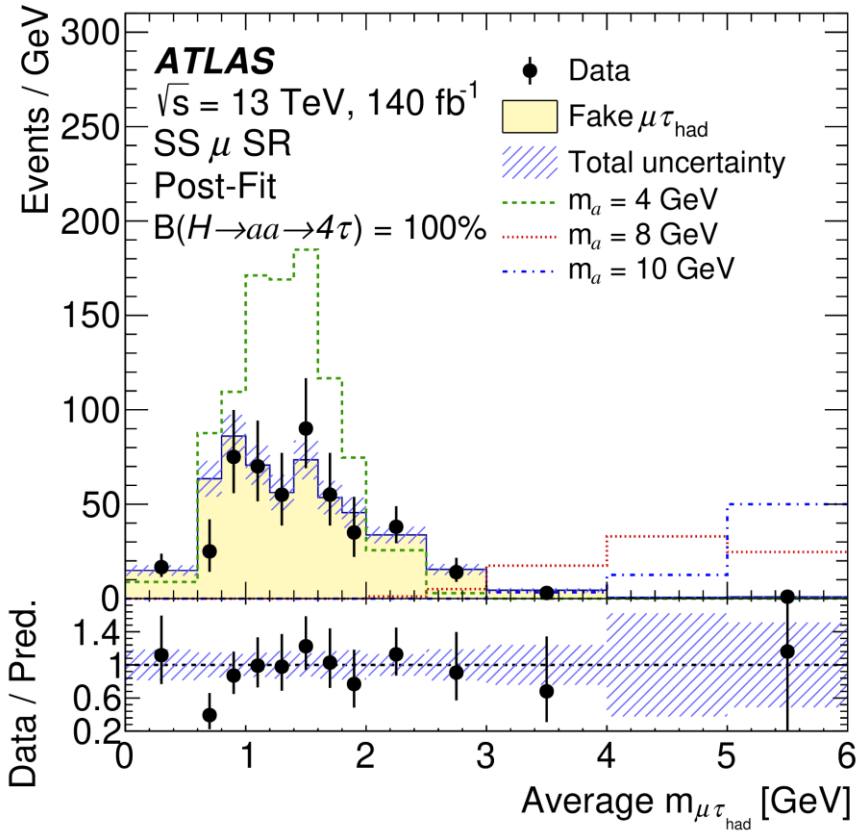

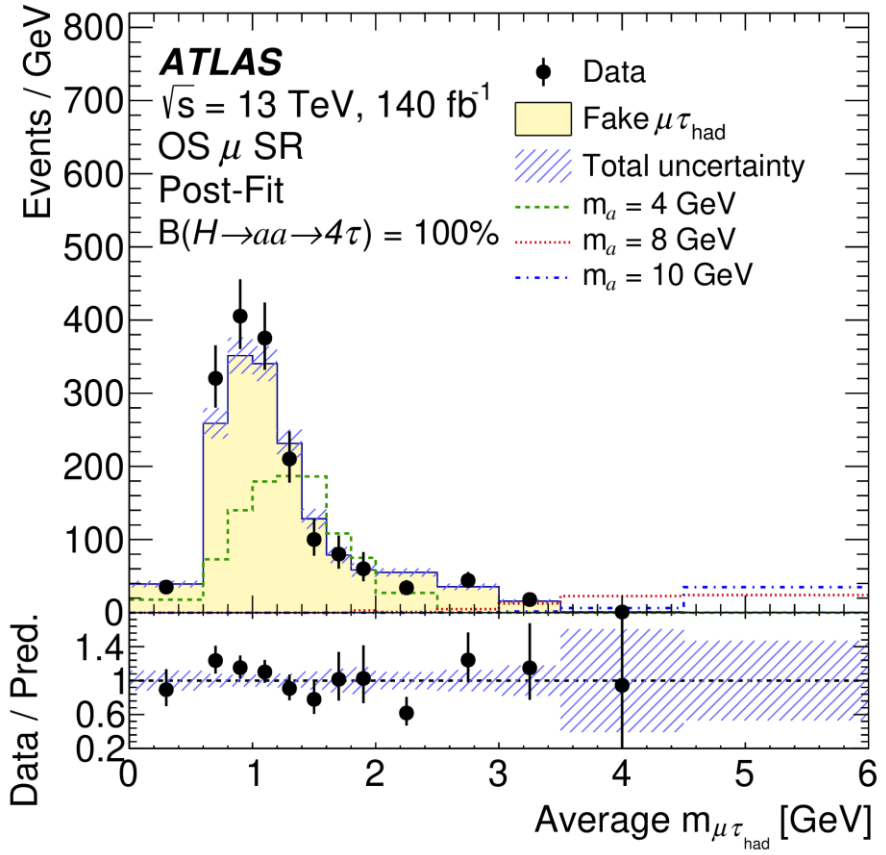

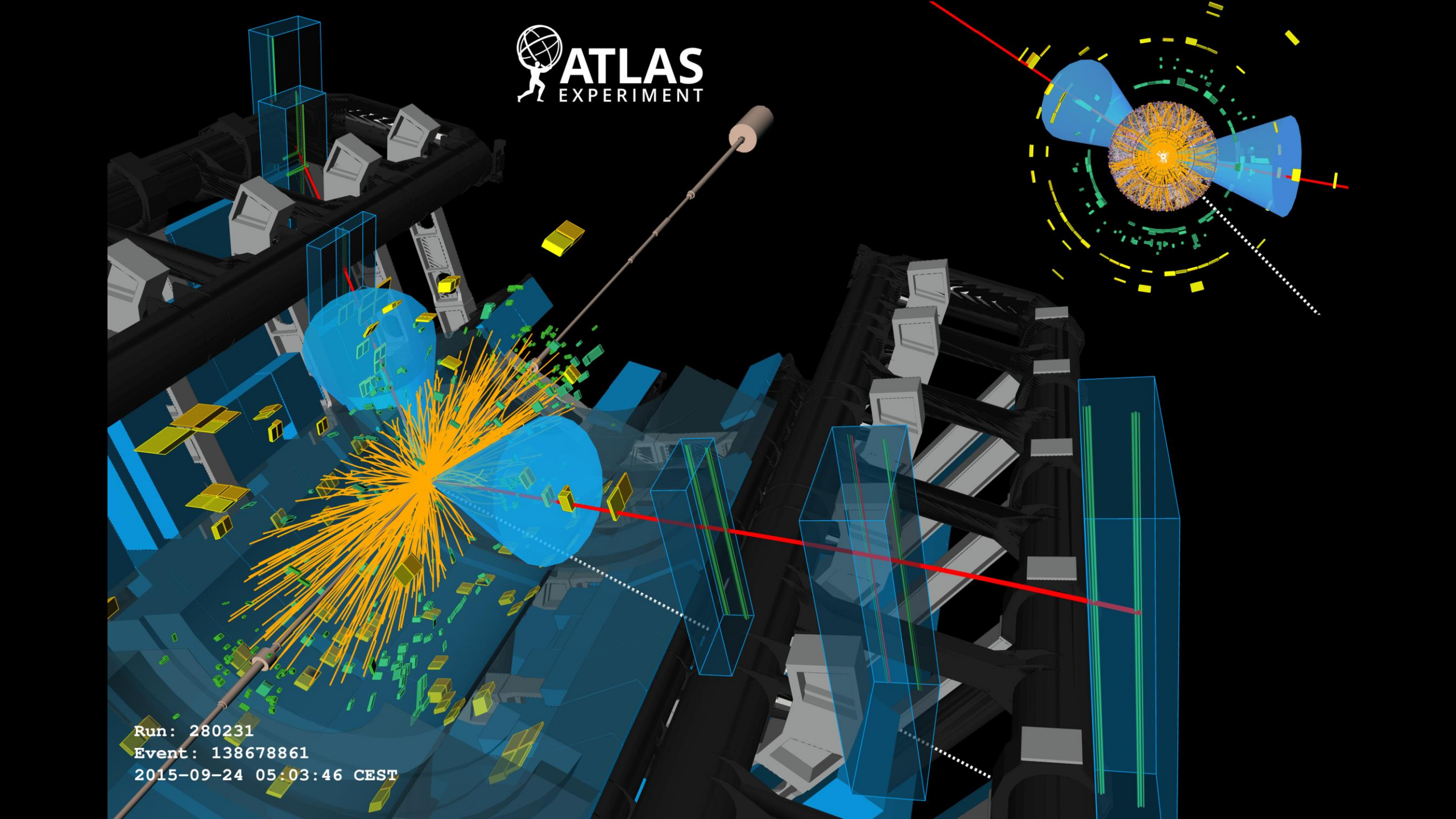
ATLAS
EXPERIMENT
Run: 280231
Event: 138678861
2015-09-24 05:03:46 CEST

Limits

- Upper limits are set at 95% CL on $\left(\frac{\sigma(H)}{\sigma SM(H)}\right) \times (B(H \to aa \to 4\tau)$ using the CL_S and pseudo-experiment method.
- The observed (expected) limit ranges from 0.03 (0.04) to 0.10 (0.13) for $m_a = 10$ GeV and $m_a = 4$ GeV.
  - The $SS\mu$ channel is more sensitive for $m_a < 6$ GeV due to less background.
  - The $SS\mu$ and $OS\mu$ channels show similar sensitivities for $m_a \geq 6$ GeV.
  - The dominant uncertainties arise from the statistical uncertainty of data.
  - Once interpreted in the 2HDM+S model, this final state offers significant improvements over previous ATLAS results.

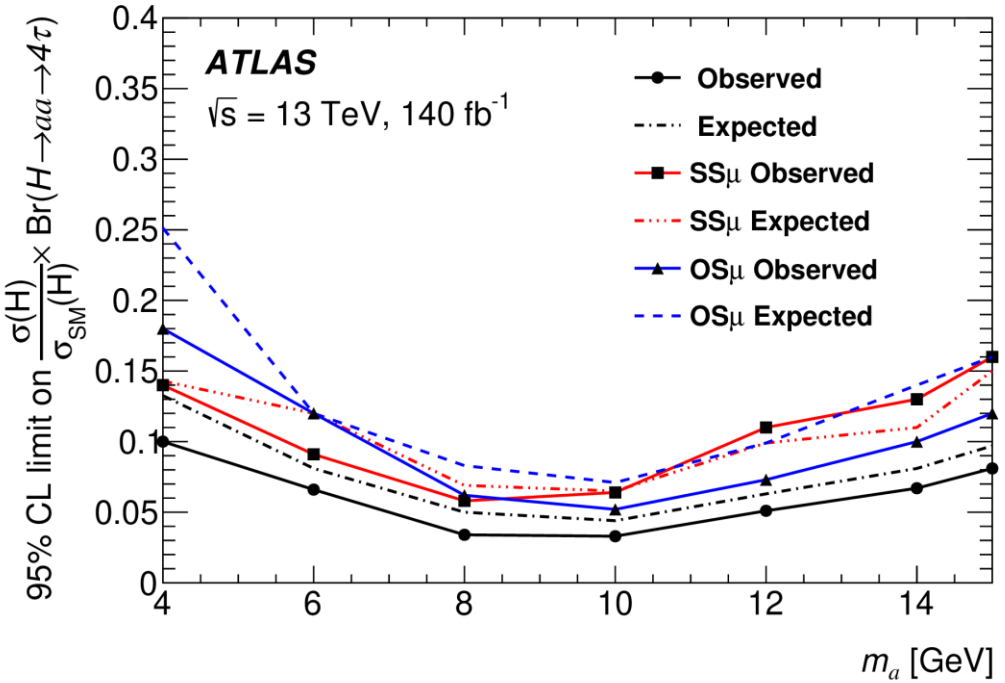

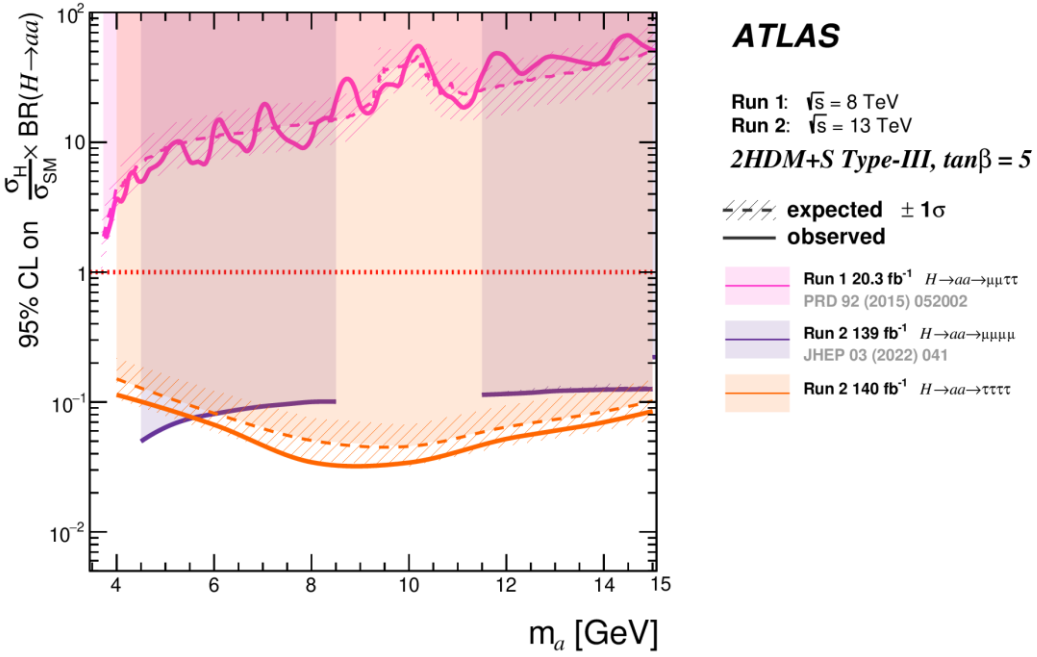

Summary of 4τ analysis

- First (boosted) 4τ search has been published in ATLAS (arXiv:2503.05463).
- A novel muon removal technique is used to reconstruct merged di-τ decays.
  - The efficiencies of merged taus are improved by an order of magnitude.
  - The first time of the muon removal technique is used in an ATLAS analysis.
- No significant excess of data over the SM background expectation is observed.
- Upper limits at 95% CL are set on $(\sigma(H)/\sigma_{SM}(H)) \times B(H \to 2a \to 4\tau)$, ranging from 0.03 at $m_a = 10$ GeV to 0.10 at $m_a = 4$ GeV.
- My contribution on this analysis:
  - I did almost the full analysis and presented all approval talks
  - Specific contributions:
    - Analysis contact, contact editor, the muon removal technique validation, MC sample production, DAOD production, signal region optimization, background estimate, systematic uncertainty estimation, statistical interpretation study, internal note editing, and paper editing

Hardware R&D for the Future

HGTD Module Assembly

Introduction of HGTD

- High Granularity Timing Detector (HGTD)
  - Located between the barrel and end-cap calorimeters
  - Based on Low Gain Avalanche Detectors (LGAD) technology
  - Chinese group makes the major contribution
  - Consists of 8032 modules
  - More than 3000 modules are planned to be assembled at IHEP
- Automation assembly with robotic gantry system is chosen for HGTD module assembly in IHEP
  - High positioning precision
  - High assembly rate

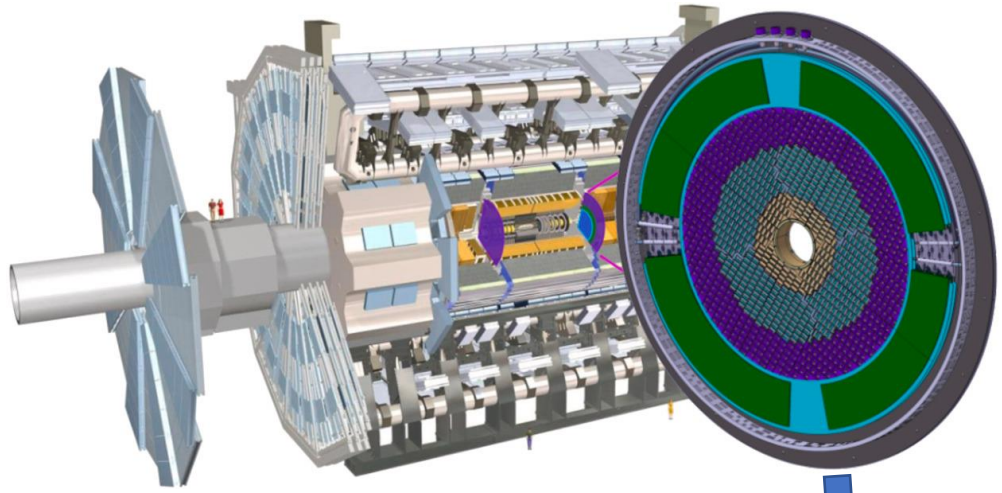

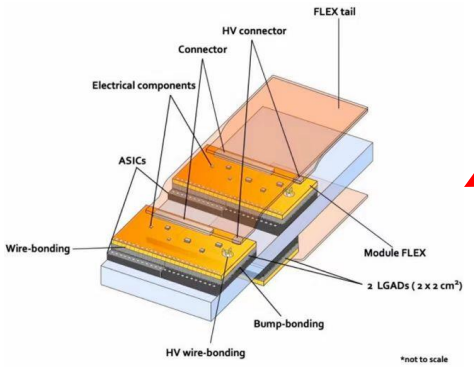

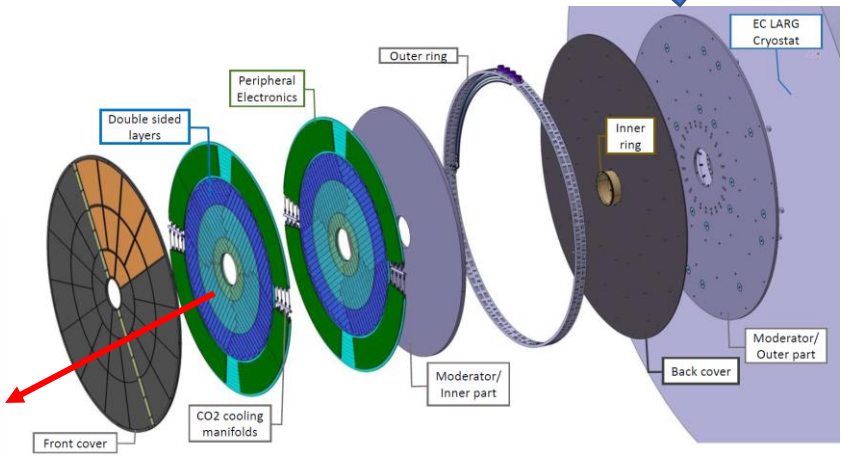

HGTD module assembly with gantry system

Glue the flex on the two bare modules

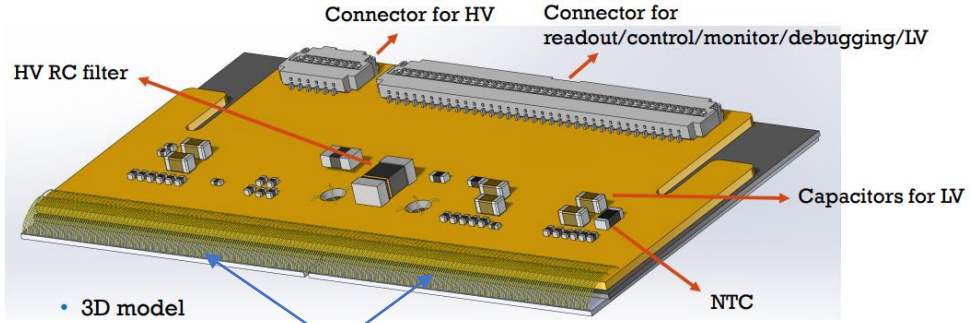

2 bare modules

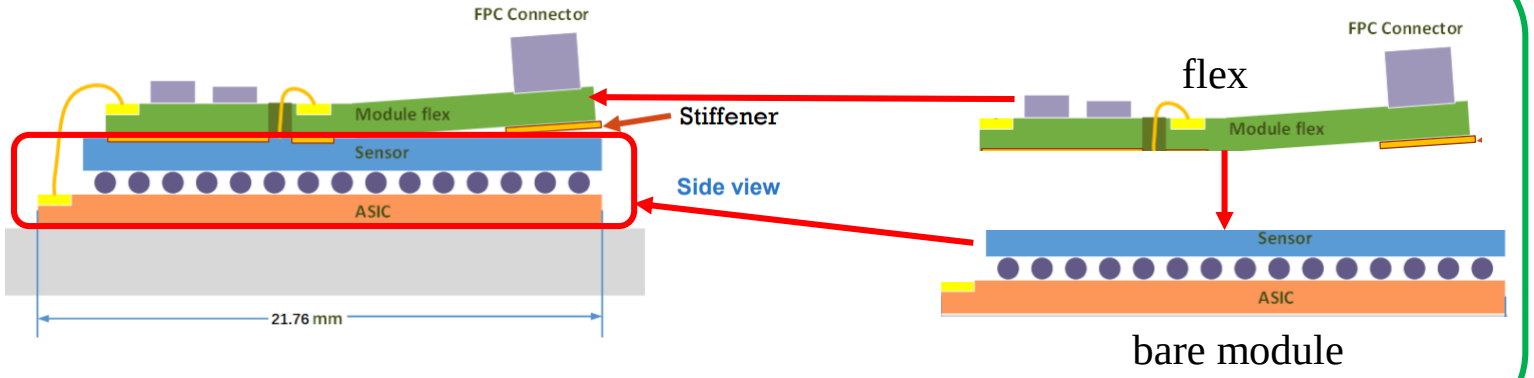

bare module

Glue the module on the support units

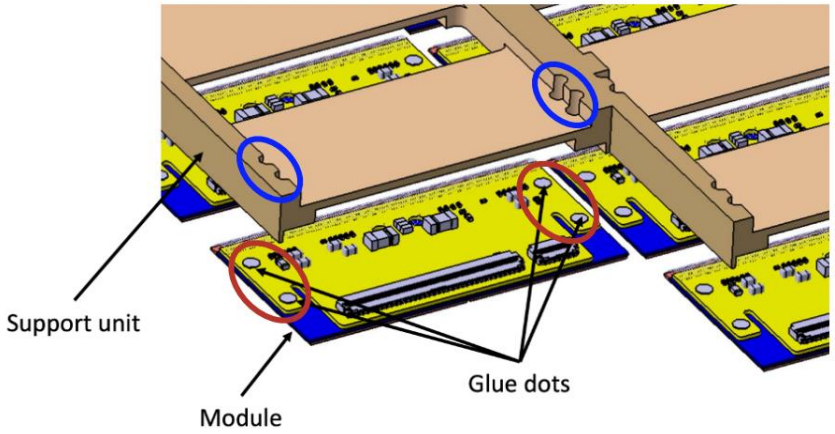

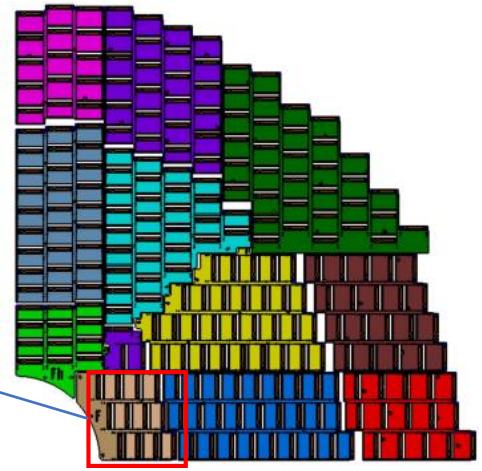

The gantry system at IHEP

- Robotic pick-and-place for systematic module assembly (gantry), consists of:
  - Coretech gantry positioning system with ACS motion controller (500 mm * 500 mm * 150 mm * 340° travel, repositioning resolution ~ 1 μm)
  - Integrated with Keyence vision system, pressure sensor, multi-channel electro-valves (maximum 32), Nordson EFD Glue Dispensing controller, flexible vacuum and air pressure piping system, and custom picking and gluing tools
  - Open source C++ Qt program with GUI to control the whole system

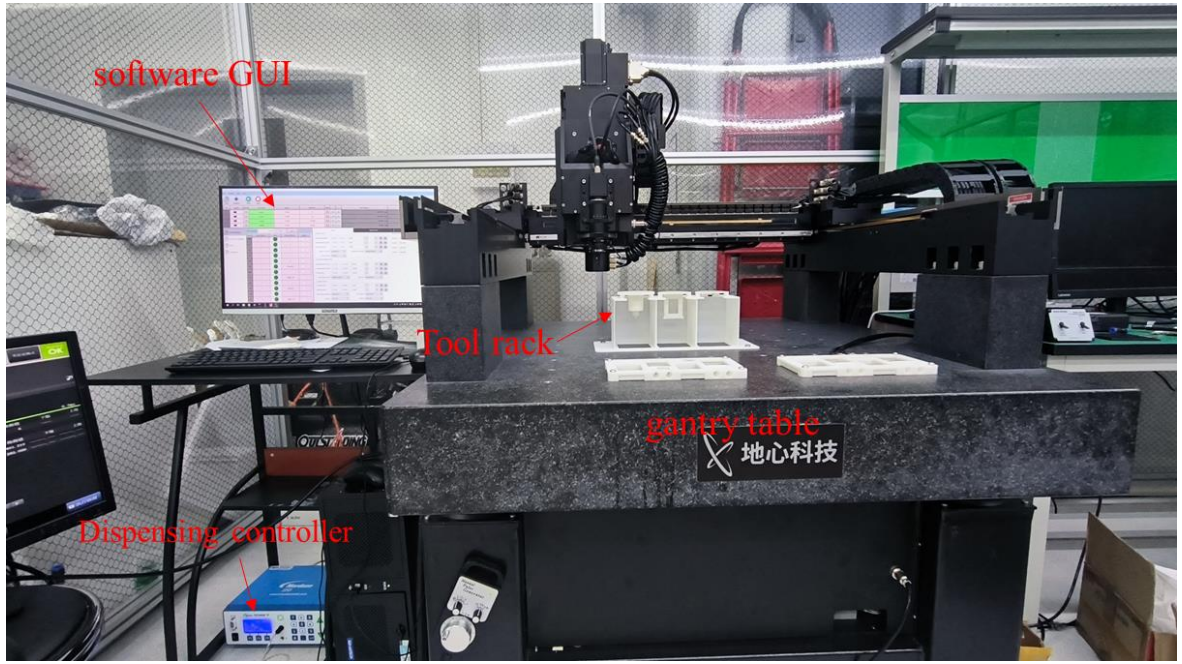

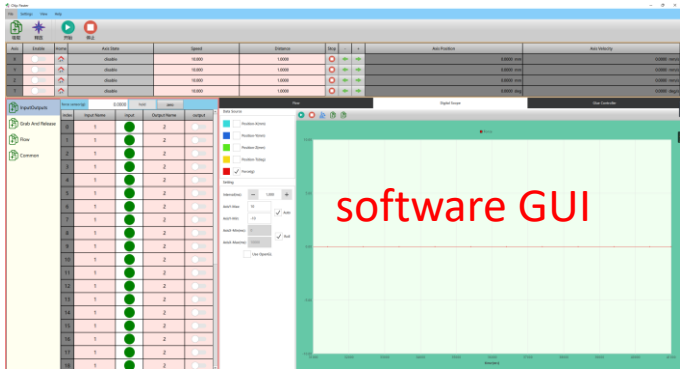

Dispensing controller

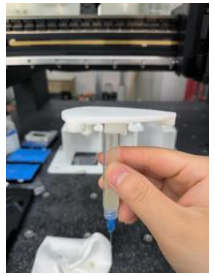

Gluing tool

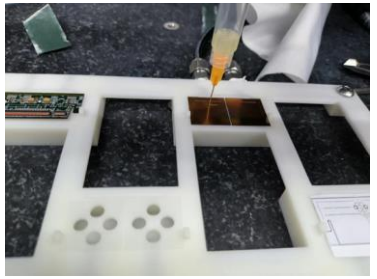

Glue dispensing

Automation dispensing system

- The gantry software controls the dispenser controller through RS232 port and the gantry motion stage
- Allows to dispense different glue patterns automatically

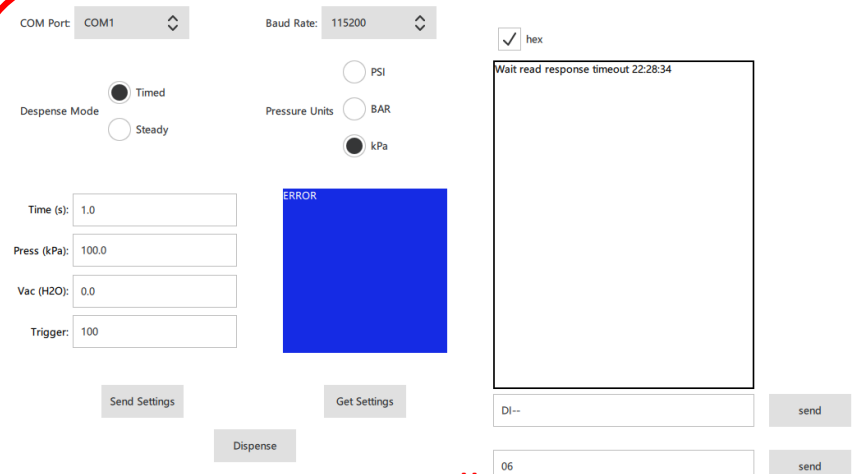

Dispenser controller GUI

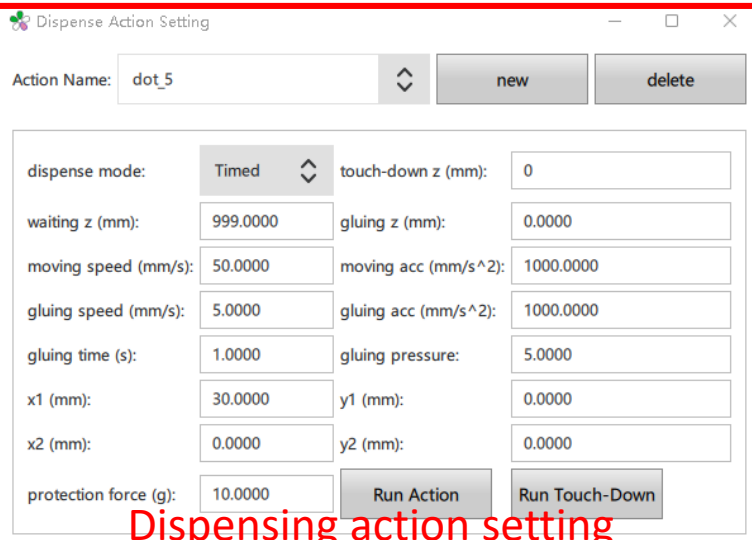

Dispensing action setting

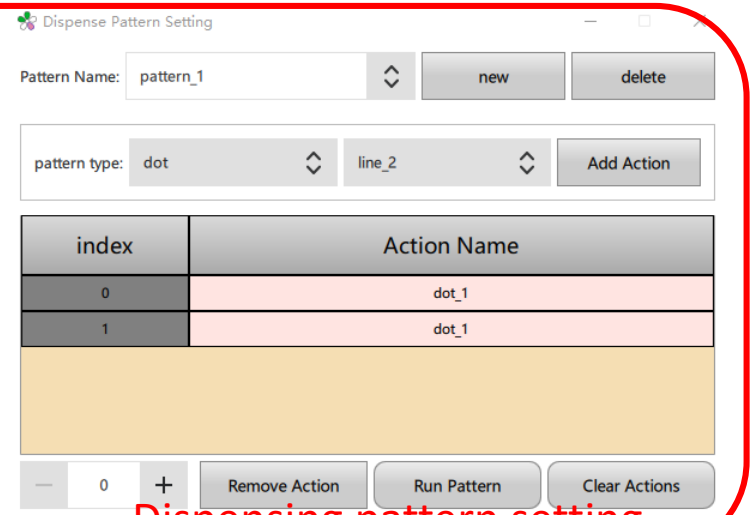

Dispensing pattern setting

RS232 port

Dispenser controller

gluing

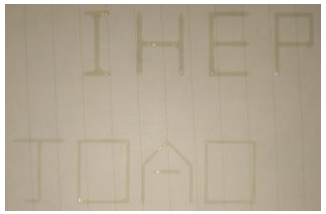

line matrix

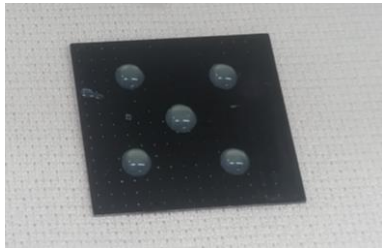

dot matrix

Assembly Procedures

Gantry table

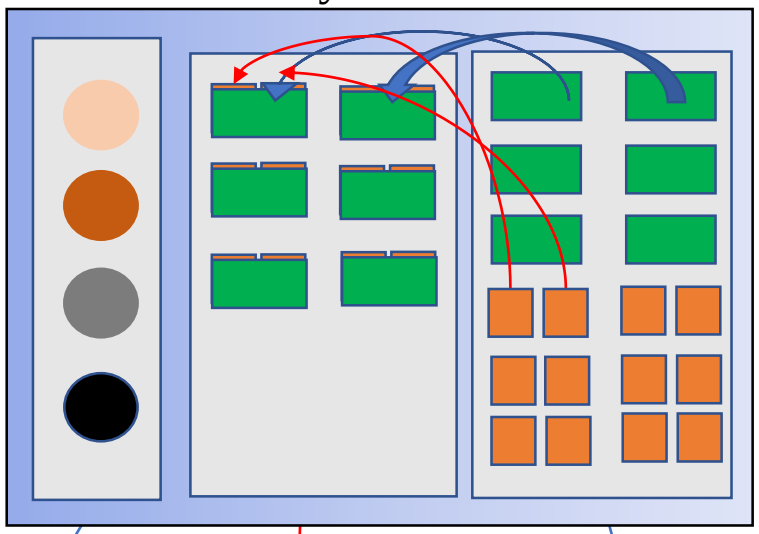

Tool rack | Full module chuck | Flex and bare module chuck

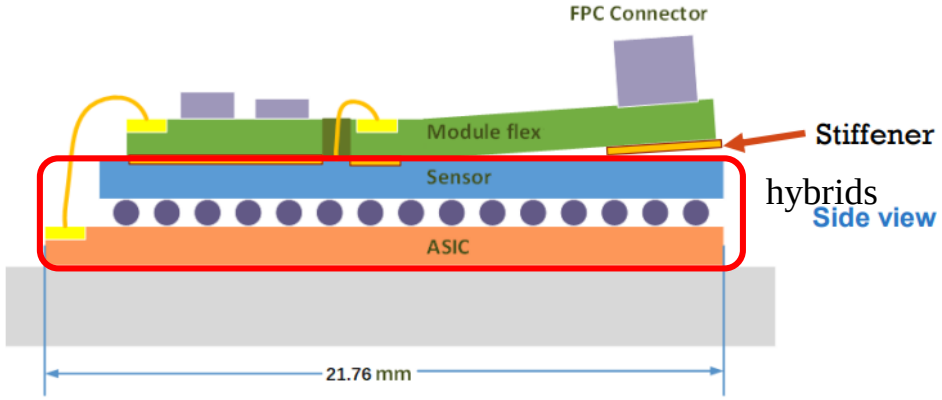

Prepare the tools, flex and hybrids

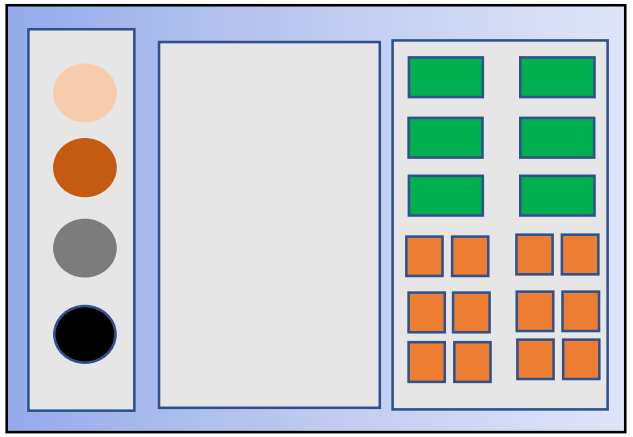

Pick-and-place the hybrids to the vacuum chuck (hybrid alignment)

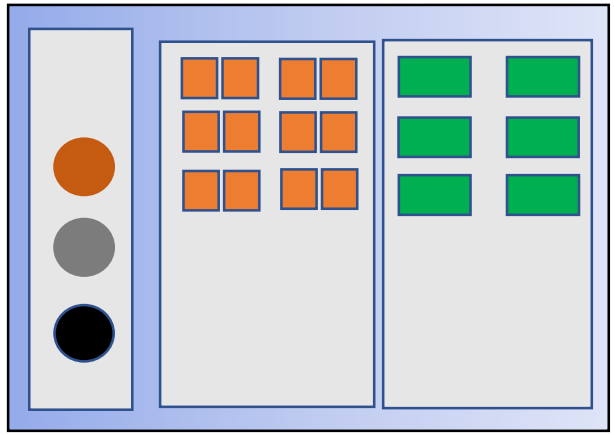

Dispense glue on the hybrids (glue weight, glue pattern)

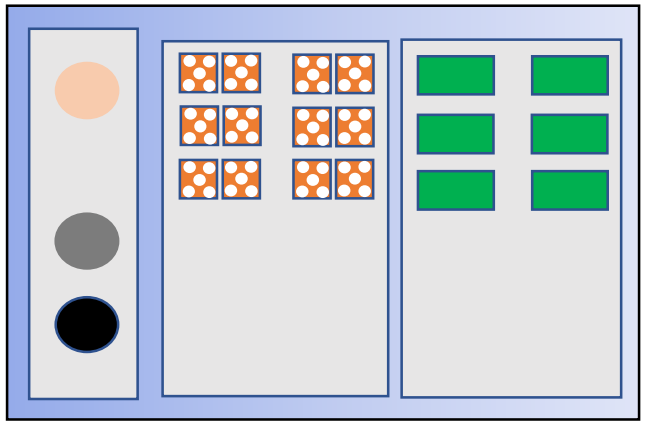

Pick the flex and place it on the hybrids (flex alignment, glue thickness)

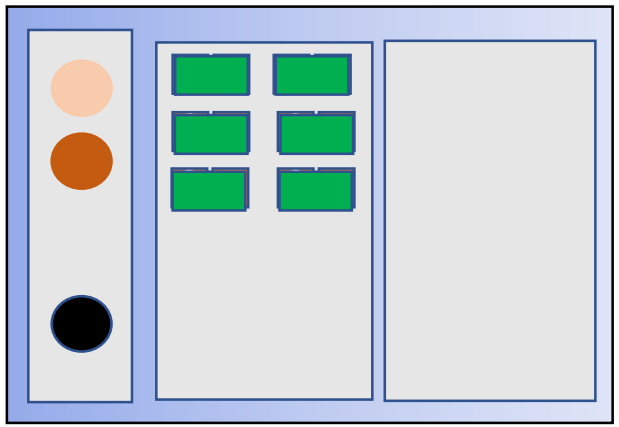

The Planarity results

- Four modules have been assembled using the gantry and custom tool
  - We chose 8 areas to measure the planarity of the modules
  - Over 80% of the thickness differences are within 60 μm, indicating good consistency in module planarity.

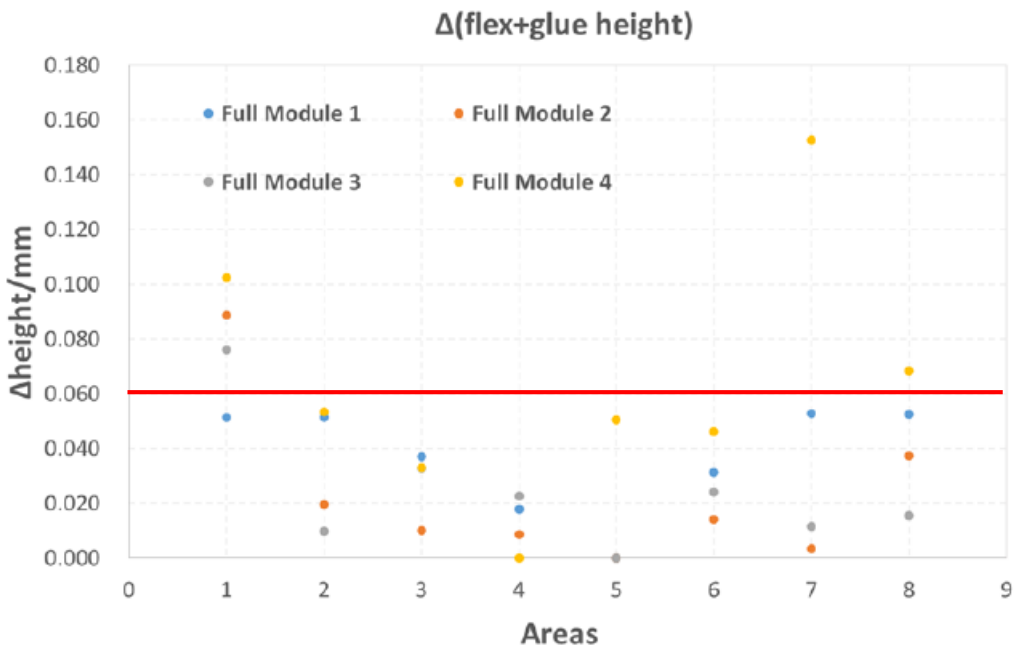

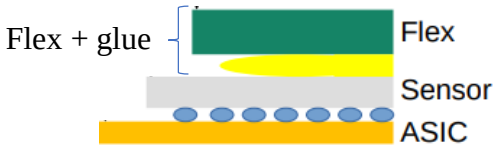

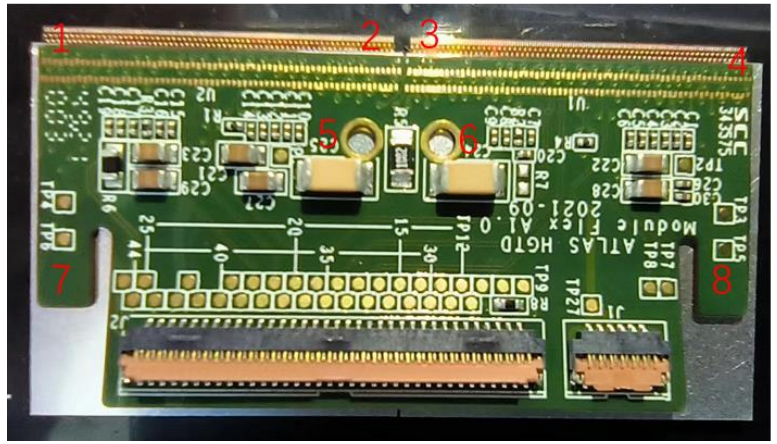

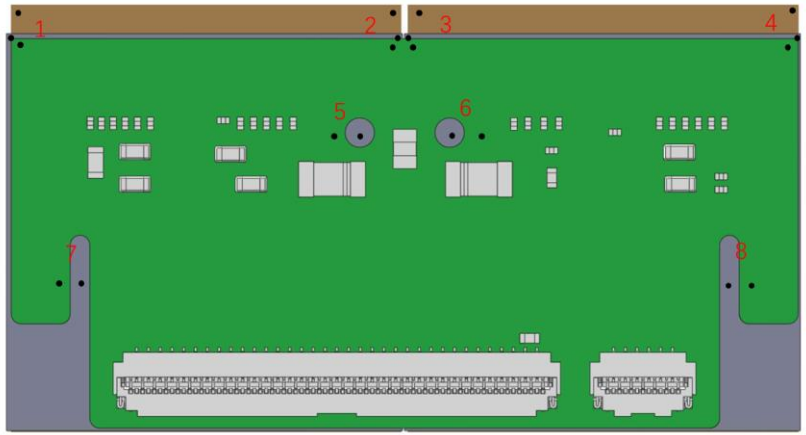

Summary of HGTD module assembly

- A high precision positioning gantry system has been built in IHEP for automatic HGTD module assembly
  - The software and hardware have been developed for the HGTD module assembly
  - Several HGTD modules has been assembled using the gantry system
  - The metrology results are mostly within the specification
  - The first time to use a homemade high-precision gantry system to assembly HEP detector modules
- My contribution:
  - ATLAS author qualification task
  - Help to set up the gantry system
  - Gantry system testing
  - Software development
  - Glue tool design
  - Glue dispenser integration
  - Glue pattern study and weight calibration
  - Module assembly and metrology measurement
  - Internal note editing

Hardware R&D for the Future

CEPC Vertex Detector Optimization

Why Vertex Detector Is Important

- Jet flavor tagging is important for CEPC Higgs study, ~70% of Z, W, and H decay products are jets
- Vertex displacement is a key variable for the jet flavor tagging and hadronic τ identification
- Silicon vertex detector is essential to measure the vertex displacement
  - An impact parameter resolution of about 5 μm is required

Physics process	Measurands	Detector subsystem	Performance requirement
$ZH, Z \to e^+e^-, \mu^+\mu^-$ $H \to \mu^+\mu^-$	$m_H, \sigma(ZH)$ $\mathrm{BR}(H \to \mu^+\mu^-)$	Tracker	$\Delta(1/p_T) =$ $2 \times 10^{-5} \oplus \frac{0.001}{p(\mathrm{GeV})\sin^{3/2}\theta}$
$H \to b\bar{b}/c\bar{c}/gg$	$\mathrm{BR}(H \to b\bar{b}/c\bar{c}/gg)$	Vertex	$\sigma_{r\phi} =$ $5 \oplus \frac{10}{p(\mathrm{GeV})\times\sin^{3/2}\theta}(\mu\mathrm{m})$
$H \to q\bar{q}, WW^*, ZZ^*$	$\mathrm{BR}(H \to q\bar{q}, WW^*, ZZ^*)$	ECAL HCAL	$\sigma_E^{\mathrm{jet}}/E =$ $3 \sim 4\%$ at 100 GeV
$H \to \gamma\gamma$	$\mathrm{BR}(H \to \gamma\gamma)$	ECAL	$\Delta E/E =$ $\frac{0.20}{\sqrt{E(\mathrm{GeV})}} \oplus 0.01$

Table 3.3: Physics processes and key observables used as benchmarks for setting the requirements and the optimization of the CEPC detector.

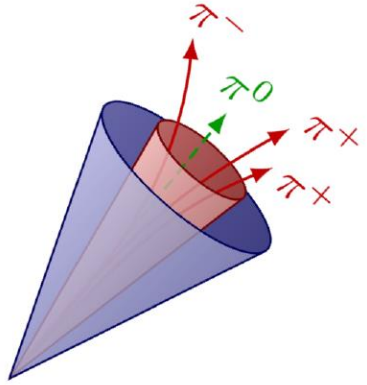

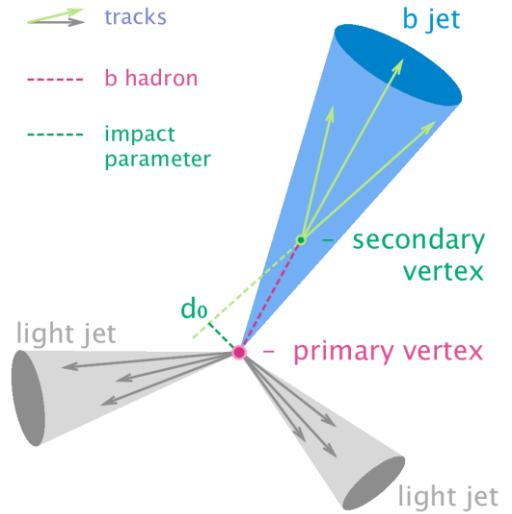

Vertex Detector Design Plan

Vertex optimization in this stage

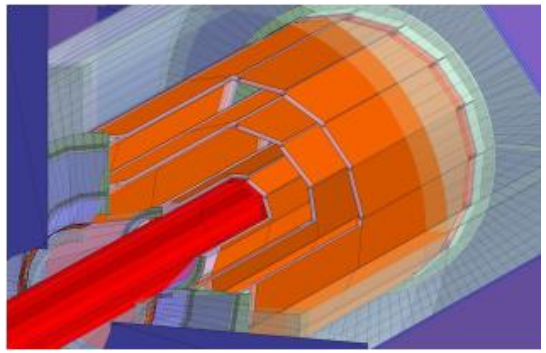

CDR vertex

Ideal concept vertex
3-layers of double-sided pixel sensors

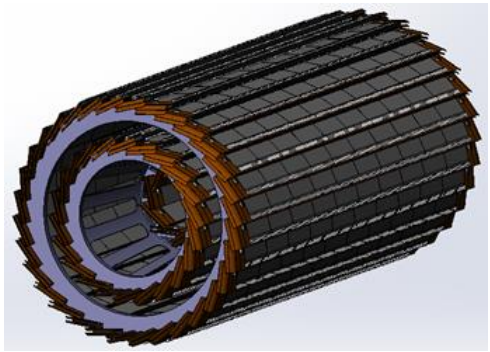

Vertex prototype

Realistic implementation of CDR vertex
Mechanics: ladder design, support structure, ladder arrangement
Electronics: chips, read-out
Cooling: air cooling

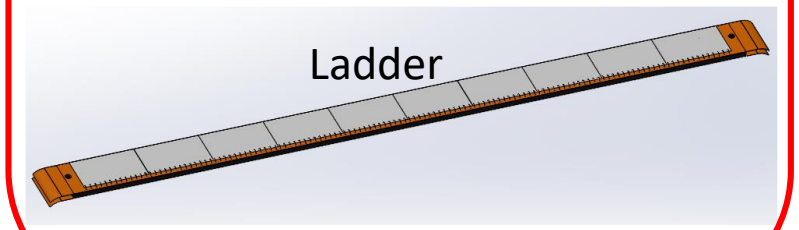

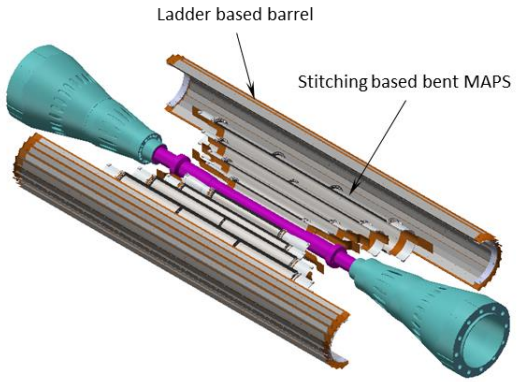

TDR detector

Realistic vertex detector for CEPC:
Based on vertex prototype (mechanics, electronics)
Full-size vertex detector (barrel + endcap)
Considering beam pipe, MDI, cooling

Vertex Detector Optimization Result

- Base on the design of vertex prototype (mechanics, electronics), we try to optimize the full-size vertex detector (d0 resolution as criteria):
  - Barrel optimization
    - The radius of vertex detector
    - The number of layers
    - The radius of second layer
    - Lengthen the innermost layer

Three equidistance double layers is best

  - Disk optimization
    - The number of disks
    - Single-disk or double-disk
    - The putting place of the disk

Improve the d0 resolution in front region

    - 3 double-disks in endcap is the best

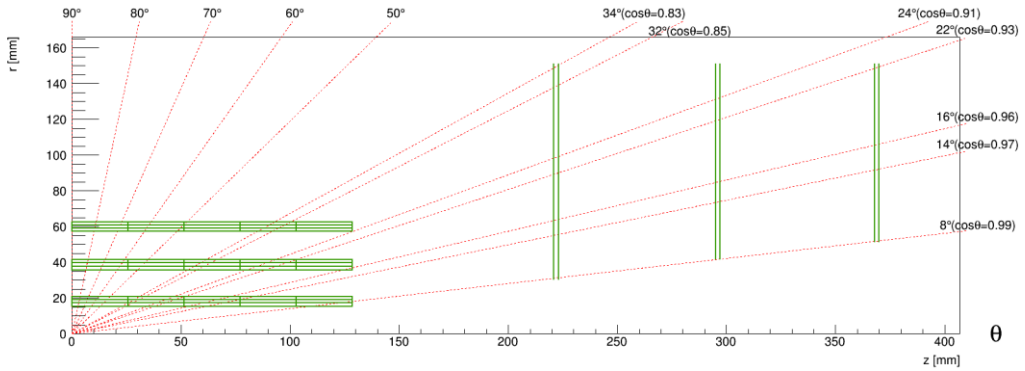

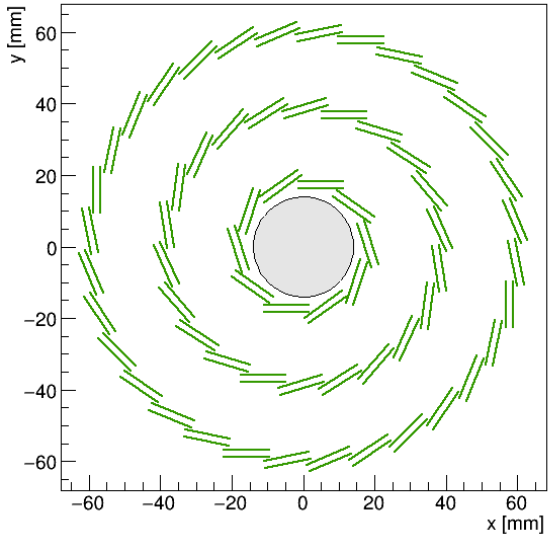

Using tkLayout tool from CMS

Vertex Detector Prototype

- The barrel of the optimal vertex detector was implemented in a prototype
- We built the prototype with full mechanic structure and 6 ladders
- Beam test has been performed for the prototype in DESY
- 5.1 μm impact parameter resolution achieved for the prototype

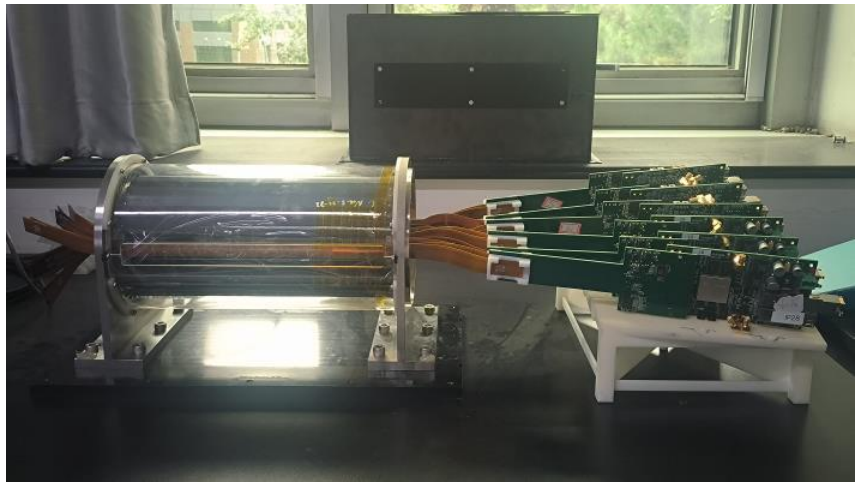

Vertex detector prototype

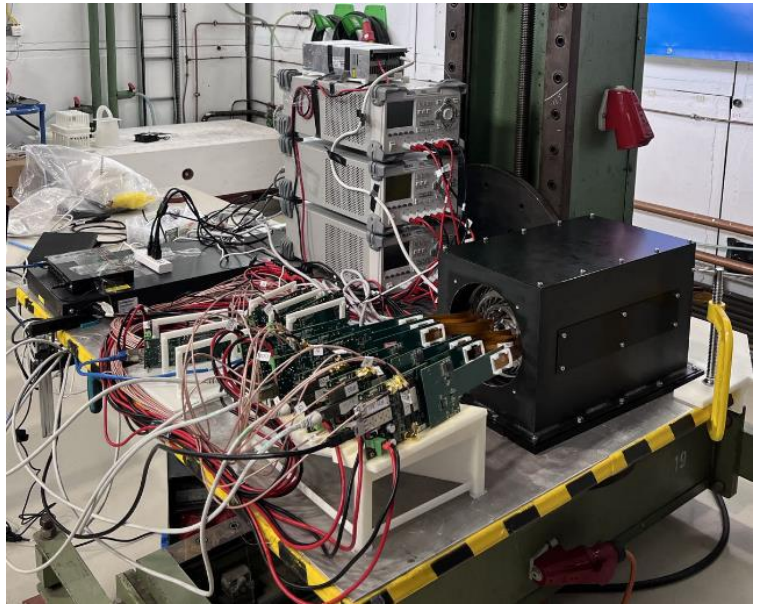

Beam test setup

arXiv:2404.03688

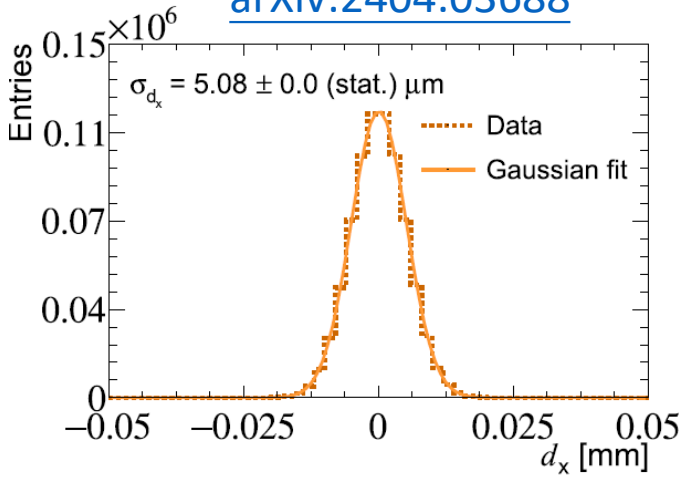

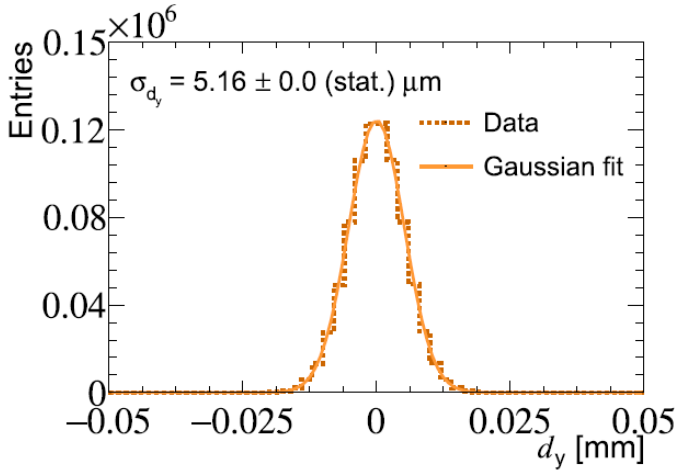

Summary of CEPC Vertex Detector Optimization

- An optimal vertex detector layout has been proposed
  - Based on mature existing electronics and mechanical technologies
  - A prototype has been built for the barrel of the optimal vertex detector layout
  - The beam test results of the prototype fulfill the CDR requirement
  - The first time to construct a high-precision silicon-pixel vertex detector prototype in China
- My contribution:
  - Vertex detector implementation in the fast simulation tool
  - Vertex detector layout optimization
  - Full simulation tool development for the vertex detector
  - Beam test shifts

Prospects for Exotic Higgs Decay

- Now reach a few percent level limits for hadronic final state ($bb/\tau\tau$), 10^{-4}- 10^{-6} level of limits for $\gamma\gamma/\mu\mu$ final state
- Not find the new physics
- Great improvement in the future for the Exotic Higgs Decay search
  - Run 3 + HL-LHC: ~ 20 times data
  - CEPC (FCC-ee): very clean signals → improve 2-3 order of magnitude
  - New machine learning techniques (AI): signal reconstruction, background rejection

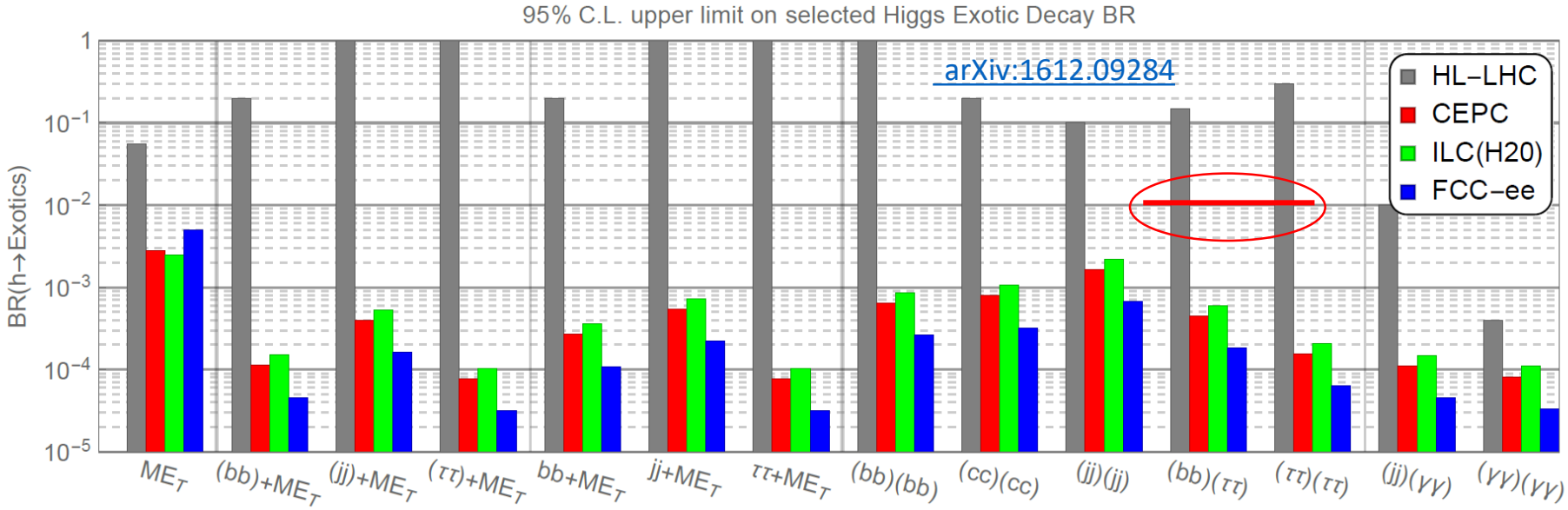

HL-LHC: 1% level

Publications and Awards

- Publications:
  - ”Search for Higgs boson exotic decays into Lorentz-boosted light bosons in the four-τ final state at $\sqrt{s}$ = 13 TeV with the ATLAS detector.” arXiv preprint arXiv:2503.05463 (2025), submitted to Phys. Lett. B
  - ”Mechanical design of an ultra-light vertex detector prototype for CEPC.” Radiation Detection Technology and Methods 6, no. 2 (2022): 159-169
  - ”Manipulating Radiation-Sensitive Z-DNA Conformation for Enhanced Radiotherapy.” Advanced Materials 36, no. 29 (2024): 2313991
  - ”Beam test of a 180 nm CMOS Pixel Sensor for the CEPC vertex detector.” Nuclear Instruments and Methods in Physics Research Section A: Accelerators, Spectrometers, Detectors and Associated Equipment 1059 (2024): 168945
  - ”Beam test of a baseline vertex detector prototype for CEPC.” IEEE Transactions on Nuclear Science (2024)
- Awards:
  - 2019.09 Second-Class Academic Scholarship, University of Chinese Academy of Science
  - 2020.09 Second-Class Academic Scholarship, University of Chinese Academy of Science
  - 2021.07 Outstanding Student Leader, University of Chinese Academy of Sciences

Answers to the Comments

- **盲审老师1**:
- 修改建议：摘要部分写的不错，但是有些太长，可以精简一下。在chapter10，建议更突出介绍哪些是自己的工作。
- **回答：**
- **1. 摘要的长度是因为国科大对于留学生外语论文有不少于5000字中文摘要的要求。**
- **2. 在chapter 10开头简介部分加上了本人的贡献说明。具体句子为 “My contributions include helping set up the gantry system, testing the gantry system, designing the glue tool, integrating the glue dispenser, assembling the first batch of modules, and conducting metrology measurements.”**

Answers to the Comments

- **盲审老师2:**
- ATLAS实验数据分析课题通常不止一人参与，建议作者在第一章“论文组织结构”后面明确是否一人完成，如果不是，需说明作者的主要贡献。
- **回答：本ATLAS分析基本由本人完成，论文中所有与物理相关内容，图片均为本人完成。其中的缪子移除技术的ATLAS代码由高能所单连友教授完成，缪子移除技术的performance研究由我完成。已经在第一章“论文组织结构”后面明确ATLAS分析主要由本人完成，并且列举了具体的贡献。**

Answers to the Comments

- **梁志均老师**:
- 论文在章节设置与研究内容之间的对应关系方面存在一些明显不足。首先，论文涵盖的多个研究方向——ATLAS实验上的四陶子物理分析、HGTD模块自动组装研发和CEPC顶点探测器布局优化——在章节布局上未能形成清晰的一一对应关系，各个部分的研究内容独立性较强，未有效呈现各研究主题之间的逻辑关联与整体科研目标。其次，各研究部分之间缺乏必要的过渡与衔接，转折较为生硬，未能以有效的章节引导或过渡段落说明多方向研究之间的内在联系与逻辑发展脉络，使读者难以快速理解不同章节内容在论文整体框架中的定位。建议作者在未来发表或修改过程中，加强对研究内容与章节对应关系的明确界定，改善各部分之间的过渡性描述，深入阐述研究背景与选题依据，以增强论文的整体结构与逻辑严密性。
- **回答：已经在两个硬件章节开头加了过渡段落用来转折。**

Answers to the Comments

- **梁志均老师：**
- 论文在四陶子末态（H → aa → 4τ）分析的引入部分显得略为简略，存在背景铺垫不足的问题。尽管绪论中提及了标准模型的局限性以及希格斯玻色子作为探索新物理的窗口，但对于为何聚焦于“四陶子”这一特定衰变通道，其理论动机、模型预测、已有实验限制与本研究的切入点，并未做出系统性和层次分明的阐述。相关背景仅在绪论中以较简略的方式介绍了轻标量粒子a的存在假设及其衰变特点，但缺乏对该末态在不同理论框架（如2HDM+S、NMSSM等）中的物理意义、参数空间中可能带来的灵敏度增益，以及为何采用μτhad对组合而非其他末态的深入讨论。此外，对ATLAS和CMS已有H→aa分析工作的对比也主要出现在正文后半部分，未在引言中作为研究动机的一部分系统整理和分析。缺乏这些内容的引导，容易使读者在进入复杂分析前缺乏对问题重要性与技术路径选择的整体认识，从而削弱分析工作的说服力和逻辑完整性。因此建议在论文后续修改或发表过程中，补充一段完整、逻辑清晰的研究背景说明，系统介绍四陶子通道的理论动机、实验挑战、已有工作及本研究的创新点和必要性，以增强整篇论文的引导性与逻辑闭环。
- **回答：在第一章节结尾加了一小节用来介绍四陶子通道的动机以及挑战和创新点。**

Answers to the Comments

- **梁志均老师：**
- 论文在结构安排上存在一定断裂，尤其体现在第四章对“boosted tau”重建的讨论与前文物理引言之间缺乏有效过渡与铺垫。尽管在绪论中提到，但未能系统说明这一现象所带来的具体识别困难及对分析策略的影响，导致第四章关于缪子去除技术的切入显得较为突然。建议在章节之间设置过渡段，或在第一章中加强对boosted tau识别问题的动机介绍，以增强各章节之间的逻辑连贯性与整体结构的完整性。
- **回答：已经在第一章节结尾处增加一小节对于boosted tau识别问题动机介绍。**

Answers to the Comments

- **梁志均老师：**
- 论文摘要虽较全面地概述了研究内容和技术方法，但在突出创新性和作者个人贡献方面表达不够明确。摘要中虽提及“缪子去除技术”的提出和应用，但未突出其为作者首次提出并在ATLAS实验中实现的原创成果，缺乏对其创新价值的明确强调；同时，摘要以客观叙述为主，未点明作者在多个研究环节中的主导地位，难以充分体现博士论文应有的独立科研贡献。此外，摘要结尾缺少对主要成果和创新点的集中归纳，建议在后续修改中增强对技术首创性与研究主导性的表述，使摘要更突出亮点，更符合博士学位论文摘要的标准要求。
- **回答：摘要第一段提及了这个是缪子去除技术首次在ATLAS上应用。同时，在四陶子分析中添加了本人做出主要贡献的描述。我也在摘要结尾添加了一小段总结了论文中所有工作的创新点。**

Answers to the Comments

- **张华桥老师：**
- 论文中大多数的图片没有ATLAS label，需要根据是否公开，标记为ATLAS/ATLAS preliminary/ATLAS internal/ATLAS thesis等
- **回答：已经经过ATLAS approval流程的图片都有ATLAS label，没有经过approval流程的按照ATLAS合作组的要求，如果博士论文要发表的话是不能直接用ATLAS label，可以不加任何label。因此本论文里面对于没有经过ATLAS approval流程的图片都是不加任何ATLAS label的。**

Answers to the Comments

- **张雷老师：**
- 1.结构上而言，目前论文把HGTD模块组装和CEPC顶点探测器单独成章，给人感觉论文结构凌乱和莫名的感觉。论文的物理分析部分足够支持一篇博士论文。目前的这两部分探测器工作无论研究深度还是内容相关性，都不值得单独成章，建议要么放在附录中，仅做博士期间工作的记录，或者放在ATLAS探测器介绍部分。
- **回答：我在前面的摘要和绪论开头部分已经阐述了，主要物理分析是针对当前LHC上面已有的ATLAS Run2 数据，但是对于未来奇异希格斯玻色子衰变的搜寻，有两个项目值得关注，那就是HL-LHC和CEPC项目，目前这两个项目处于硬件生产或者研发阶段，我在这两个项目中所作的硬件方面的工作就是为未来希格斯玻色子奇异衰变搜寻做贡献。因此整篇论文的主要内容就是现有ATLAS Run2数据的直接物理分析，加上未来能进行希格斯玻色子奇异衰变搜寻的HL-LHC和CEPC项目的硬件研发工作，这样其实所有工作都是在一个大的希格斯玻色子奇异衰变搜寻的主题下。因此我觉得可以把硬件相关工作内容写入正文，这样也可以体现一个高能物理博士生在博士期间得到了物理分析和探测器研发各方面的训练。**
- 2.论文有多处引用后续章节，如Figure 4-18，引了Section 6.2。应当避免提前引用。
- **回答：从论文的组织结构来说，我们应该先写di-tau重建和鉴别的内容，区间的定义应该是在这个object重建之后才能定义的。但是在di-tau重建和鉴别章节里面有一个关于tau动量修正的小节，其中的Figure 4-18是为了说明陶子动量修正在data中的效果，因此挑选了一个与信号区间无关的区间来加以验证，也就是论文后面才提到的Cross Check 区间，引用Section 6.2是为了提醒读者如果对Cross Check区间的定义感兴趣，可以跳到Section 6.2阅读。**
- 3.小文字问题：摘要中“预测的标准模型本底跟数据吻合的很好”，第二个“的”应当为“得”。
- **回答：已经修改。**

Answers to the Comments

- Rafael：
- * There are two things that I think it is a bit unfortunte. I find the discussion about how the tau variables were corrected to be quite shallow. I really hoped for a more in-depth discussion.
- **Answer： I added some sentences on how we did the correction in R21 software. We removed the layer information and track information for the merged taus.**
- * The description of the analysis is really good, but I wish you had done an assessment of the result. What does it say about the several models it motivates? How does it compare to other analyses?
- **Answer: In section 9.7.2, I compared our results with other searches including both ATLAS and CMS mumutautau and 4tau searches.**
- * In the technical chapters, about the timing detector modules and about the CEPC vertexdetector, I wish you made it clearer what was the development that you, yourself, did.
- **Answer: Added the contributions I did for the HGTD module assembly. “My contributions include helping set up the gantry system, testing the gantry system, designing the glue tool, integrating the glue dispenser, assembling the first batch of modules, and conducting metrology measurements.” For the CEPC vertex detector optimization, all the layouts I wrote in the thesis are done by myself, so I added clarify sentence in the beginning of this chapter. The sentence is “All simulations included full silicon outer trackers as described in the CEPC CDR. All the optimization work in this chapter is carried out by me.”**

Backup

LHC/HL-LHC Plan

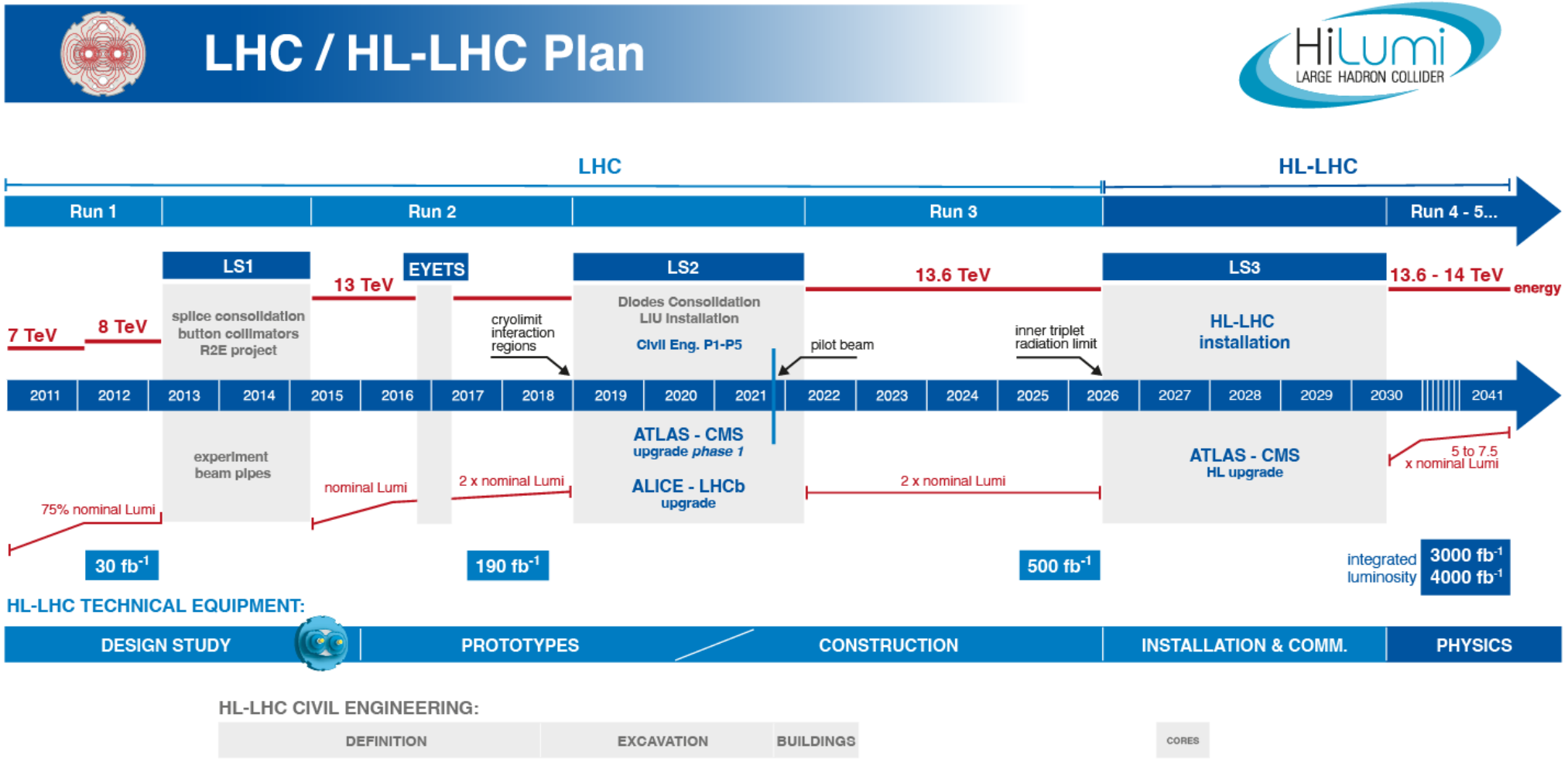

Data and simulated samples

- Data:
  - Full pp collision dataset collected by ATLAS during Run 2 of LHC (L = 140 fb^{-1})
- Signal simulation:
  - Powheg + Pythia8 + AFII, ggF production, $H \to aa \to 4\tau$
  - 2lep2had tau filter
  - m_a= 4, 6, 8, 10, 12, 14, 15 GeV
- Background simulation:
  - Prompt background
    - $q\bar{q}/gg \to ZZ^*$: Sherpa 2.2.2
    - $H \to ZZ^*$: Powheg + Pythia8
    - Triboson, $t\bar{t} + Z/W$: Sherpa
  - Non-prompt background (only used for fake composition study and signal optimization)
    - $t\bar{t}$: Powheg + Pythia8
    - Z/W + jets: Sherpa
    - Single top: Powheg + Pythia8
    - Semi-leptonic diboson: Sherpa
    - Dijet: Powheg + Pythia8
- Derivation:
  - Customized TAUP6

Trigger

- Combination of single muon and di-muon triggers:

Trigger Type	Year	HLTs
Single Muon	2015-2018	HLT_mu50
Di-muon	2015	HLT_mu18_mu8noL1 HLT_2mu10
	2016-2018	HLT_mu22_mu8noL1 HLT_2mu14

- Since the muons in the signals are close to the hadrons, only triggers without isolation requirements are considered.
- The proposed trigger set efficiency is comparable with other trigger sets.
- The combined trigger efficiency SF is directly obtained from the official TrigGlobalEffciencyCorrectionTool (twiki).

cut name	4 GeV	6 GeV	8 GeV	10 GeV	15 GeV
FullTrig	54	58	56	68	84
ResolvedTrig	42	44	40	46	53
AllmuTrig	50	55	52	63	82
AlltauTrig	23	13	11	25	52
AllmuOrtauTrig	53	56	53	64	84
DoubleMuTrig	39	40	35	40	43
SingleDoubleMuTrig	40	44	39	46	53
SingleDoubleMuNonIsoTrig	39	42	37	43	47
SingleDoubleTriMuTrig	41	45	40	47	53
SingleDoubleTriMuTauTrig	49	50	46	60	79

- FullTrig: full un-prescaled triggers in run2
- CurrentTrig: the triggers currently in use, from the resolved analysis
- AllmuTrig: all the triggers including mu in run2
- AlltauTrig: all the triggers including tau in run2
- AllmuOrtauTrig: all the triggers including mu or tau in run2
- DoubleMuTrig: hand-picked dimu triggers
- SingleDoubleMuTrig: hand-picked single muon and dimu triggers
- SingleDoubleMuNonIsoTrig: hand-picked single non-isolated muon and dimu triggers
- SingleDoubleTriMuTrig: hand-picked single muon, dimu and triple muon triggers
- SingleDoubleTriMuTauTrig: hand-picked single muon, dimu, and triple muon triggers + tau triggers

The efficiency of different trigger set in run2 trigger menu (in percent %)

Event selection (1)

- Event selection in the SRs:
  - Leading $p_T^{\mu} > 14$ GeV
  - Leading $p_{T,\tau}^{Uncorr} > 30$ GeV, subleading $p_{T,\tau}^{Uncorr} > 25$ GeV
  - 2 signal $\mu\tau_{had}$ pairs ($\Delta R(\mu, \tau_{had}) < 0.4$, $m_{\mu\tau_{had}} < 15$ GeV and τ_{had} passing Medium RNN ID)
  - $60 < m_{2\mu\tau_{had}}^{Uncorr} < 120$ GeV
  - $SS\mu$ channel: same-sign charge muons
  - $OS\mu$ channel: opposite-sign charge muons and $m_{\mu\mu} < 50$ GeV

cut name	4 GeV	6 GeV	8 GeV	10 GeV	12 GeV	14 GeV	15 GeV
AOD generation	5.5e+05	3.2e+05	2.7e+05	2.4e+05	2.3e+05	2.3e+05	2.2e+05
Preselection	5707.6	2773.7	2222.1	1955.2	1725.5	1561.7	1493.3
N(baseline μ) $\geq$ 2	5289.1	2554.3	2020.8	1785.3	1587	1441.8	1372
N(baseline τ) $\geq$ 1	5276.2	2546.2	2014.3	1779.4	1579.5	1432.1	1364
N(baseline τ) $\geq$ 2	2441	1200	872	683	524	456	410
2 baseline $\mu\tau$	2332.6	1135.4	818	576	334	222	176
μ leadpt > 14 GeV	2319.6	1128.2	813	573	334	222	176
2 OS $\mu\tau$	2229	1092.7	784	556	323	215	168
2 mVis15 $\mu\tau$	2229	1092.7	784	556	323	215	168
Lead $p_T^{\tau} > 30$ GeV	2047.7	1010.3	706	500	299	207	164
Sublead $p_T^{\tau} > 25$ GeV	1678.8	845	581	417	260	184	149
2 signal $\mu\tau$	477	231	167	141	86	67	54
60 GeV < $m_{2\mu\tau}^{vis}$ < 120 GeV	420	206	150	128	77	60	49
2 SS μ	202±9.0	97±4.8	78±4.4	66±3.7	37±2.5	31±2.3	24±2.0

$SS\mu$ channel cutflow table

Event selection (2)

- Cutflow table for $OS\mu$ channel:

cut name	4 GeV	6 GeV	8 GeV	10 GeV	12 GeV	14 GeV	15 GeV
AOD generation	5.5e+05	3.4e+05	2.7e+05	2.4e+05	2.3e+05	2.3e+05	2.3e+05
Preselection	5707.6	2773.7	2222.1	1955.2	1725.5	1561.7	1493.3
N(baseline μ) $\geq$ 2	5289.1	2554.3	2020.8	1785.3	1587	1441.8	1372
N(baseline τ) $\geq$ 1	5276.2	2546.2	2014.3	1779.4	1579.5	1432.1	1364
N(baseline τ) $\geq$ 2	2441	1200	872	683	524	456	410
2 baseline $\mu\tau$	2332.6	1135.4	818	576	334	222	176
μ leadpt > 14 GeV	2319.6	1128.2	813	573	334	222	176
2 OS $\mu\tau$	2229	1092.7	784	556	323	215	168
2 mVis15 $\mu\tau$	2229	1092.7	784	556	323	215	168
Lead p_T^τ > 30 GeV	2047.7	1010.3	706	500	299	207	164
Sublead p_T^τ > 25 GeV	1678.8	845	581	417	260	184	149
2 signal $\mu\tau$	477	231	167	141	86	67	54
60 GeV < $m_{2\mu\tau}^{vis}$ < 120 GeV	420	206	150	128	77	60	49
2 OS μ	218	109	72	62	40	29	24
$m_{\mu\mu}$ < 50 GeV	214±9.1	107±5.0	69±4.0	60±3.3	39±2.6	27±2.2	24±2.0

Table 10: A summary of weighted cutflow of signal region in OSμ channle for m_a = 4, 6, 8, 10, 12, 14, 15 GeV (BR($H \to 2a \to 4\tau$) = 1.0 at 140 fb^{-1}), starting from the AOD generation level.

Muon Working Points

• **Loose WP**: This WP maximizes efficiency for prompt muons, particularly in analyses such as Higgs boson decays into four muons, accepting a trade-off with lower purity. It encompasses CB, IO, CT, ST, ME, and SiF muons. Within $|\eta| < 2.5$, it includes CB and IO muons from the Medium WP, as well as CT and ST muons in the MS gap region ($|\eta| < 0.1$). For low-p_T muons ($p_T < 7\,\text{GeV}$), IO muons with one precision station are included in $|\eta| < 1.3$ if also reconstructed as ST muons. Outside the ID ($2.5 < |\eta| < 2.7$), ME and SiF muons with three precision stations are added. The Loose WP covers p_T from 3 GeV to several hundred GeV and the full MS range $|\eta| < 2.7$, achieving efficiency gains of roughly 20% at $3-5\,\text{GeV}$ and 1-2% at higher p_T.

• **Medium WP**: Designed as a balanced option for most analyses, this WP offers good efficiency and purity with manageable systematic uncertainties. It employs CB, IO, ME, and SiF muons. Within $|\eta| < 2.5$, it requires CB and IO muons to have at least two precision stations (or one in $|\eta| < 0.1$ with at most one precision hole), and a q/p compatibility of less than 7. Beyond the ID ($2.5 < |\eta| < 2.7$), ME and SiF muons must have three precision stations. This WP applies to p_T ranging from 3 GeV to several hundred GeV across $|\eta| < 2.7$, with over 98% of prompt muons in $t\bar{t}$ events being CB muons.

• **Tight WP**: This WP prioritizes high purity and background rejection, making it ideal for analyses sensitive to non-prompt muons, albeit with a slight efficiency cost. It includes only CB and IO muons that pass the Medium WP criteria. Requirements consist of at least two precision stations, a combined track fit $\chi^2 < 8$, and stricter q/p and ρ' cuts optimized for p_T and $|\eta|$, significantly reducing background by over 50% at $6-20\,\text{GeV}$. It targets p_T from 4 GeV (with 91% efficiency) to above 20 GeV (with 96% efficiency) within $|\eta| < 2.5$, excluding ME, ST, and CT muons to ensure high quality.

Tau RNN Identification

Table 1: List of observables used as inputs in the different parts of the RNN. The markers indicate which observables are used to identify 1-prong and 3-prong $\tau_{\text{had-vis}}$. See Section 5.1 for the definitions of the observables.

	Observable	1-prong	3-prong
Track inputs	$p_{\text{T}}^{\text{seed jet}}$	•	•
	$p_{\text{T}}^{\text{track}}$	•	•
	$\Delta\eta^{\text{track}}$	•	•
	$\Delta\phi^{\text{track}}$	•	•
	$\lvert d_0^{\text{track}}\rvert$	•	•
	$\lvert z_0^{\text{track}}\sin\theta\rvert$	•	•
	$N_{\text{IBL hits}}$	•	•
	$N_{\text{Pixel hits}}$	•	•
	$N_{\text{SCT hits}}$	•	•
Cluster inputs	$p_{\text{T}}^{\text{jet seed}}$	•	•
	$E_{\text{T}}^{\text{cluster}}$	•	•
	$\Delta\eta^{\text{cluster}}$	•	•
	$\Delta\phi^{\text{cluster}}$	•	•
	λ_{cluster}	•	•
	$\langle\lambda_{\text{cluster}}^2\rangle$	•	•
	$\langle r_{\text{cluster}}^2\rangle$	•	•
High-level inputs	$p_{\text{T}}^{\text{uncalibrated}}$	•	•
	f_{cent}	•	•
	$f_{\text{leadtrack}}^{-1}$	•	•
	ΔR_{max}	•	•
	$\lvert S_{\text{leadtrack}}\rvert$	•	
	$S_{\text{T}}^{\text{flight}}$		•
	$f_{\text{iso}}^{\text{track}}$	•	•
	$f_{\text{track}}^{\text{EM}}$	•	•
	$p_{\text{T}}^{\text{EM+track}}/p_{\text{T}}$	•	•
	$m^{\text{EM+track}}$	•	•
	m^{track}		•

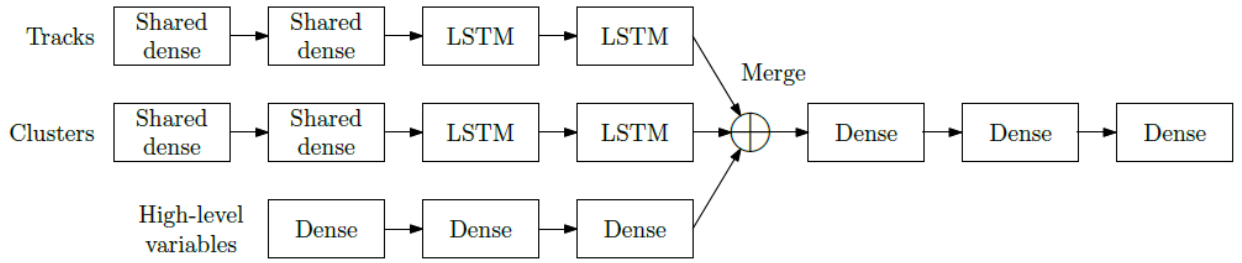

Figure 2: Schematic view of the network architecture used for tau identification. Layers marked as *dense* are fully connected to adjacent layers.

Table 2: List of defined working points with fixed true $\tau_{\text{had-vis}}$ selection efficiencies and the corresponding background rejection factors for misidentified $\tau_{\text{had-vis}}$ in dijet events for the BDT and RNN classifiers.

	Signal efficiency		Background rejection BDT		Background rejection RNN	
Working point	1-prong	3-prong	1-prong	3-prong	1-prong	3-prong
Tight	60%	45%	40	400	70	700
Medium	75%	60%	20	150	35	240
Loose	85%	75%	12	61	21	90
Very loose	95%	95%	5.3	11.2	9.9	16

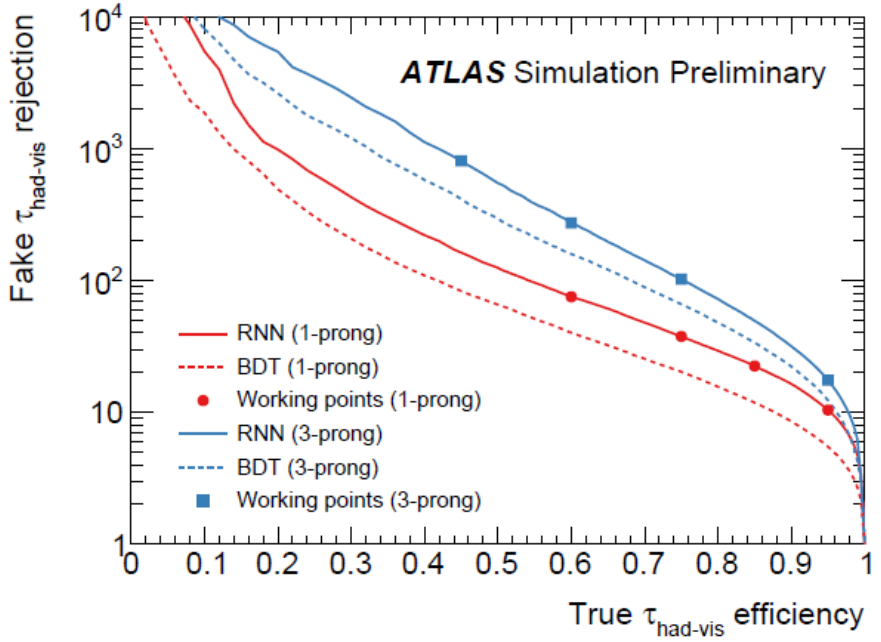

Background estimation

- Prompt background
  - Estimate using MC: $q\bar{q}/gg \rightarrow ZZ, H \rightarrow ZZ4l$
- Non-prompt/fake background
  - Data-driven fake factor method
  - Measure the FF of $\mu\tau$ in the $Z(\mu\mu)$ + jets($\mu\tau_{had}$) control region
  - $$FF = \frac{N^{Z+\mu\tau}_{pass\ RNNLoose, Data} - N^{Z+\mu\tau}_{pass\ RNNLoose, truth\ matched\ MC}}{N^{Z+\mu\tau}_{fail\ RNNLoose, Data} - N^{Z+\mu\tau}_{fail\ RNNLoose, truth\ matched\ MC}}$$
  - FF parameterized as function of p_T^{Uncorr} and prongness (FF(p_T^{Uncorr}, $prongness$))
  - Apply the FFs to $2\mu\tau_{had}$ regions by using the events with at least one $\mu\tau_{had}$ candidate failing ID
    - $Fake(\mu\tau_1^P\mu\tau_2^P) = [\boldsymbol{FF_2\mu\tau_1^P\mu\tau_2^F + FF_1\mu\tau_1^F\mu\tau_2^P - FF_1FF_2\mu\tau_1^F\mu\tau_2^F}]_{data} - [\boldsymbol{FF_2\mu\tau_1^P\mu\tau_2^F + FF_1\mu\tau_1^F\mu\tau_2^P - FF_1FF_2\mu\tau_1^F\mu\tau_2^F}]_{truth\ matched\ MC}$
    - $\boldsymbol{FF_2\mu\tau_1^P\mu\tau_2^F}$, $\boldsymbol{FF_1\mu\tau_1^F\mu\tau_2^P}$: estimate the single fake $\mu\tau$ events, fake $\mu\tau_1$ and fake $\mu\tau_2$
    - $\boldsymbol{FF_1FF_2\mu\tau_1^F\mu\tau_2^F}$: estimate the double fake $\mu\tau$, minus sign is to remove the double counting double-fake-$\mu\tau$ events

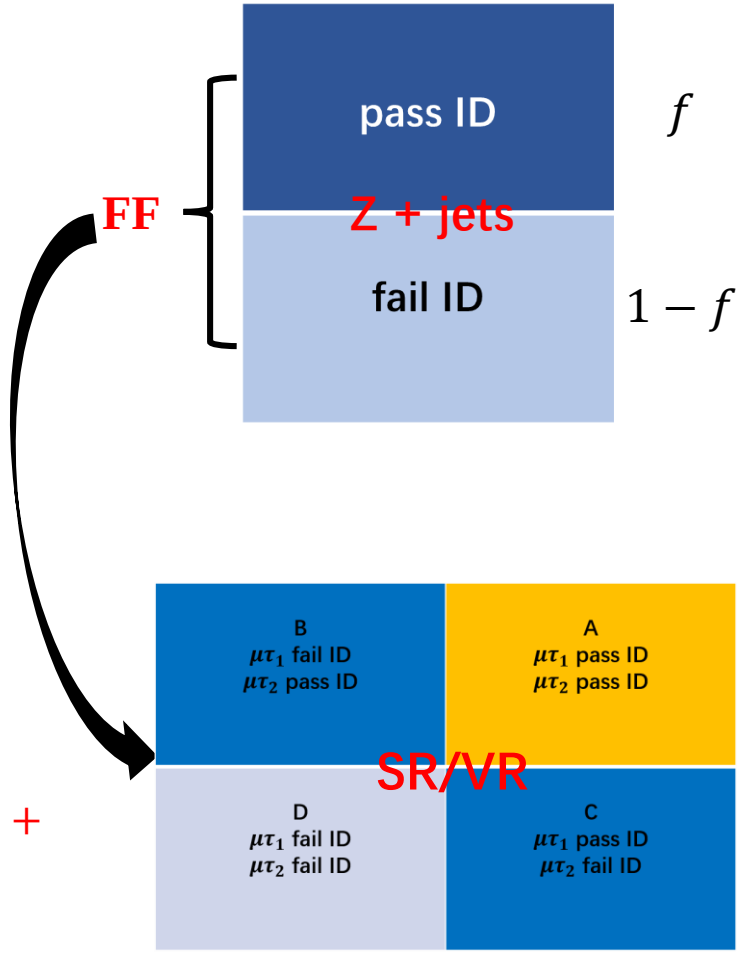

A: $\mu\tau_1$ pass ID, $\mu\tau_2$ pass ID (SR,VR)
B: $\mu\tau_1$ fail ID, $\mu\tau_2$ pass ID
C: $\mu\tau_1$ pass ID, $\mu\tau_2$ fail ID
D: $\mu\tau_1$ fail ID, $\mu\tau_2$ fail ID

Average $m_{\mu\tau_{had}}$ Distributions in SRs

- The binning strategy for the SSμ and OSμ signal regions is optimized to target approximately 20% statistical uncertainty for background events
- The last two bins were specifically optimized to enhance the signal significance over all mass hypothesis simultaneously while ensuring non-zero background events in each bin.

$m_a = 4$ GeV

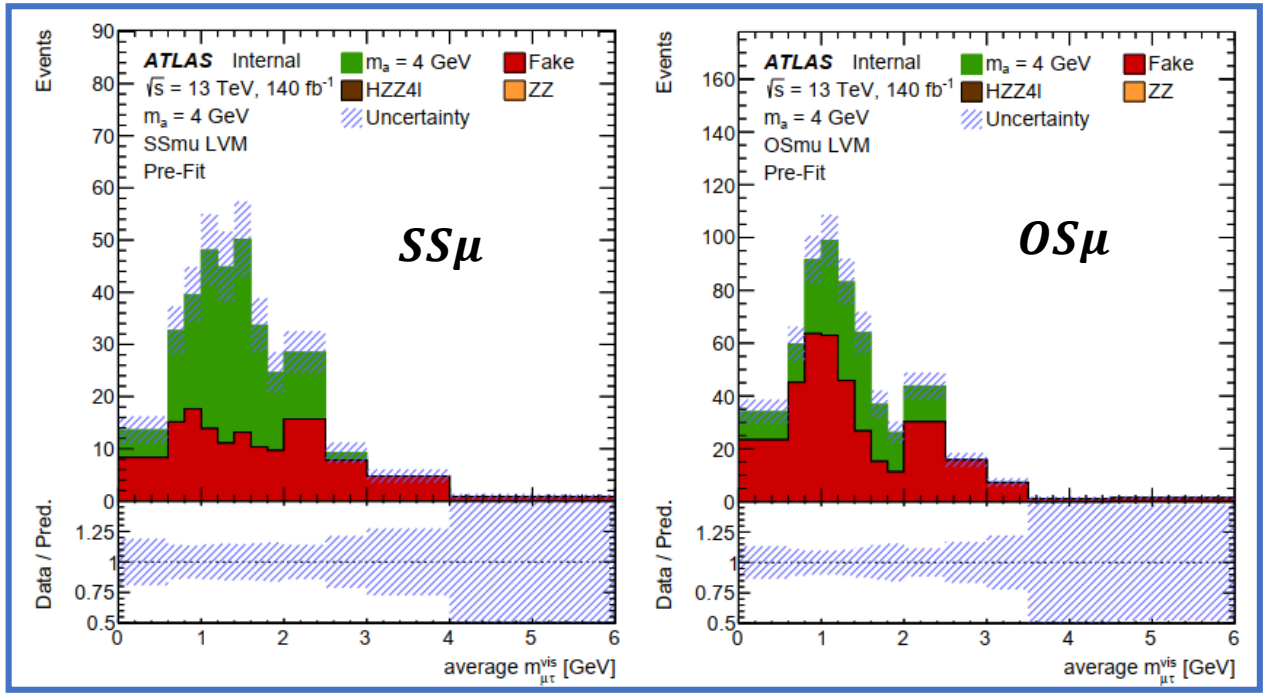

$m_a = 8$ GeV

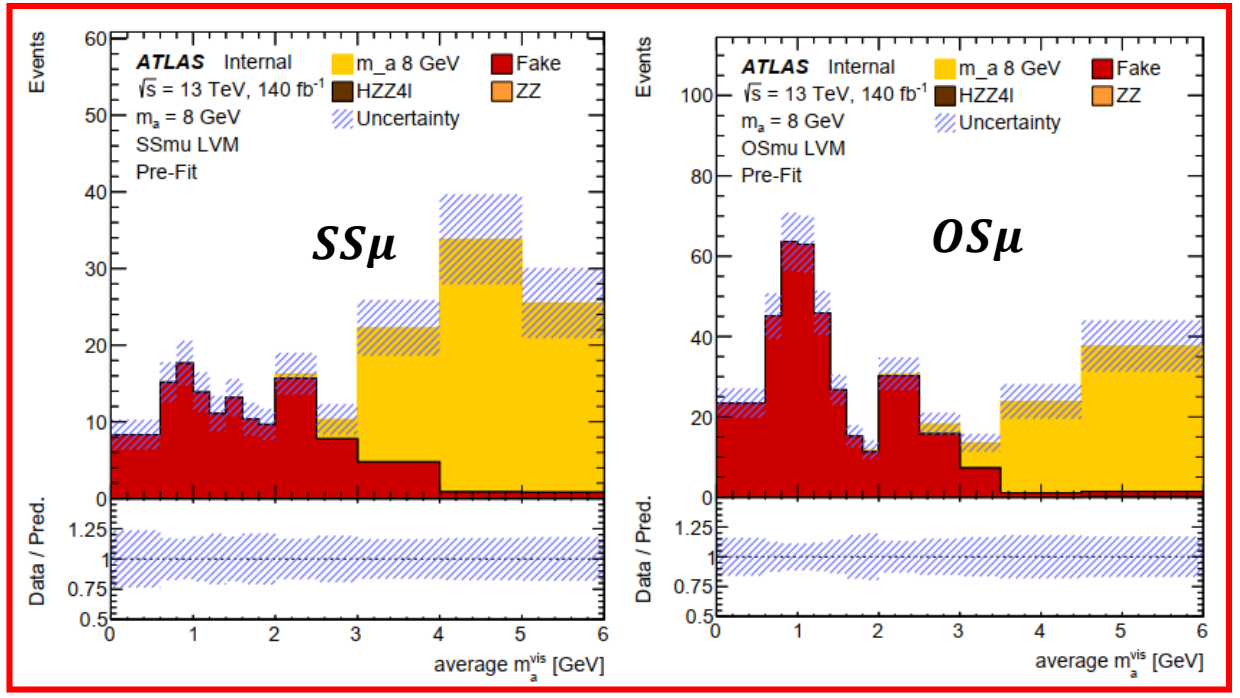

Average $m_{\mu\tau_{had}}$ distributions in SRs

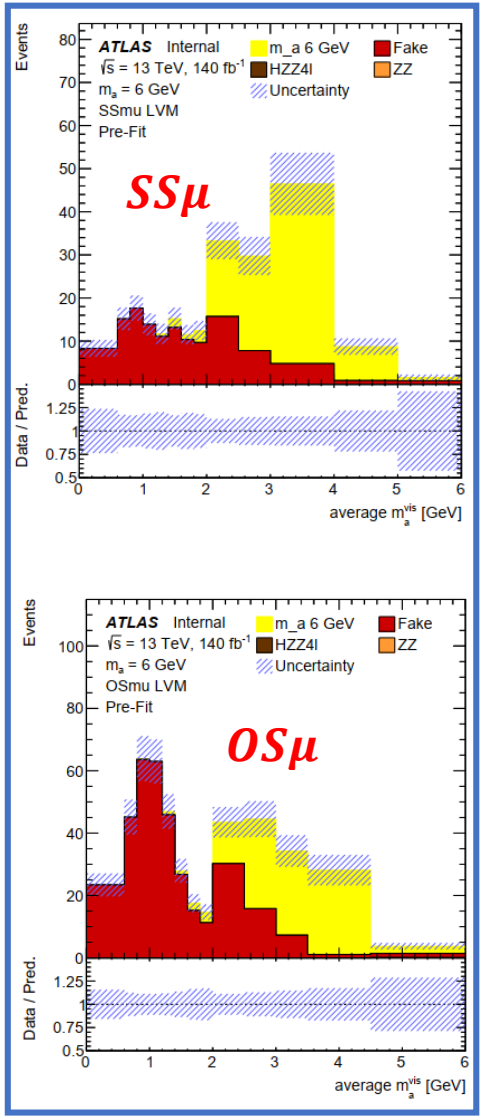

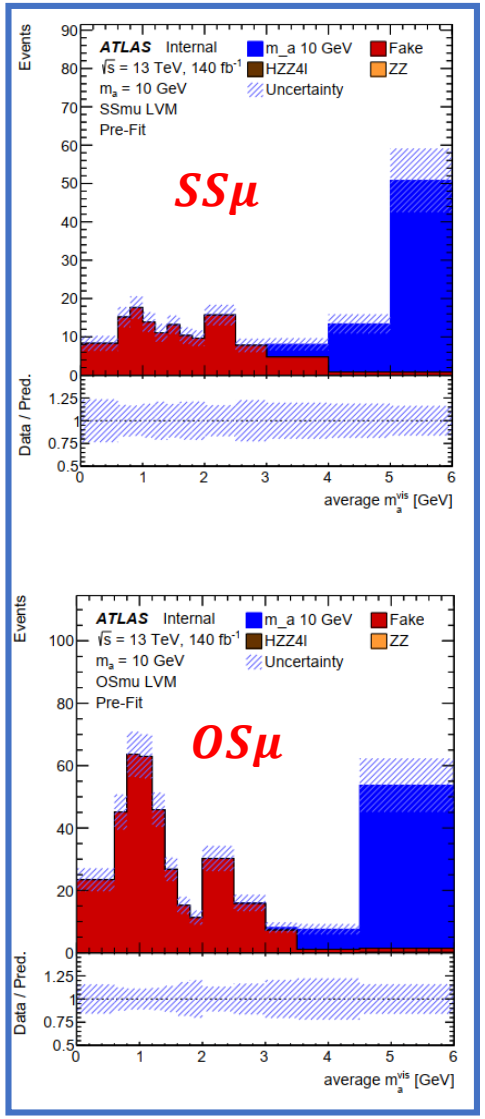

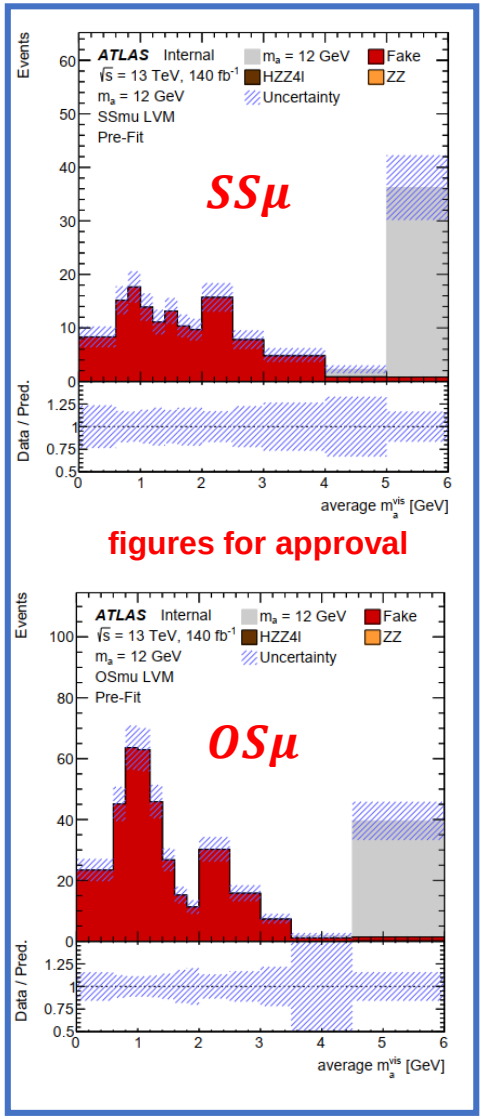

figures for approval

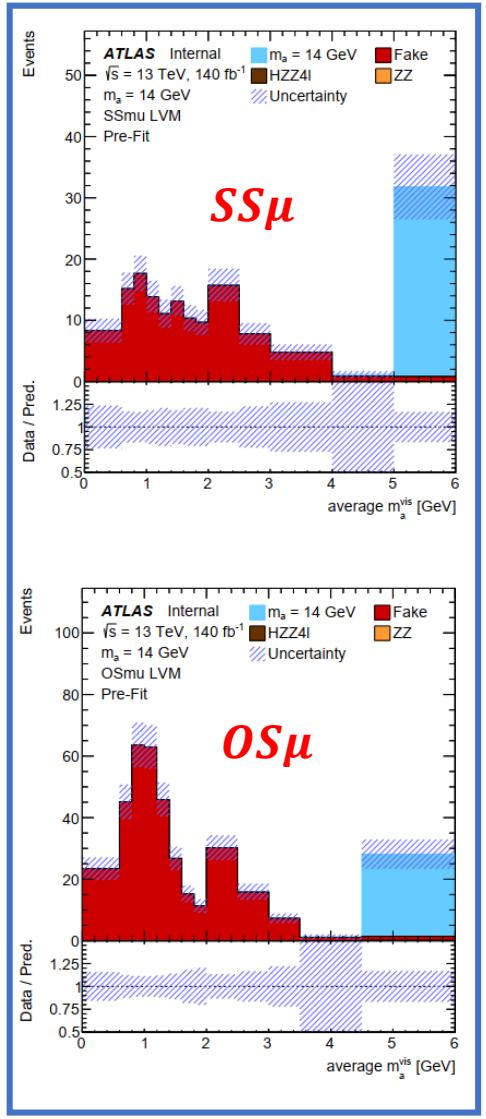

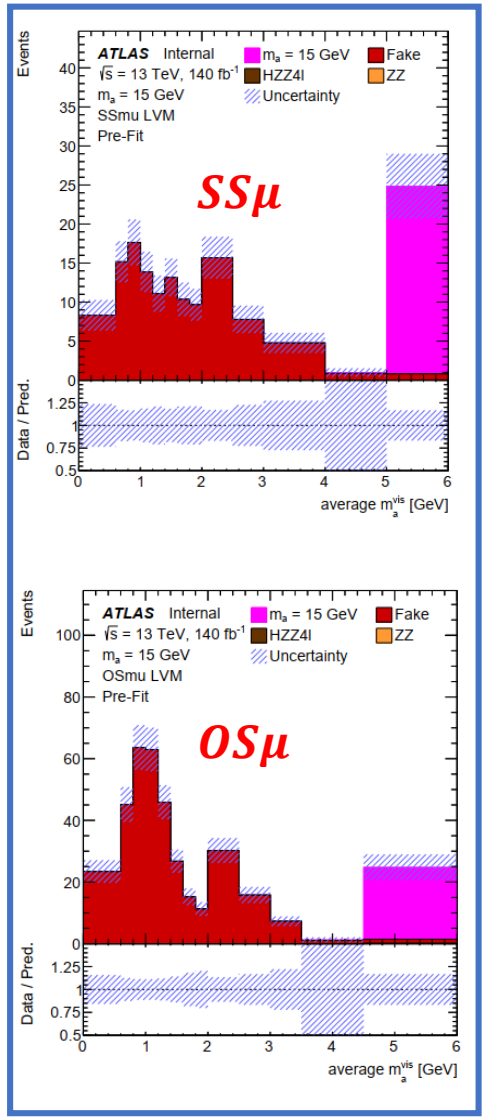

$m_a = 6$ GeV | $m_a = 10$ GeV | $m_a = 12$ GeV | $m_a = 14$ GeV | $m_a = 15$ GeV

Observed yields in SRs

- The observed number of events in data is consistent with the background prediction within 1σ in both $SS\mu$ and $OS\mu$ channels.
- No excess is found. The fake prediction shows very good agreement with the data.

Process	SSμ region	OSμ region
Data	121	380
Fake background	129.1 ± 11.5	349.7 ± 31.4
$q\bar{q} \to ZZ$ and $gg \to ZZ$	< 0.01	< 0.01
$H \to ZZ^*$	0.01 ± 0.01	0.09 ± 0.04
Total background	129.1 ± 11.5	349.8 ± 31.4
$H \to aa \to 4\tau$ ($m_a = 4$ GeV)	20.2 ± 3.2	21.4 ± 3.3
$H \to aa \to 4\tau$ ($m_a = 6$ GeV)	9.7 ± 1.5	10.7 ± 1.7
$H \to aa \to 4\tau$ ($m_a = 8$ GeV)	7.8 ± 1.3	6.9 ± 1.1
$H \to aa \to 4\tau$ ($m_a = 10$ GeV)	6.6 ± 1.1	6.0 ± 1.0
$H \to aa \to 4\tau$ ($m_a = 12$ GeV)	3.7 ± 0.6	3.9 ± 0.6
$H \to aa \to 4\tau$ ($m_a = 14$ GeV)	3.1 ± 0.5	2.7 ± 0.5
$H \to aa \to 4\tau$ ($m_a = 15$ GeV)	2.4 ± 0.4	2.4 ± 0.4

Limits

- The likelihood function is built as a product of Poisson probability functions for each average $m_{\mu\tau_{had}}$ bin in the SSμ and OSμ SRs.
- Nuisance parameters with Gaussian constraints are introduced to model sources of systematic uncertainties and their impact on the expected signal and background yields.

$$L(\vec{n}|\vec{\theta},\vec{k}) = \prod_i P(n_i|S_i(\vec{\theta},\vec{k}) + B_i(\vec{\theta},\vec{k})) \times \prod_i G(\theta_j)$$

- 95% CL upper limits are set on $(\sigma(H)/\sigma SM(H))(\mathrm{B}(H \to aa \to 4\tau)$ using the CL_S method.
- The upper limits for each signal mass are obtained by using both pseudo-experiment and asymptotic method.
  - The expected and observed upper limits are comparable for pseudo-experiment and asymptotic method.
  - The upper limits using pseudo-experiment method are considered as the final upper limits for publication.
- The observed (expected) limit ranges from 0.033 (0.044) to 0.10 (0.13) for $m_a = 10$ GeV and $m_a = 4$ GeV.

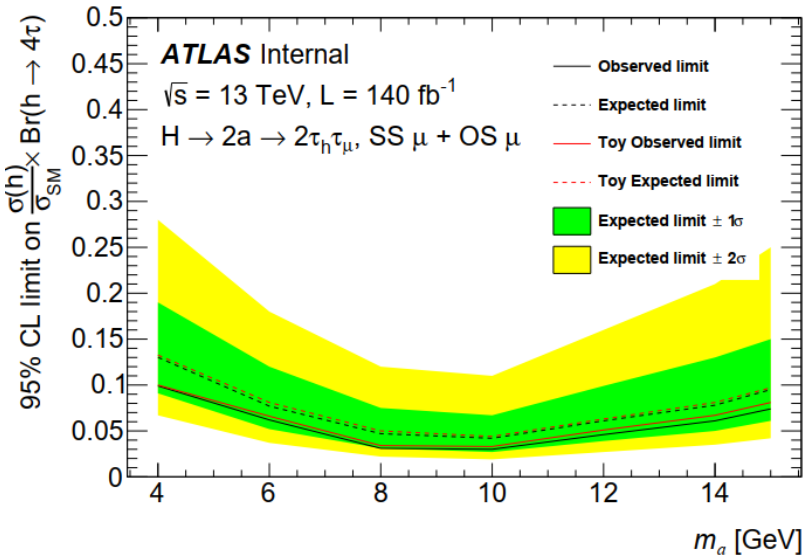

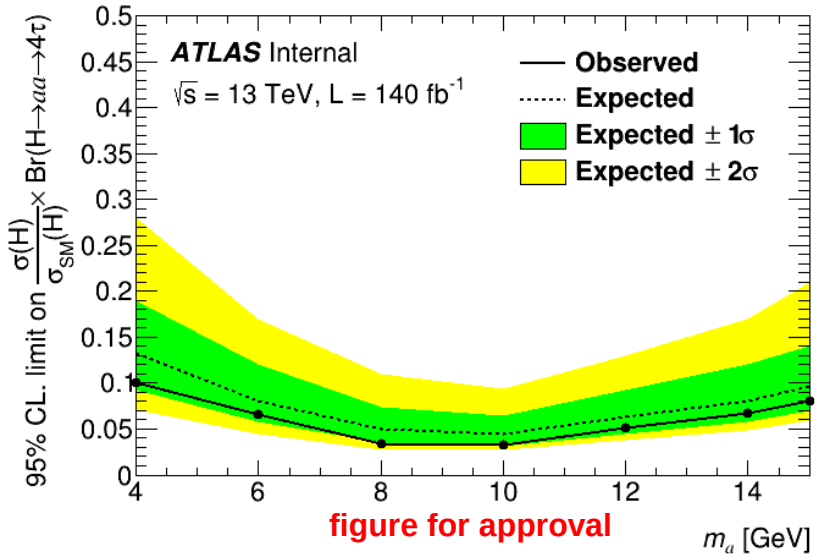

figure for approval

Acceptance in different Higgs production modes

UMassAmherst

Acceptance in $H \to aa \to 4\tau$ analysis

- We use $m_a = 6$ GeV. The study is done at truth level. We use MG5_aMC + Pythia for this study.

Cutflow	ggF		VBF		VH	
	Events	Acceptance	Events	Acceptance	Events	Acceptance
All	50,000	100%	50,000	100%	50,000	100%
τ_{had} (p_{T}, η)	9,178	18.36%	11,167	22.33%	8,537	17.07%
μ (p_{T}, η)	1,793	3.59%	2,748	5.50%	1,972	3.94%
$\mu\tau_{\text{had}}$ ΔR	1,788	3.58%	2,731	5.46%	1,964	3.93%
$\mu\tau_{\text{had}}$ mass	1,788	3.58%	2,724	5.45%	1,964	3.93%
Higgs mass	1,519	3.04%	2,267	4.53%	1,615	3.23%

Process	Total xsec [pb]	Fiducial xsec [fb]	With ggF acc [fb]	Relative diff
ggF	48.58	1,475	1,475	0.00%
VBF	3.78	171	114	49.24%
VH	2.26	73	69	6.32%
Total	**54.62**	**1,719**	**1,658**	**3.68%**

41

CMS latest results

CMS PAS SUS-24-002

A search for a pair of light pseudoscalar bosons (a_1) produced from the decay of the 125 GeV Higgs boson (H) is presented. The analysis examines decay modes where one a_1 decays into a pair of tau leptons, and the other decays into either another pair of tau leptons or a pair of muons. The a_1 mass probed in this study ranges from 4 to 15 GeV. The data sample used was recorded by the CMS experiment in proton-proton collisions at a center-of-mass energy of 13 TeV and corresponds to an integrated luminosity of 138 fb^{-1}. The study uses the $2\mu 2\tau$ and 4τ channels in combination to constrain the product of the Higgs boson production cross section and the branching fraction to the 4τ final state, $\sigma(pp \to H + X)\mathcal{B}(H \to a_1 a_1)\mathcal{B}^2(a_1 \to \tau\tau)$. This methodology takes advantage of the linear dependence of the fermionic coupling strength of pseudoscalar bosons on the fermion mass. Model-independent upper limits at 95% confidence level (CL) on $\sigma(pp \to H + X)\mathcal{B}(H \to a_1 a_1)\mathcal{B}^2(a_1 \to \tau\tau)$, relative to the standard model Higgs boson production cross section σ_{SM}, are set. The observed (expected) upper limits range between 0.007 (0.011) and 0.079 (0.066) across the mass range considered. Exclusion limits at 95% on $\sigma(pp \to H + X)\mathcal{B}(H \to a_1 a_1)$, relative to σ_{SM}, are derived for various Two Higgs Doublet Model + Singlet scenarios.

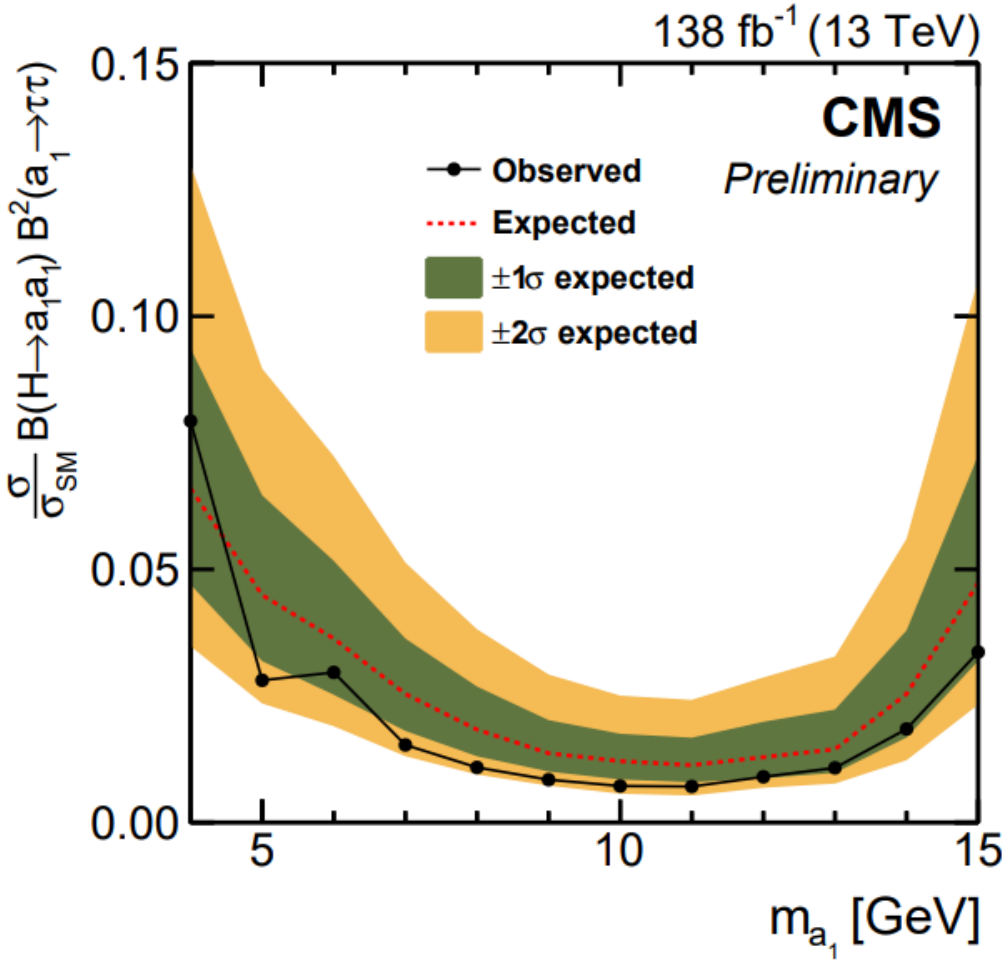

The gap and rotation results

- ✓ Several digital module and full module has been assembled using the gantry and custom tooling (semi-automation assembly)
  - ✓ Wire-bonding was performed successful
  - ✓ The metrology results are very close the specifications

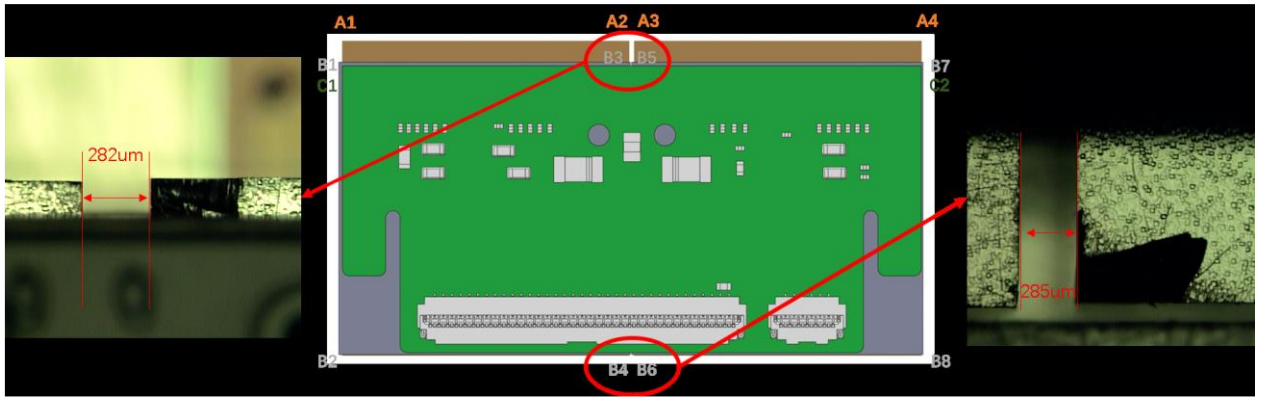

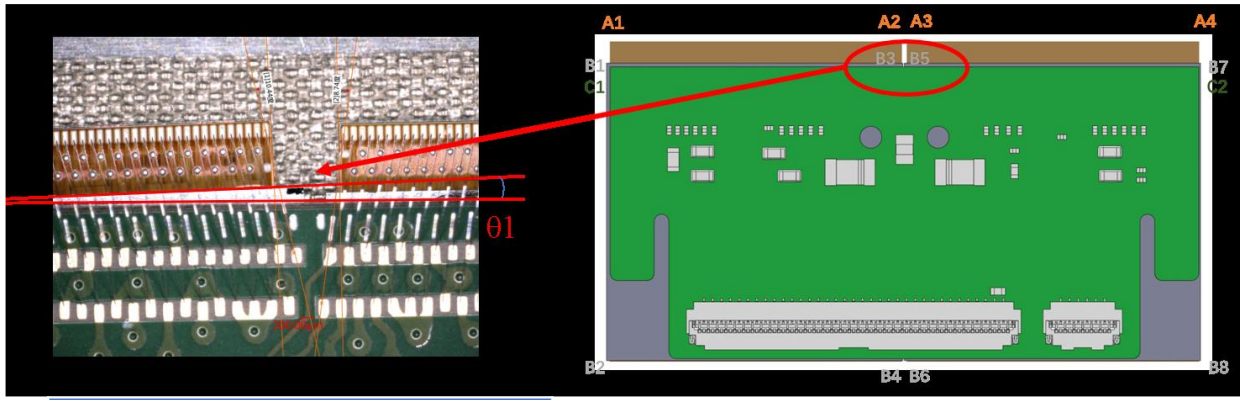

	B3B5(mm)	B4B6(mm)	Nominal gap(um)	Average Δ nominal(um)
Full Module 1	0.215	0.200	280	-72
Full Module 2	0.235	0.311	280	-7
Full Module 3	0.157	0.196	280	-104
Full Module 4	0.282	0.285	280	3

	Full Module 1	Full Module 2	Full Module 3	Full Module 4
Average rotation angle[°]	-0.067	0.128	0.070	-0.182

Specification of the module mass and dimension
Module weight 3.0 g
Nominal thickness of the module 2.52 mm
Maximum thickness of the module 3.32 mm
Maximum width of the module 40.6 mm
Nominal gap between two bare modules 200 μm
Minimum gap between two bare modules 50 μm

Specifications on the module flex to bare module attachment
Glue thickness: 50±30μm
Single lap shear force: >2N
Total coverage of glue area: 80%, no spillage
Alignment between module flex and bare modules: < 100μm displacement, < 0.1° rotation

Vertex Detector Prototype Resolution

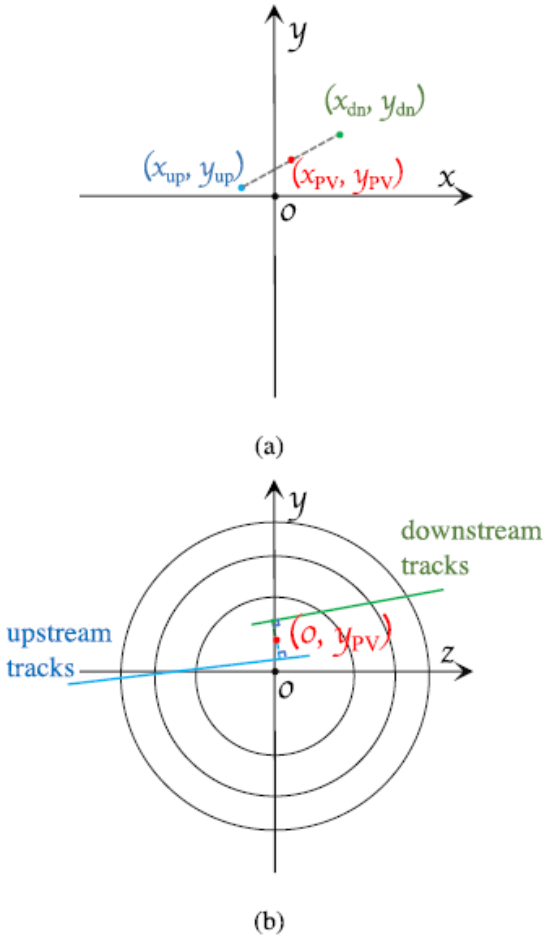

Fig. 11. (a) (x_{up}, y_{up}) and (x_{dn}, y_{dn}) represent the extrapolated positions of the upstream track and downstream track, respectively, at $z = 0$ plane. The point (x_{PV}, y_{PV}) denotes the midpoint between (x_{up}, y_{up}) and (x_{dn}, y_{dn}). (b) Projection to the y-z plane. The impact parameter is the perpendicular distance between the PV and the tracks.

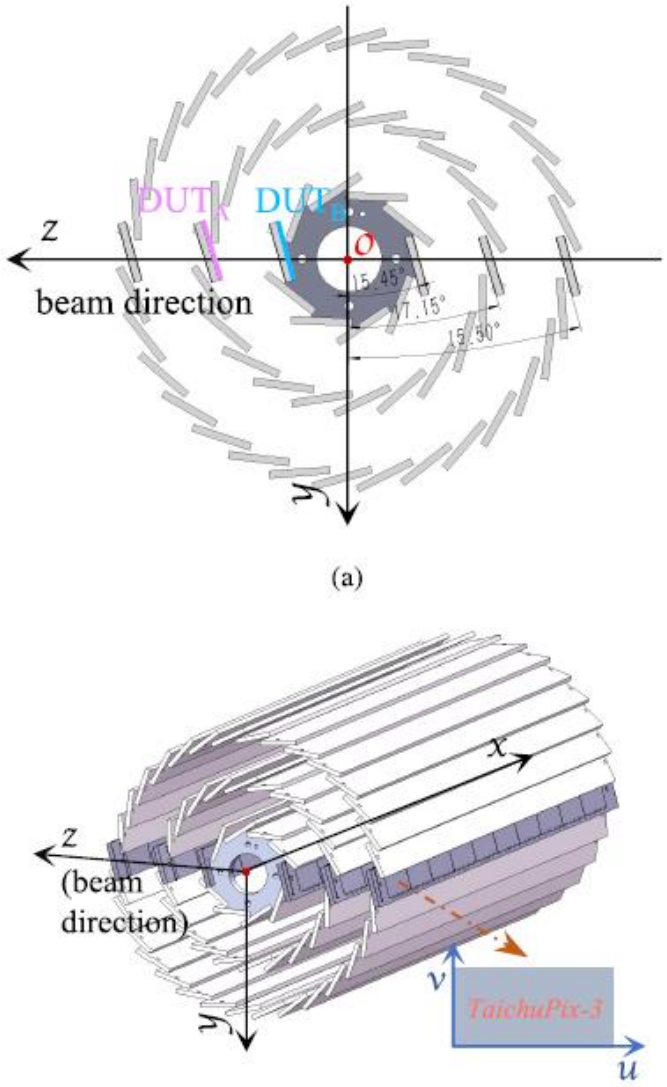

$\mu\tau$ pair finding in the signal sample

- Taking μ as the seed
- Finding the closest τ to construct the $\mu\tau$ pairs
- Selecting the $\mu\tau$ pairs with $\Delta R(\mu,\tau) < 1.0$ (0.4 used in analysis), $m_{\mu\tau}^{vis} < 15$ GeV
- If one τ matches to more than one μ, only keep the $\mu\tau$ pair has the smallest $\Delta R(\mu,\tau)$
- No duplicated μ or τ in different $\mu\tau$ pairs

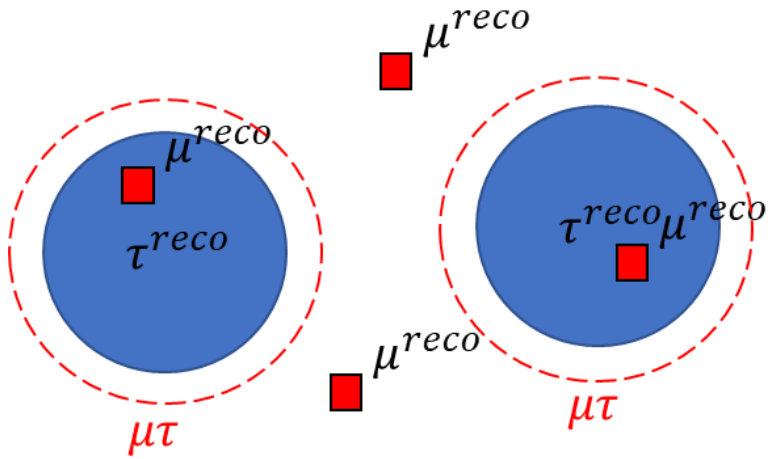

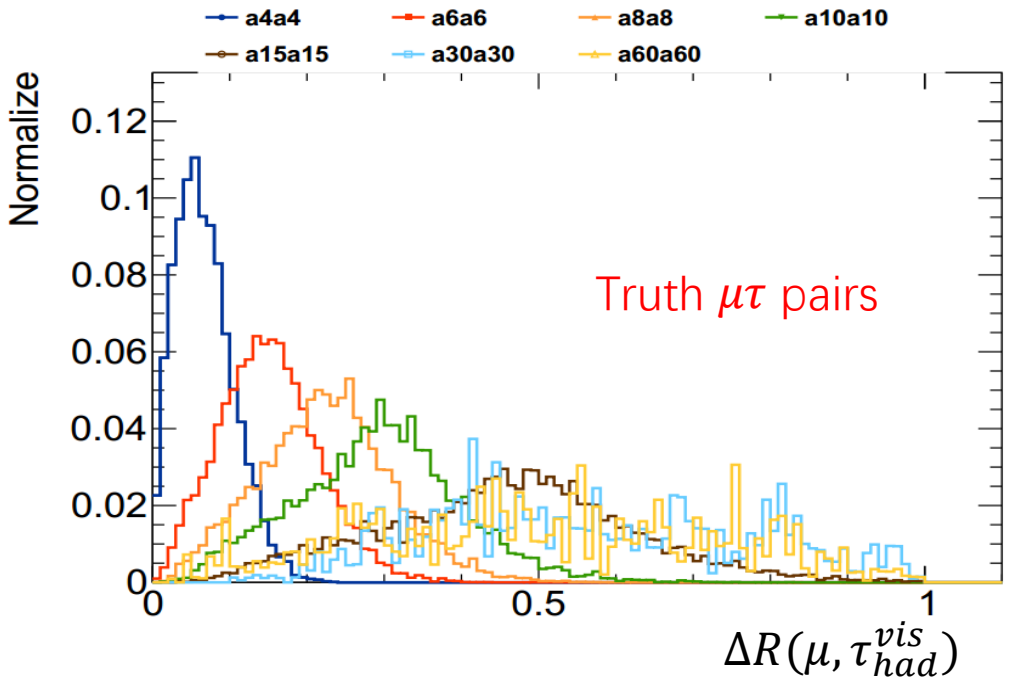

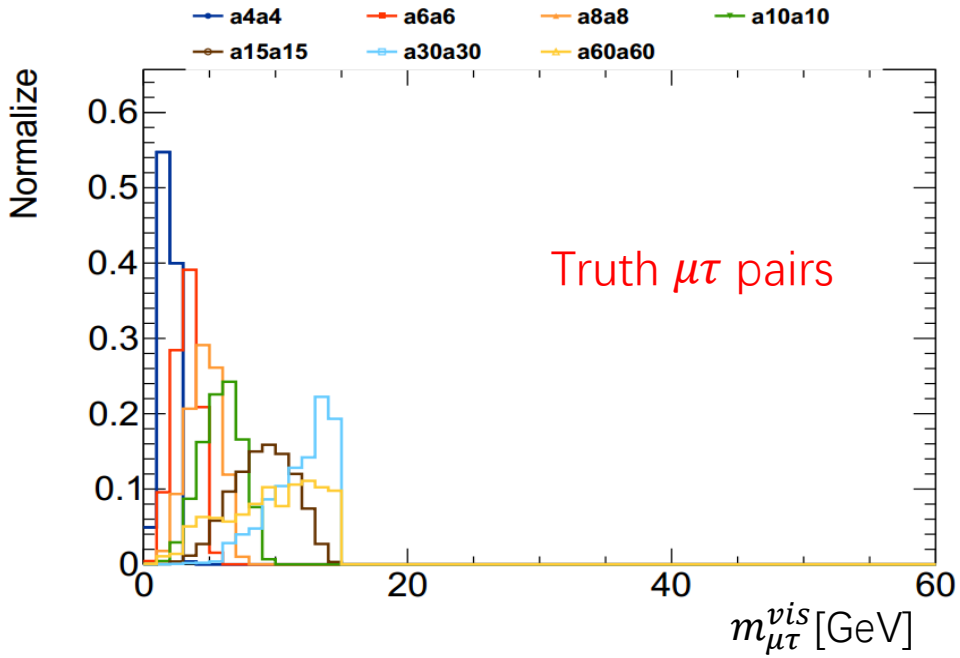

Tau ID variables distribution after muon removal

- After proper muon removal, tau id variables are recovered to the similar distribution of standard taus
- All the RNN variables are re-calculated after muon removal

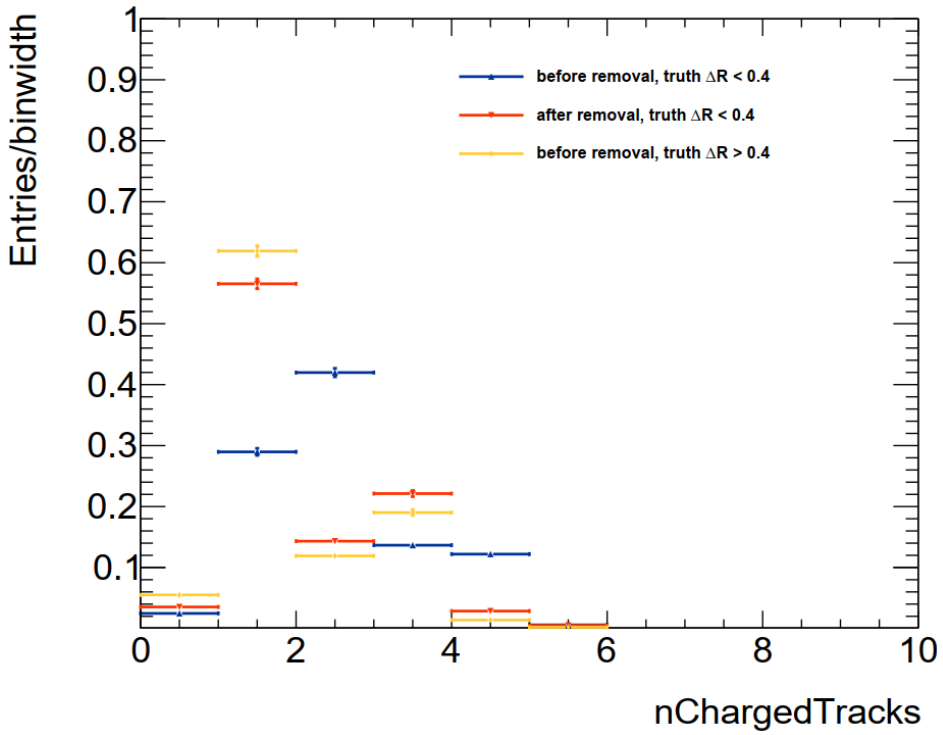

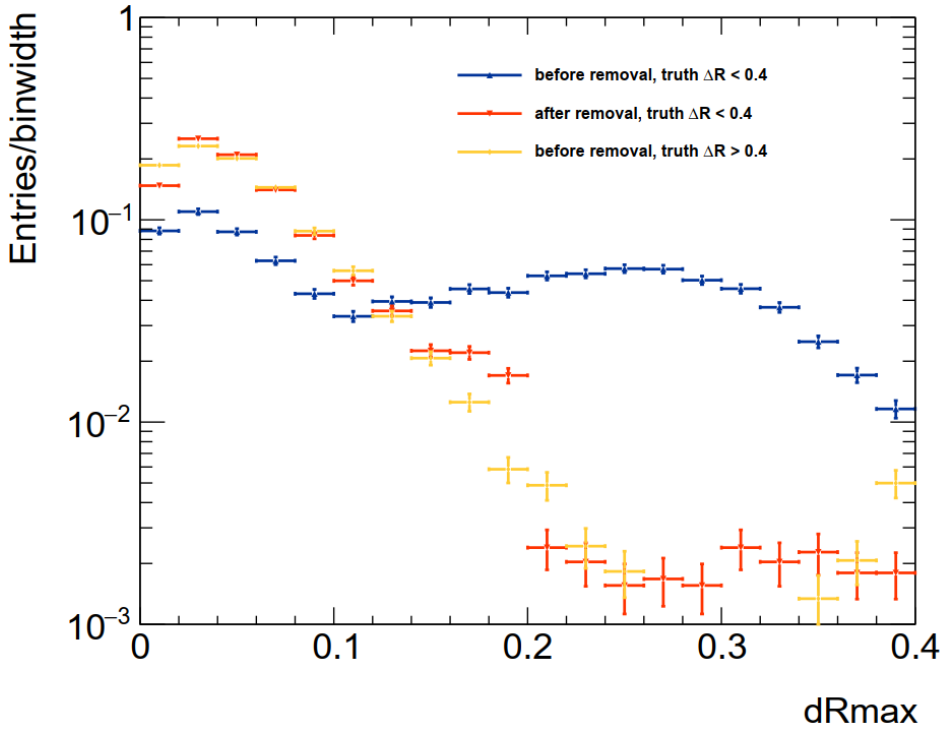

Recalculated tau RNN variables

- ipZ0SinThetaSigLeadTrk
- trFlightPathSig
- innerTrkAvgDist
- SumPtTrkFrac
- massTrkSys
- centFrac
- ptRatioEflowApprox
- dRmax
- mEflowApprox
- etOverPtLeadTrk
- EMPOverTrkSysP

Flow diagram of TauID algorithms

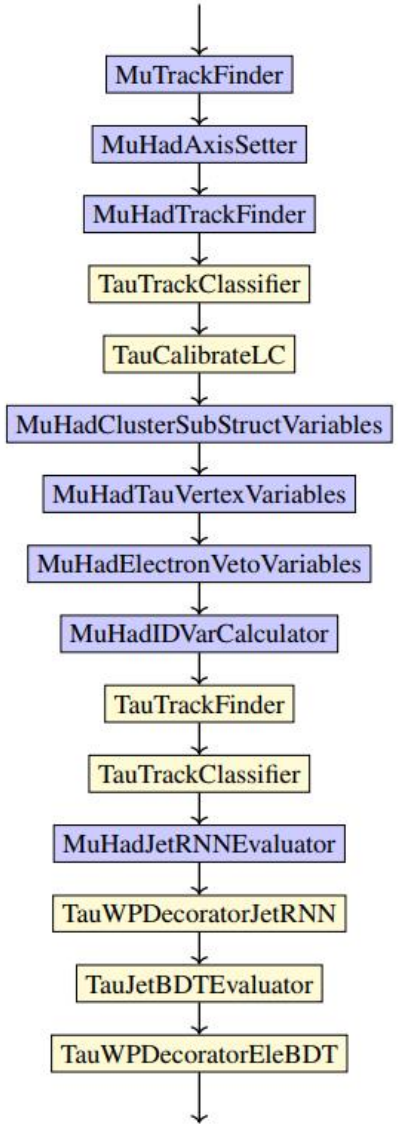

Official algorithms

Adapting algorithms

Tau reco & id efficiency definition

- The reconstruction efficiency is defined as the fraction of 1-prong (3-prong) hadronic tau decays which are reconstructed as 1-track (3-track) $\tau_{had-vis}$ candidates:
  - reco efficiency $= \frac{N(\tau_{had-vis}^{truth}\ reconstructed\ as\ 1-track\ (3-track)\ \tau)}{N(\tau_{had-vis}^{truth})}$

Ref: ATL-PHYS-PUB-2015-045

- The identification efficiency is defined as the fraction of 1-prong (3-prong) hadronic tau that are reconstructed as 1-track (3-track) $\tau_{had-vis}$ candidates, which also pass the RNN score selection:
  - id efficiency $= \frac{N(\tau_{had-vis}\ passed\ RNN\ score\ selction)}{N(\tau_{had-vis}^{truth} reconstructed\ \ as\ 1-track\ (3-track)\ \tau)}$, reco + id = reco eff × id eff

Muon removal efficiency

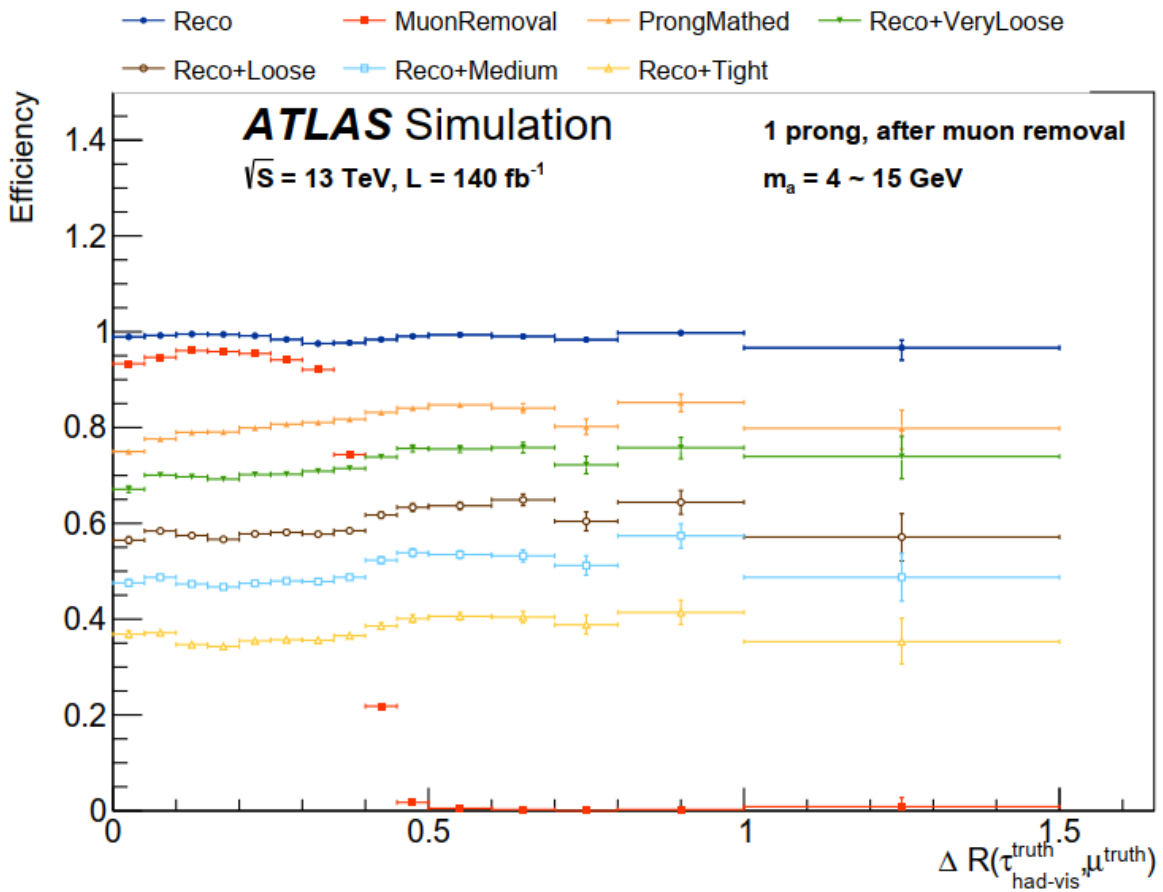

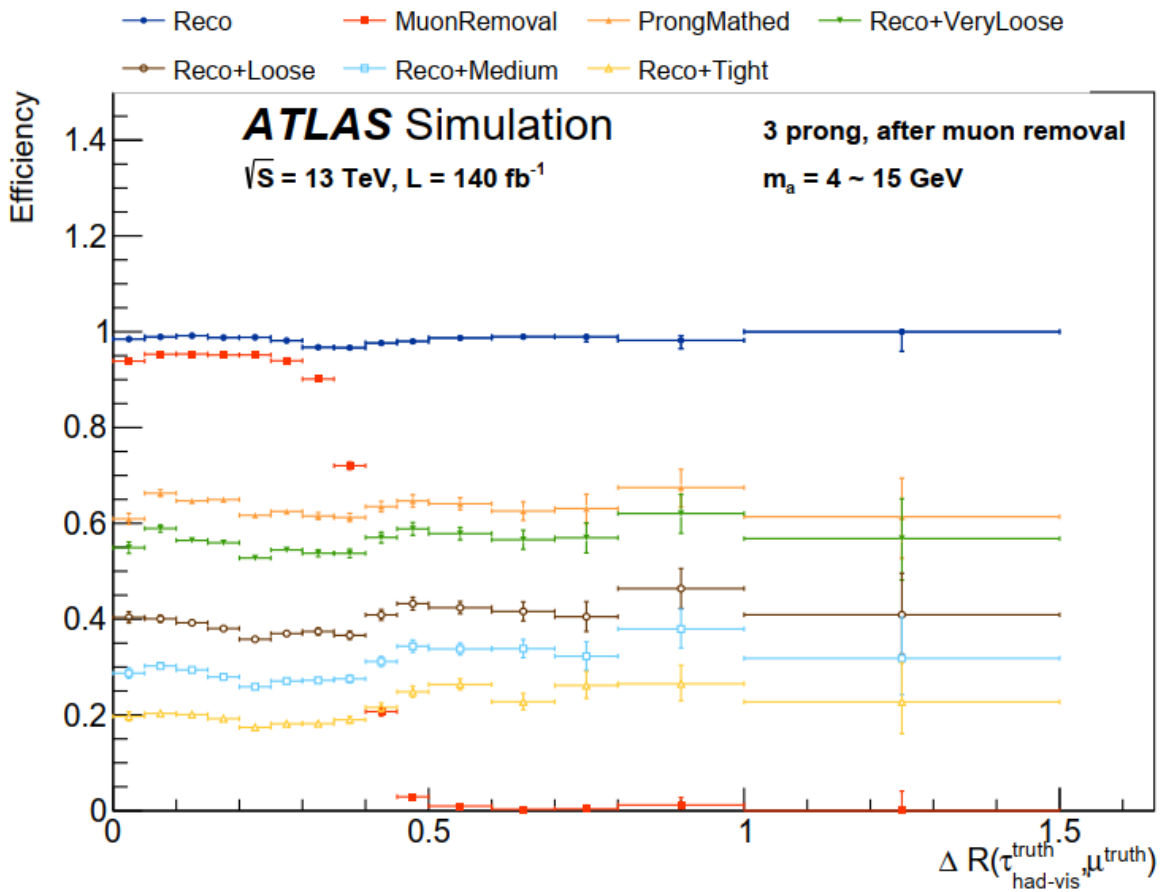

Stability of Tau ID Efficiency

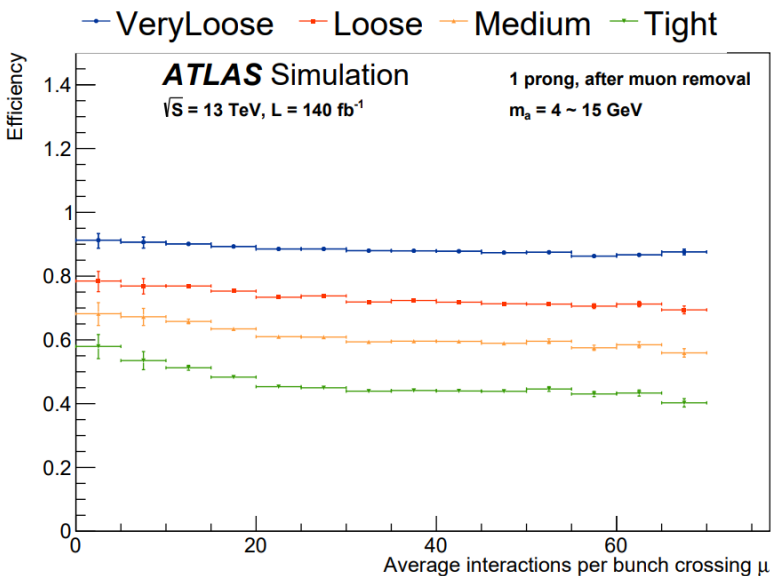

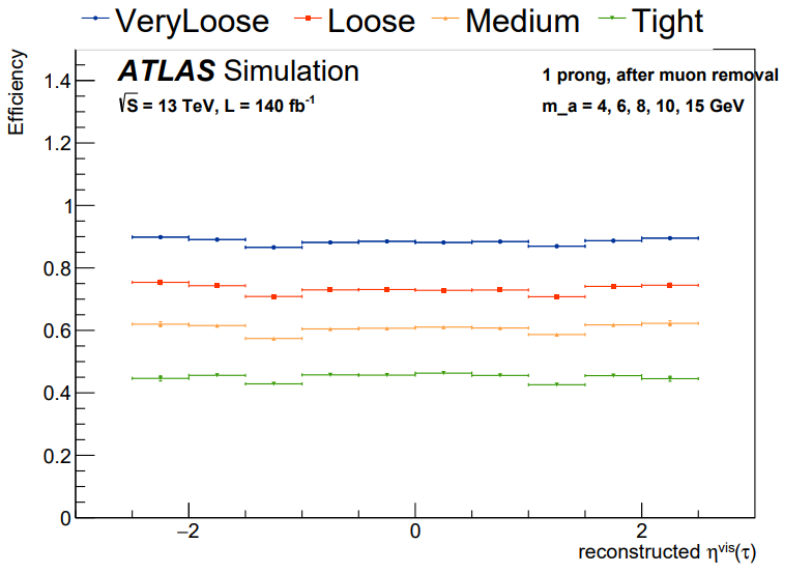

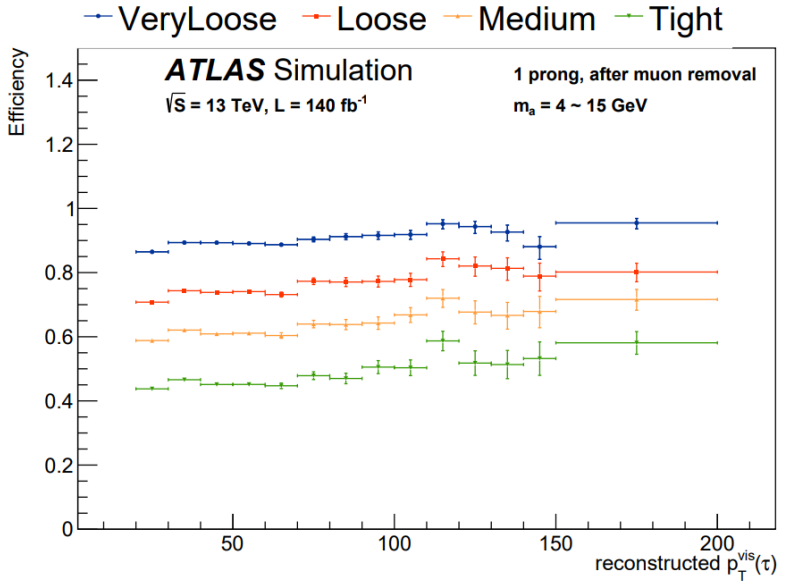

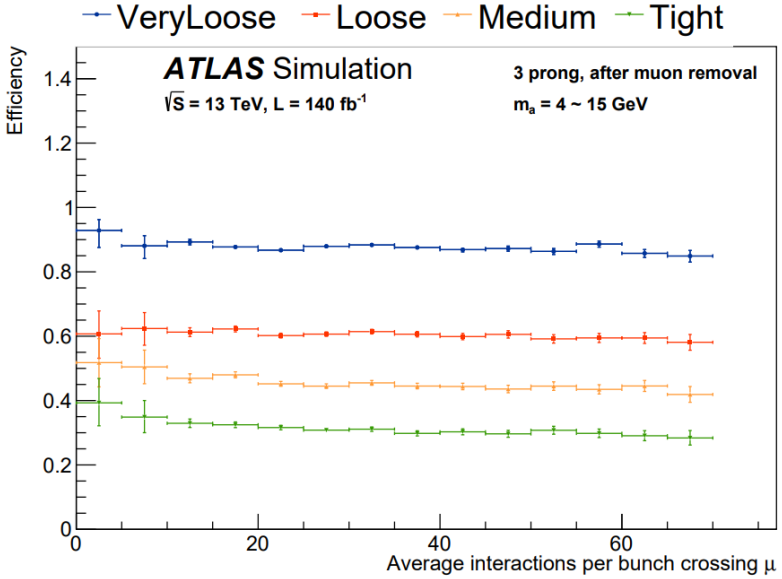

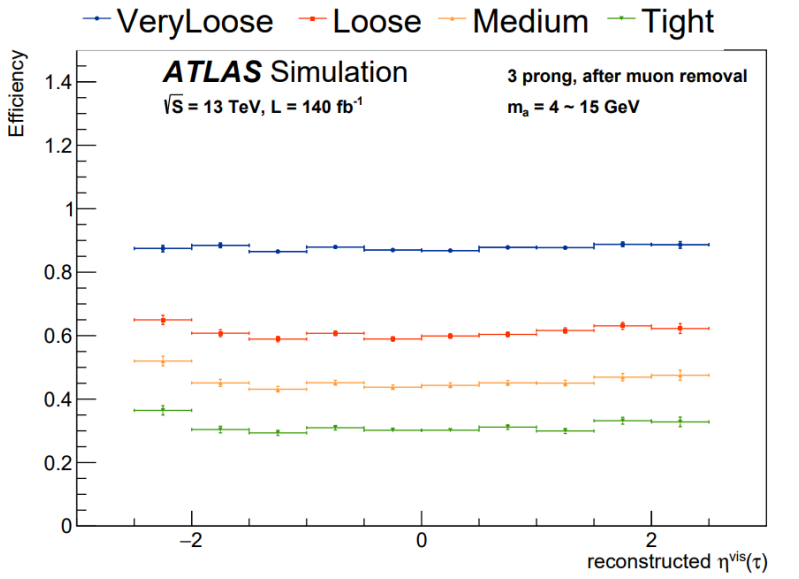

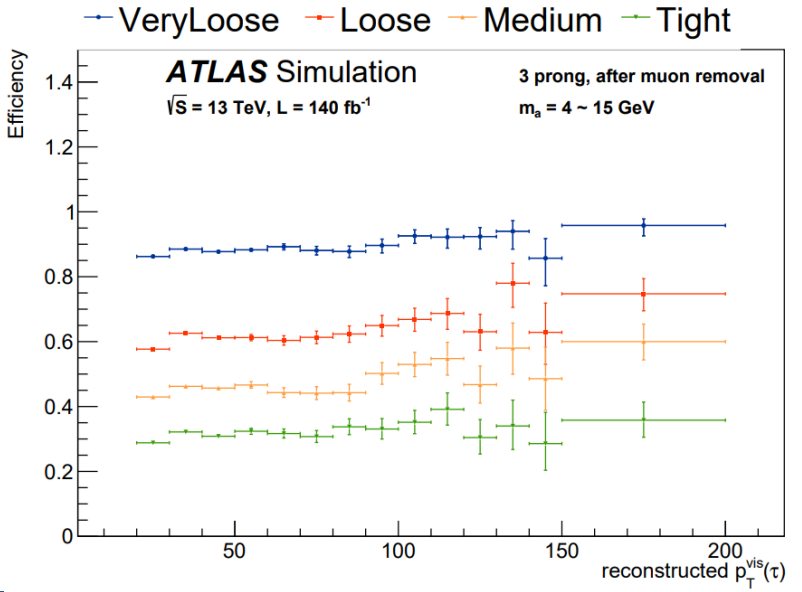

Tau Energy difference

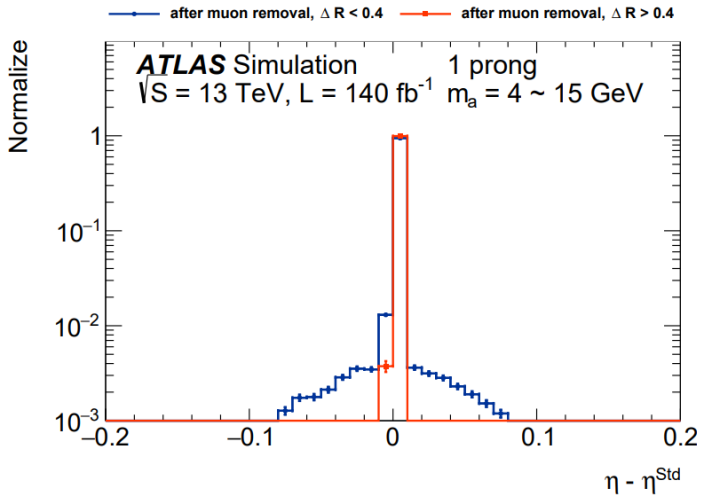

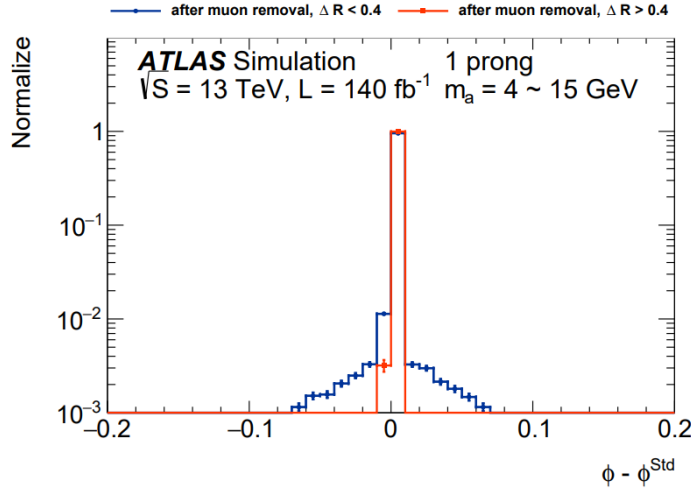

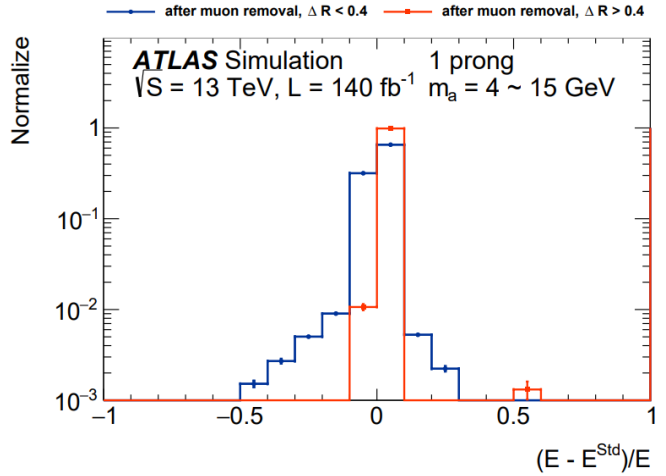

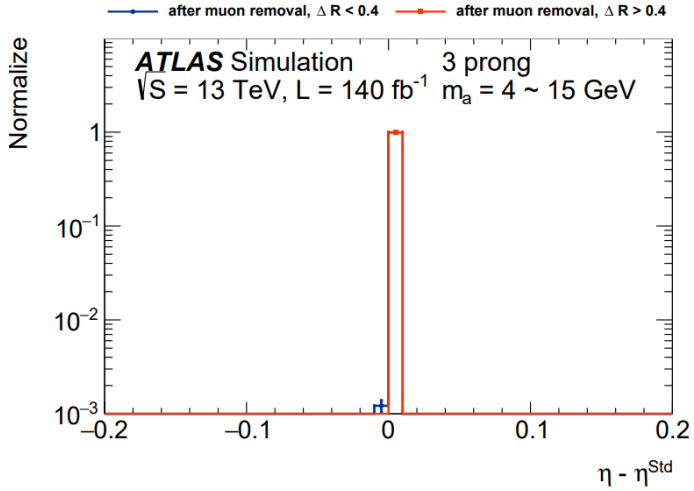

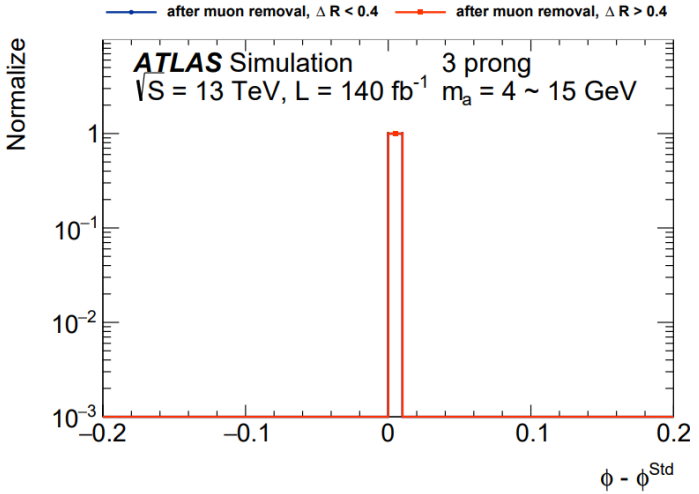

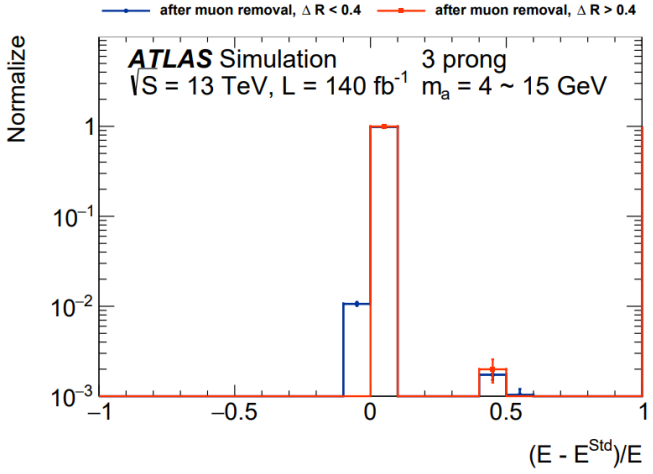

- Very small difference between MuRm taus and Std taus (~3%), which is comparable with the public tau energy scale uncertainty (2-4%) [Eur. Phys. J. C75 (2015) 303]

Tau id variables distribution after muon removal

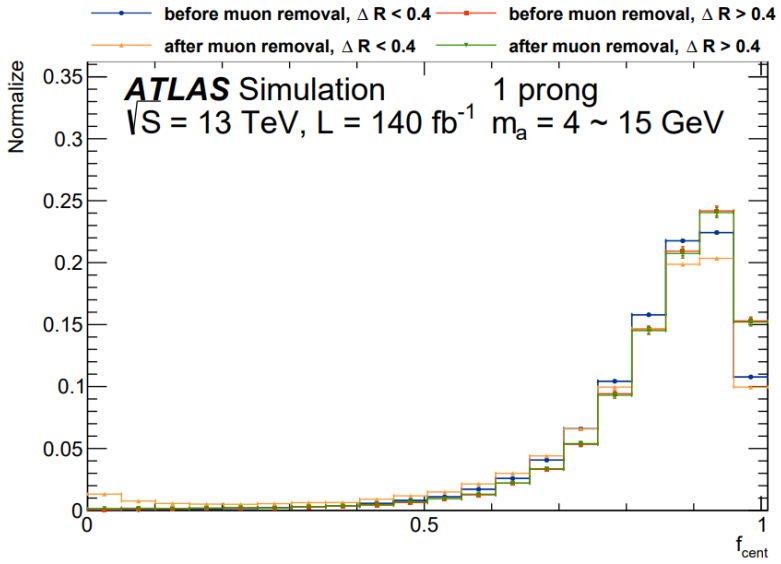

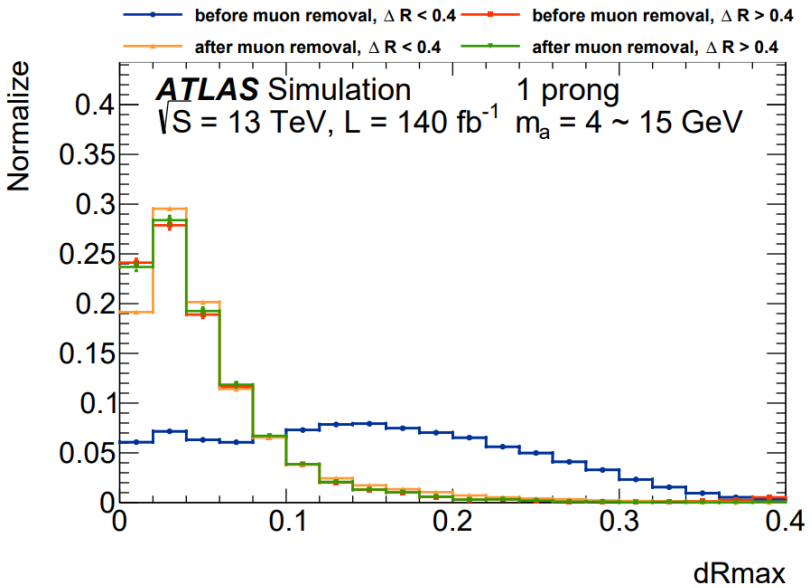

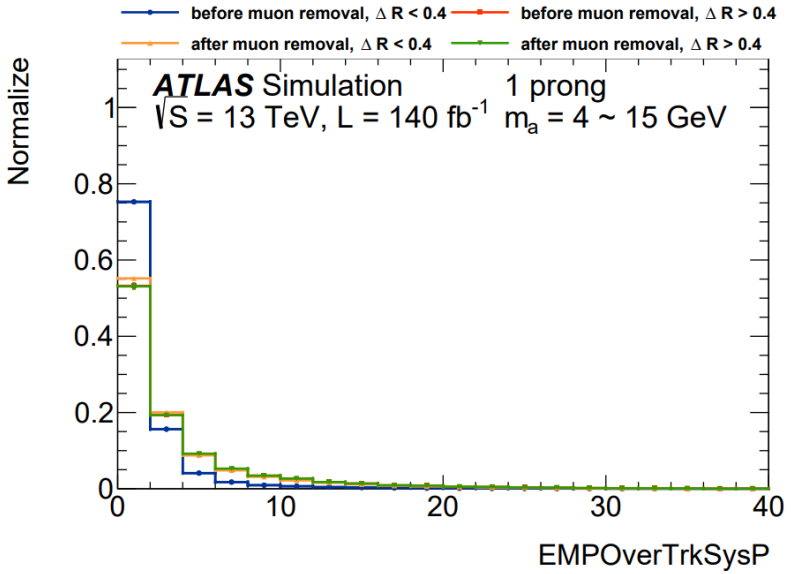

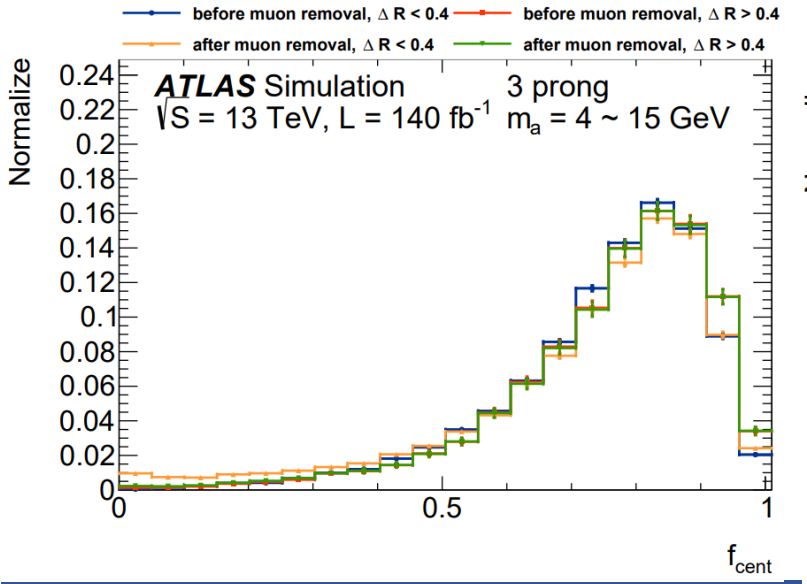

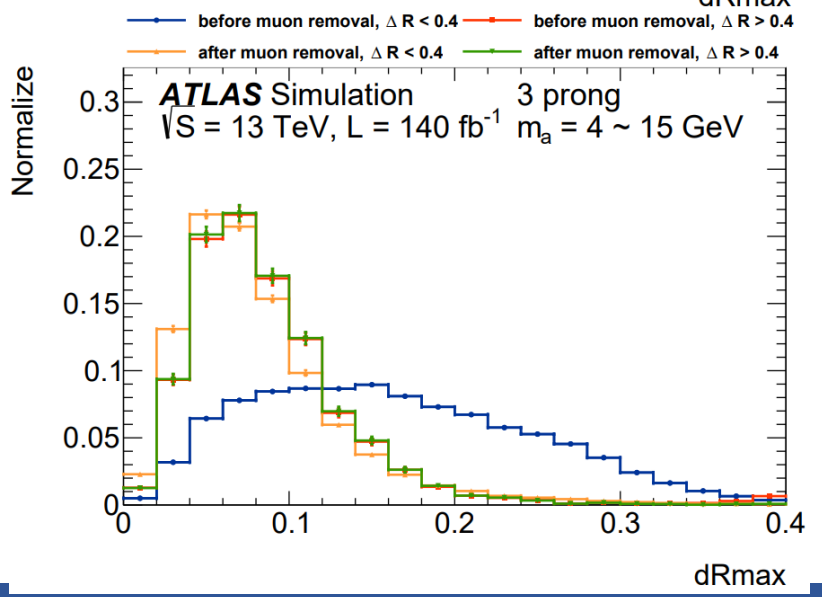

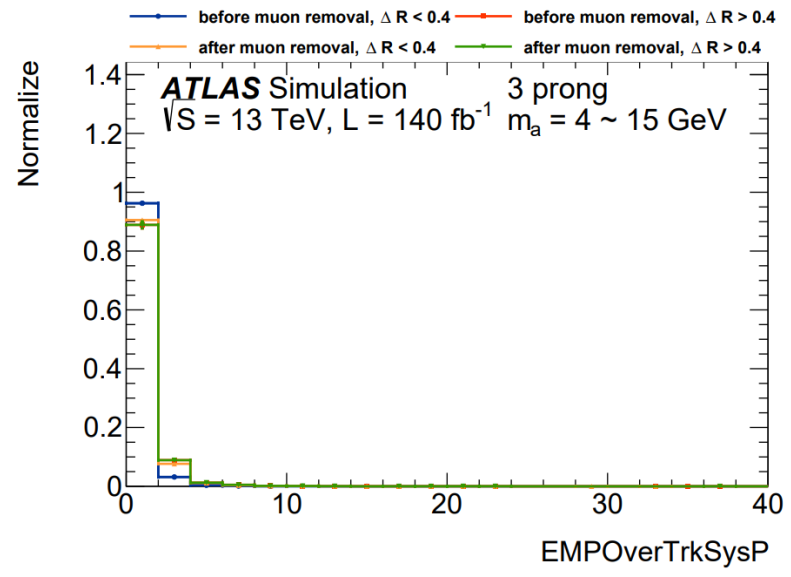

Tau id variables distribution after muon removal

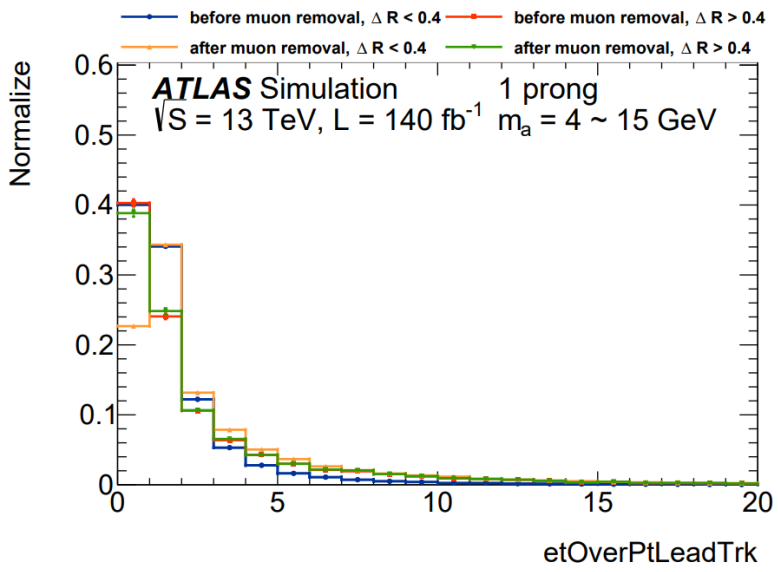

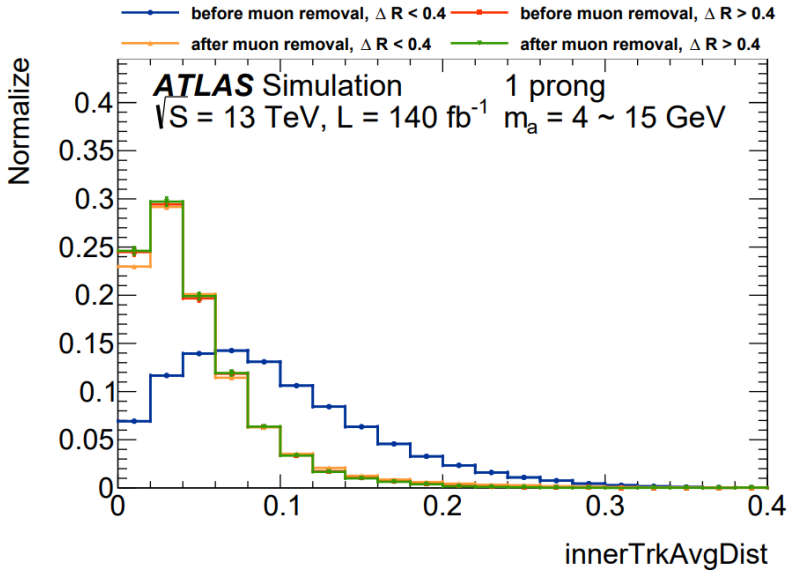

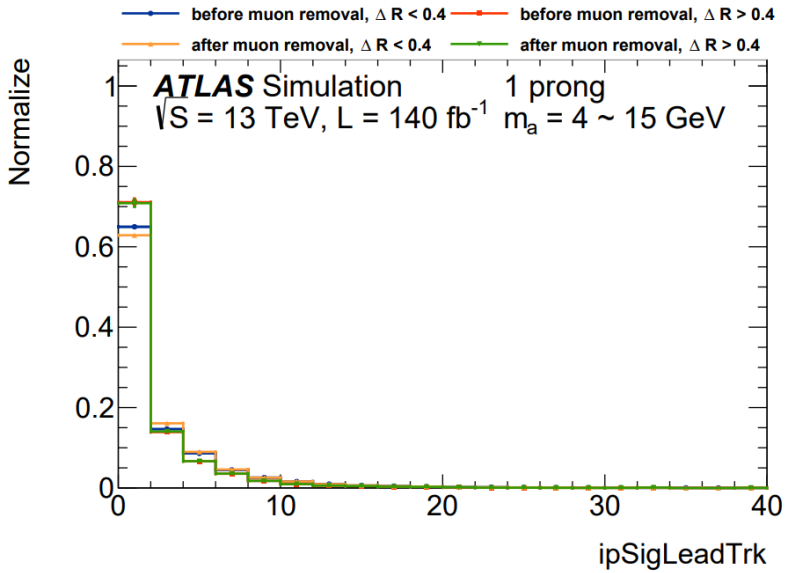

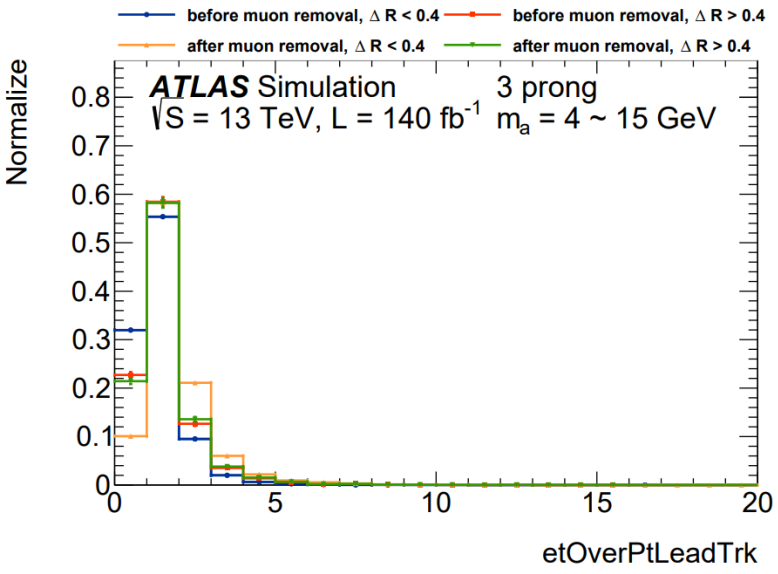

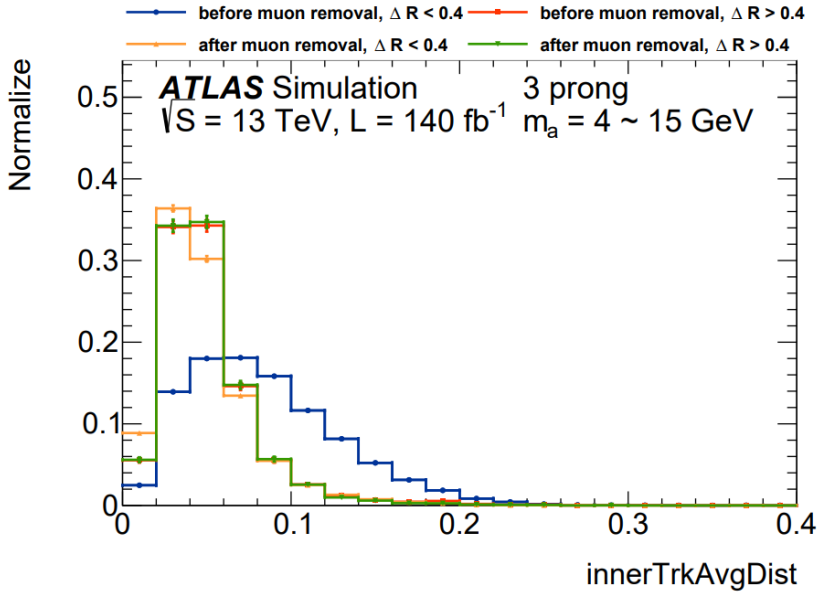

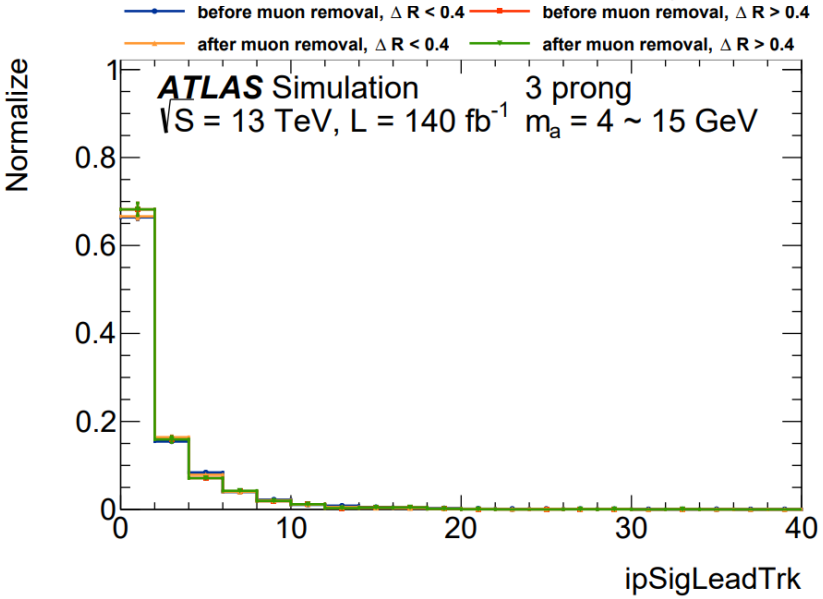

Tau id variables distribution after muon removal

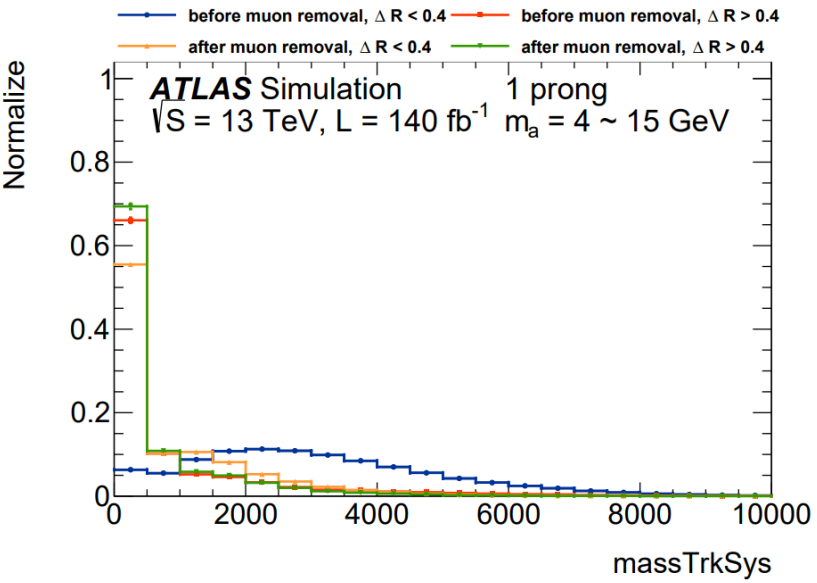

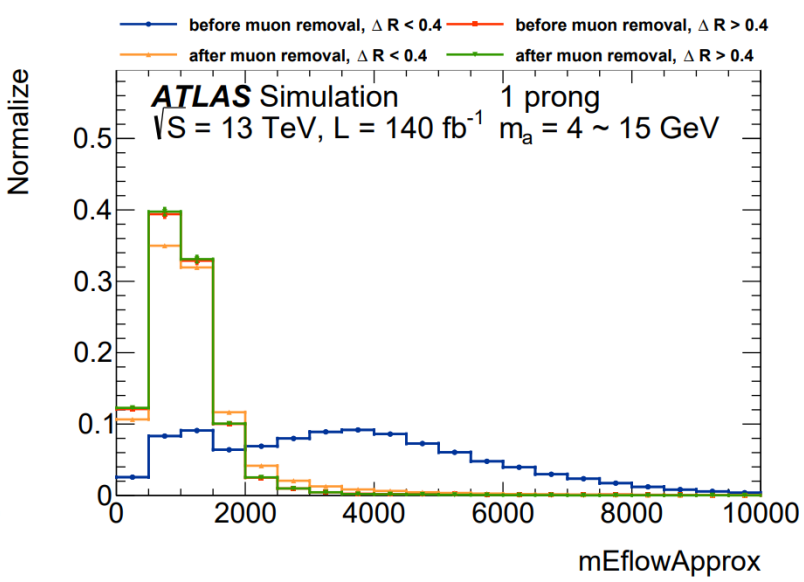

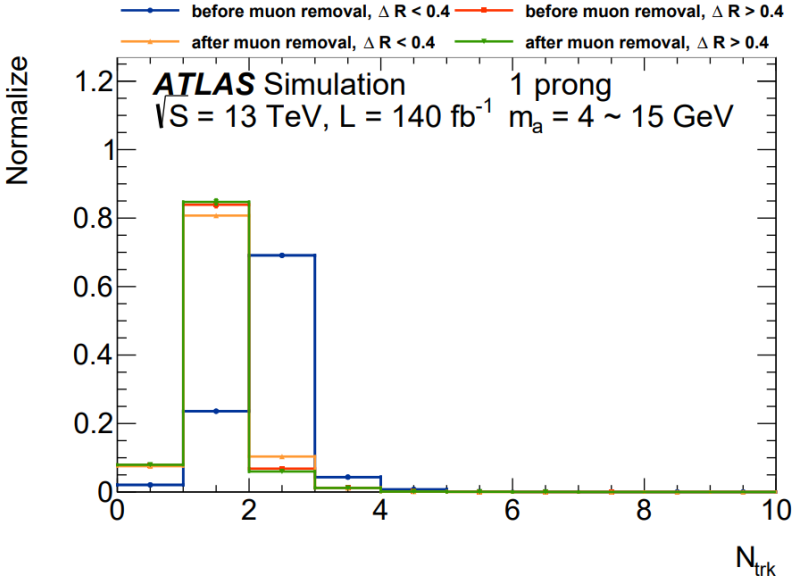

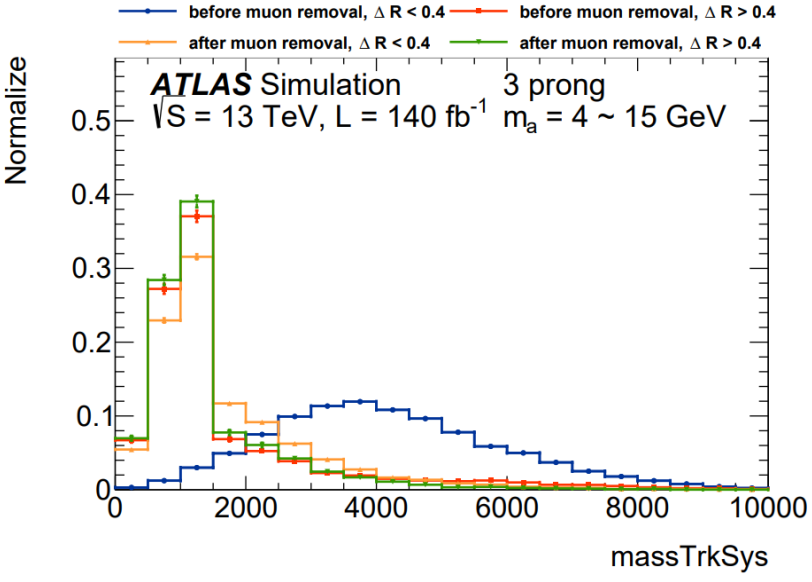

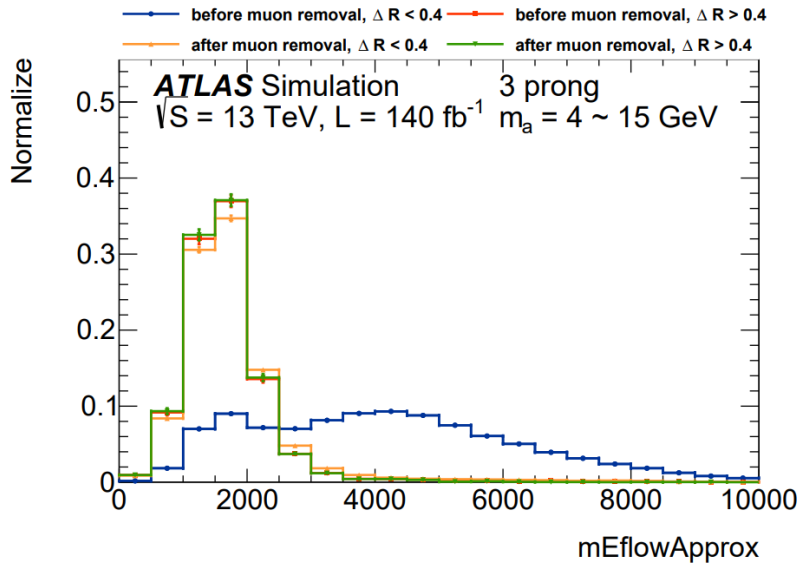

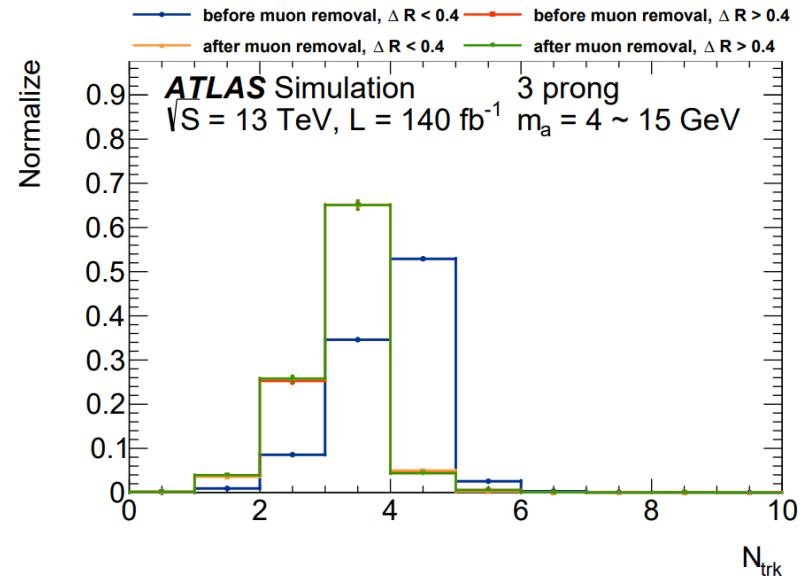

Tau id variables distribution after muon removal

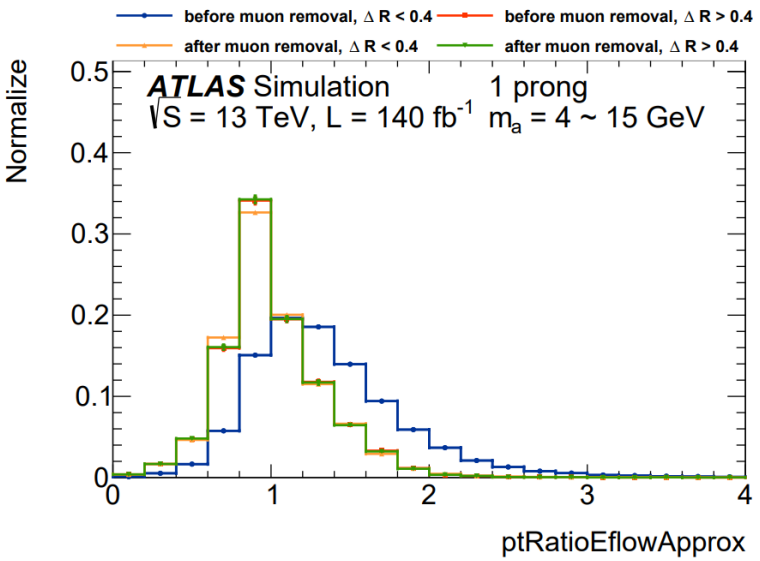

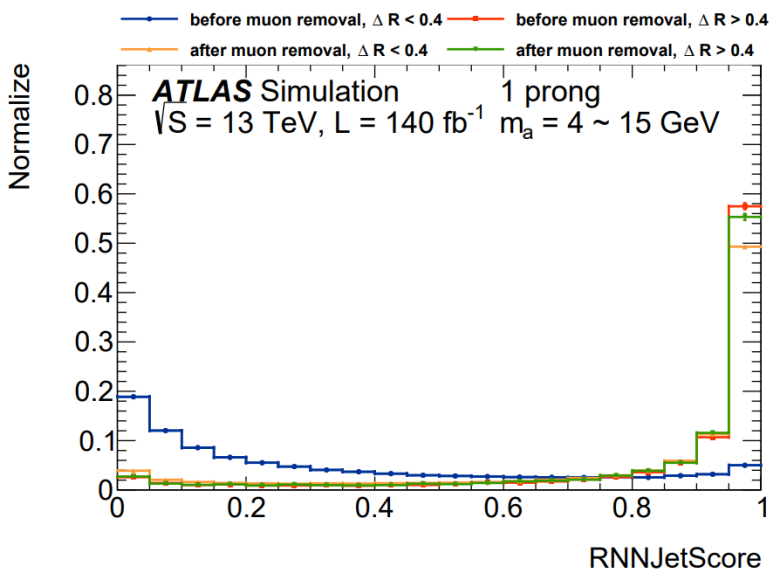

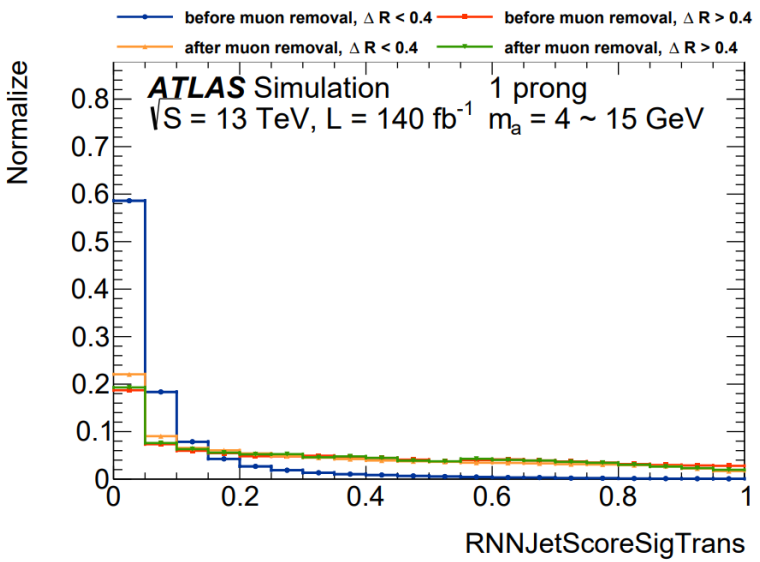

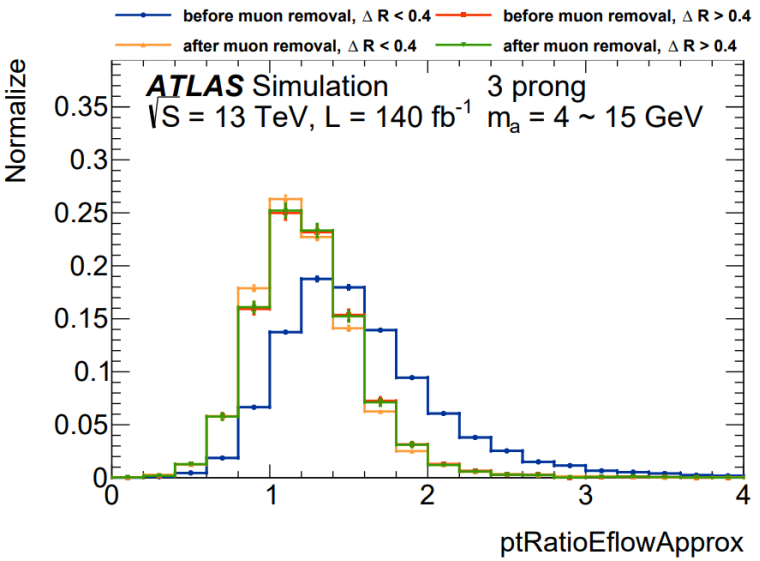

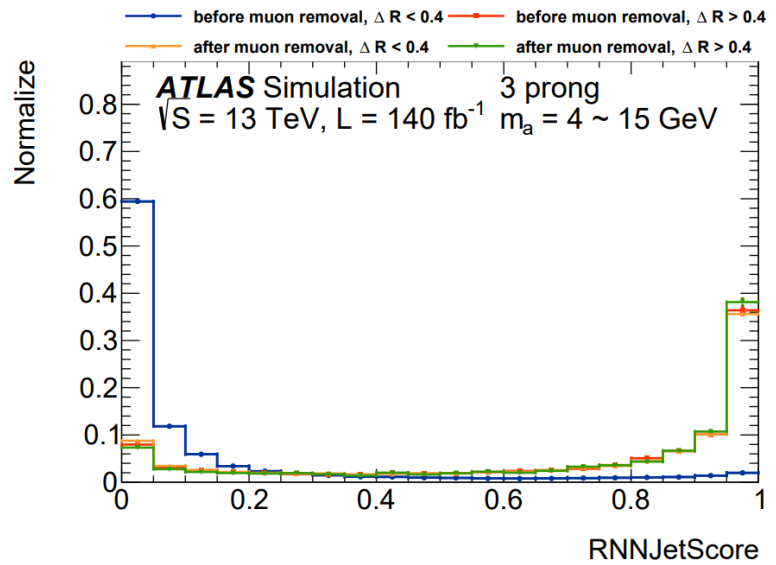

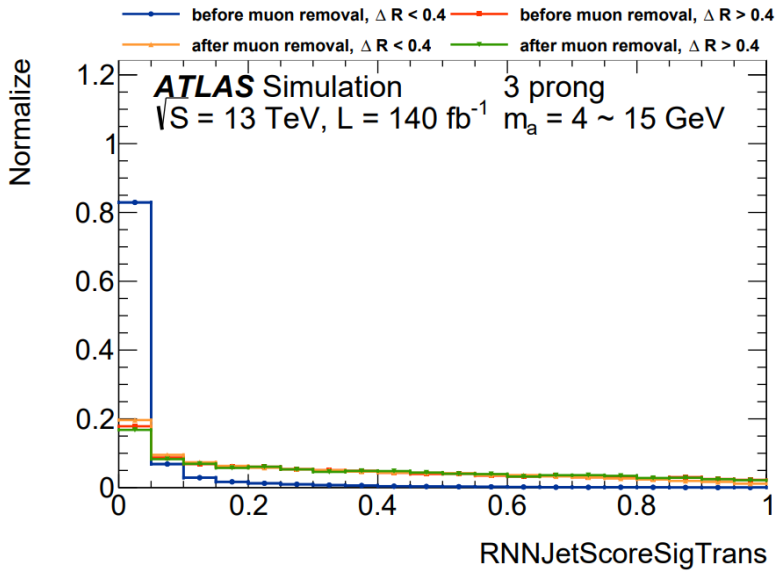

Tau id variables distribution after muon removal

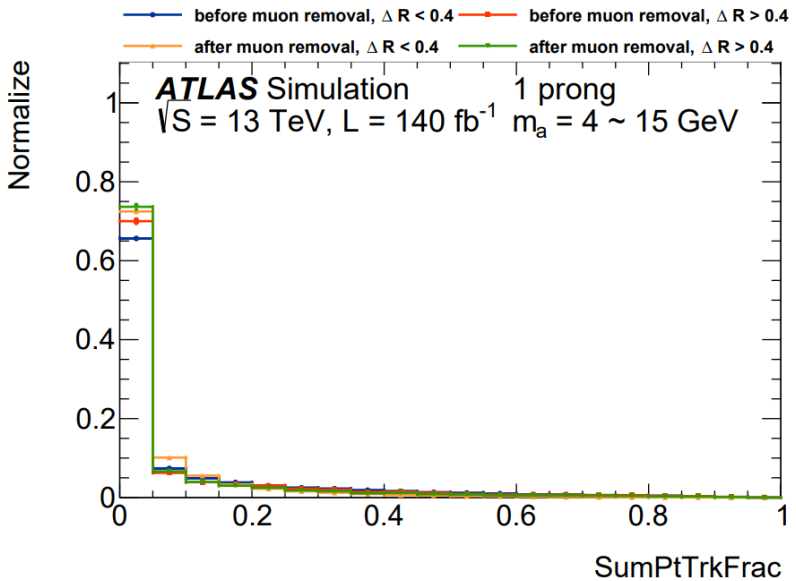

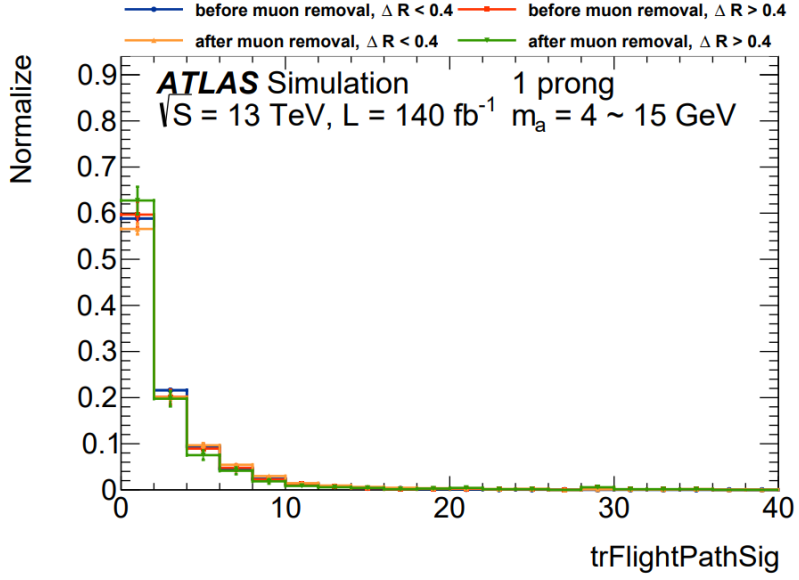

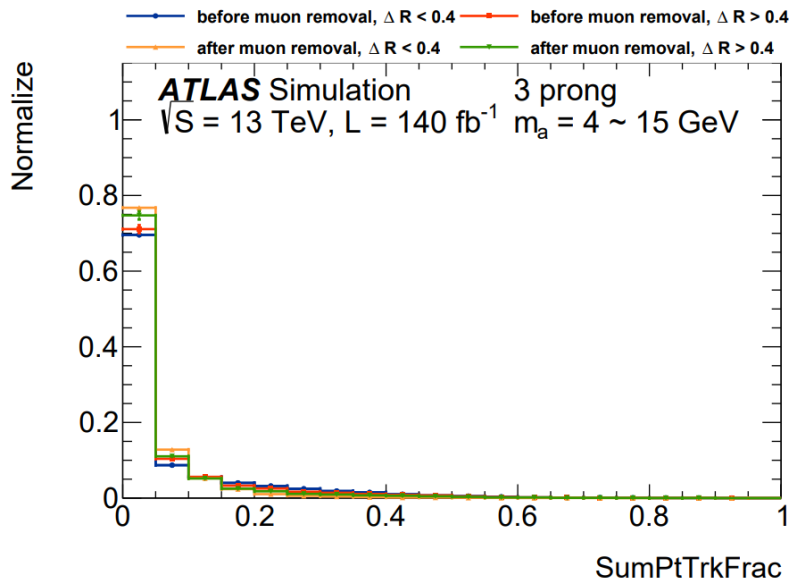

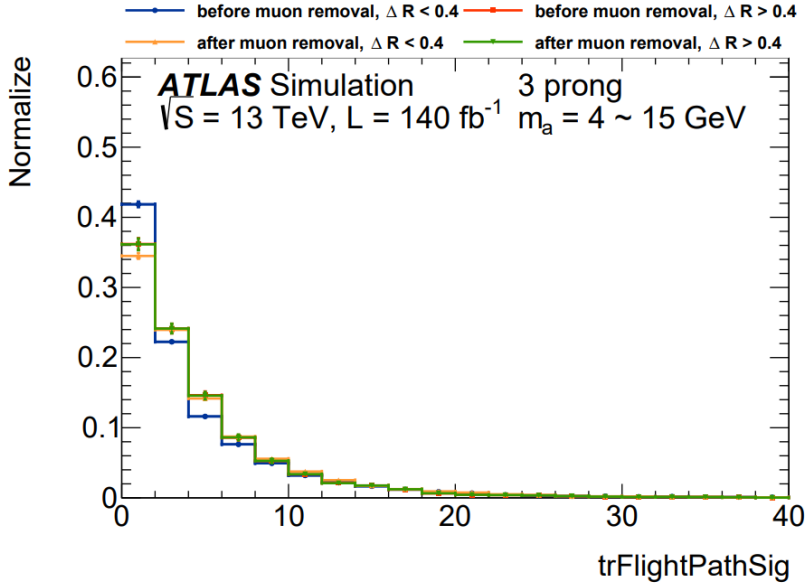

Efficiency from truth tau

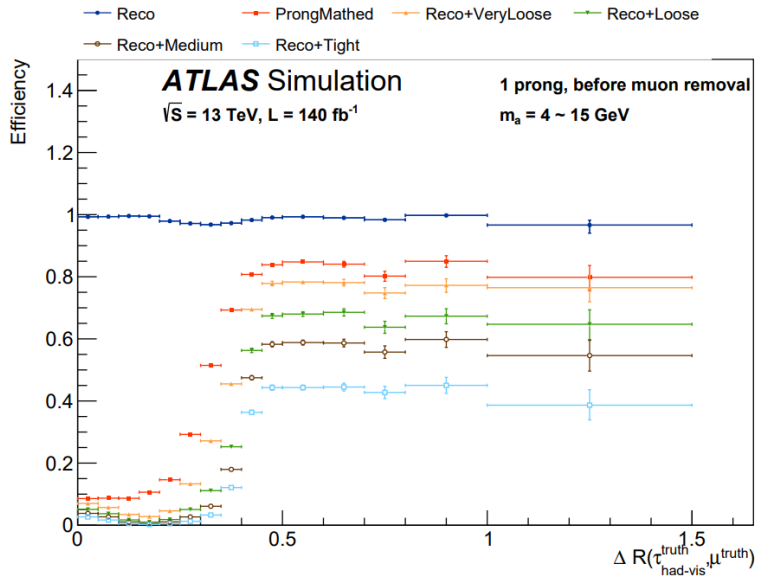

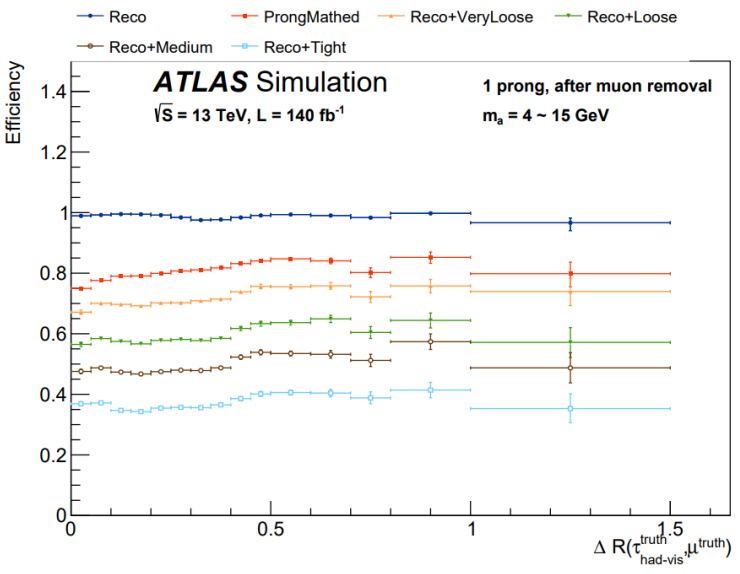

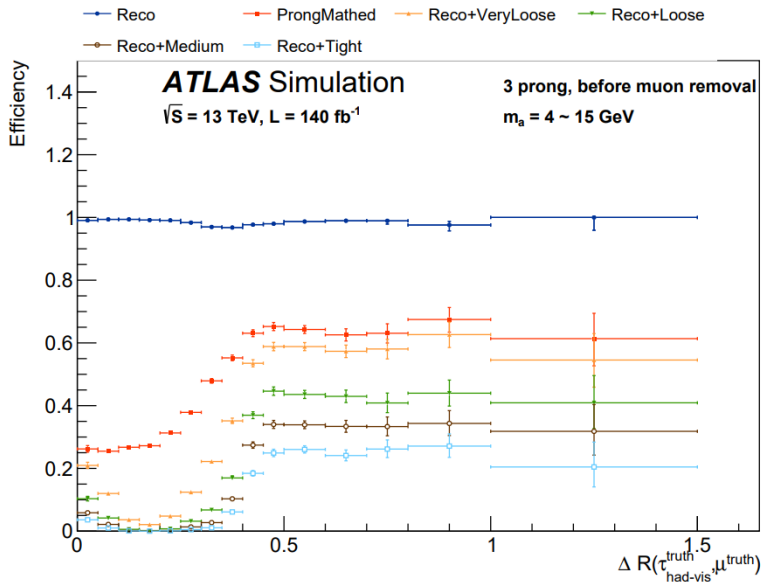

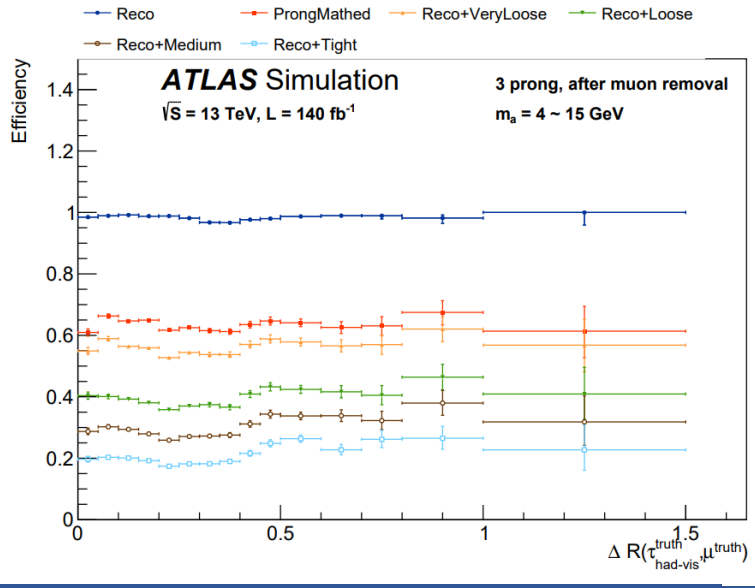

Efficiency from truth tau

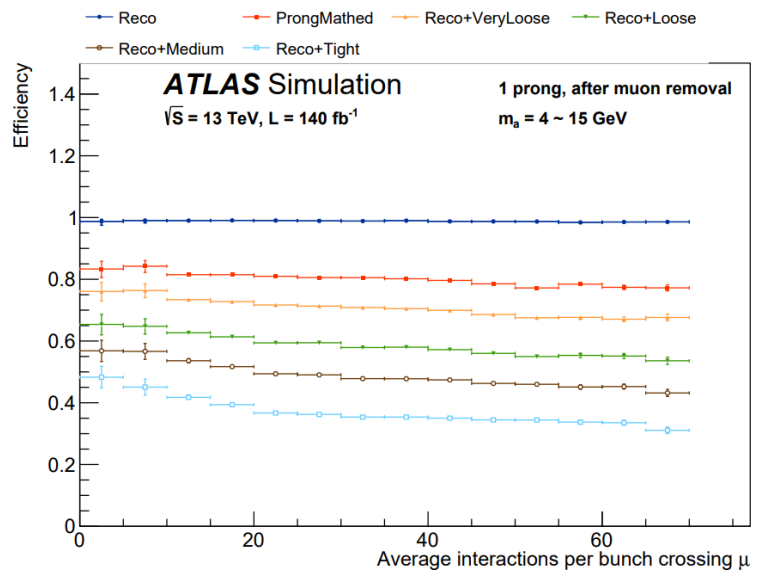

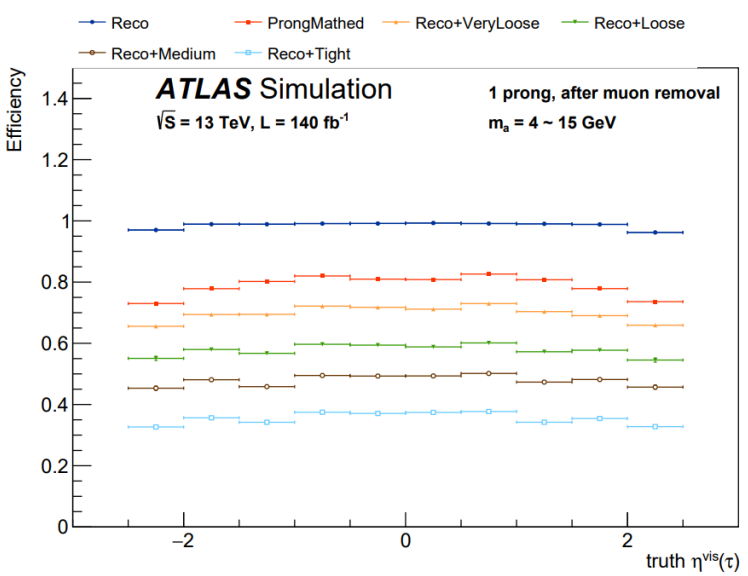

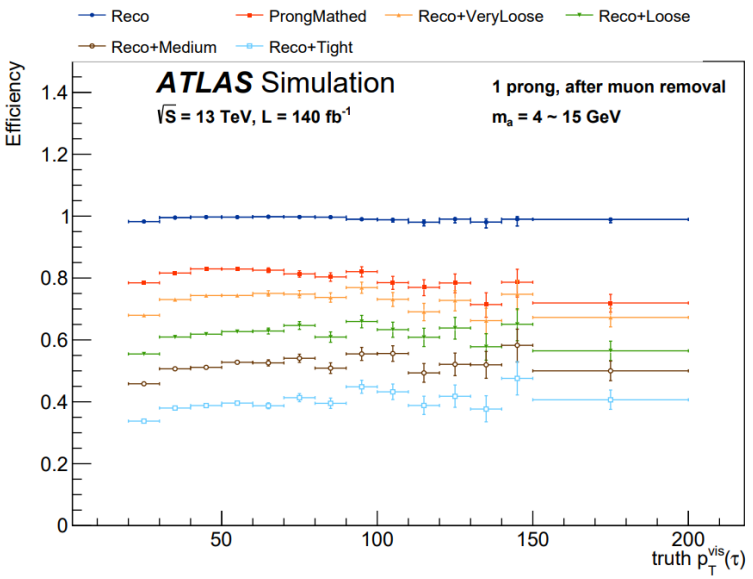

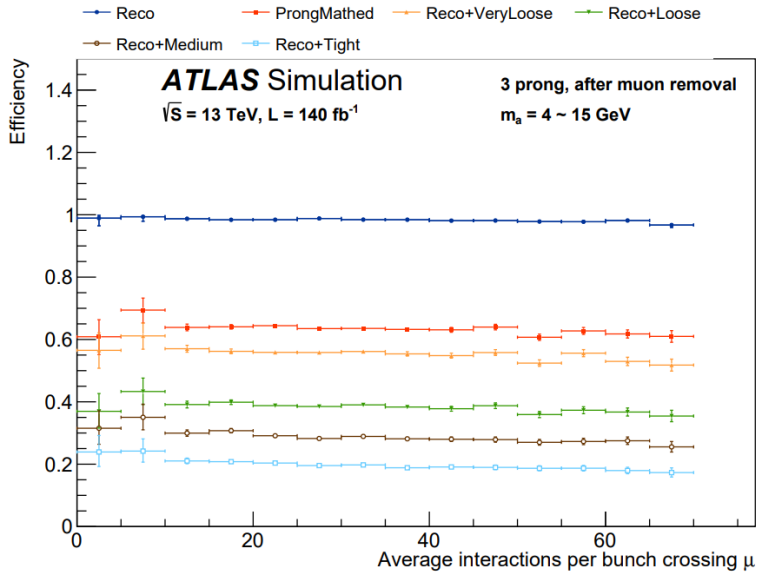

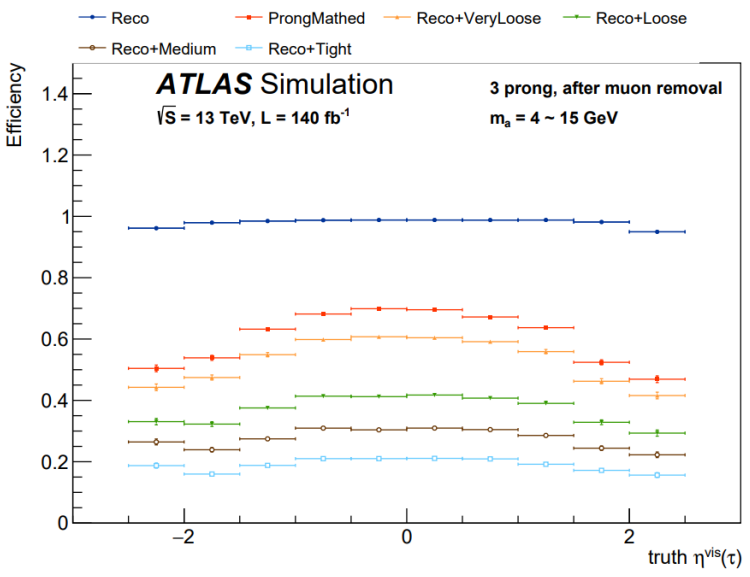

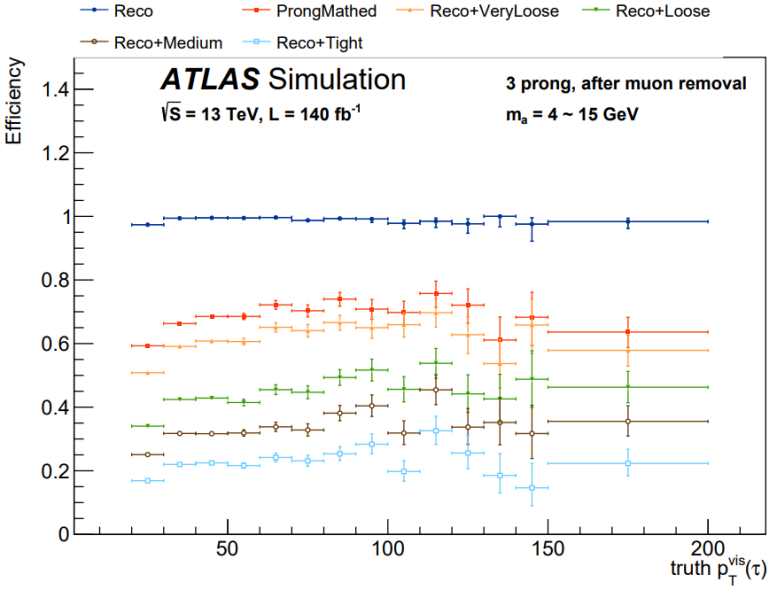

Efficiency from reconstructed tau

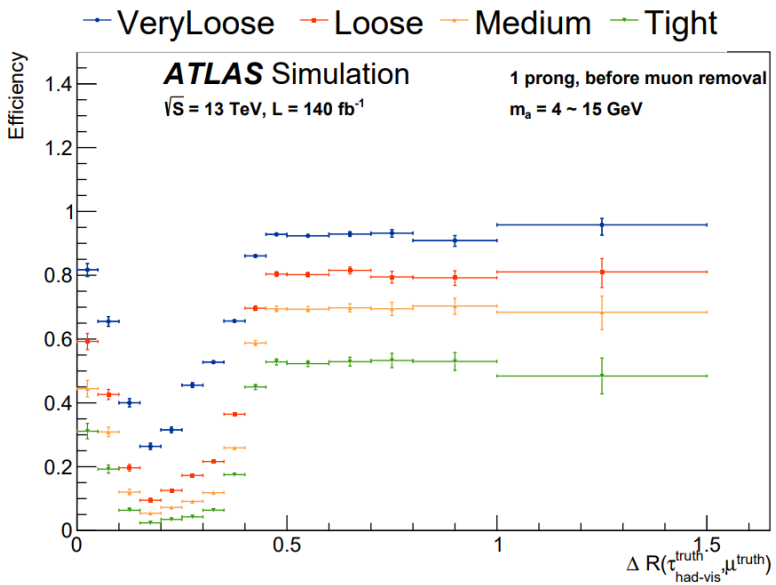

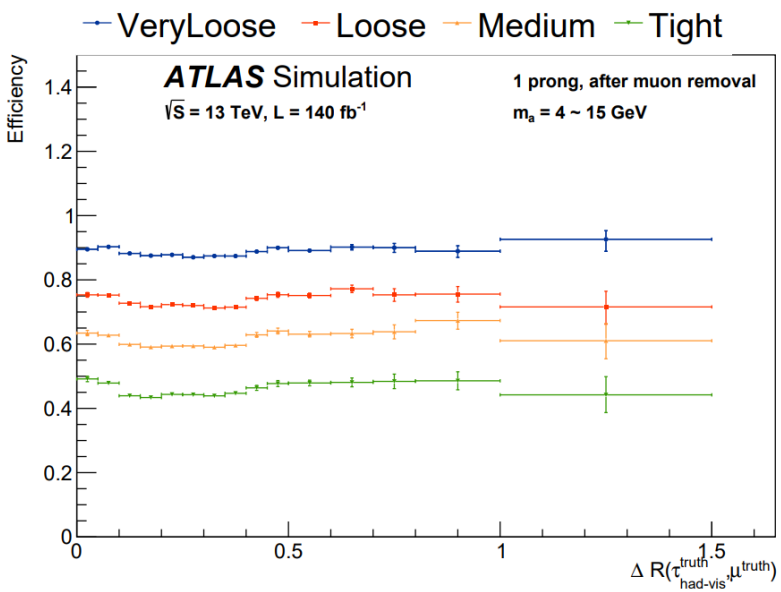

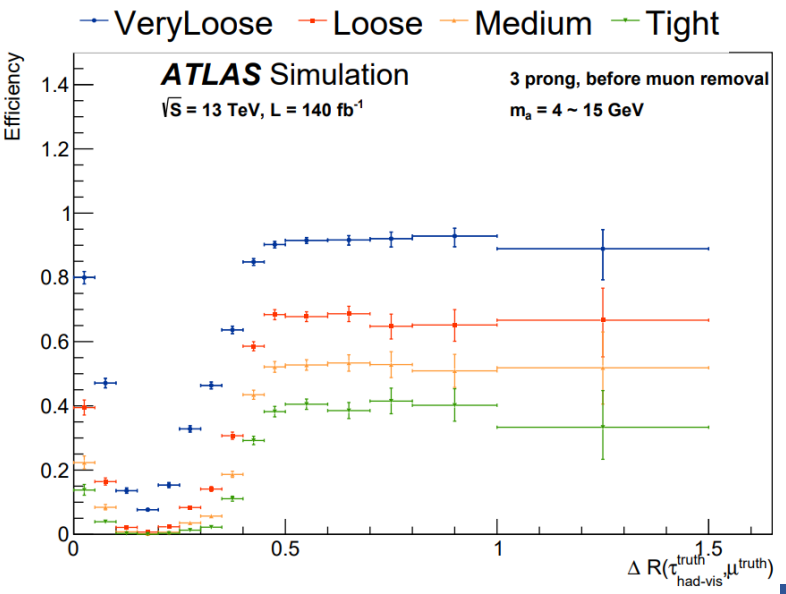

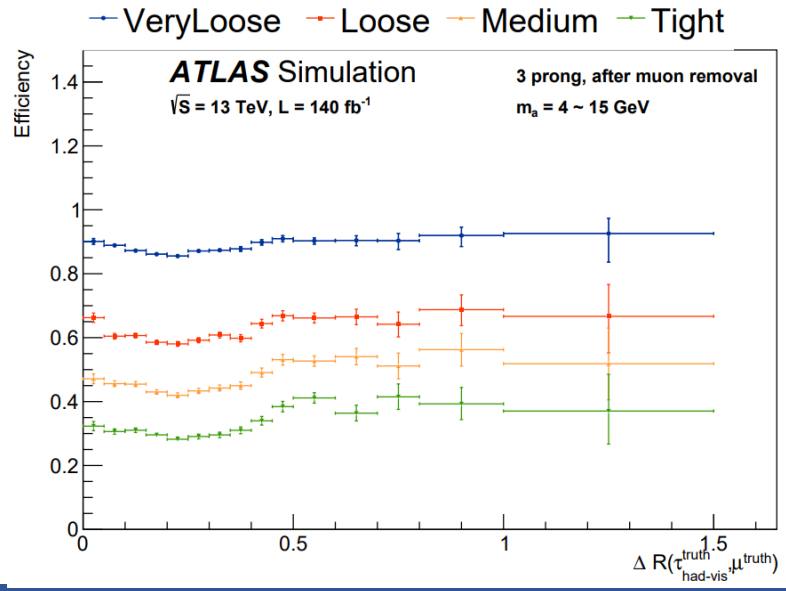

Efficiency from reconstructed tau

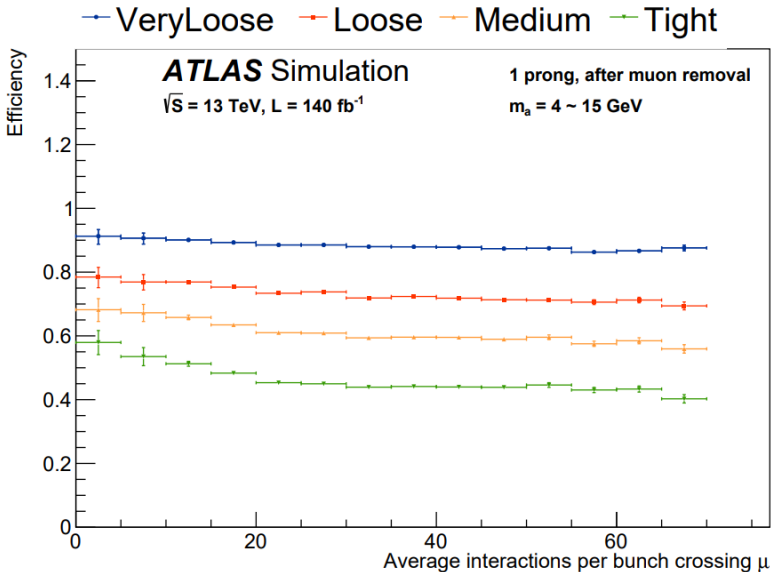

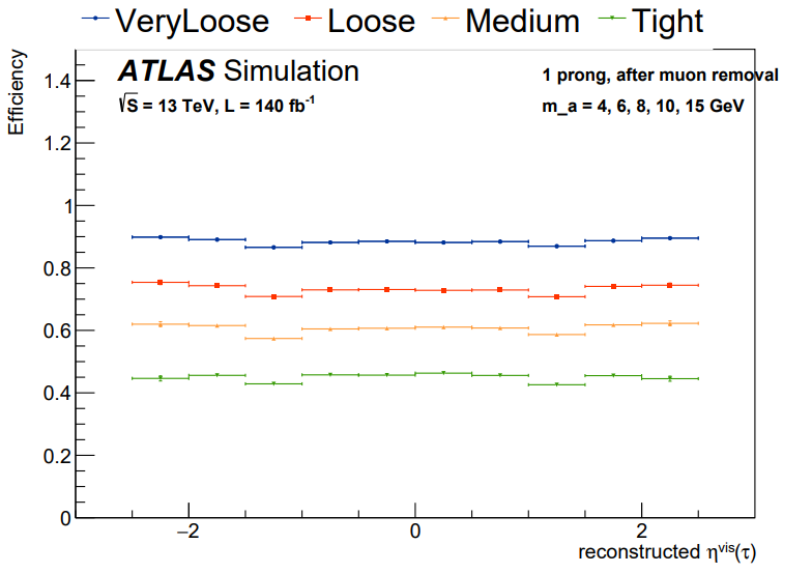

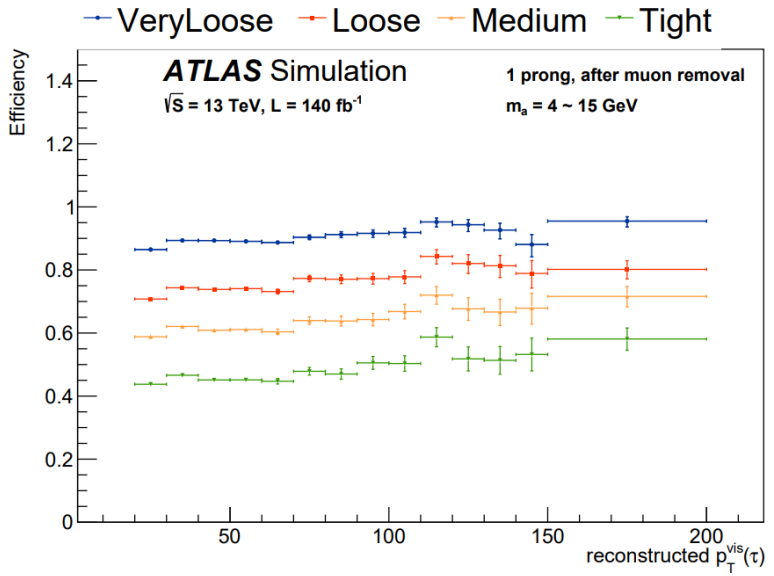

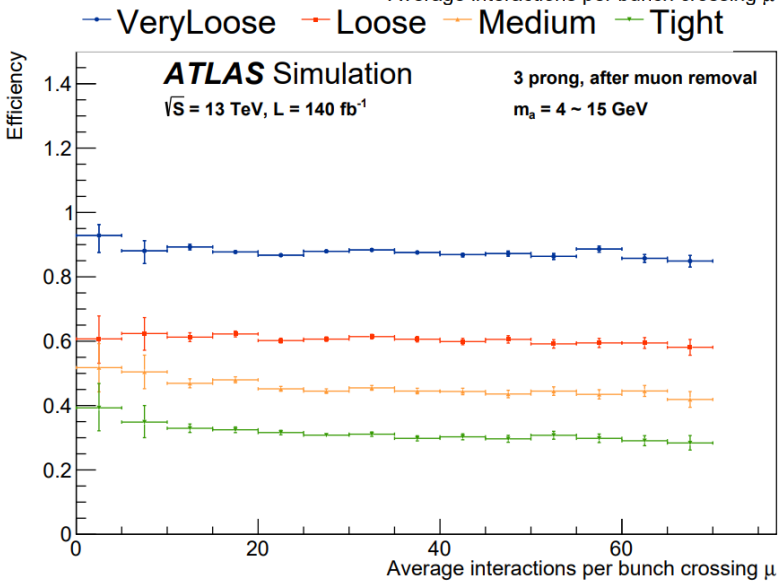

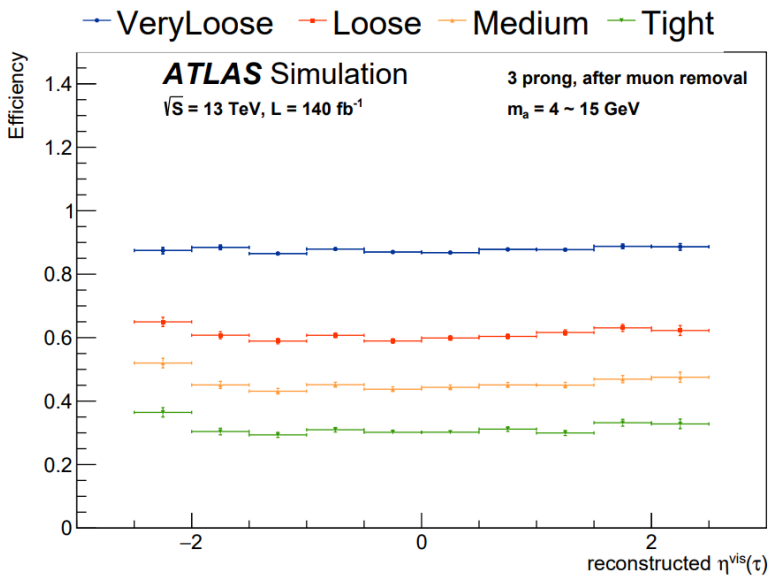

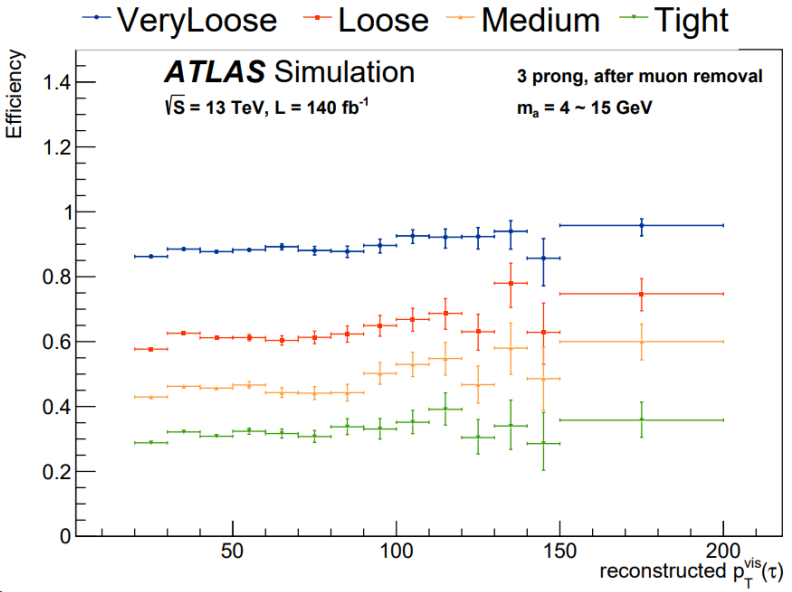

Tau Energy difference

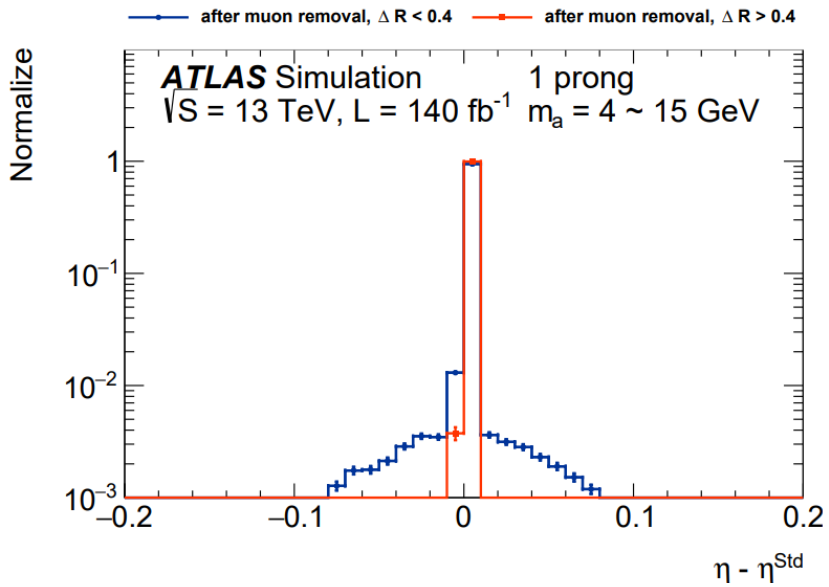

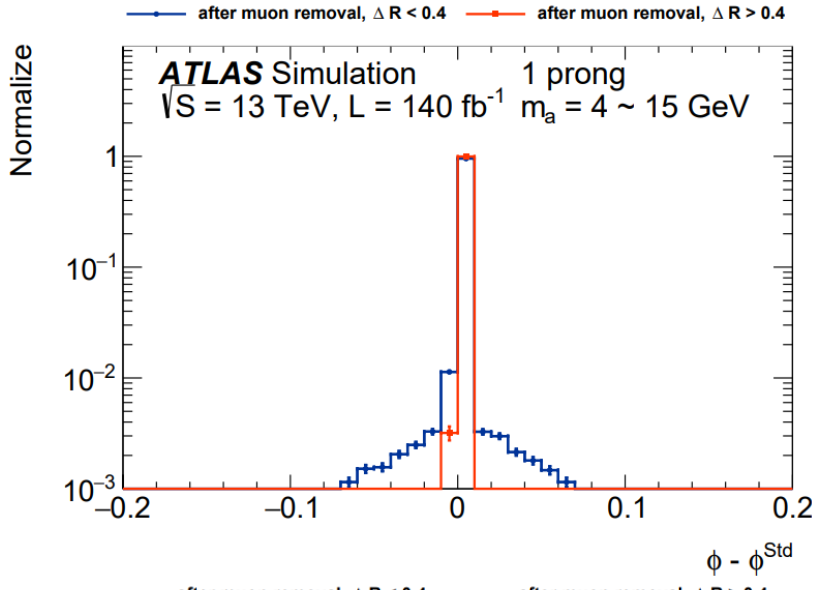

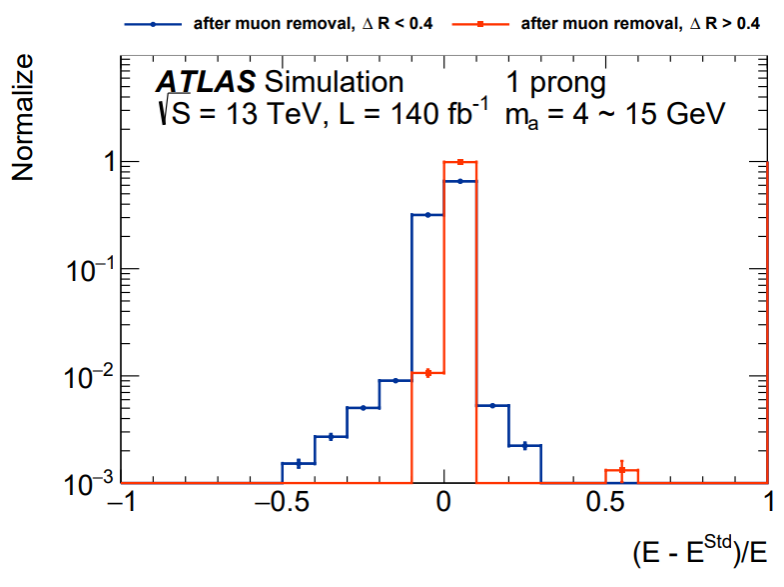

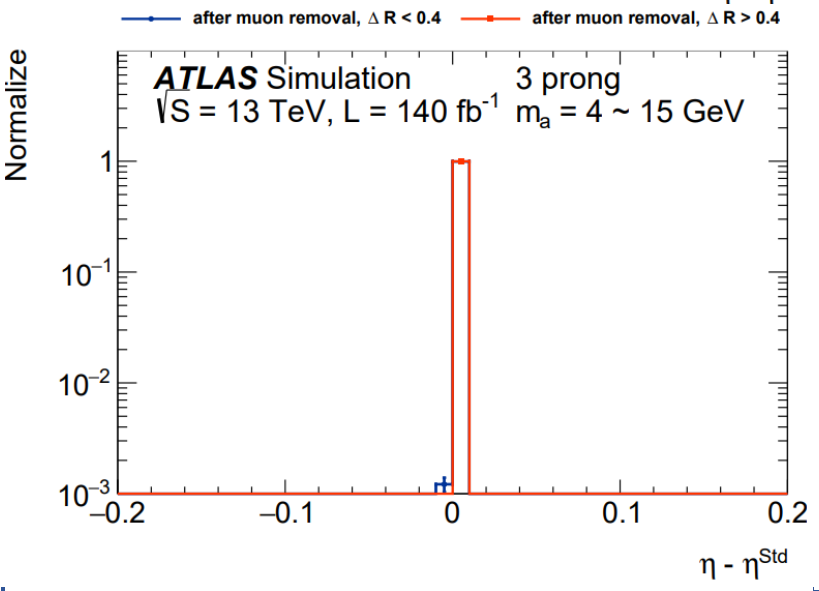

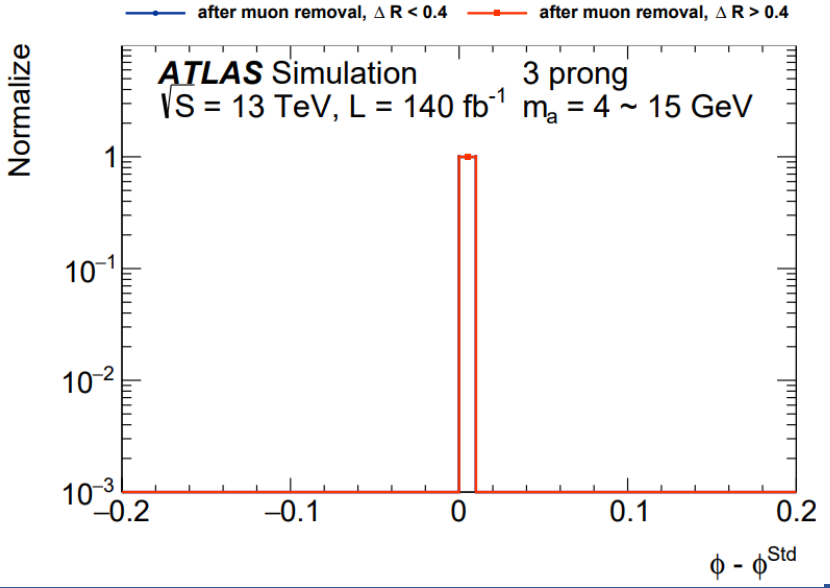

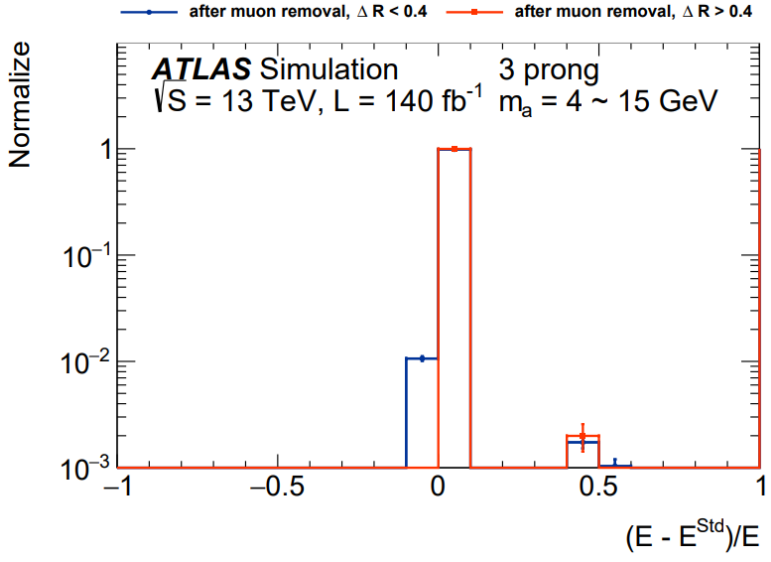

The discrepancy between truth and reco visible mass

- The variable "average $m_{\mu\tau}^{vis}$" is used for the final fitting.
  - average $m_{\mu\tau}^{vis} = (m_{\mu\tau_1}^{vis} + m_{\mu\tau_2}^{vis})/2$,
  - $m_{\mu\tau}^{vis} = \sqrt{2p_T^{\mu}p_T^{\tau}(\cosh(\eta^{\mu}-\eta^{\tau}) - \cos(\phi^{\mu}-\phi^{\tau}))}, (m=0, E \gg m)$
- The reco average $m_{\mu\tau}^{vis}$ shifts to lower value compared to the truth value.
- The reason is because we only re-calculate the RNN ID variables in the muon removal algorithm, but not re-calculate the tau momentum variables (p_T, η, ϕ).
- Solution : Correct the tau momentum in the SR and VR.
  - Only taus having charged tracks overlapped with muon should be corrected
  - The total number of events for each region keeps the same

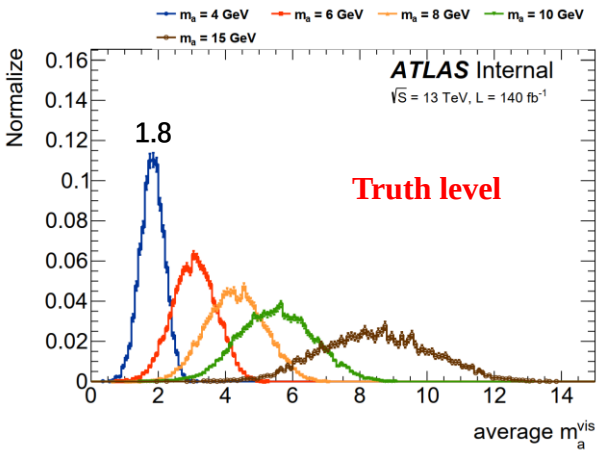

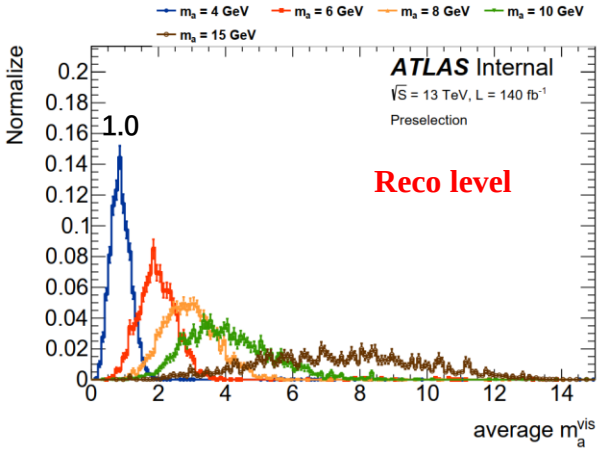

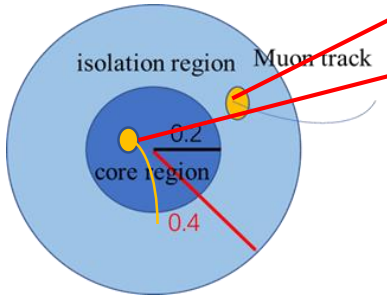

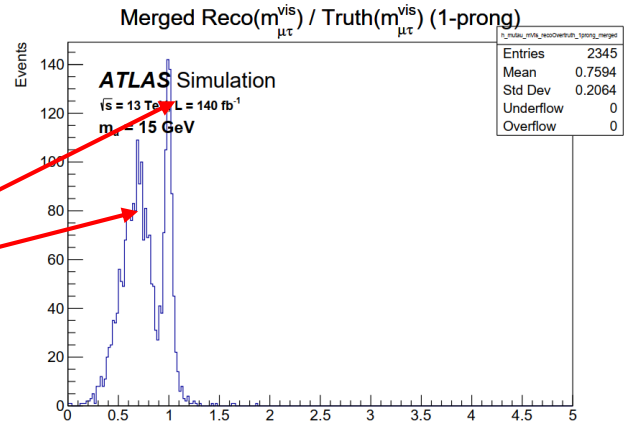

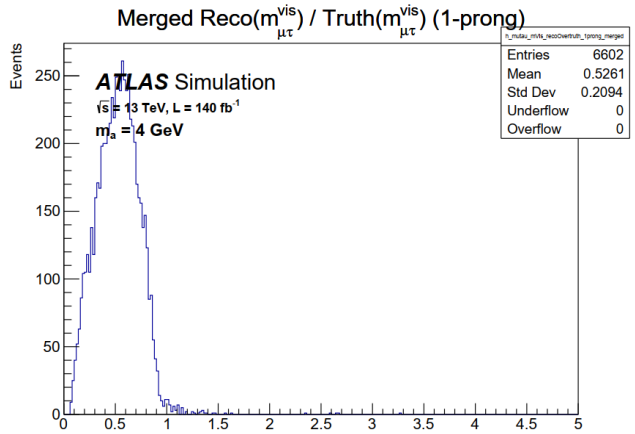

How to correct the tau momentum

- Step 1: Correct the p_T^τ
  - In the same truth p_T bin, the average reco p_T are different for the taus with OL muon and without OL muon.
  - We can make the ratio of overlapped tau p_T to unoverlapped tau:
    - OL taus: having charged track overlapped with muon; UnOL: no charged track overlapped with muon
    - $R(p_T^{OL}, p_T^{\mu}, n_p, \eta) = p_T^{OL}/p_T^{UnOL}$
    - Fit the ratio with a function
  - Correct the p_T^{OL} to p_T^{UnOL} using p_T^{OL}/R

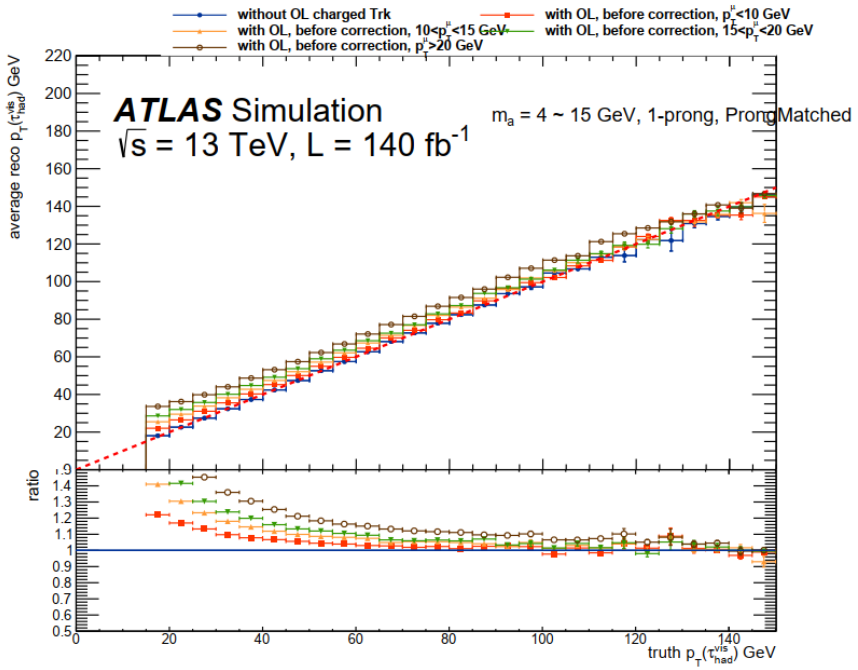

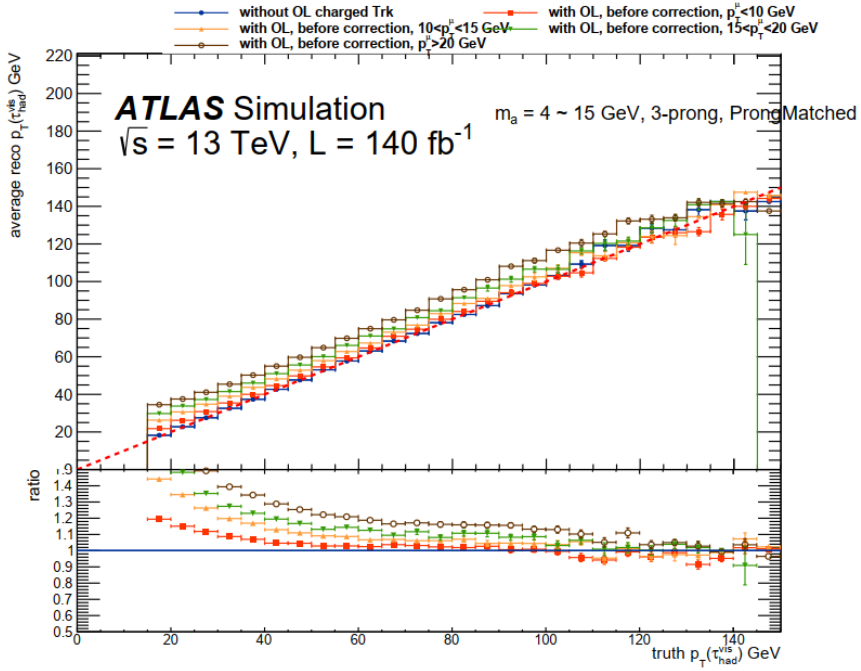

How to correct the tau momentum

- Step 2: Correct the η^{τ} and ϕ^{τ}
  - After correcting the p_T , we have:
    - $\vec{p}_{\mu\tau}(p_T^{\mu\tau}, \eta^{\mu\tau}, \phi^{\mu\tau})$
    - $\vec{p}_{\tau}(p_T^{\tau}, \eta^{\tau}, \phi^{\tau})$
    - $\vec{p}_{\mu}(p_T^{\mu}, \eta^{\mu}, \phi^{\mu})$
    - Where variables marked with green color are already known, variables marked with red color are unknown
  - According to the momentum conservation, we have $\vec{p}_{\mu\tau} = \vec{p}_{\mu} + \vec{p}_{\tau}$
  - We solve the equation:
    - $\phi^{\tau} = \phi^{\mu\tau} - sin^{-1}[p_T^{\mu}/p_T^{\tau}\, sin(\phi^{\mu} - \phi^{\mu\tau})]$
    - $p_T^{\mu\tau} = (p_T^{\tau}\cos\phi^{\tau} + p_T^{\mu}\cos\phi^{\mu})/cos\phi^{\mu\tau}$
    - $\eta^{\tau} = tanh^{-1}[(p_T^{\mu\tau}tanh(\eta^{\mu\tau}) - p_T^{\mu}tanh(\eta^{\mu}))/p_T^{\tau}]$
  - Finally, we can correct η^{τ} and ϕ^{τ} using the above formulas.

Fit the ratio p_T^{OL}/p_T^{UnOL}

- The function used to fit the p_T ratio is the energy resolution parametrization function:
  - energy resolution parameterization: $\frac{\sigma_E}{E} = \frac{a}{\sqrt{E}} + b + \frac{c}{E}$
  - $R(p_T^{OL}, p_T^{\mu}, \eta, n_p) = p_T^{OL}/p_T^{UnOL} = \frac{a}{p_T^{OL}} + b + \frac{c}{p_T^{OL}}$
- The barrel and endcap have almost the same ratio curves, so I merged them into one ratio curve for final parameterization:
  - $R(p_T^{OL}, p_T^{\mu}, n_p) = p_T^{OL}/p_T^{UnOL} = \frac{a}{p_T^{OL}} + b + \frac{c}{p_T^{OL}}$

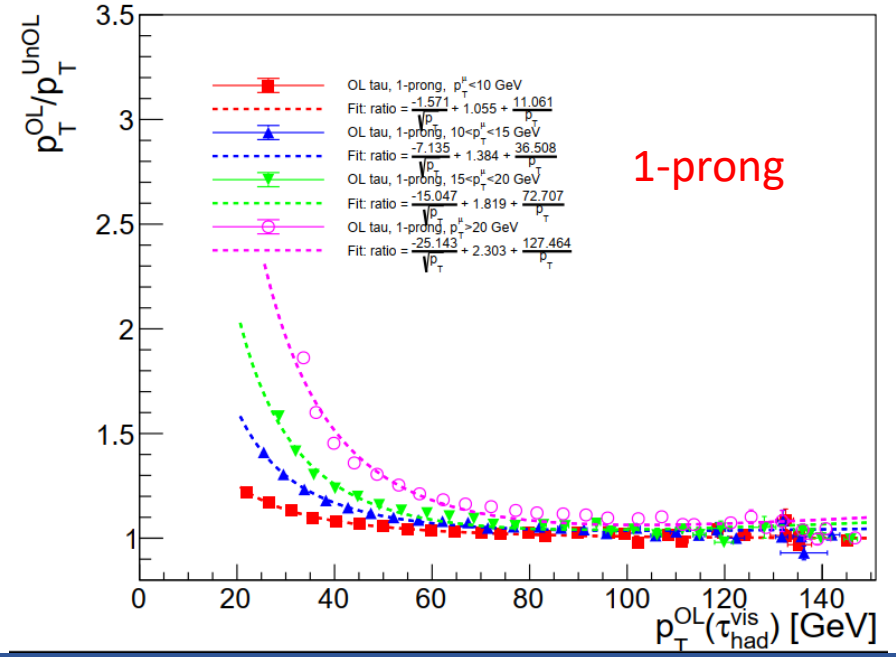

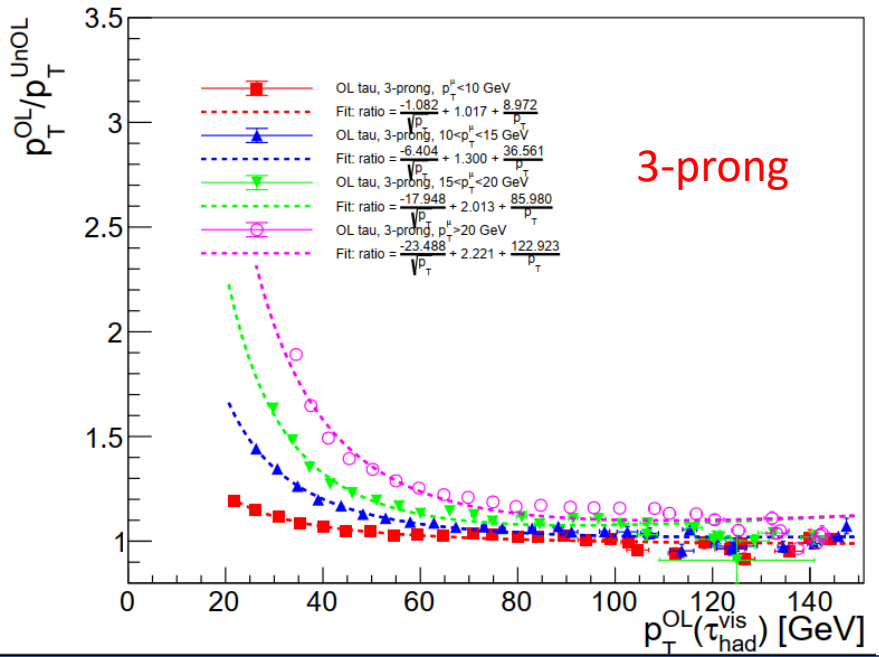

Visible mass $m_{\mu\tau}^{vis}$ correction results

- The reco $m_{\mu\tau}^{vis}$ is consistent with truth $m_{\mu\tau}^{vis}$ after tau momentum correction.
- The m_{τ}^{vis} has a relatively large effect on $m_{\mu\tau}^{vis}$ for the lower mass signal. If we consider truth $m_{\tau}^{vis} = 0$, reco $m_{\mu\tau}^{vis}$ is also consistent with truth $m_{\mu\tau}^{vis}$ for lower masses after correction.

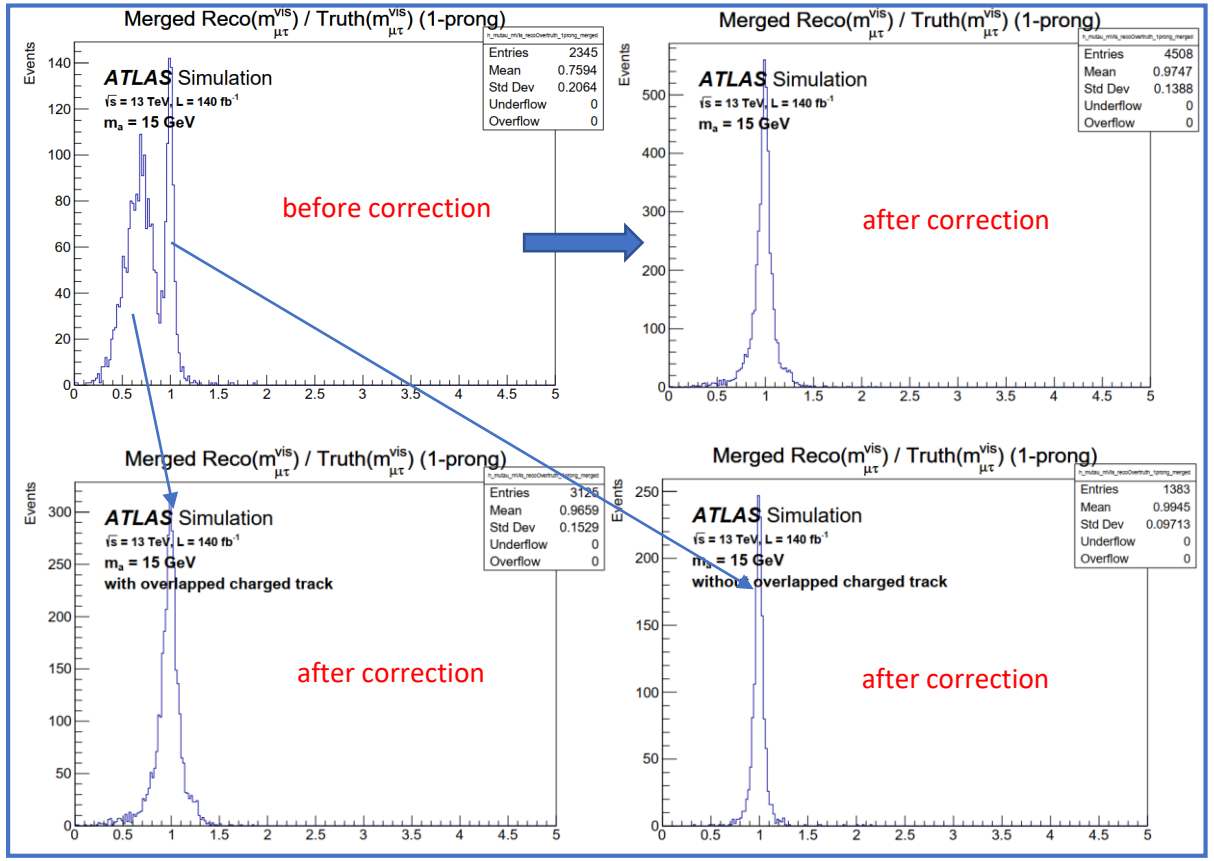

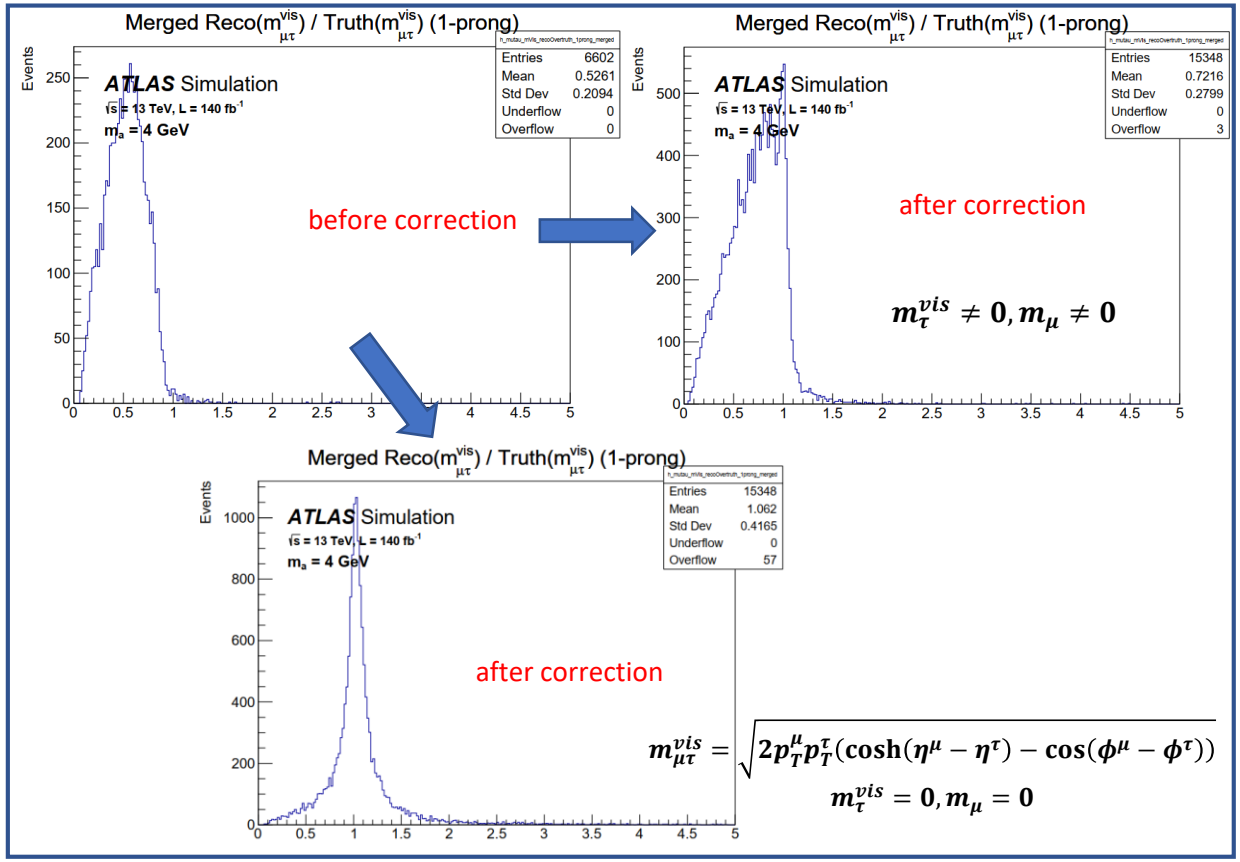

Correction check in validation region

- The tau momentum correction is applied for both data and background in the VRs, then the relevant variables are re-calculated after tau momentum correction.
- The fake prediction still agrees with data after correction.

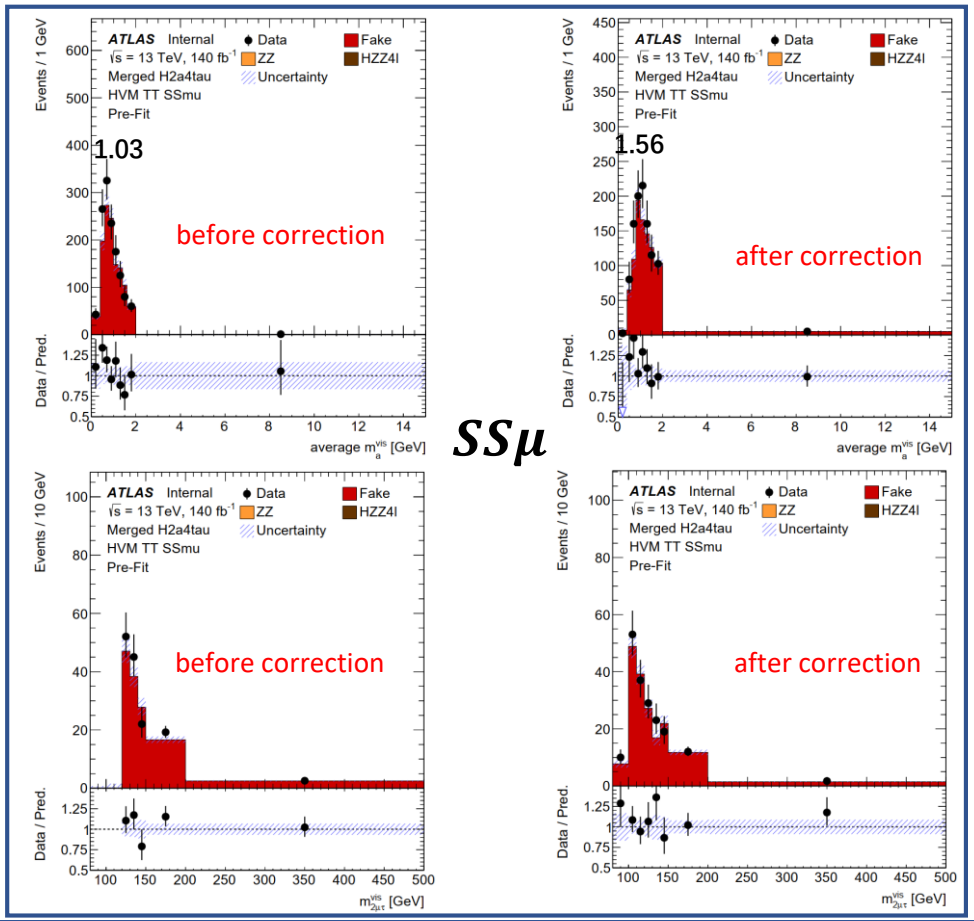

$SS\mu$

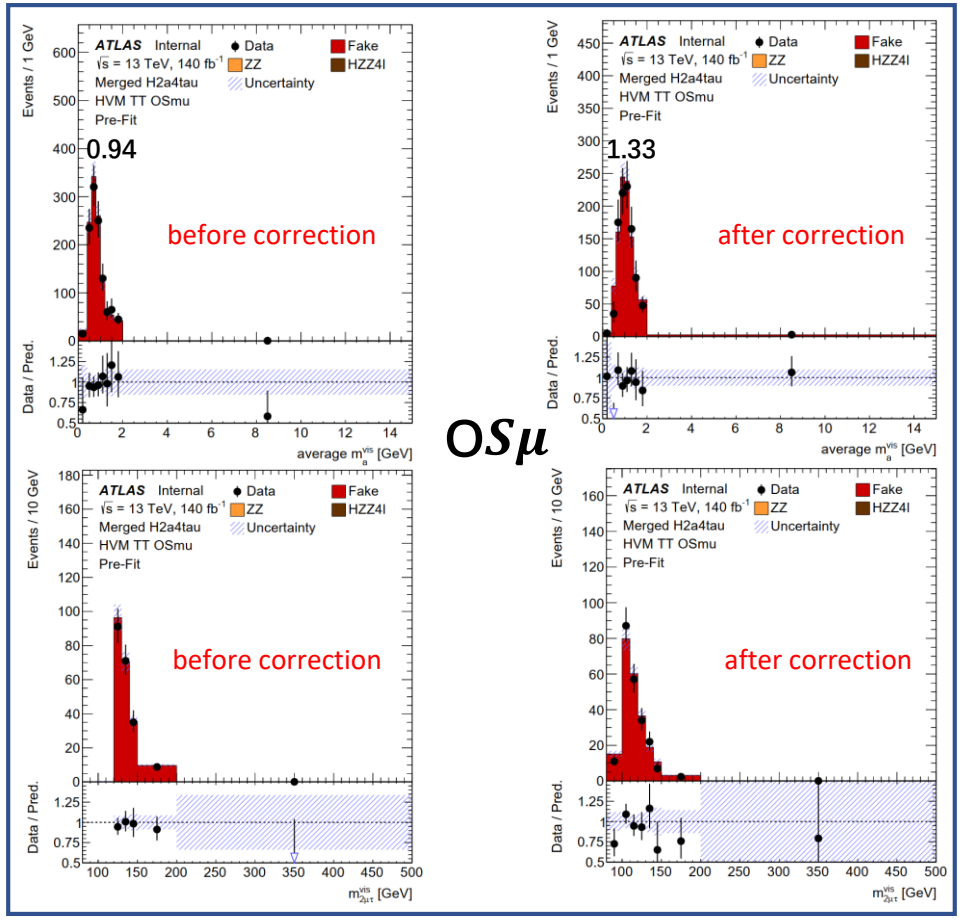

$OS\mu$

Correction check in cross-check region

- The fake prediction still agrees with data in the cross-check region after correction.

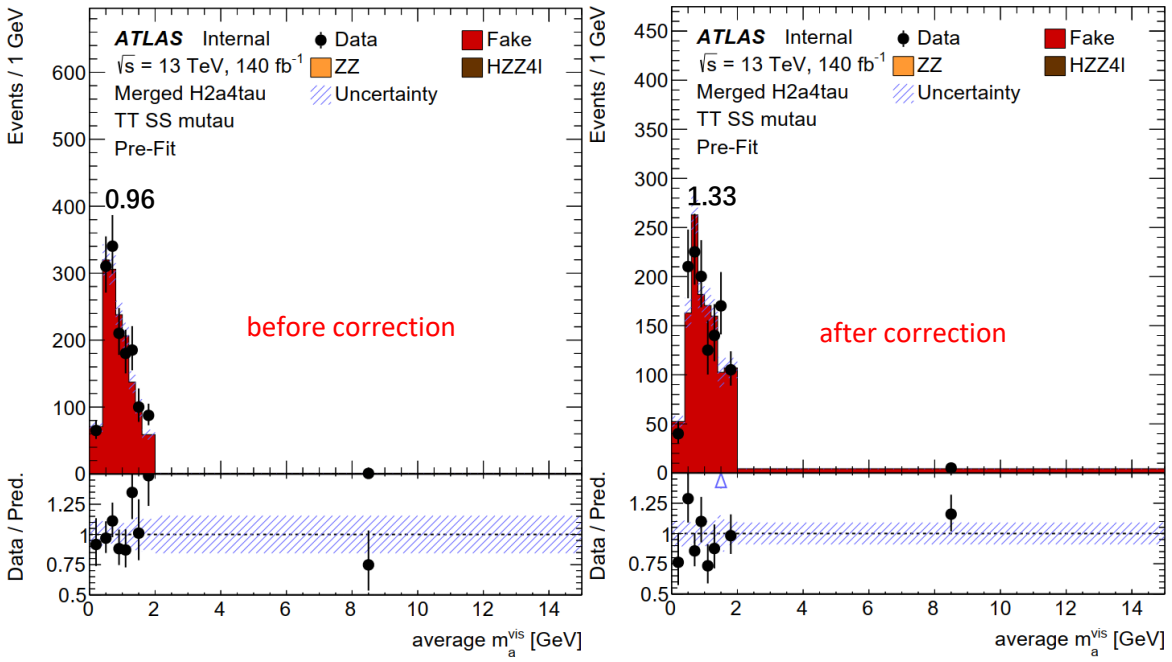

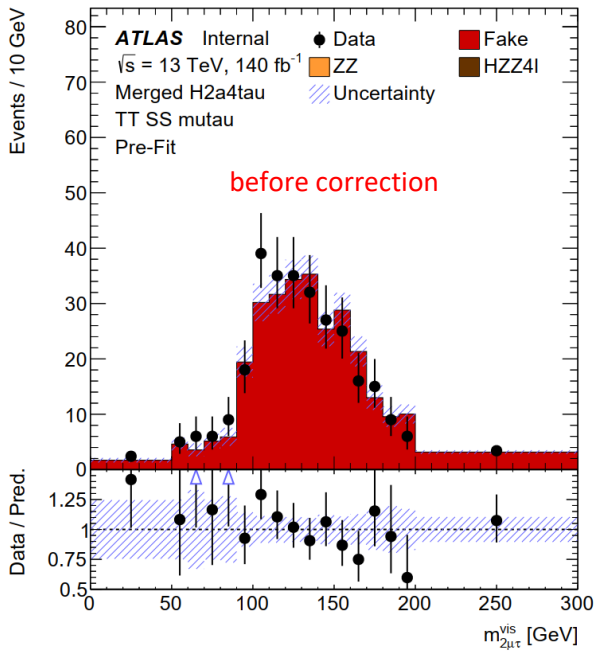

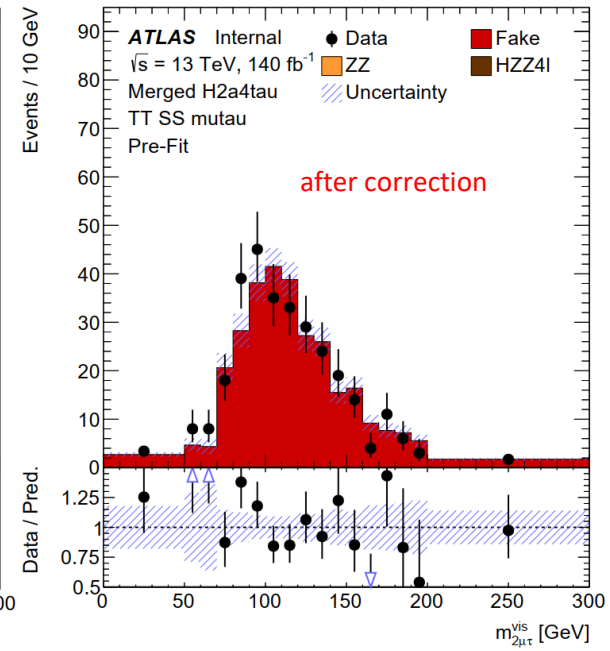

The effects of visible mass correction on the limits

signal mass (GeV)	4	6	8	10	12	14	15
expected limits without $m_{\mu\tau}^{vis}$ correction	0.134	0.0846	0.0493	0.0414	0.0624	0.0767	0.0957
expected limits with $m_{\mu\tau}^{vis}$ correction	0.131	0.0769	0.0471	0.0418	0.0609	0.0775	0.0946
Δlimits	2%	10%	5%	-1%	2%	-1%	1%
expected limits with additional correction systematic	0.131	0.0782	0.0473	0.0418	0.0609	0.0775	0.0946

- The limits with and without the $m_{\mu\tau}^{vis}$ correction are shown in the table. Δlimits are the differences between the limits with $m_{\mu\tau}^{vis}$ and without $m_{\mu\tau}^{vis}$ correction: (expected limits without $m_{\mu\tau}^{vis}$ correction)/(expected limits with $m_{\mu\tau}^{vis}$ correction) - 1.
- The Δlimits can already reflect the impact of 100% variation of $m_{\mu\tau}^{vis}$ correction on the final limits. The impact of any other variations should be smaller than this variation. We can clearly see the impacts are very small on the limits after the correction.
  - The relatively large effects on the limits of 6 and 8 GeV after performing the $m_{\mu\tau}^{vis}$ are because the separation between signal and background is better after the $m_{\mu\tau}^{vis}$ correction as shown in next few pages.
  - The limits for $m_a > 8$ GeV signal almost keep the same as before the correction, because the signal and background are always well separated before and after correction.
- The Δlimits are then applied as cross-section uncertainties in the fit for each mass point.
  - After applying the additional $m_{\mu\tau}^{vis}$ correction uncertainties, the limits are almost the same as before. The maximum effect on limits is only 2% for 6 GeV signal.
- The conclusion is that the $m_{\mu\tau}^{vis}$ correction has very small impact on the analysis. We don't need to apply an uncertainty for the $m_{\mu\tau}^{vis}$ correction because it will contribute negligible effects on the final limits compared to other major systematics.

Average $m_{\mu\tau}^{vis}$ ($m_a = 6,8$ GeV)

- The same binning strategy is used for $m_a = 6,8$ GeV signal.

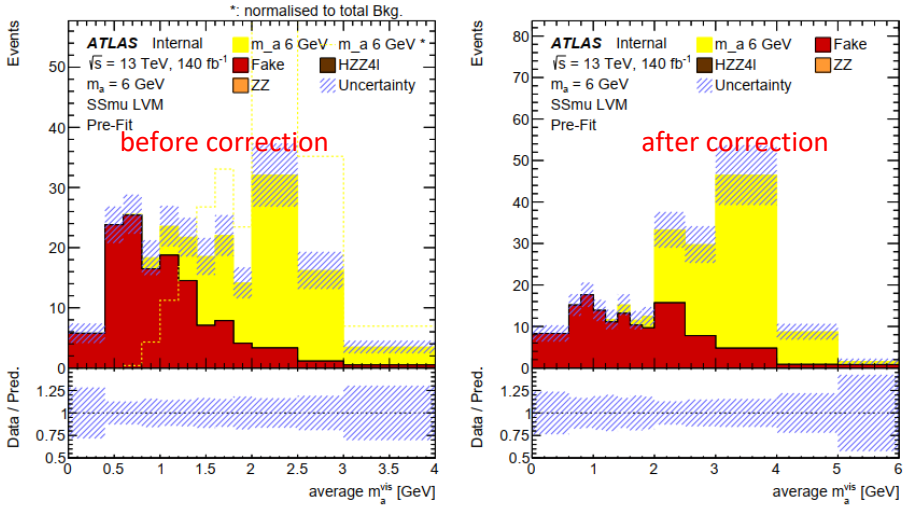

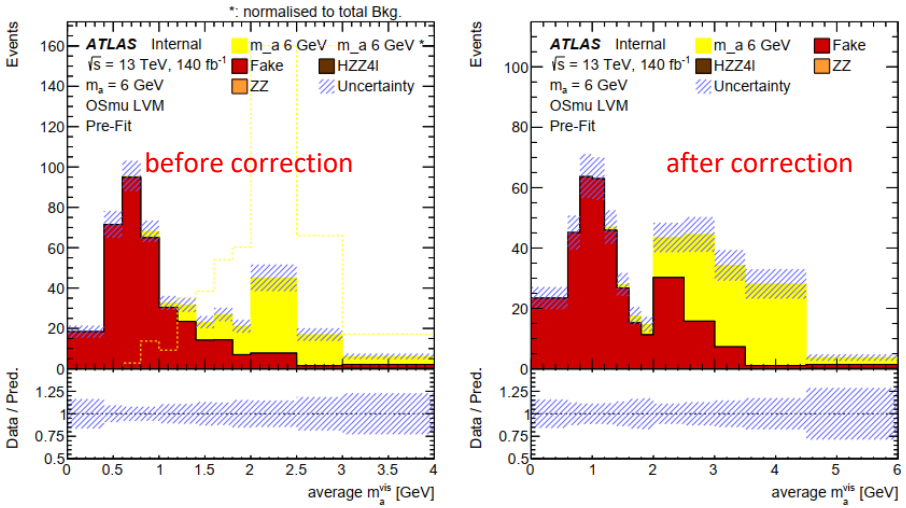

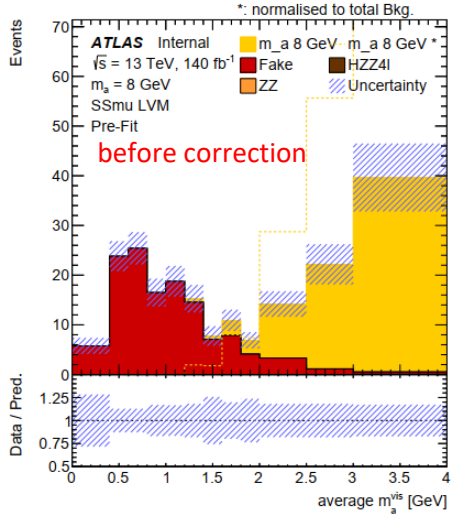

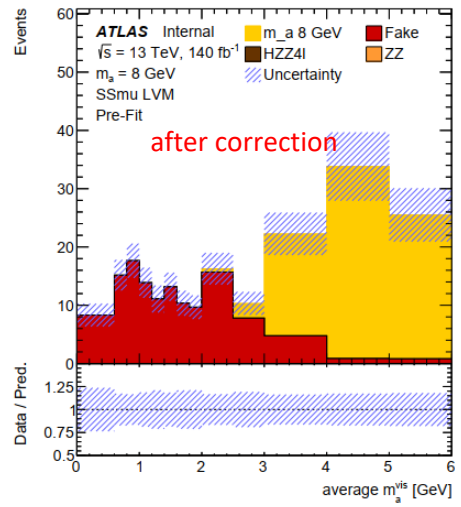

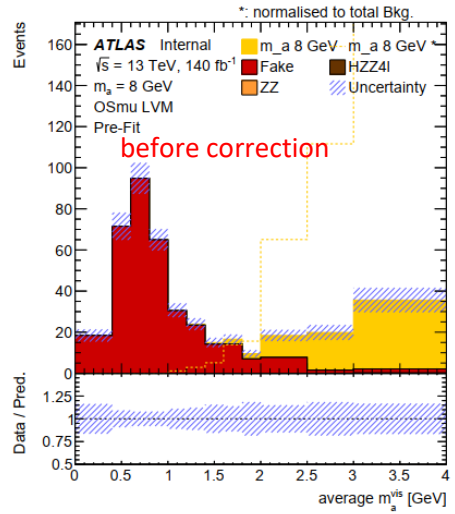

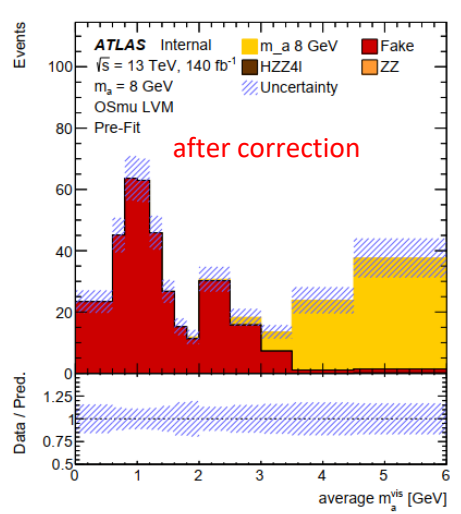

More cutflow table

cut name	4 GeV	6 GeV	8 GeV	10 GeV	12 GeV	14 GeV	15 GeV
AOD generation	5.5e+05	3.4e+05	2.7e+05	2.4e+05	2.3e+05	2.3e+05	2.3e+05
Preselection	5707.6	2773.7	2222.1	1955.2	1725.5	1561.7	1493.3
N(baseline μ) ≥ 2	5289.1	2554.3	2020.8	1785.3	1587	1441.8	1372
N(baseline τ) ≥ 1	5276.2	2546.2	2014.3	1779.4	1579.5	1432.1	1364
N(baseline τ) ≥ 2	2441	1200	872	683	524	456	410
2 baseline $\mu\tau$	2332.6	1135.4	818	576	334	222	176
μ leadpt > 14 GeV	2319.6	1128.2	813	573	334	222	176
2 OS $\mu\tau$	2229	1092.7	784	556	323	215	168
2 mVis15 $\mu\tau$	2229	1092.7	784	556	323	215	168
Lead $p_T^\tau > 30$ GeV	2047.7	1010.3	706	500	299	207	164
Sublead $p_T^\tau > 25$ GeV	1678.8	845	581	417	260	184	149
2 signal $\mu\tau$	477	231	167	141	86	67	54
60 GeV < $m_{2\mu\tau}^{vis}$ < 120 GeV	420	206	150	128	77	60	49
2 OS μ	218	109	72	62	40	29	24
$m_{\mu\mu} < 50$ GeV	214±9.1	107±5.0	69±4.0	60±3.3	39±2.6	27±2.2	24±2.0

Table 10: A summary of weighted cutflow of signal region in OSμ channle for $m_a = 4, 6, 8, 10, 12, 14, 15$ GeV (BR($H \to 2a \to 4\tau$) = 1.0 at 140 fb^{-1}), starting from the AOD generation level.

cut name	Events passed	Efficiency	Cumulative efficiency
AOD generation	5.5e+05	1	1
Preselection	5707.6	0.010459	0.010459
N(baseline μ) ≥ 2	5289.1	0.92668	0.0096917
N(baseline τ) ≥ 1	5276.2	0.99755	0.0096679
N(baseline τ) ≥ 2	2441	0.46264	0.0044728
2 baseline $\mu\tau$	2332.6	0.95562	0.0042743
μ leadpt > 14 GeV	2319.6	0.99441	0.0042504
2 OS $\mu\tau$	2229	0.96094	0.0040843
2 mVis15 $\mu\tau$	2229	1	0.0040843
Lead $p_T^\tau > 30$ GeV	2047.7	0.91866	0.0037521
Sublead $p_T^\tau > 25$ GeV	1678.8	0.81986	0.0030762
2 signal $\mu\tau$	477	0.28435	0.00087474
60 GeV < $m_{2\mu\tau}^{vis}$ < 120 GeV	420	0.88021	0.00076995
2 SS μ	202	0.48146	0.0003707

Table 7: Weighted cutflow of signal region in the SSμ channel for $m_a = 4$ GeV (BR($H \to 2a \to 4\tau$) = 1.0 at 140 fb^{-1}), starting from the AOD generation level.

cut name	Events passed	Efficiency	Cumulative efficiency
AOD generation	5.4574e+05	1	1
Preselection	5707.6	0.010459	0.010459
N(baseline μ) ≥ 2	5289.1	0.92668	0.0096917
N(baseline τ) ≥ 1	5276.2	0.99755	0.0096679
N(baseline τ) ≥ 2	2441	0.46264	0.0044728
2 baseline $\mu\tau$	2332.6	0.95562	0.0042743
μ leadpt > 14 GeV	2319.6	0.99441	0.0042504
2 OS $\mu\tau$	2229	0.96094	0.0040843
2 mVis15 $\mu\tau$	2229	1	0.0040843
Lead $p_T^\tau > 30$ GeV	2047.7	0.91866	0.0037521
Sublead $p_T^\tau > 25$ GeV	1678.8	0.81986	0.0030762
2 signal $\mu\tau$	477	0.28435	0.00087474
60 GeV < $m_{2\mu\tau}^{vis}$ < 120 GeV	420	0.88021	0.00076995
2 OS μ	218	0.51854	0.00039925
$m_{\mu\mu} < 50$ GeV	214	0.98207	0.00039209

Table 9: Weighted cutflow of signal region in the OSμ channel for $m_a = 4$ GeV (BR($H \to 2a \to 4\tau$) = 1.0 at 140 fb^{-1}), starting from the AOD generation level.

Cross-check on the fake factor method

- The SS $\mu^{\pm}\tau^{\pm}_{had}$ and OS $\mu^{\pm}\tau^{\mp}_{had}$ have similar fake composition
  - Quark jet is dominant
- Cross-check the fake estimation method using SS $\mu^{\pm}\tau^{\pm}_{had}$
  - Measure the FFs of SS $\mu^{\pm}\tau^{\pm}_{had}$ in Z + jets region
  - Apply the FFs into a signal-like region with 2 SS $\mu^{\pm}\tau^{\pm}_{had}$

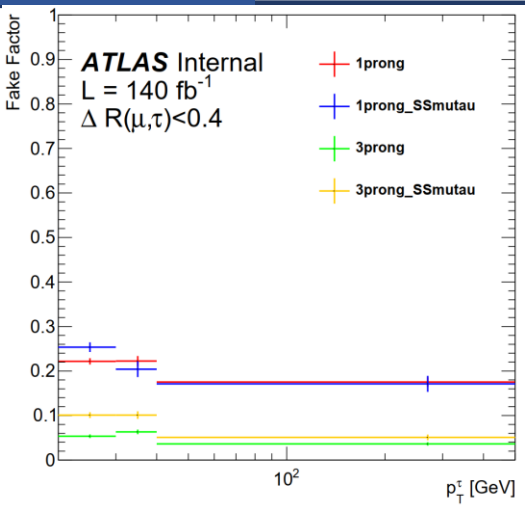

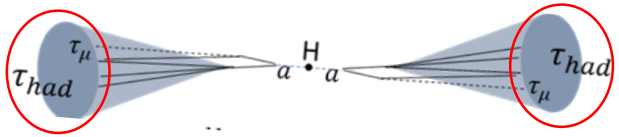

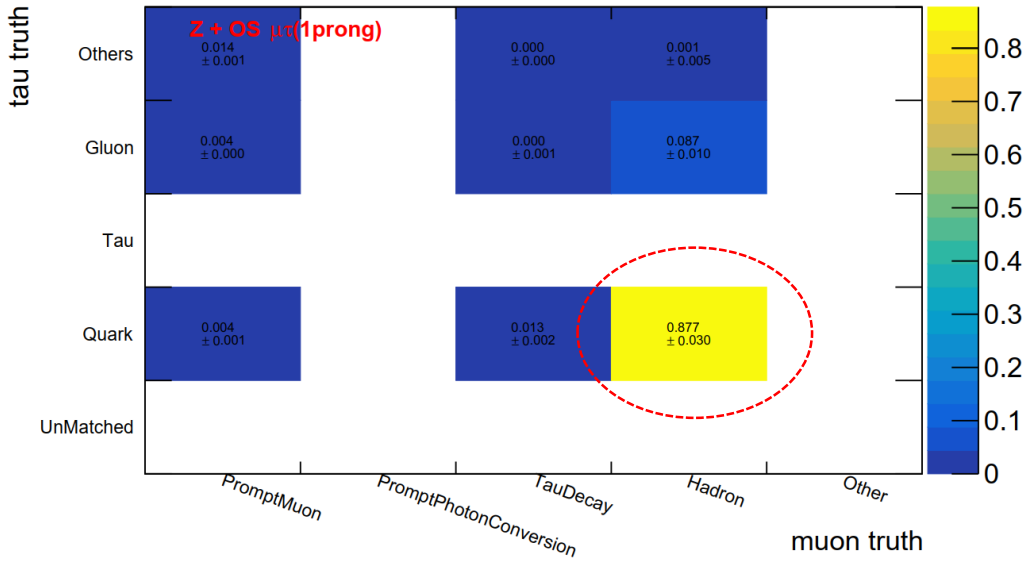

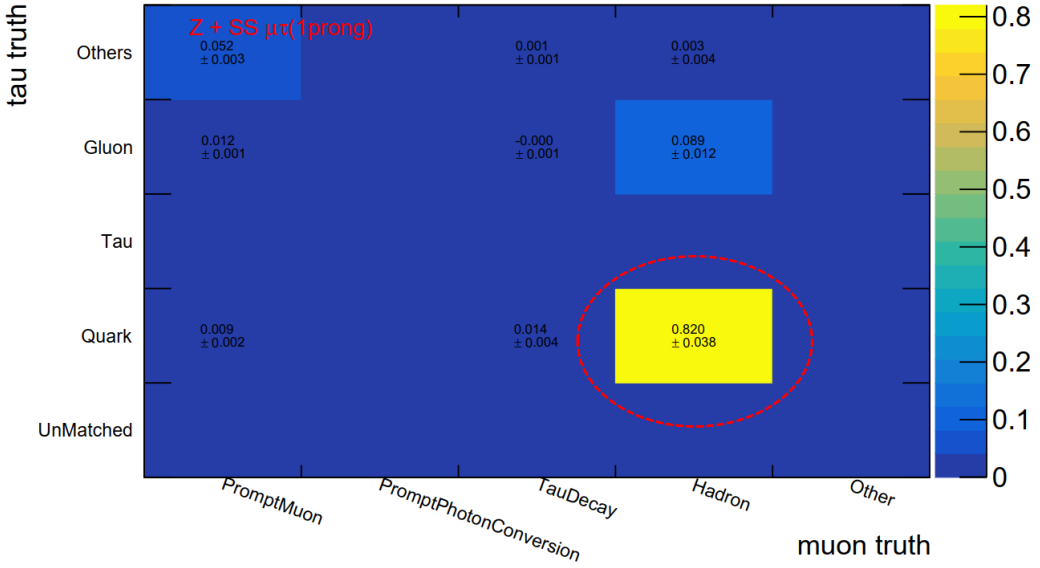

Cross-check on the fake factor method

- Only select two pass-id SS $\mu^{\pm}\tau^{\pm}_{had}$ without any other cuts to increase the statistics
- The fake in the cross-check region is estimated using the same equation
- The prediction shows very good agreement with data (discrepancy < 3%)

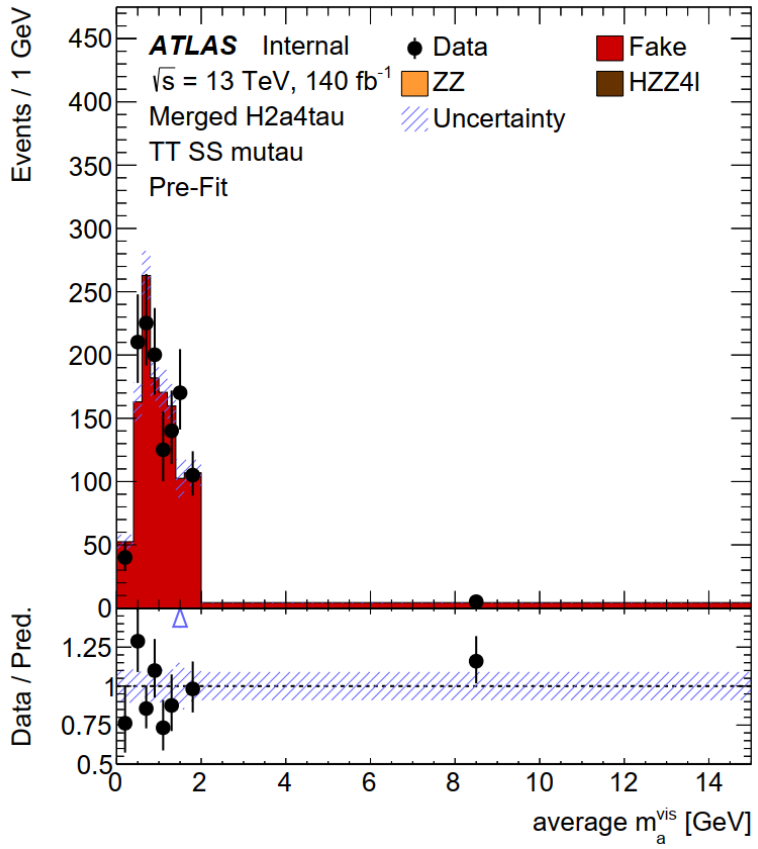

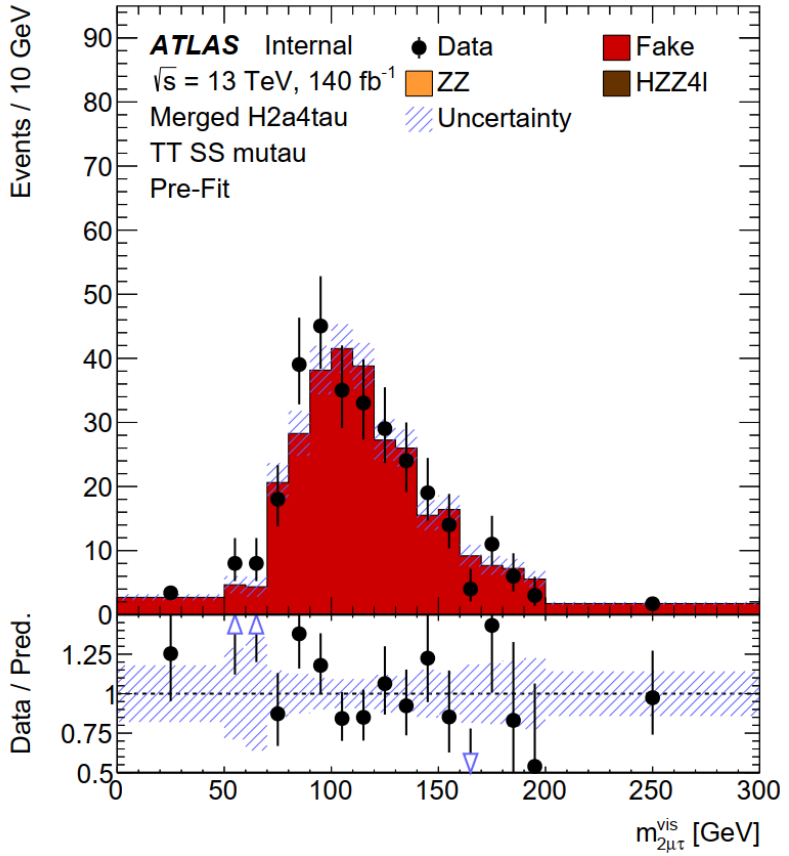

Fake Composition from MC

- The fake compositions in the signal-like region (2 OS $\mu^{\pm}\tau_{had}^{\mp}$) are consistent with the ones in the Z+jets CR
  - Quark is dominant
  - Gluon is sub-dominant

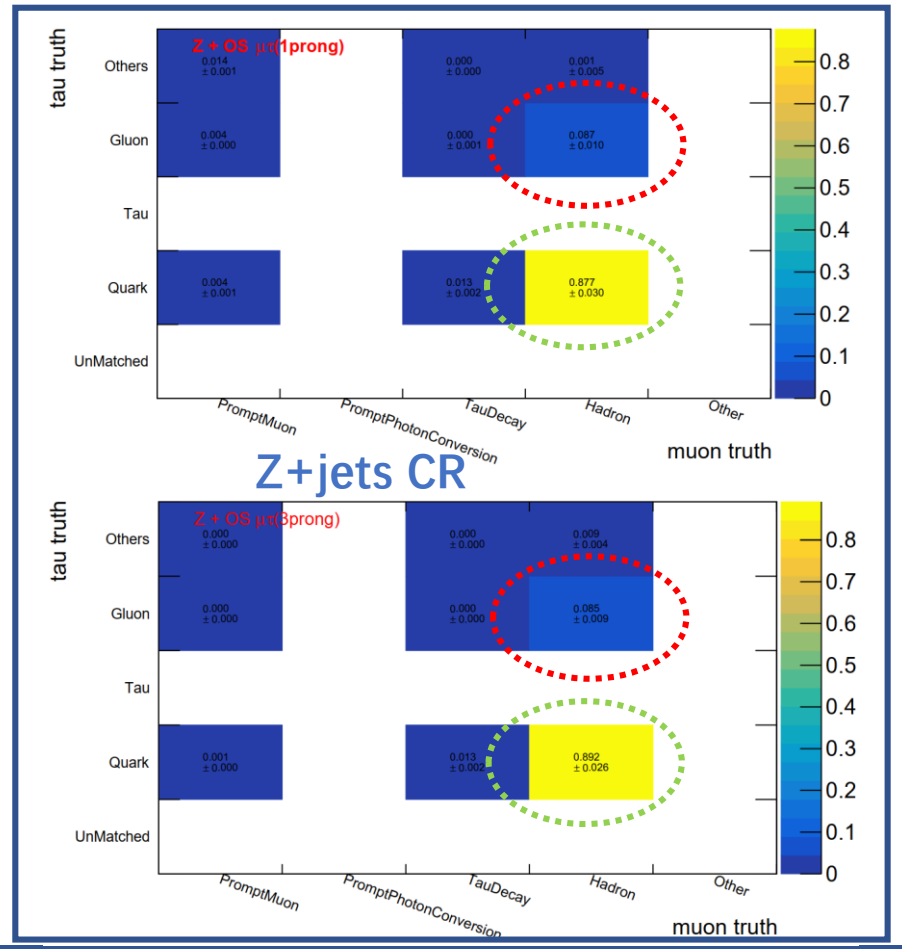

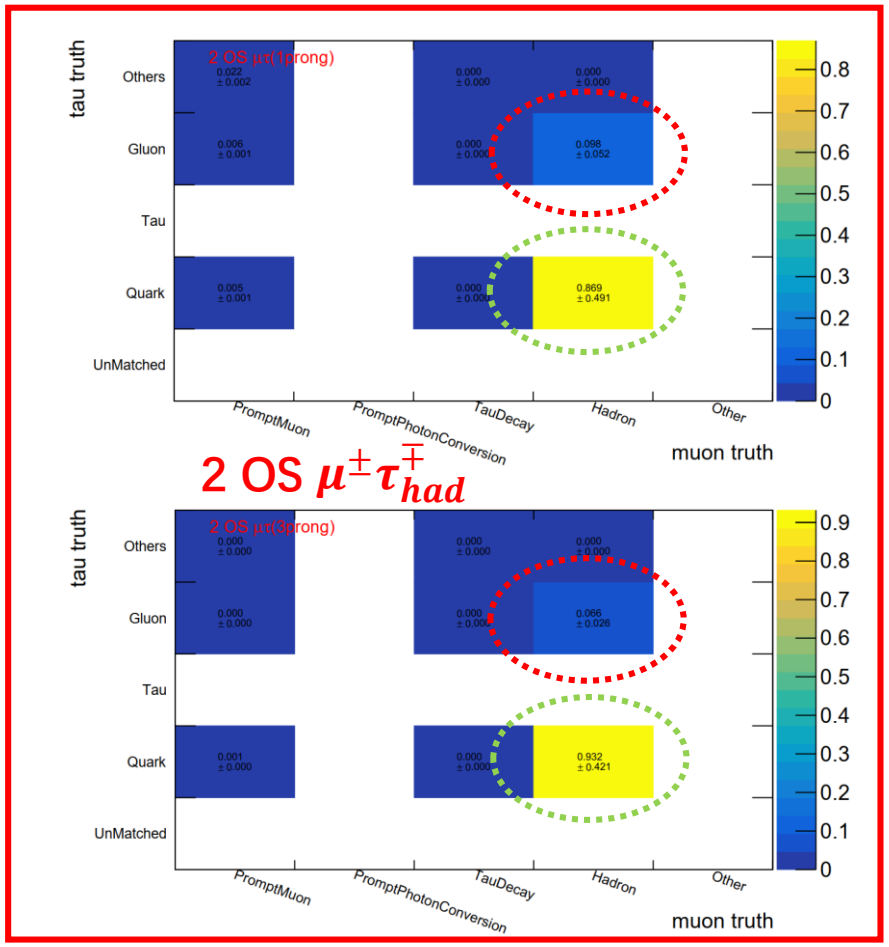

Average $m_{\mu\tau}^{vis}$ in signal region

- The binning of each signal mass point is optimized to make the statistical error of signal + background of each bin around 20% and never 0 background events in each bin.
- The edge of each bin is manually chosen to separate the shape of the signal and background.
- The overflow bin is added to the rightmost bin of each distribution.

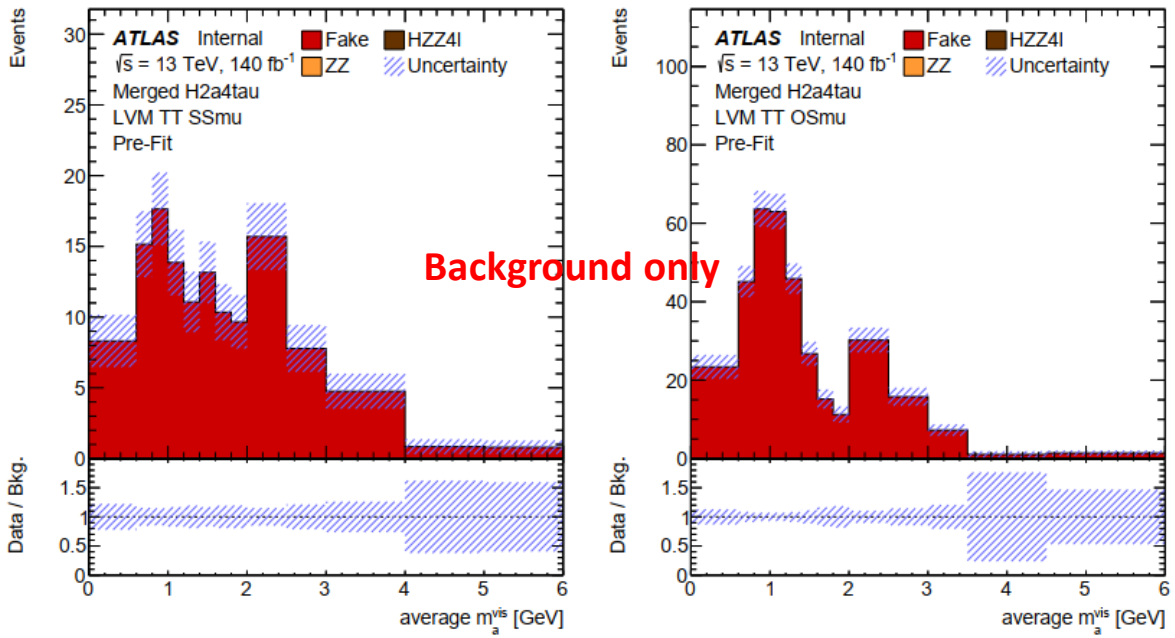

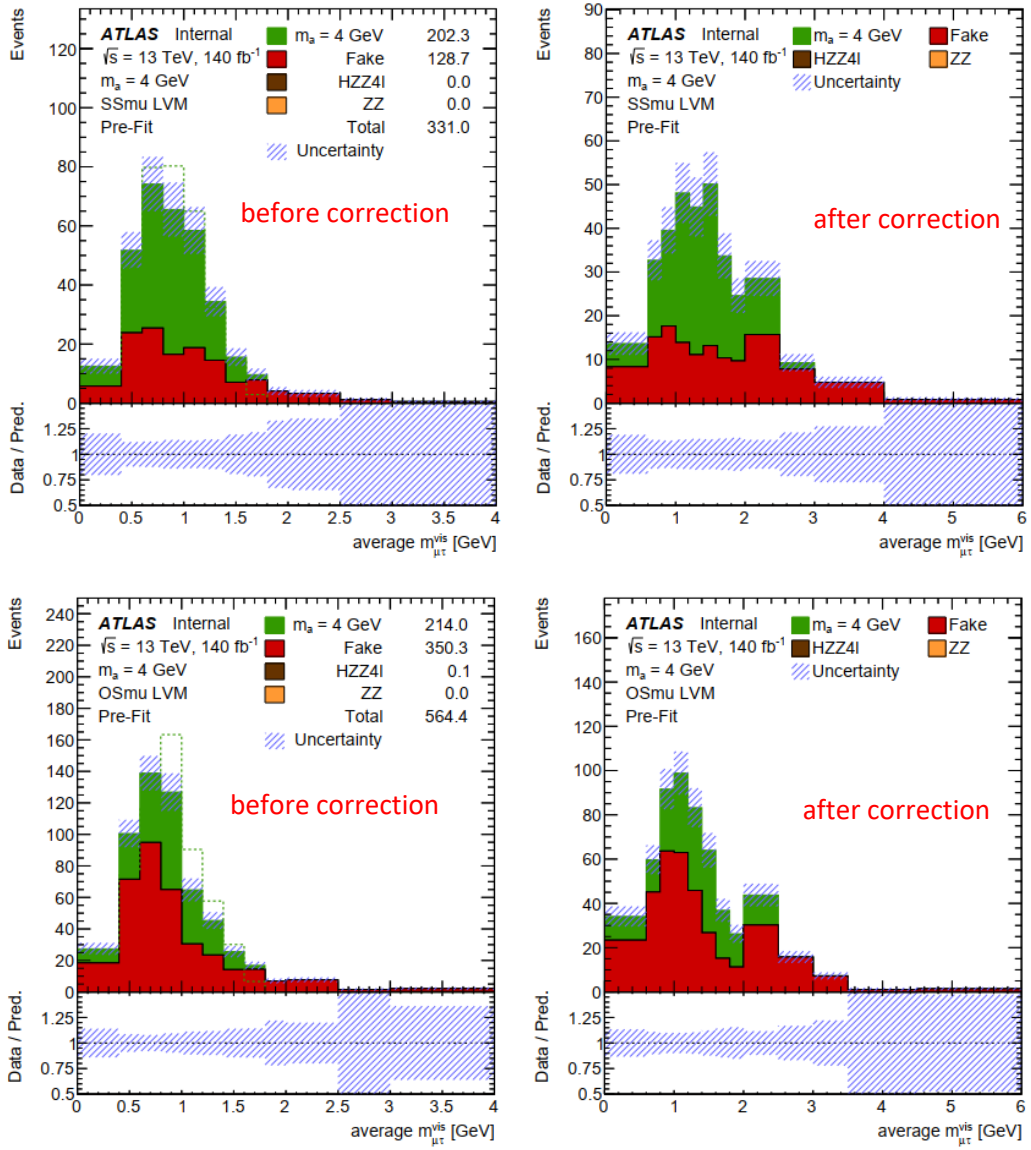

Average $m_{\mu\tau}^{vis}$ ($m_a = 6,8$ GeV)

- The same binning strategy is used for $m_a = 6{,}8$ GeV signal.

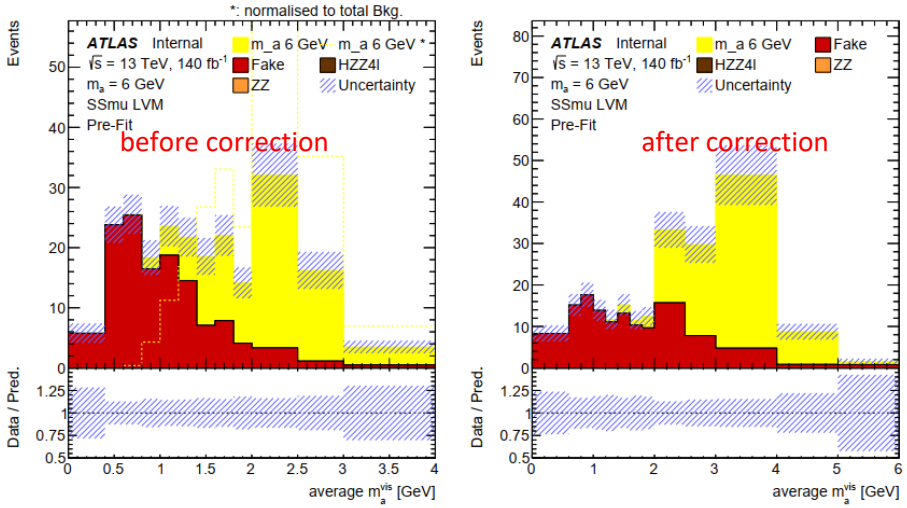

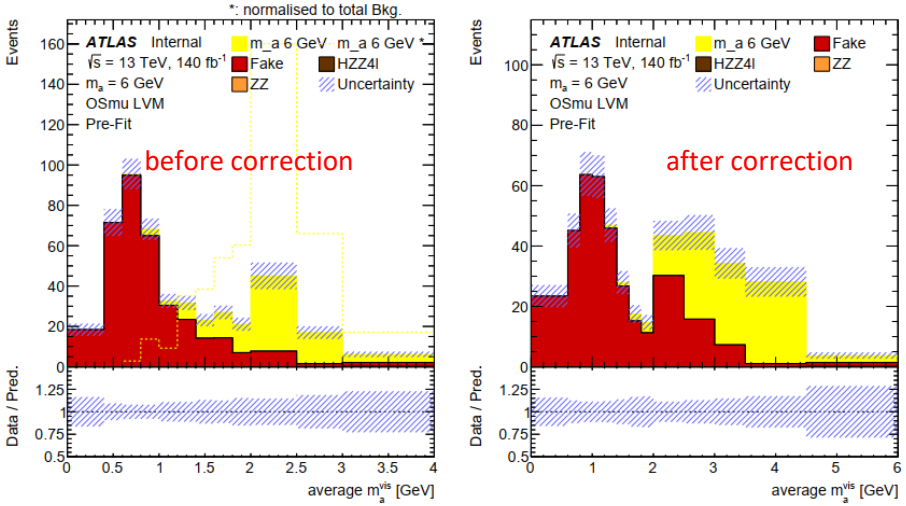

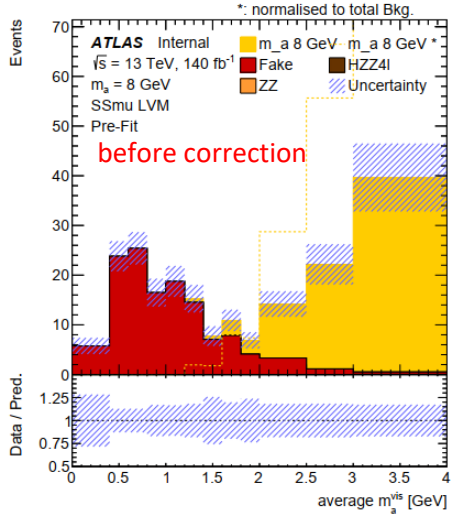

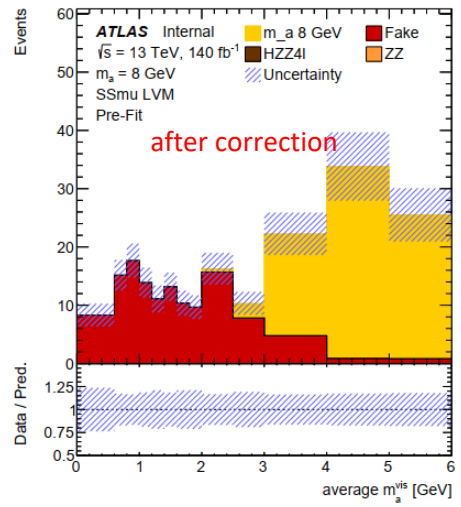

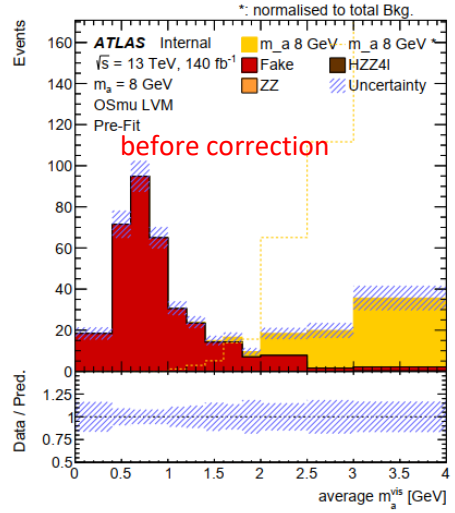

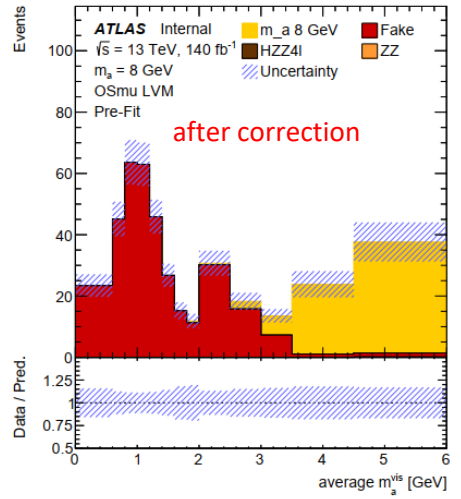

Average $m_{\mu\tau}^{vis}$ ($m_a = 10, 12$ GeV)

- The same binning strategy is used for $m_a = 10,12$ GeV signal.

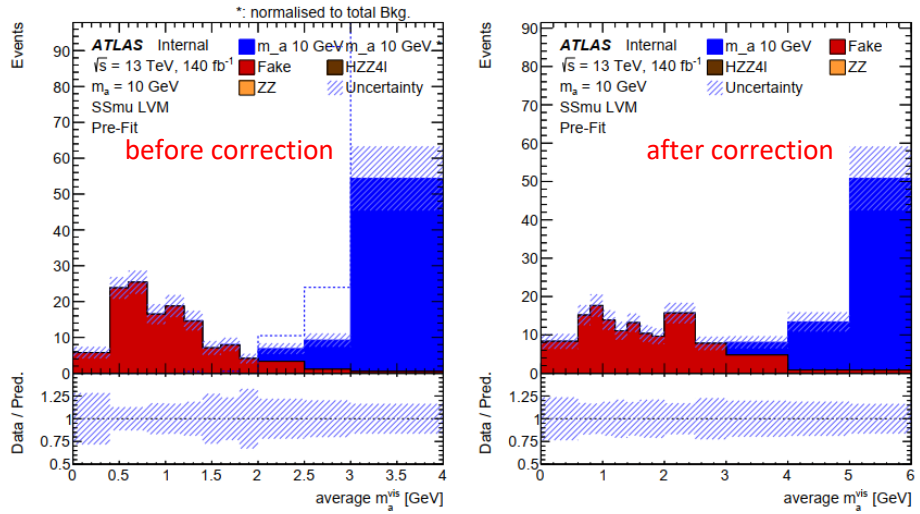

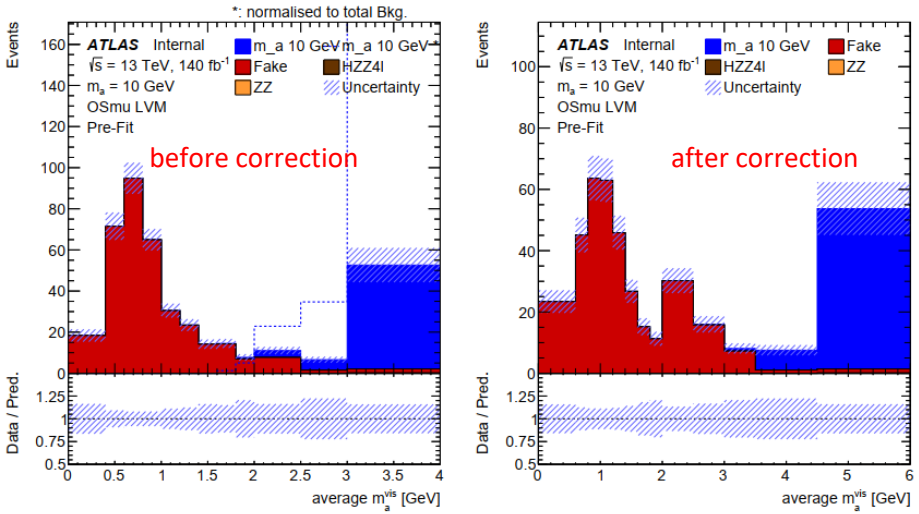

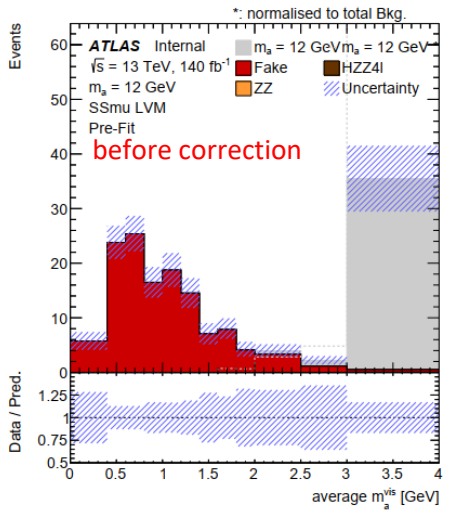

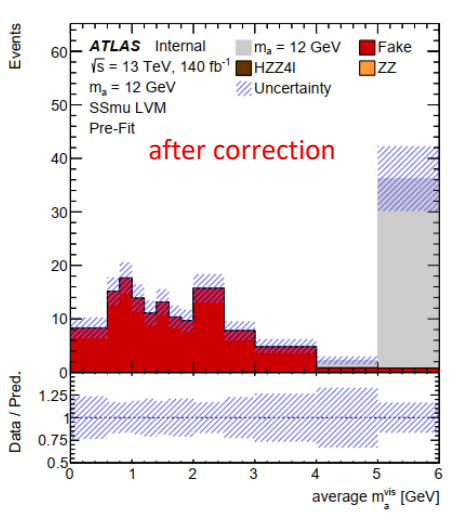

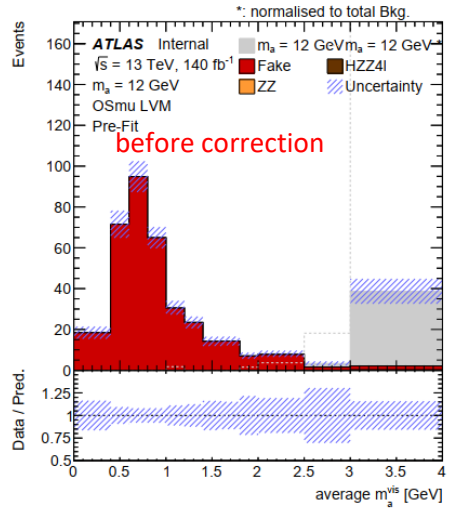

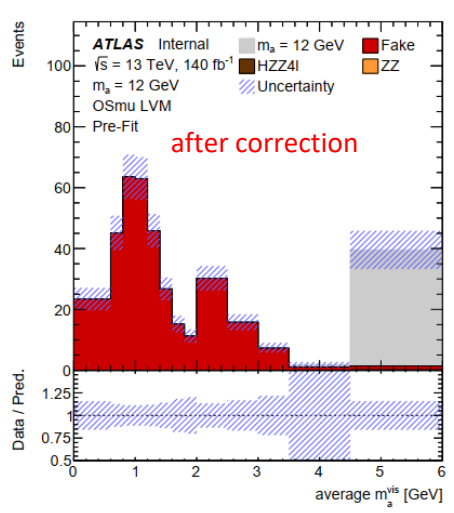

Average $m_{\mu\tau}^{vis}$ ($m_a = 14, 15$ GeV)

- The same binning strategy is used for $m_a = 14,15$ GeV signal.

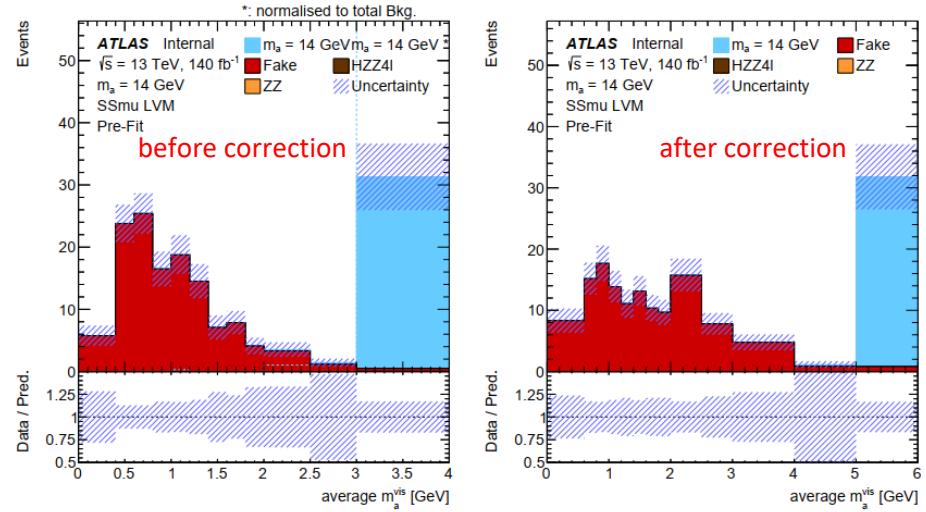

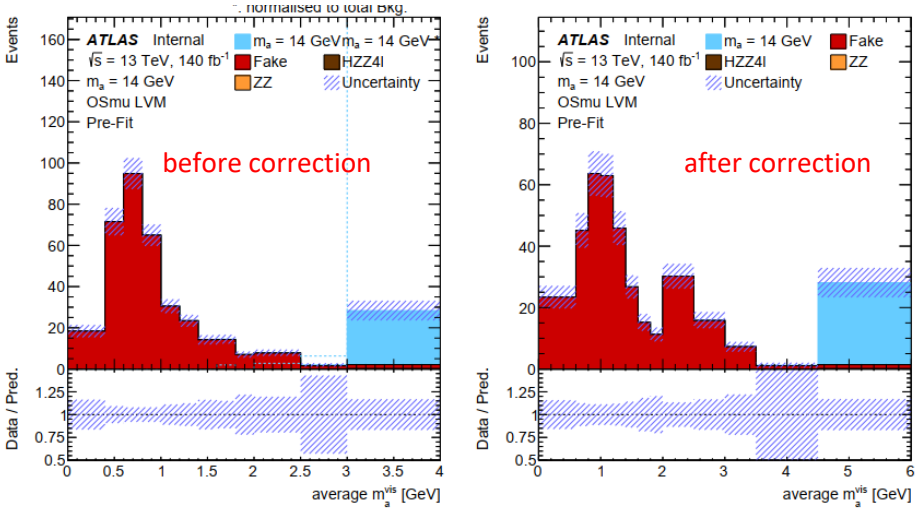

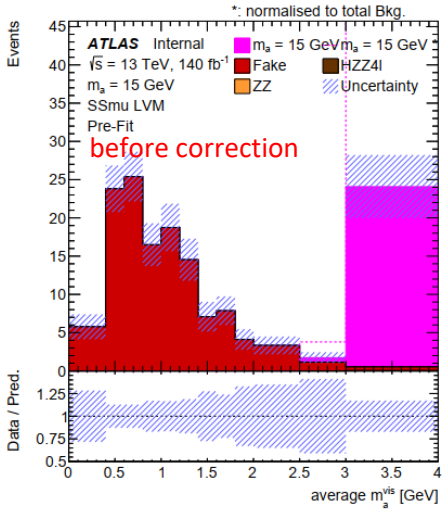

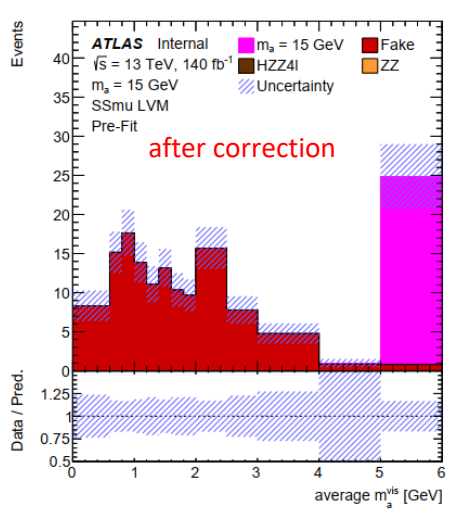

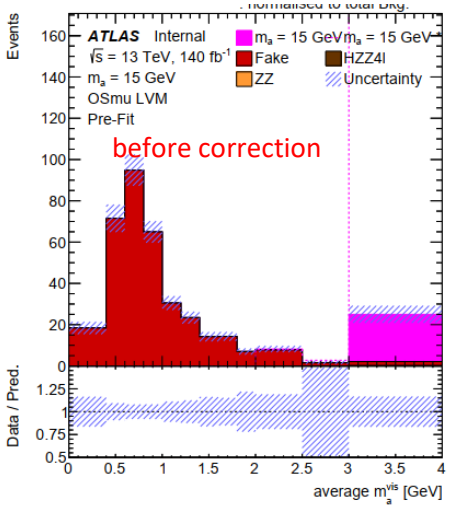

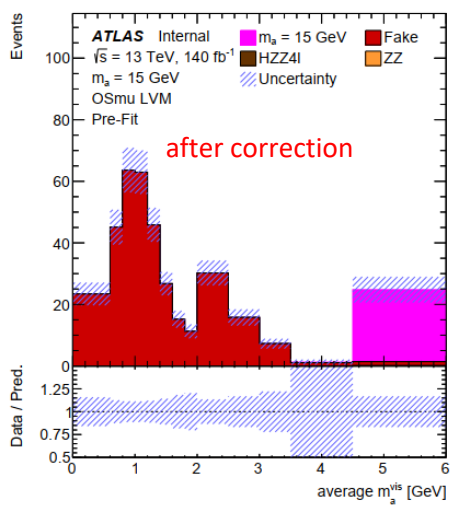

Impact of fake composition uncertainties

- fake_FF_Bcomposition and fake_FF_2MuTau

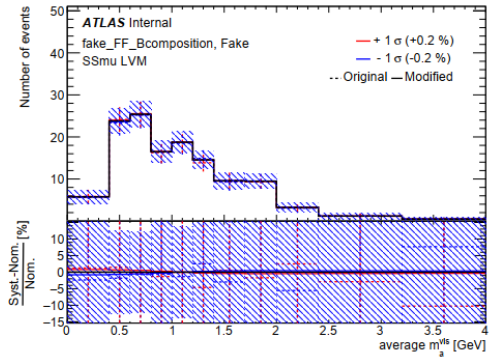

(a) Average $m_{\mu\tau}^{vis}$ for SSμ channel

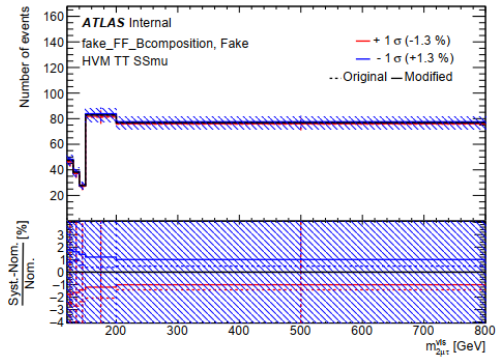

(b) $m_{2\mu\tau}^{vis}$ for SSμ channel

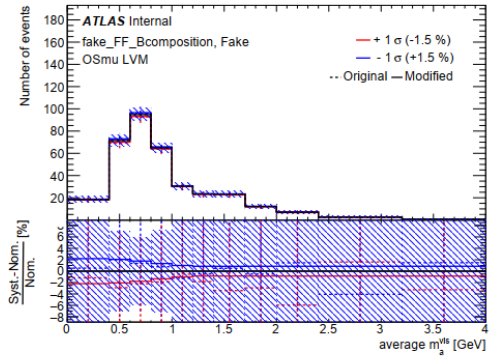

(c) Average $m_{\mu\tau}^{vis}$ for OSμ channel

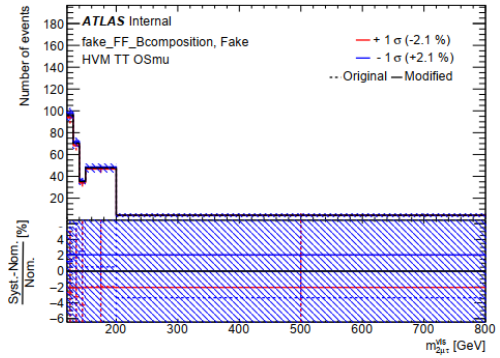

(d) $m_{2\mu\tau}^{vis}$ for OSμ channel

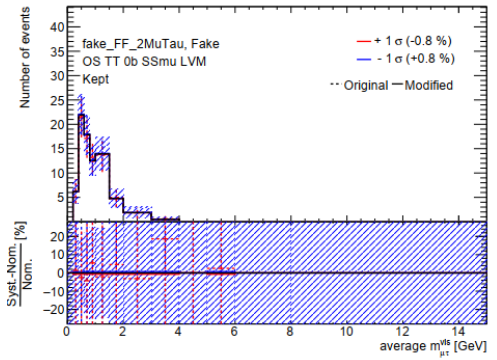

(a) Average $m_{\mu\tau}^{vis}$ for SSμ channel

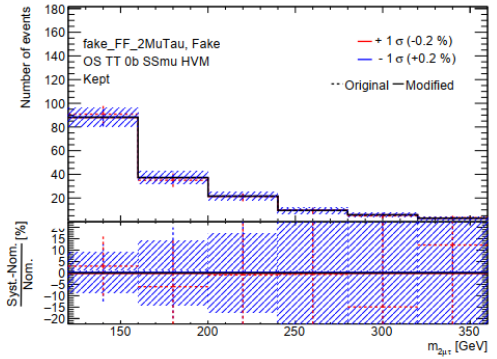

(b) $m_{2\mu\tau}^{vis}$ for SSμ channel

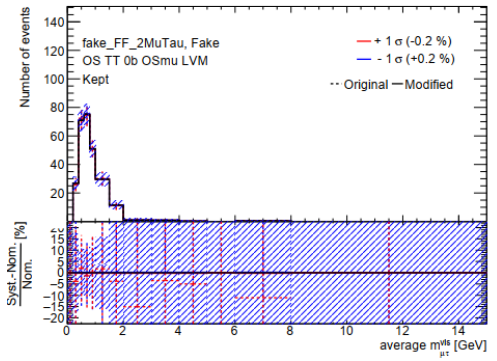

(c) Average $m_{\mu\tau}^{vis}$ for OSμ channel

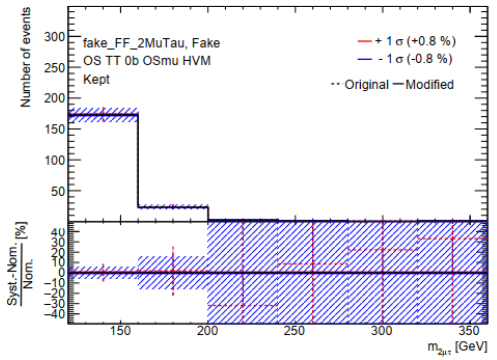

(d) $m_{2\mu\tau}^{vis}$ for OSμ channel

Impact of fake composition uncertainties

- fake_FF_1jet and fake_FF_2jets

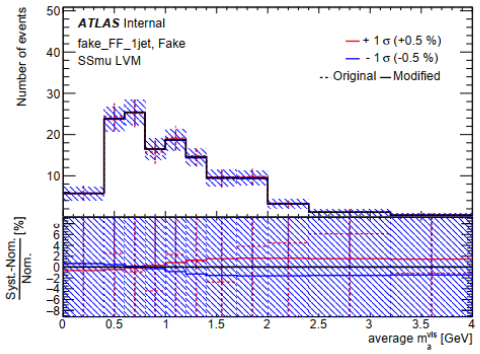

(a) Average $m_{\mu\tau}^{vis}$ for SSμ channel

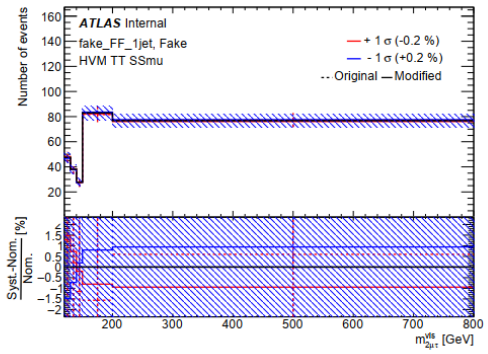

(b) $m_{2\mu\tau}^{vis}$ for SSμ channel

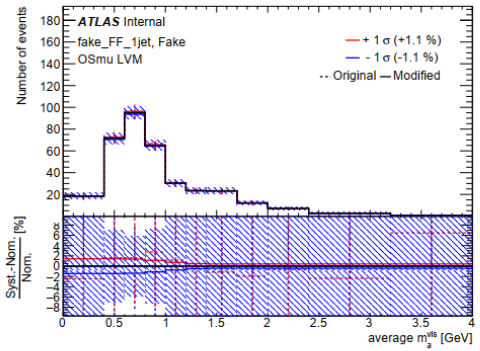

(c) Average $m_{\mu\tau}^{vis}$ for OSμ channel

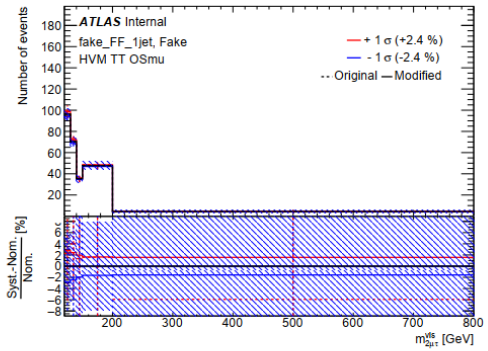

(d) $m_{2\mu\tau}^{vis}$ for OSμ channel

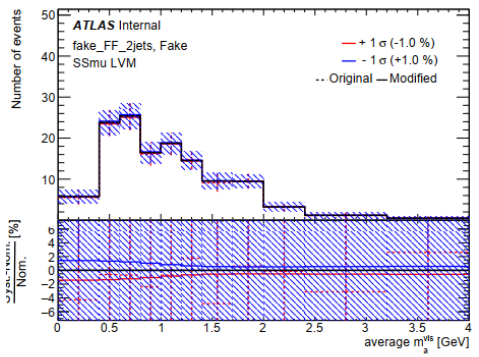

(a) Average $m_{\mu\tau}^{vis}$ for SSμ channel

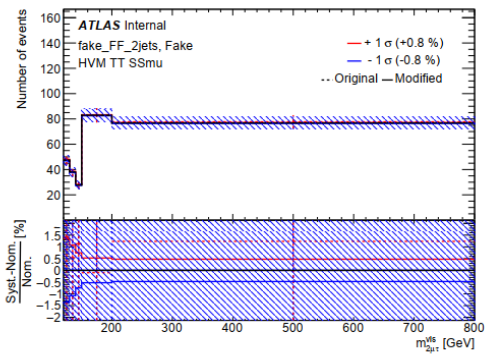

(b) $m_{2\mu\tau}^{vis}$ for SSμ channel

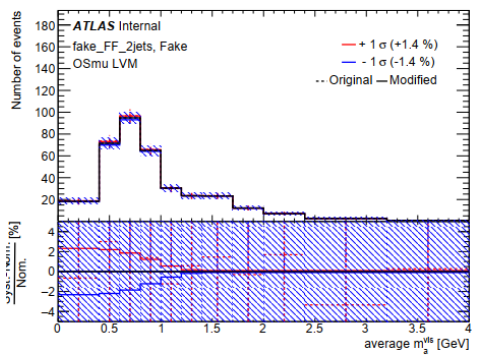

(c) Average $m_{\mu\tau}^{vis}$ for OSμ channel

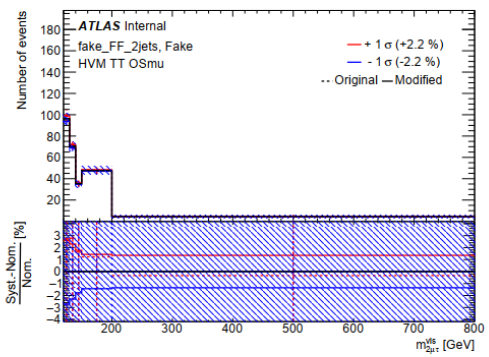

(d) $m_{2\mu\tau}^{vis}$ for OSμ channel

Systematic Impact of Muon Removal Uncertainty

- 1-prong uncertainties are quite large because there are much more 1-prong taus than 3-prong taus

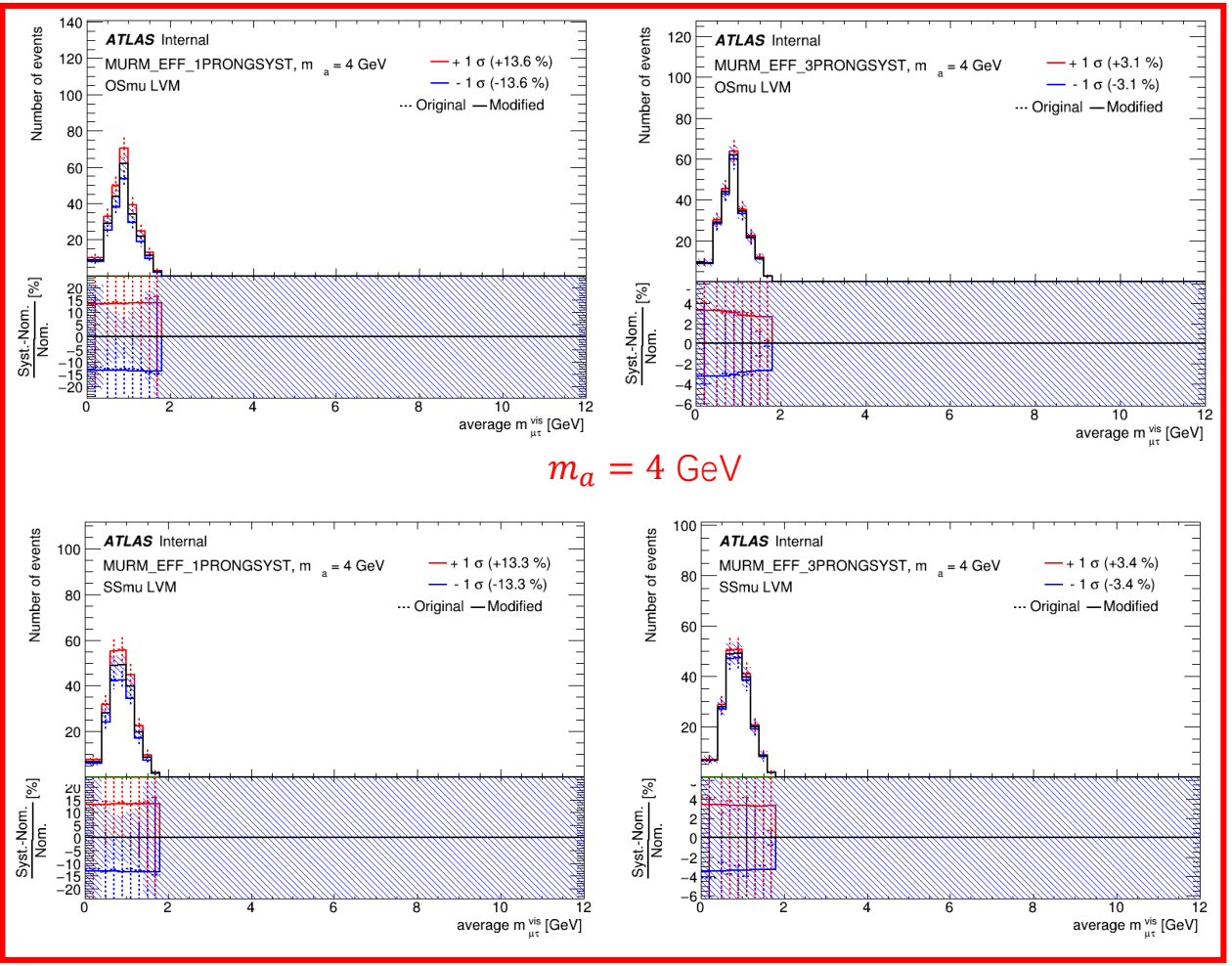

$m_a = 4$ GeV

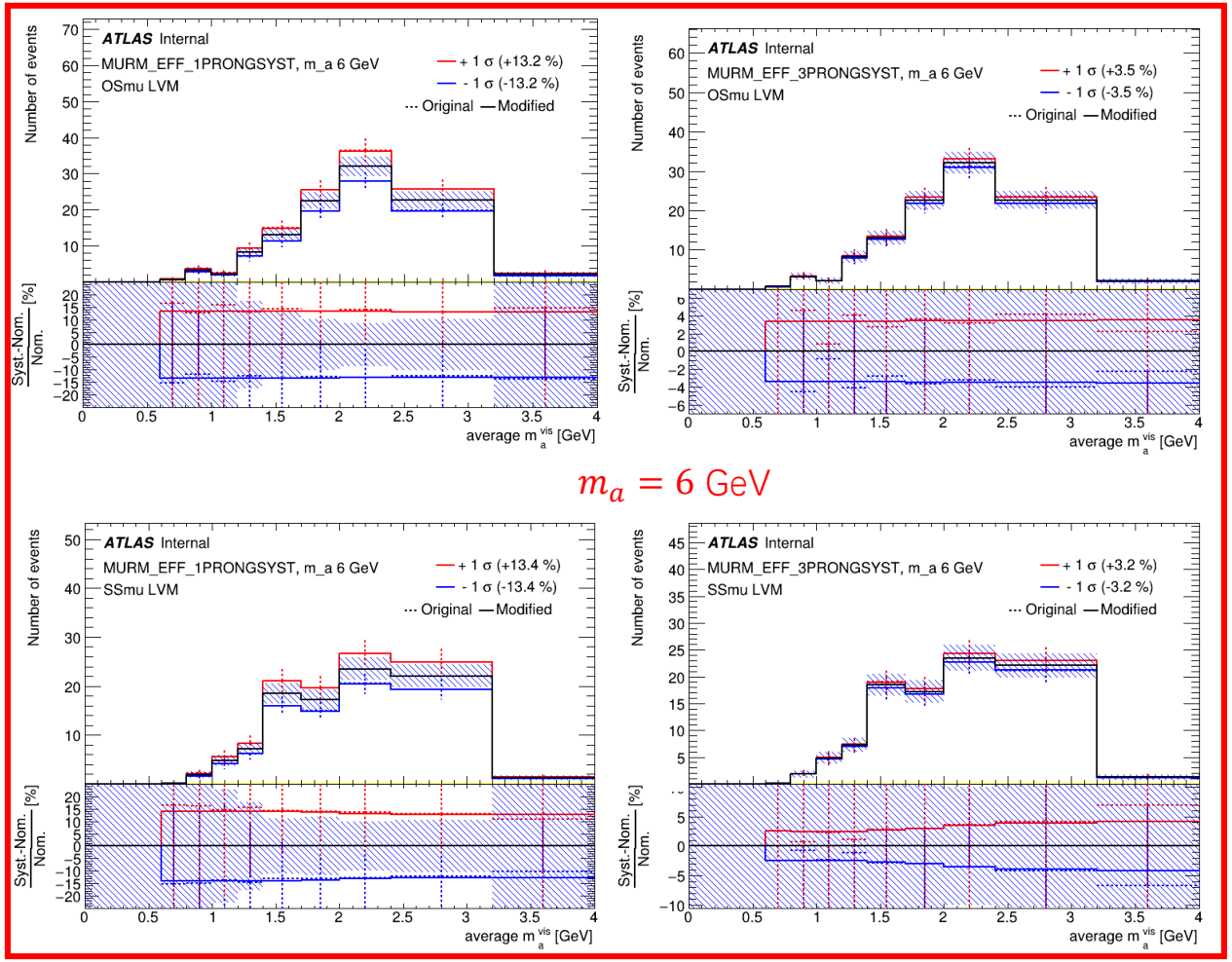

$m_a = 6$ GeV

Background only fit

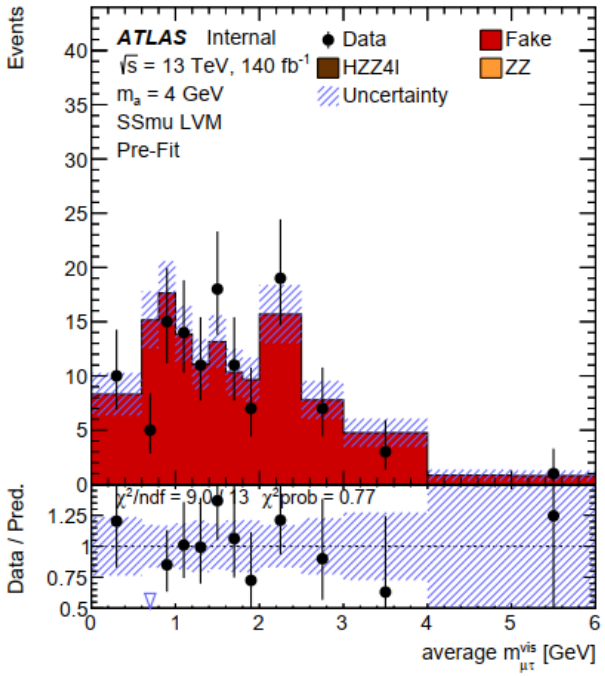

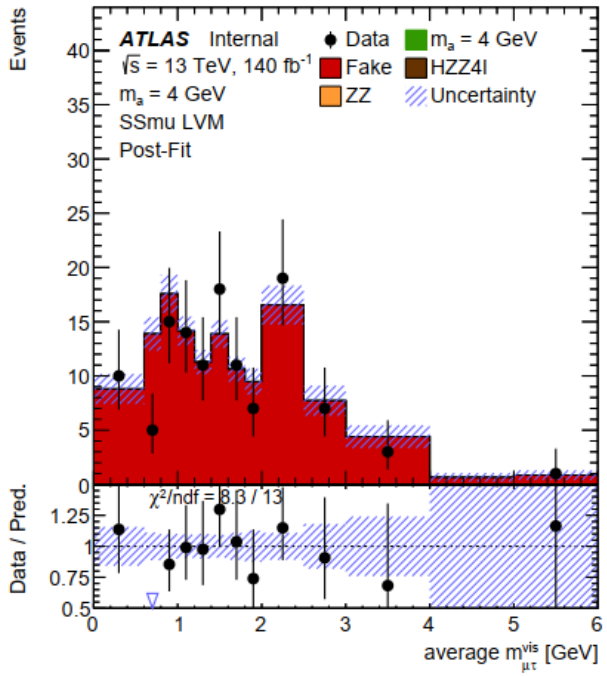

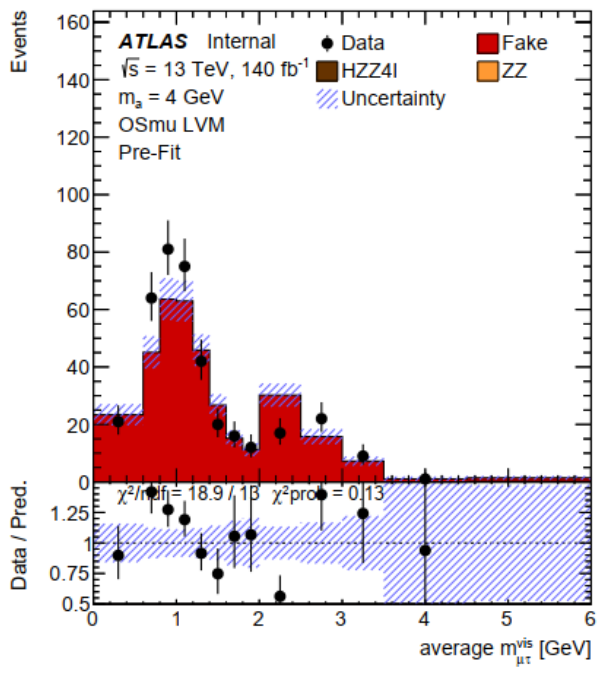

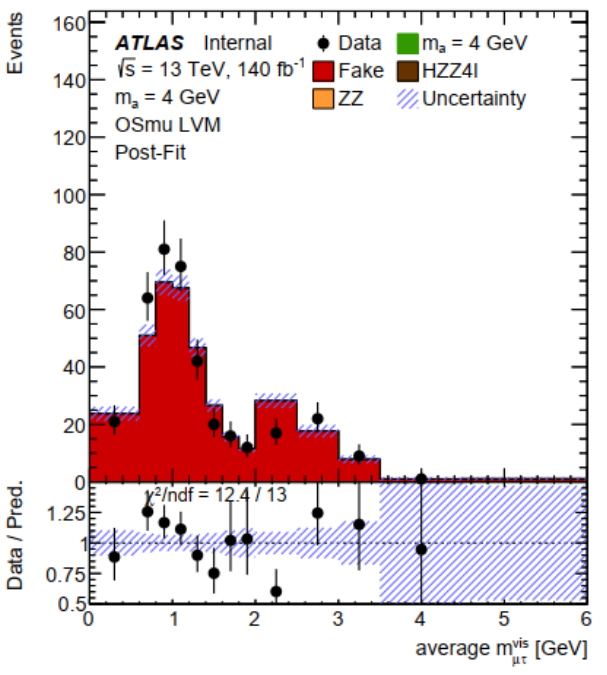

Background only fit

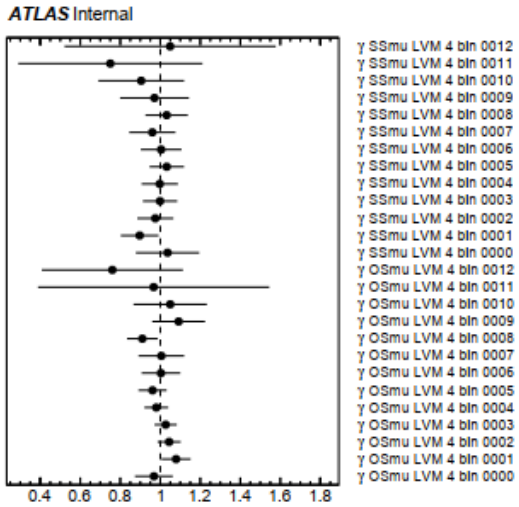

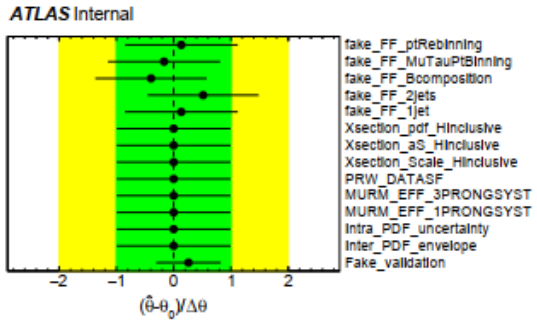

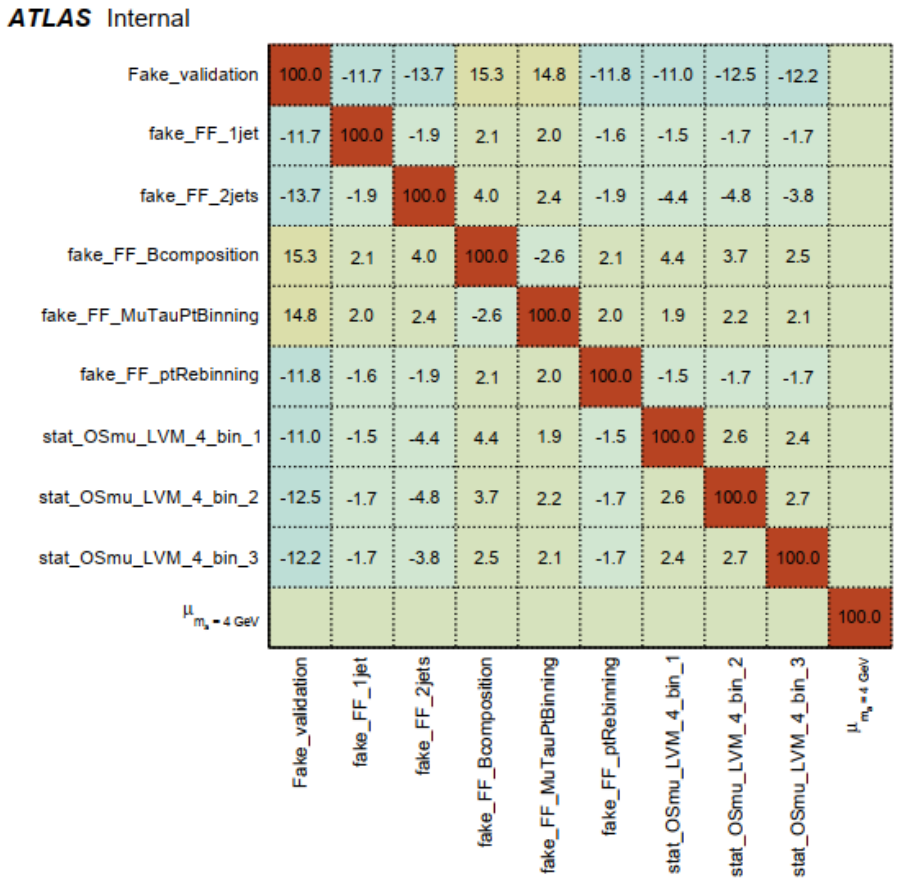

Signal + background fit (m_a = 4 GeV)

- Capped the μ at 0 ($\mu > 0$). (SSμ)
- The fit gets converged and the errors are all good.

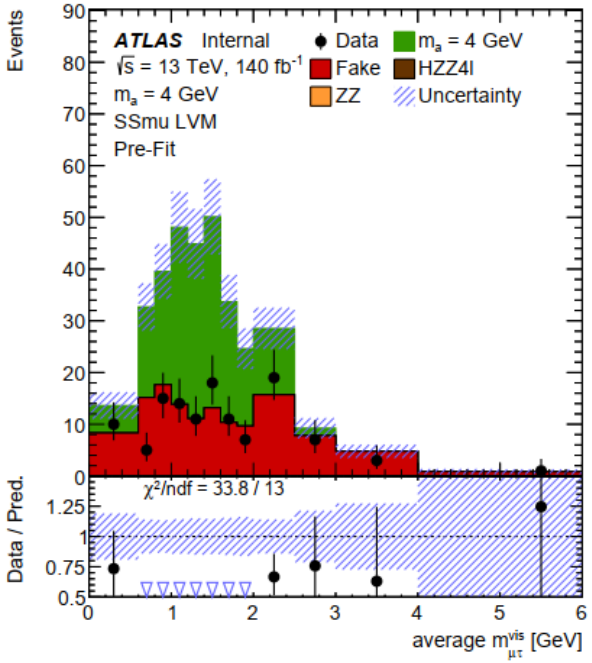

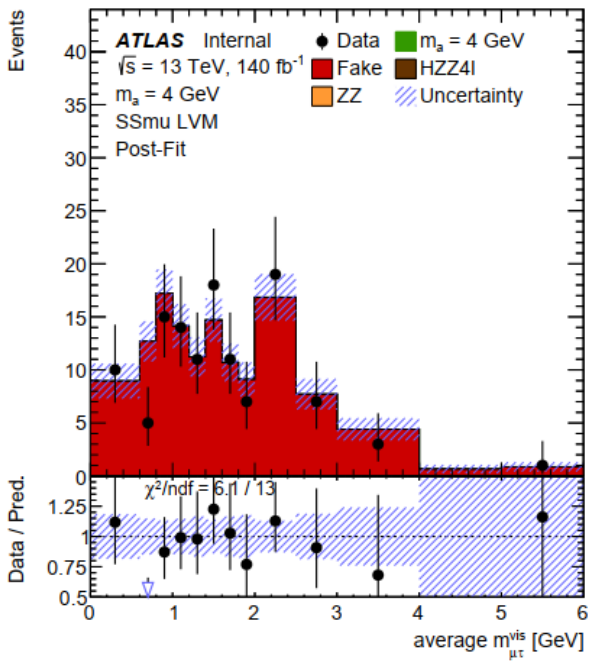

- Capped the μ at 0 ($\mu > 0$). (OSμ)

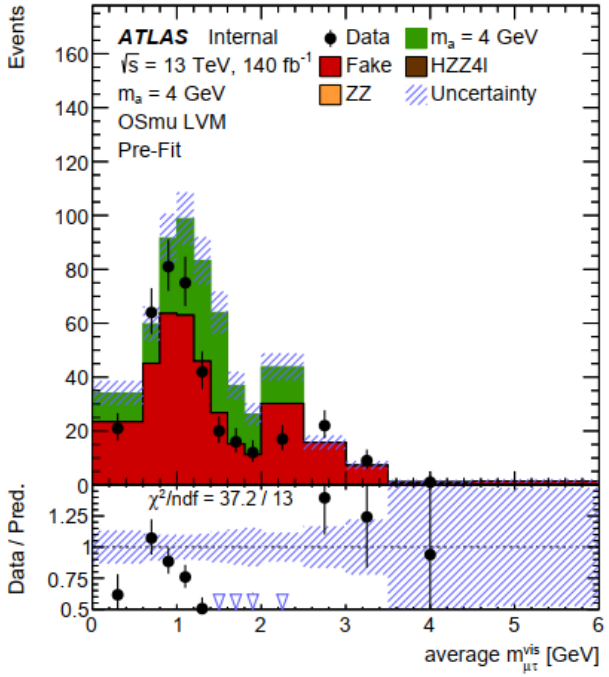

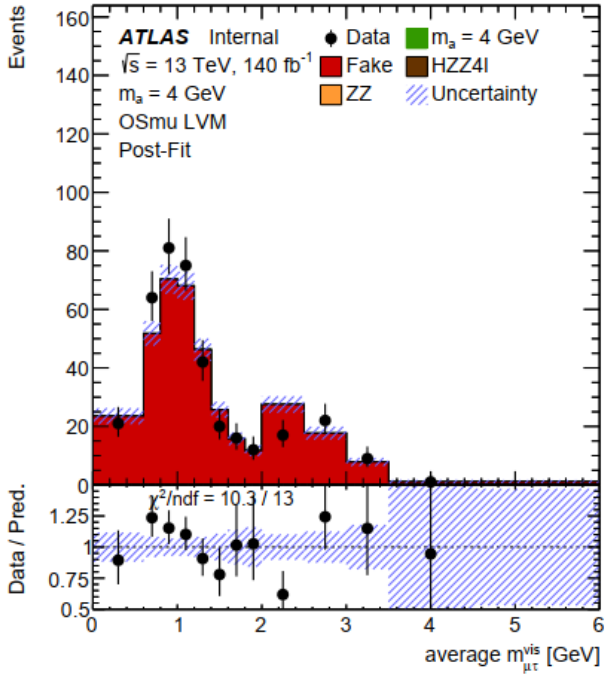

Signal + background fit (m_a = 4 GeV)

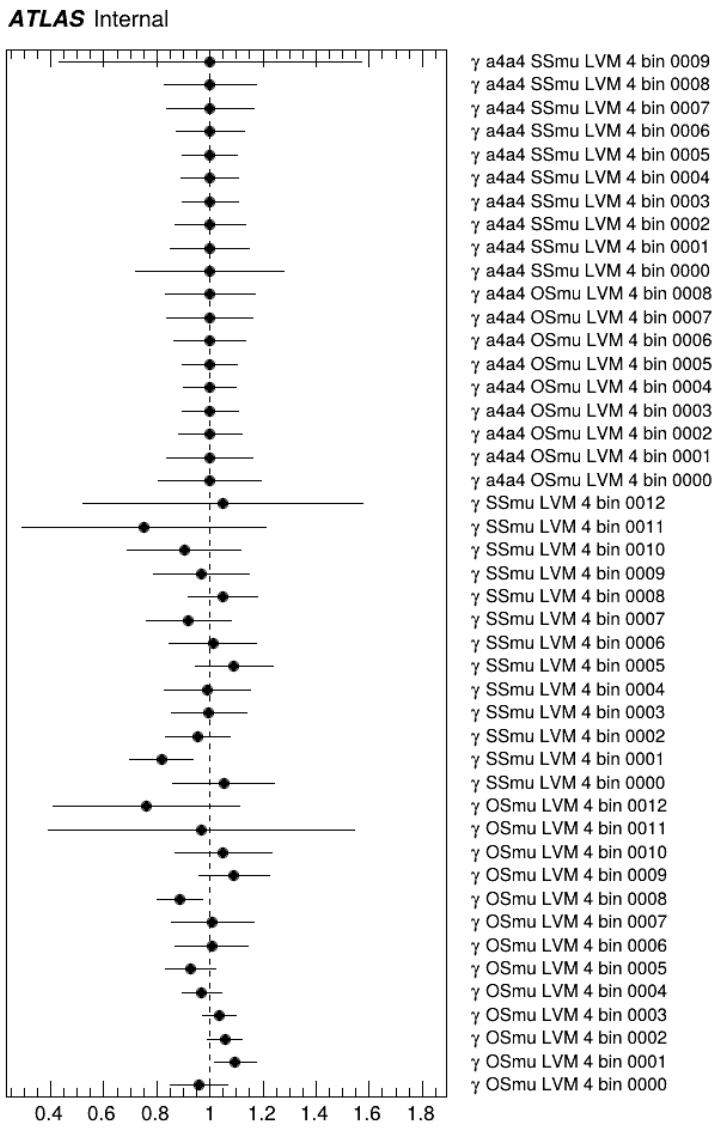

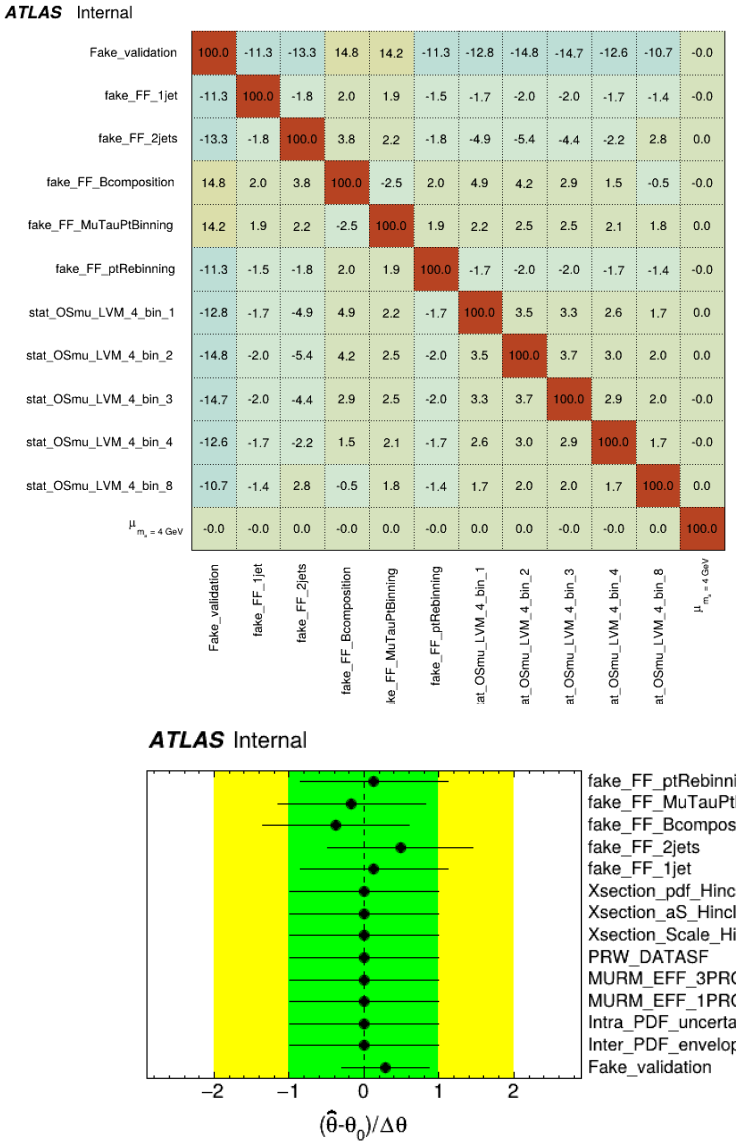

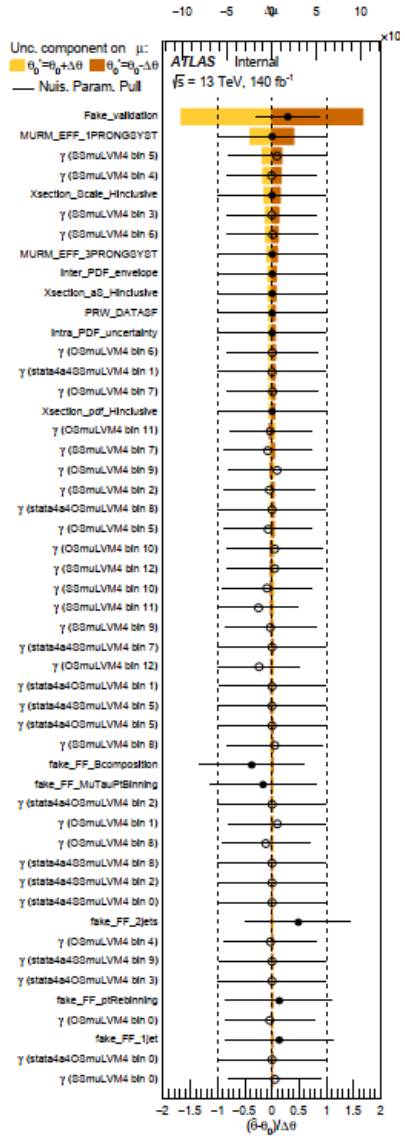

Signal + background fit (m_a = 8 GeV)

- Capped the μ at 0 ($\mu > 0$). (SSμ)
- The fit gets converged and the errors are all good.

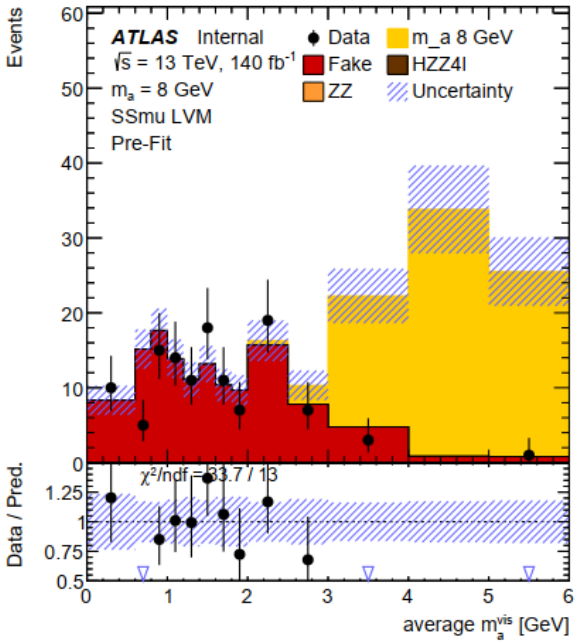

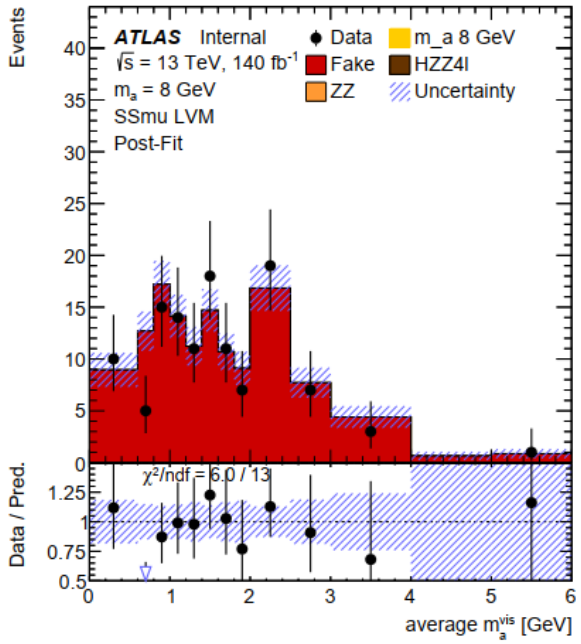

- Capped the μ at 0 ($\mu > 0$). (OSμ)

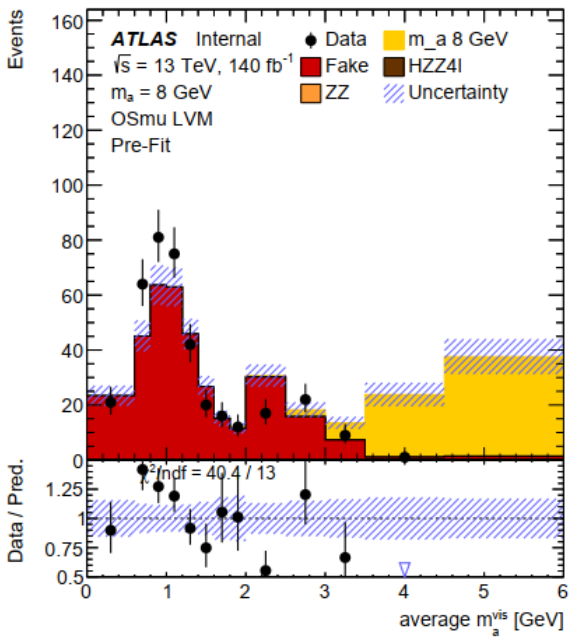

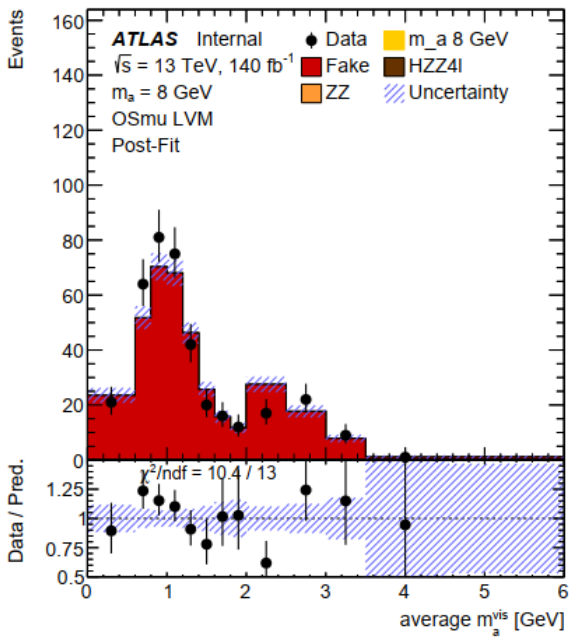

Signal + background fit (m_a = 8 GeV)

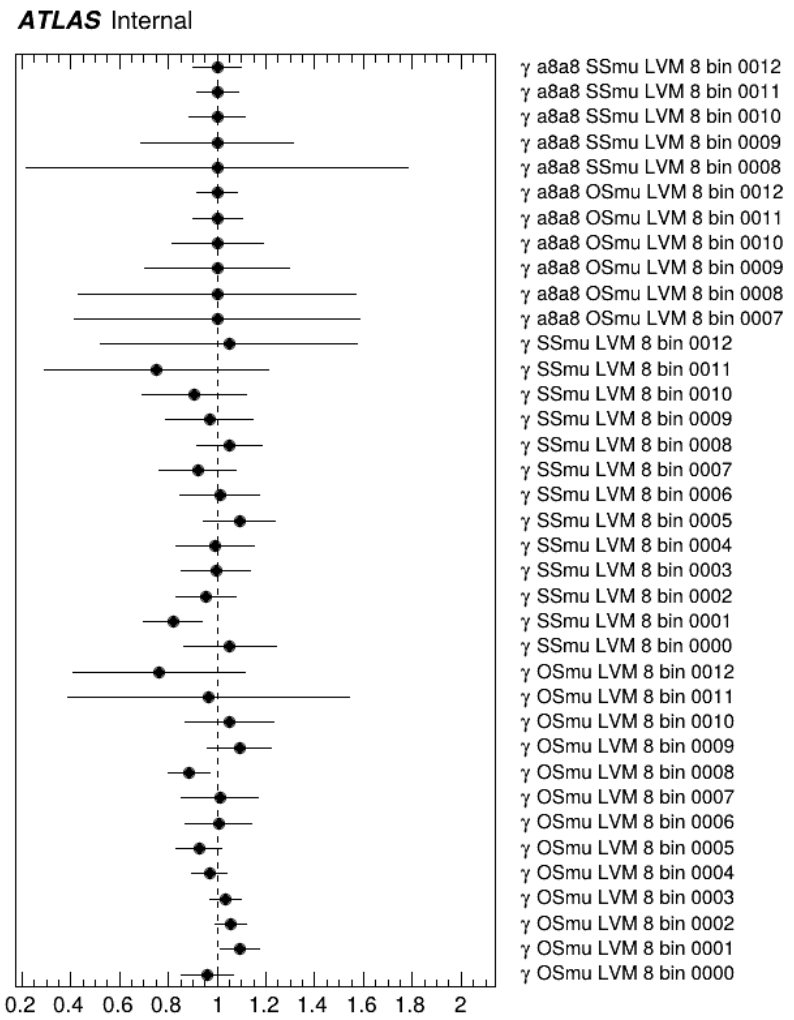

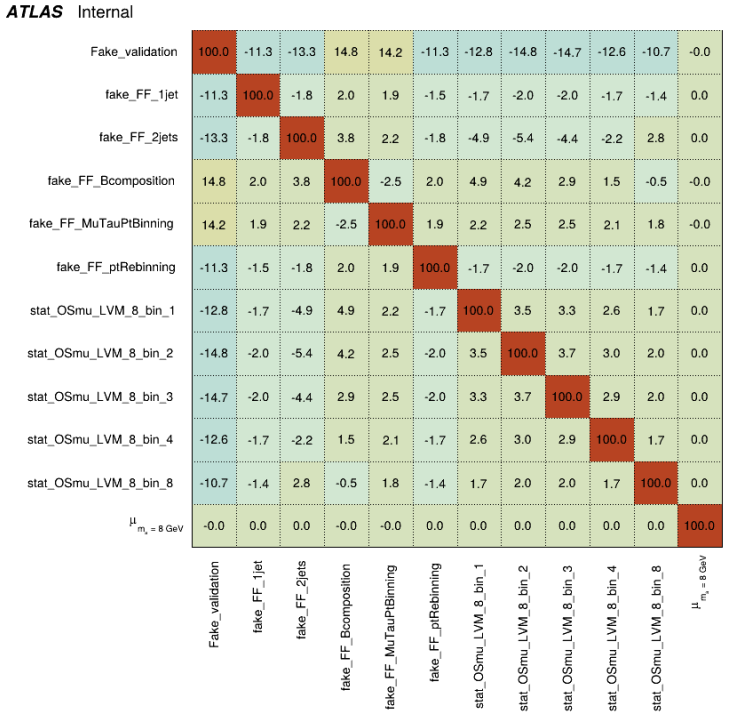

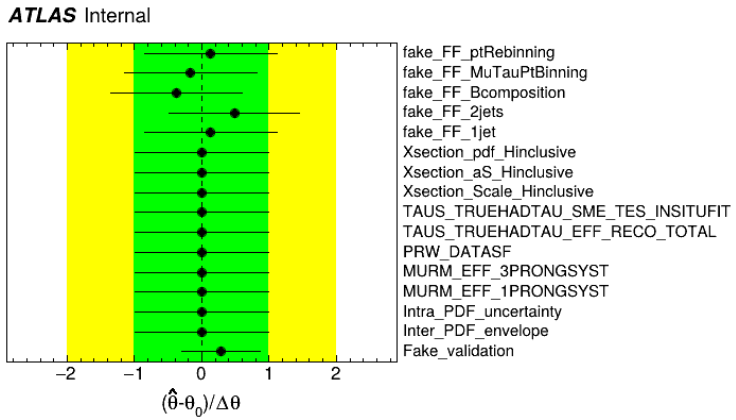

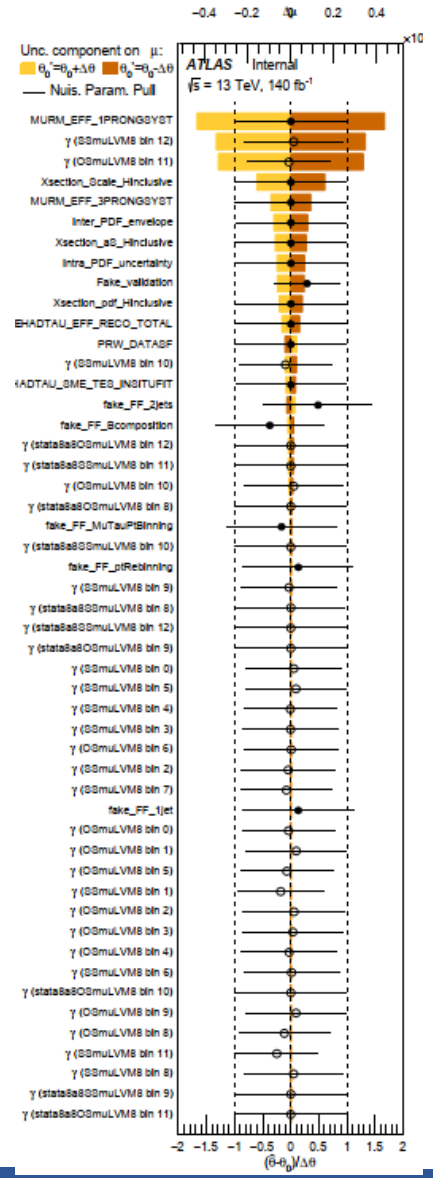

Limits using asymptotic mthod

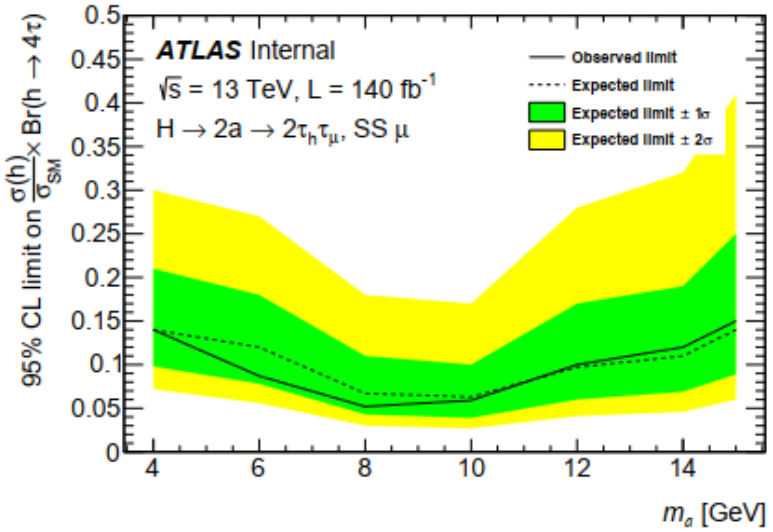

(d) SSμ

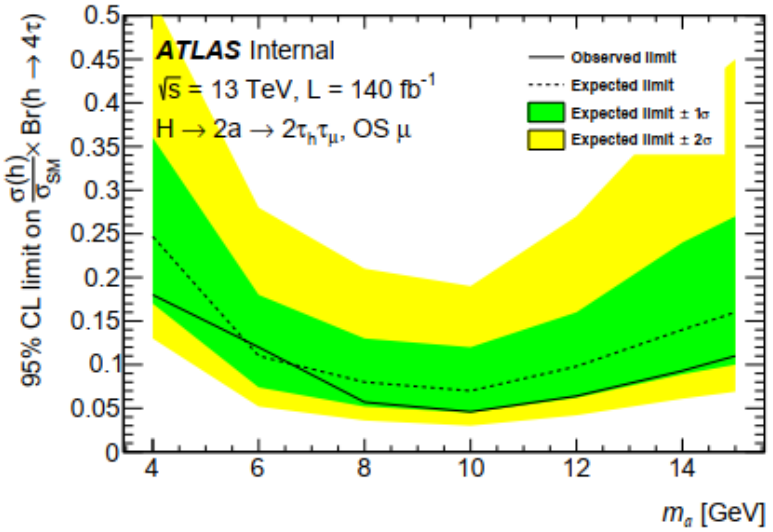

(e) OSμ

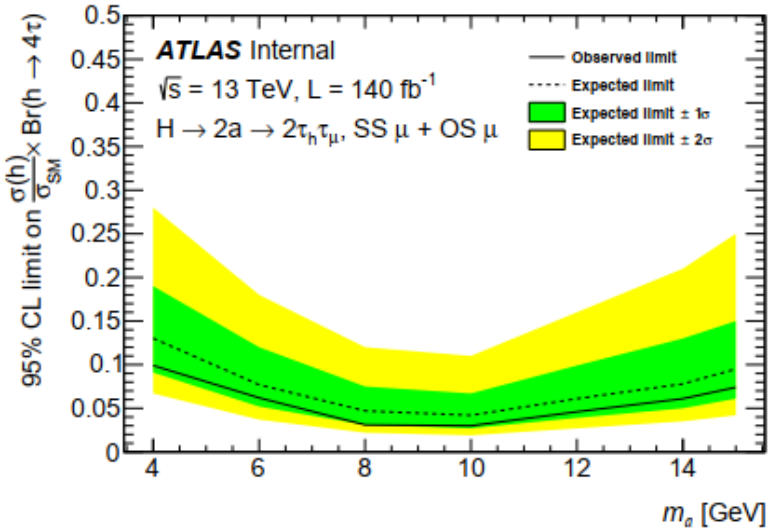

(f) Combination

- The combined observed limits are always better than the expected limits.

Combined toy limits

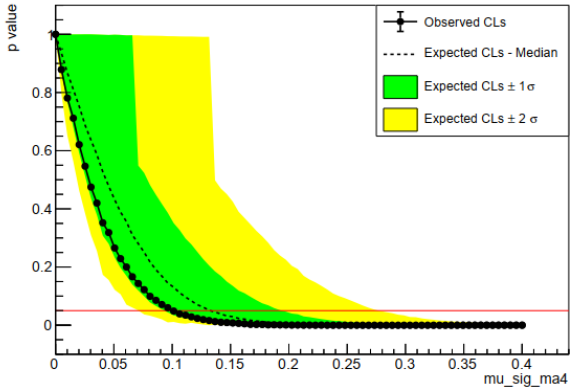

(g) $m_a = 4$ GeV

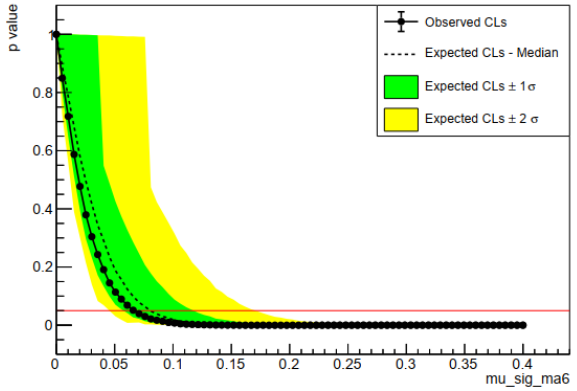

(h) $m_a = 6$ GeV

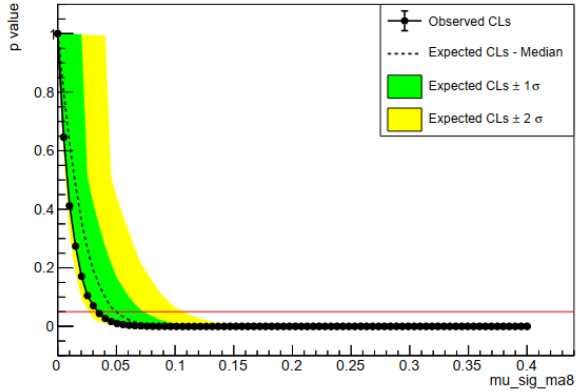

(i) $m_a = 8$ GeV

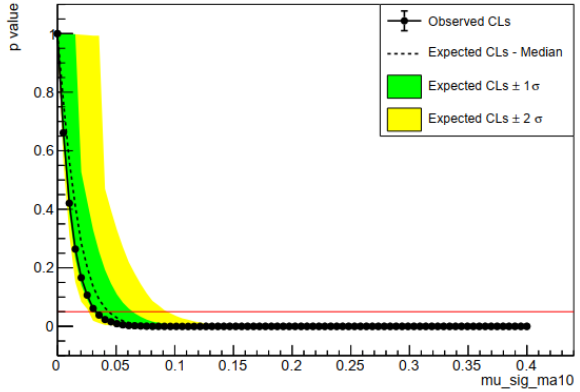

(j) $m_a = 10$ GeV

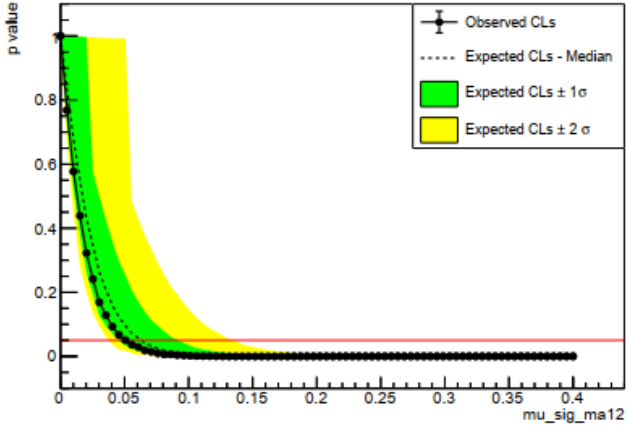

(k) $m_a = 12$ GeV

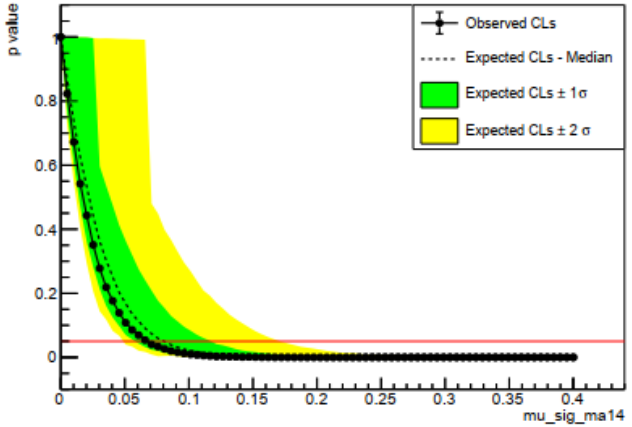

(l) $m_a = 14$ GeV

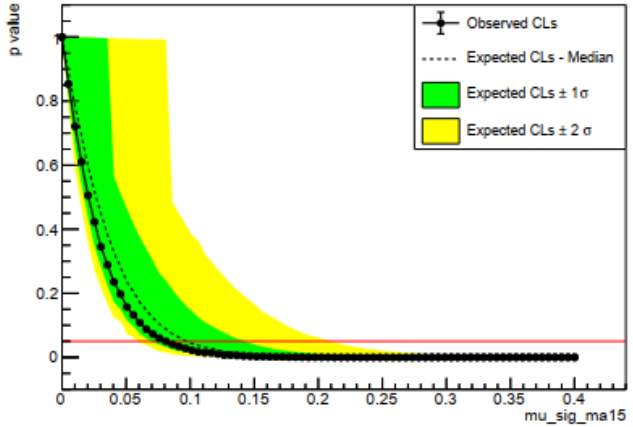

(m) $m_a = 15$ GeV

Comparison between asymptotic and pseudo-experiment (toy) method

- The expected and observed limits are summarized below.
- The differences between the asymptotic and toy methods are within 6% for the expected limits and within 11% for the observed limits.

signal mass (GeV)	4	6	8	10	12	14	15
asymptotic expected limits	0.13	0.077	0.047	0.042	0.061	0.078	0.095
toy expected limits	0.13	0.081	0.050	0.044	0.063	0.081	0.097
asymptotic observed limits	0.099	0.062	0.031	0.030	0.046	0.061	0.074
toy observed limits	0.10	0.066	0.034	0.033	0.051	0.067	0.081
Δ expected limits	0%	5%	6%	5%	3%	4%	2%
Δ observed limits	1%	6%	10%	10%	11%	10%	10%

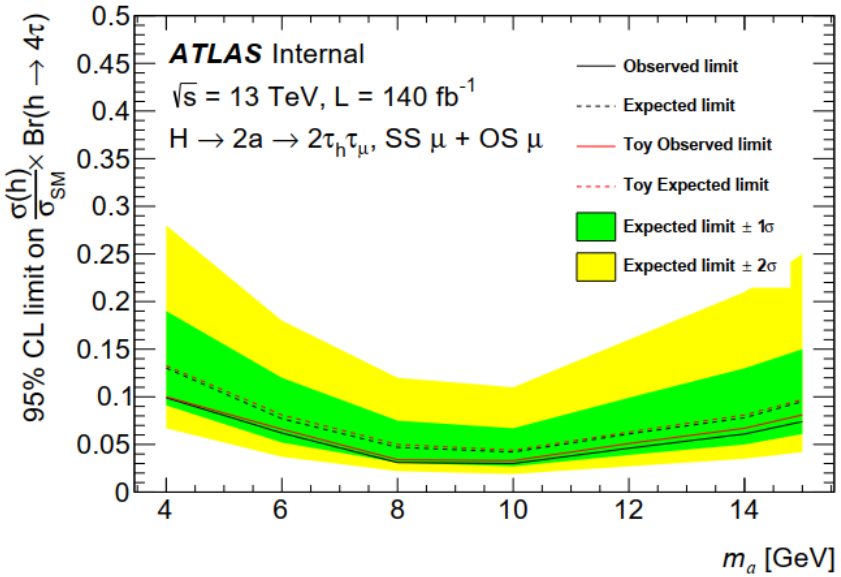

MC backgrounds